Author:
O'Sullivan, Michael Francis

Title:
Microcapsules with liquid cores and solid shells for pressure release applications

Microcapsules with Liquid Cores and Solid Shells for Pressure Release Applications

Michael Francis O'Sullivan

A thesis submitted to the University of Bristol in accordance with the requirements of the degree of Doctor of Philosophy in the Faculty of Science.

Physical and Theoretical Section, School of Chemistry
University of Bristol, BS8 1TS

March 2007

Abstract

The encapsulation of one material by another, to form core-shell particles, has many applications: principally the containment, protection, and distribution of an active material. This thesis describes the development of core-shell particles with liquid cores and solid shells of tunable thickness.

Two main systems are studied. Firstly, polydimethylsiloxane (PDMS) emulsions, or microgels if cross-linked, are employed as templates for the formation of solid shells. The templates are prepared by a surfactant-free emulsion polymerization of dimethyldiethoxysilane (DMDES) that allows monodisperse emulsions to spontaneously form, subject to appropriate monomer concentrations. The viscosity of the microgel is controlled by variation of the cross-linking component's concentration. Silica shells were grown upon silica-skinned templates in a seeded growth process through slow addition of tetraethoxysilane (TEOS) under basic and ethanolic conditions. Solid silica-silicone composite shells were formed, in the absence of ethanol, through condensation of TEOS and DMDES. Shell thickness may be controlled by manipulation of relative TEOS and DMDES concentrations, or by quenching the shell maturation step.

The second system involves the encapsulation of acidic or basic water-in-hexadecane emulsions. These are prepared and exposed to small quantities of TEOS, thereby forming a thin silica membrane at the water/oil interface. This skin was observed to crenellate, with an optical microscope, upon evaporation of the aqueous core. Similar particles were also prepared from emulsions initially stabilized with hydrophobic fumed silica. Thicker membranes may be prepared if the aqueous phase also contains alkoxysilane monomer; these skins survive washing with heptane, or centrifugation into water, and may be viewed by SEM.

The coated PDMS particles were subjected to compression using a micromanipulator. The capsule breaking force was found to be proportional to the shell thickness, as quantified using SEM and ultramicrotomy. Model actives, such as dyes, may be incorporated into the PDMS templates prior to shell formation through use of a vector solvent that swells the core material.

Author's Declaration

I declare that the work presented in this thesis was carried out in accordance with the Regulations of the University of Bristol. The work is original except where indicated by special reference in the text and no part of the thesis has been submitted for any other degree. Any views expressed in the thesis are those of the author and in no way represent those of the University of Bristol. The thesis has not been presented to any other university for examination either in the United Kingdom or overseas.

Michael O'Sullivan

For my family,
and in loving memory of
my grandfather Percival Francis Pallot
and Susan Parnell

Acknowledgements

Firstly, I'd like to thank Professor Brian Vincent for giving me this research project: it's been an adventure! His support and encouragement, including transportation to Australia, is much appreciated and I have very much enjoyed working in his group.

The micromanipulation study, which is a key aspect of this work, would not have been possible without the co-operation of Professor Zhibing Zhang and Katie Min Lui at the School of Chemical Engineering, University of Birmingham. I'd like to take this opportunity to express sincere thanks to them both. And again to Katie for exhibiting phenomenal patience with me while I continually lost glass probes from the force transducer.

S. Shahnaz Tasrin Wahid worked with me as an undergraduate project student and made some of the PDMS in ethanol PCS measurements reported in Chapter 3.

I would also like to thank Jonathan Jones and Philip Newberry of the Electron Microscopy Unit. Phil taught me how to use SEM, and Jon TEM. My thanks also to Sarah Lawrence and Sue Williams, without whom I'd have been lost at sea.

This PhD was supported by Schlumberger Cambridge Research and the Douglas Everett Postgraduate Scholarship. I'd like to thank Dr Jonathan Phipps, Dr Louise Bailey, Professor Geoff Maitland, Dr Jeroen van Duijneveldt, and Professor Terence Cosgrove for guidance.

The BV Lab makes life interesting (in a good way!) and so I am indebted to Pierre Starck, Kath Rees, Jess Tsiopani, Bernd Neumann, Rob Atkin, Mel Bradley, David Snoswell, Aaron Olsen, Jirut Wattoom, Haruna Musa, and Herely Cassanova. Darby Kozak, Ruth Dunleavey, and Phil Dale imparted wisdom. Discussions with Voss Gibson, Erol Hassan, Beth Foster, Ben Cheesman, Nils Elsner, Verawan Nerapusri and Paul Davies were always fun. Ciarán Martin, Andy Cheesman, and Mogens Hinge were inspiring. And Brother Joël Manuvelpillai brought that *je ne sais quoi*, for which we should all be grateful. Outside of the lab, I'd like to acknowledge my friends David Rees, Joel Loveridge, Lisa Nickolds, Neil Timmins, Jasmine Cockcroft, Nico, Andy and Samm, Phil, Paul, Ciarán, and Joël.

Finally, I thank my parents for sustaining me as I write, for all the other times, and for all the vegetable soup, chocolate, and peanut butter sandwiches. Special mention should go to Dougal, Dylan, and Paige for keeping my feet warm, for diversionary tactics (including slumbering atop much-needed journal articles) and, of course, for moral support.

Contents

List of Figures

Chapter 1

Introduction

1.1 Background

Microcapsules are particles that have two components: the active centre or core material, and the shell material or coating. Generally microcapsules are classified such that those smaller than 1 μm are known as nanocapsules, and those larger than 1000 μm are known as macrocapsules [1]. It is typical for a commercial microcapsule to have a diameter between 3 and 800 μm and to have a core that is 10 to 90 % by weight of the capsule. Numerous types of core material have been encapsulated, including adhesives, agrochemicals, live cells, active enzymes, flavours, fragrances, pharmaceuticals, and inks. Recently core-shell particles have been used as precursors to form hollow gold spheres, which have optical applications [2]. Shell materials may be formed from organic polymers (natural or synthetic), fats, or waxes. They may be made permeable, selectively permeable, or impermeable. These properties allow different methods for controlled release of core material, either through mechanical damage of the envelope (as in carbonless copy paper) or permeation [3]. In some microcapsule systems, permeability depends on external salt concentration [4], pH [5], or temperature, e.g. a porous shell has thermoresponsive molecules grafted onto the pores that regulate the passage of material into or out of the capsule [6], or hydrogen bonds within the wall material are disrupted to cause swelling [7].

It is often desirable for microcapsules to be of a small and uniform size. Smaller particle sizes reduce irritation at the site of injections [8]. Uniform size is important as it

allows consistent kinetics of dispersion, and release of core materials, and simplifies their manipulation [6]. Size also determines the distribution of microcapsules in a body, and their interaction with biological cells [9].

A focus of this project is the development of generic core-shell systems for use in oil well drilling. Encapsulated active ingredients, which include electrolytes, enzymes and polymers, are already employed for this purpose. These capsules are prepared using a fluidized bed deposition process, whereby solids are suspended in a gas stream and coated with shell material, that yields particles of millimetre size. This size range imposes limitations on the performance of the particles, both in terms of their combination with other ingredients and in their subsequent distribution in the drilling environment. Encapsulating these materials in the micro- or nanoscale would enable better mixing, and could also offer applications for controlled release and increased permeation. An ideal system would involve a water core and tunable shell thickness. Control of shell thickness would allow application for pressure-triggered release, with higher pressures required for thicker shells.

1.2 Objectives

1. Develop core-shell particles, with liquid (aqueous and oil) cores, in a micrometre size range.
2. Control and quantify shell thickness.
3. Quantify particle response to compression, including the applied breaking force, as a function of shell thickness.
4. Investigate incorporation of model active materials.

1.3 Nomenclature

This work involves the synthesis of polydimethylsiloxane (PDMS) oligomers. All references to PDMS is this text refer to this oligomeric form, rather than to that of high molecular weight, unless otherwise stated.

1.4 Microencapsulation: A Review

Capsule production may be broadly classified as chemical or mechanical. Chemical processes tend to involve chemical reactions that trigger phase changes to form wall materials, while the mechanical processes usually involve aerosol dispersion of material to form shells, either as a point of combination with shell precursors or as a drying step [1]. In general, mechanical methods can allow control of size distribution or shell thickness, but not both; a new technique has been reported, however, that involves extrusion through charged coaxial jets, and may allow simultaneous control of both properties by manipulation of fluid flow rates [10]. This work is primarily concerned with chemical processes, and a review of these is presented here.

1.4.1 Polymer Capsules

Capsules have been prepared by the controlled phase separation of polymer from within an oil-in-water (O/W) emulsion [11]. The oil phase consisted of both a good and bad solvent for the shell polymer. Upon evaporation of the good solvent the polymer was forced to precipitate and migrate to the oil-water interface, where it formed a shell. Interfacial tensions had to be carefully controlled, through selection of specific components and stabilizers, to obtain particles with core-shell morphology. Without this control, alternative non-encapsulating morphologies predominate. Shell thickness was determined by the concentration of the dissolved shell-polymer in the oil phase of the initial emulsion. More recently, a W/O variant of this method was developed that used a combination of acetone, as the volatile solvent, and water in the aqueous phase [12]. Mono-nuclear capsules could be formed using this latter method with poly(tetrahydrofuran) (PTHF) as the encapsulating material; this polymer, however, has a low glass transition temperature (T_g) and was too soft to be transferred into water by centrifugation. Use of alternative higher T_g polymers, such as poly(methylmethacrylate), lead to formation of multinuclear cores; these polymers also required more acetone in the core phase to render them soluble. Final particle size and dispersity is dictated by those properties of the initial emulsion, and, as such, specialized emulsifying equipment, or fractionation, would be required to form a monodisperse dispersion.

Polymer shell formation at the oil-water interface in O/W emulsions has also been achieved following incorporation of oil-soluble monomer in emulsion droplets, water-soluble co-monomer in the continuous phase [13]. Formation of the shells in interfacial reactions limits interactions of reagents, leading to relatively thin capsule walls.

1.4.2 The Layer-by-Layer Method

The Layer-by-Layer (LBL) method of encapsulation typically involves the sequential deposition of complementary or interacting polymers onto a sacrificial colloidal template. A variety of wall materials may be used. These include synthetic or natural polyelectrolytes; nanoparticles, and biomacromolecules [14, 15]. The alternating layers may bind together through electrostatic interactions [16], hydrogen bonds [7], or hydrophobic interactions [17]. The layers may also be cross-linked to improve capsule stability [14].

The method is versatile: It allows unparallelled fine control over wall thickness, and tunable selective permeability; use of sacrificial templates can endow monodispersity; modification and functionalization of the wall surfaces is possible. The method also presents complications [14]: The alternating deposition steps are time consuming; wide distributions in permeability have been observed within the same batch due to pore formation upon core removal; sub-micron capsules are prone to aggregate; and some systems exhibit low reproducibility.

Conventional wall formation can require many steps if thick shells are required. In recent work, however, adsorbed pyrrole was polymerized upon thin LBL capsules to give thicker shells [18]. The multilayer nature of LBL capsule walls can allow formation of multiple shell particles that have structural advantages. LBL deposition of polyelectrolyte upon melamine formaldehyde latex cores, followed by deposition of silica nanoparticles with poly(allylamine hydrochloride) (PAH), succeeded by poly(styrene sulfonate) (PSS)/ PAH LBL, formed capsule walls with three discrete layers. Removal of the core with HCl and the silica with HF presented a hollow shell-in-shell particle. The inter-shell space was filled with a PAH solution that was found to act as an osmotic pressure buffer and rendered the particles more resistant to osmotic-driven collapse [19].

1.4.3 Capsules formed from Adsorbed Particles

Core shell particles have been formed from the heterocoagulation of oppositely charged latex particles. Smaller particles, with a low T_g, formed a coating when melted and allowed spread under elevated temperatures to form a shell. The extent of coverage was determined by the packing density of the shell-precursor particles on the core. Voids and cracks were observed in the shells made with this method [20, 21].

The assembly of latex particles at oil-water interfaces have been exploited to make core-shell particles with selectively permeable membranes. Permeability was determined by the porosity of the shell, which arose due to interstices between the surface-bound particles. Such systems have been called Colloidosomes [22]. The fabrication process involves the formation of an emulsion that is stabilized by particles dispersed in the continuous phase. The stabilizing particles may then be interconnected by some suitable method, such as sintering or application of a cross-linking agent. In the case of water-in-oil (W/O) systems, the colloidosomes have been successfully transferred into an aqueous continuous phase by centrifugation in the presence of non-ionic surfactant.

Another approach, using particle-stabilized emulsions, employed an aqueous lysine monohydrate modified latex system dispersed into 1-octanol. The aqueous phase dissolves into the octanol, leaving spherical latex assemblies with cavities in their centres; this was attributed to alcohol-triggered latex coagulation following core dissolution [23].

O/W systems were formed from the dispersal of a non-aqueous phase that contained microgel particles into water [24]. The microgels were subsequently cross-linked through addition of a cross-linking agent that reacted with the surface groups of neighbouring particles. Soft, swellable microgels were used for the shell particles for controlled release applications.

1.4.4 Silica Capsules

Silica particles present a readily functionalized surface that may be modified to enable their dispersal in non-polar solvents [25]. Silica shells tend to be smooth because growth takes place on a molecular scale [26], which is beneficial if the shells need to be well defined.

Silica-coated emulsion droplets have been formed by interfacial sol-gel reactions [27].

For example, aqueous NH_3 solution is emulsified into hexadecane in the presence of TEGOPREN 7008 surfactant [28, 29]. TEGOPREN 7008 (from Goldschmidt) is an alkyl- and polyether-modified siloxane comb polymer Alkoxysilanes are then added, which hydrolyse at the basic W/O interface and are thought to cross-link the TEGOPREN surfactant at the terminal OH of the polyether groups, forming a silica-type skin. The shell is expected to grow until a continuous silica layer has formed around the droplet that prevents further interaction between the aqueous phase and the external alkoxysilane.

Silica shells have also been grown on zinc sulfide cores by the Stöber process [30]; the cores were subsequently dissolved with nitric acid to yield hollow silica particles. The ZnS particles were prepared by precipitation from acidic zinc nitrate using thermal decomposition of thioacetamide (TAA) as a source of sulfide ions. Particle size may be controlled by reaction time and monodispersed systems of 1.5–2 μm have been prepared [31, 32].

Monodisperse polydimethylsiloxane (PDMS) emulsions have be used as a liquid templates (see Chapters 3 and 4). The emulsions are prepared by surfactant-free emulsion polymerization of dimethyldiethoxysilane (DMDES) [33]. Silica coatings on such droplets have been grown by precipitation of a thin silica skin, from saturated sodium silicate, followed by Stöber-type shell growth [34].

More recently, a solid composite silica-silicone shell material has been formed around PDMS by adding tetraethoxysilane (TEOS), as cross-linking agent, during the emulsion growth process [35, 36]. The latter method demonstrated tunable shell thickness and is further discussed in Chapter 4.

1.4.5 Principal methods to Incorporate Active Materials into Capsules

There are three principle methods to incorporate active ingredients into capsules. Firstly, capsules whose wall material permeability may be tuned by external conditions are introduced into a continuous phase that contains dissolved active. The capsule is rendered permeable through change in pH [5], or temperature [37], or addition of salt [4], to allow active to diffuse into the capsule. A range of materials may be loaded into capsules with this method provided the wall material is sufficiently permeable. The final active concentration within the

capsule is limited by that of the active in the continuous phase. This method's reproducibility is poor and the shell swelling conditions may be unsuitable for many biomolecules [15]. Use of sequestering agents can enhance active uptake into capsules, however [38].

Secondly, if a material may be crystallized then direct encapsulation of the solid leads to a concentrated core-shell particle, but the crystals must be insoluble in shell-forming reagents [39].

Lastly, the most versatile method of active incorporation is to use an absorbent or solid porous media as a core material [15]. Active molecules, such as enzymes, can be adsorbed onto the pore surfaces prior to encapsulation. The core can be dissolved subsequently. Typical sacrificial templates are silica [40] and calcium carbonate [41].

1.5 Summary

The use of series of emulsions stabilized with particles of various size as core-shell precursors offers a route for control of shell thickness. This has, in part, already been achieved with the colloidosome system. O/W shelled systems were produced by sintering the surface bound latex. For water-cored systems this may be problematic, as core evaporation might occur. The W/O shelled systems depended on chemical linkage of particle surface groups, leaving interstitial space as pores. Such porosity, though advantageous for loading of the capsules, may be problematic for some applications—particularly where release is intended by shell rupture alone, rather than diffusion. Interfacial polymerization produces capsules with thin shells and, without subsequent growth or deposition steps, offers limited scope for control of shell thickness. Phase separation of polymer from an internal emulsion phase to form the shell relies on specific conditions of interfacial tension to form a well defined mononuclear structure. Layer-by-layer deposition offers control of shell thickness, and methods for introducing macromolecules to the capsule. Capsule preparation requiring multiple deposition steps may be unsuitable for large scale production, however.

This project focuses on the formation of core-shell particles with liquid cores and solid shells for purposes of controlled release. A key aim is to control shell thickness. Monodisperse core-shell particles, with liquid cores, may be formed by shell growth upon a sacrificial

solid template or liquid droplets. Use of monodisperse templates can engender monodispersity to the final particles. A variety of fabrication routes to form monodisperse solid particles are available, but the subsequent solid removal can cause disruption, e.g. by pore formation, of the shell.

Approaches whereby actives may be loaded into core material prior to shell formation are preferable, and use of emulsions as a core material may offer scope to do this. Monodisperse emulsion formation tends to require the use of specialized equipment, such as cross-flow membranes [42] or microfluidic devices [43]. The use of spontaneously formed monodisperse PDMS emulsions as templates, however, seems a promising alternative, at least as a model system, but would not be directly suitable for delivery of aqueous media.

1.6 Thesis Outline

Chapter 2 discusses the principal methods used to characterize the particles, with the exception of micromanipulation, which is discussed in Chapter 5. Chapter 3 introduces the concept of surfactant-free PDMS emulsion synthesis, reviews previous work in this area and describes investigations into growth of a silica shell around these dispersions as mentioned in Section 1.4.4. Chapter 4 follows with an alternative method to grow a solid silica-silicone composite shell upon PDMS, and its modification to enable scope for active incorporation prior to shell formation. Chapter 5 introduces and reviews micromanipulation, the method used to quantify the particles' mechanical properties, and presents results and discussion from that study. Chapter 6 details investigations into incorporation of dyes as model actives into the encapsulated PDMS particles. Chapter 7 describes the preparation of capsules with aqueous cores.

Chapter 2

Methods

2.1 Photon Correlation Spectroscopy

Photon Correlation Spectroscopy (PCS), also known as dynamic light scattering, or quasi-elastic light scattering, measures the hydrodynamic diameter of colloidal particles: the sum of the particle diameter and any adsorbed solvent.

Electromagnetic radiation, as described by classical electromagnetic theory, consists of perpendicularly fluctuating electric and magnetic fields that propagate as a wave through space at the velocity of light. Radiation intensity I is proportional to the square of the amplitude of the wave motion. The electric field constituent of radiation may interact with electron distributions within molecules causing them to oscillate. This electronic oscillation generates electromagnetic radiation, effectively rendering the particle as a point source of light, and is the basis for light scattering.

If a coherent light source, such as a laser, is projected through a stationary array of particles, scattered light experiences systematic constructive and destructive interference so that an interference pattern is produced. If, instead, the particles undergo Brownian motion in a dispersion, a continuously shifting diffraction pattern is produced. Scattered light presents variables that may be quantifiably measured: average intensity as a function of angle, polarization, wavelength, and fluctuations about the average intensity. In the latter case, a detector positioned at a fixed angle from the incident beam may measure the fluctuations. A fluctuation's decay time relates to the diffusion constant, and hence the size, of the particle. Small,

rapidly moving particles create fluctuations that decay more rapidly than those generated by larger, slower particles.

In PCS, the intensity fluctuations are passed to a photon correlator. The total time over which the measurement is made is divided into small time intervals called delay times (τ). These times are small relative to the time taken for an intensity fluctuation to decay to the average intensity. The output from the photon correlator is the autocorrelation function $C(\tau)$ (Equation 2.1.1). The autocorrelation function effectively measures the probability of a particle moving a given distance in time τ [44] and is the relationship between the average intensity at time $(t+\tau)$ and time t. When τ is large, $I(t)$ and $I(t+\tau)$ are independent of one another and the function approaches the background value B; for very small τ values, $I(t)$ and $I(t+\tau)$ are closely related.

$$C(\tau) = A\exp\left(-\frac{\tau}{\tau_C}\right) + B \tag{2.1.1}$$

The parameter τ_C relates to the particle diffusion coefficient D.

$$\tau_C = \frac{1}{DQ^2} \tag{2.1.2}$$

Q is calculated from the scattering angle θ, the laser wavelength λ and the refractive index n of the continuous phase.

$$Q = \frac{4\pi n}{\lambda}\sin\left(\frac{\theta}{2}\right) \tag{2.1.3}$$

Particle diffusion coefficients may be related to particle hydrodynamic diameter d. Equation 2.1.4, the Stokes-Einstein Equation, assumes a spherical morphology, in which k_B is the Boltzmann constant, T is the absolute temperature, and η is the viscosity of the continuous phase that the particles move through.

$$D = \frac{k_B T}{3\pi\eta d} \tag{2.1.4}$$

In effect, the technique measures the autocorrelation function and fits Equation 2.1.1 to that function to determine τ_C. The diffusion coefficient may then be calculated from Equa-

tion 2.1.2 for known values of n, θ. Hydrodynamic diameter follows from Equation 2.1.4.

The equations assume purely Brownian motion, which are solvent-particle rather than particle-particle interactions, and neglect gravitational influences. Dilute dispersions are required, both for the former reason and to minimize subsequent scattering of already scattered light (so-called secondary scatter).

When the particle size approaches the magnitude of the light wavelength used, the scattering behaviour becomes more complex, forward scattering is more pronounced, and the recorded measurement becomes less reliable above a size of approximately 1 μm. PCS is however quicker, more convenient and less invasive than transmission electron microscopy (TEM). Although this method applies well to monodisperse dispersions, the analysis is complicated by polydispersity because the correlation function must account for the movement of differently sized particles.

2.2 Microscopy

Microscopy involves the magnification of an object to allow its fine detail to be observed. The technique is limited by the resolving power; resolution is the smallest separation between two bodies at which they may be observed to be discrete. The resolving limit δ is determined by the wavelength λ of the illuminating radiation, the refractive index n of the medium it has to pass through and α, which is half the angle of the maximum cone of light that can enter the aperture (Equation 2.2.1) [45]. This means the resolving power is principally limited by the illuminating wavelength: the larger λ, the larger the minimum separation.

$$\delta = \frac{\lambda}{2n\sin\alpha} \tag{2.2.1}$$

2.2.1 Optical Microscopy

Optical microscopes use an array of glass lenses to focus and enlarge a light-illuminated image. The wavelength range of light is between 400–750 nm, while 2α is 70° [46]. The maximum theoretical resolution limit of an optical microscope, using oil immersion, is 200 nm.

Magnification above x1000 will increase size, but not definition of the image. Practically this means optical microscopy will impose large and scaling systematic errors upon particle size measurements for diameters in the region of ≈ 2 μm [45]. A further limitation is the lack of optical contrast between the object and its surroundings.

2.2.2 Electron Microscopy

Electron microscopes use a focused beam of electrons as an illuminating source. The focusing principle is analogous to that of optical microscopy, but electromagnets are used in place of glass lenses. The technique has a higher resolving power than its optical analogue because the electron beam may exhibit wavelengths in the region of 0.0025–0.01 nm, depending on the accelerating voltage, and a 2α value of 35' [46]. The maximum theoretical δ is 0.03 nm, but in practise 0.2–0.3 nm is achieved due to chromatic (the distribution of electron energy) and achromatic (path length distribution) aberrations. Use of a coherent electron source may reduce chromatic aberration, but inelastic scattering upon interaction with the sample restores the effect. For conventional electron microscopy, it is necessary for the sample and electron beam to be contained in a vacuum, as atmosphere would scatter the electrons. As such, experimental samples must survive a drying process and should be stable when exposed to the electron beam to present a representative image.

Transmission Electron Microscopy

Transmission electron microscopy (TEM), involves the passage of a focused electron beam through a thin specimen to a phosphorous screen to form an optical image. Samples are deposited on a carbon film-coated copper grid and presented to the beam. The carbon film supports deposited particles and, due to its low atomic weight, presents little interference. Thick or dense structures scatter electrons and create contrast in the final image.

Scanning Electron Microscopy

In scanning electron microscopy (SEM), an electron beam is focused to a point at, and raster scanned across, a sample surface. The incident beam displaces electrons from a conduction

band that are in turn emitted, these are called secondary electrons. The detected secondary electrons provide high resolution topographic information. Interaction with the electron beam also leads to back-scattered electrons through elastic collisions. Electrons derived from both mechanisms impinge upon a phosphorus screen to provide an optical image. Secondary electrons provide a diffusely lit image that allows determination of particle size, while back-scattered electrons act to provide a point illumination source leading to shadow formation that allows depth perception [45].

The resolving power of SEM tends to be less than TEM, $\delta \approx 5$ nm, as lower accelerating voltages are used, but the technique provides a depth of focus $\approx$ 1 mm, while that of an optical microscope provides 1 μm, and thereby yields valuable information about particle size and shape. Use of higher acceleration voltages lead to beam penetration of the sample, which provides less surface detail and may cause sample damage. High resolution work requires a narrow beam diameter and a high accelerating voltage to give a good signal. A field emission gun (FEG) is used to provide a point electron source for such work, rather than a simpler filament. To produce the narrow bean, a FEG incorporates a single crystal tungsten wire cathode that is sharpened by electrolytic etching.

It is a requirement of the technique that the sample presents a conductive surface to the beam, either through its own nature or following deposition of a thin metallic coating, to prevent charge build-up that leads to a distortion that manifests itself as glare in the final optical image.

2.3 Instrument Details

A Zeta Plus Zeta Potential Analyser from the Brookhaven Instruments Corporation was used to conduct PCS. Samples were placed into 1 cm path-length polystyrene cuvettes and all measurements were conducted at 25 °C. All samples were diluted to achieve a photon count rate in the region of 100 x10^3 counts s^{-1}. The instrument used a 30 mW 676 nm wavelength laser source, and the photomultiplier (used to amplify the scattered light signal) and detector were fixed at 90° to the source.

A Nikon Optihot Optical Microscope, fitted with Nikon x20 and x40 objective lenses,

was used to view the experimental systems. A Pulnix TM-1020-15CL video camera was used to capture still images. The microscope was calibrated with a stage micrometre (Agar Scientific) using 50 x 2 μm divisions.

High resolution SEM micrographs were taken with a Jeol JSM 6330F, fitted with a field emission gun. Typically 10–20 keV acceleration was used. Lower resolution images were taken with a Jeol 5600LV. Samples were air dried on stub-mounted adhesive carbon tabs and coated with Pd/Pt alloy films, typically 15–20 nm thick, using an Agar high resolution splutter coater. TEM images were taken with Jeol JEM 1200 EX MKI.

Chapter 3

Silica Growth on PDMS Microgels

3.1 Introduction

A key aim of this work is to develop core-shell particles with liquid cores, tunable shell thickness, and a narrow size distribution, which may be achieved if the core material is monodisperse.

3.1.1 PDMS Emulsions

Monodisperse polydimethylsiloxane (PDMS) emulsions may be formed by base catalysed hydrolysis and condensation of dimethyldiethoxysilane (DMDES) [33], a process thought to be analogous to the nucleation and growth of silica particles in the Stöber process [47, 26]. The method is simple and does not require any special apparatus.

To form the emulsion, DMDES is shaken with an ammonia solution, whereupon the monomer forms a soluble ionic intermediate that condenses to form insoluble PDMS macromolecules, which in turn form nucleation sites for subsequent emulsion growth.

$$\mathrm{EtO-Si(Me)_2-OEt} \xrightarrow[-\mathrm{EtOH}\,+\,\mathrm{OH^-}]{\mathrm{H_2O}\,+\,\mathrm{OH^-}} \mathrm{EtO-Si(Me)_2-O^-} \xrightarrow[-\mathrm{EtOH}\,+\,\mathrm{OH^-}]{\mathrm{DMDES}\,+\,\mathrm{H_2O}} \mathrm{PDMS} \quad (3.1.1)$$

The nucleating centres combine until a threshold size is reached because the stabilizing surface groups are of sufficient density to prevent further coalescence; further droplet growth is a result of direct condensation with, or adsorption of, monomer or oligomer residues. The re-

action occurs at a steady state and is limited by the initial rate of monomer hydrolysis. Ionic strength influences the maximum coalescent size of the nascent droplets, while monomer concentration affects the droplet number density, polydispersity and final droplet size.

The final emulsions were observed to be stable to coalescence, although longer-term stability could be achieved through lowering the ionic strength by dialysis.

Static light scattering studies showed PDMS emulsion droplet growth to exhibit a first order behaviour and could be fitted by Equation 3.1.2 in which R_t is the droplet radius at time t, R_f is the final droplet radius, and t_1 is a fitting parameter.

$$R_t^3 = R_f^3 \left[1 - \exp\left(-\frac{t}{t_1} \right) \right] \tag{3.1.2}$$

PDMS oil formed by this method has a density of 0.95 kg dm^{-3}, based upon the observed density balance that occurred in an emulsion prepared in 35 % v/v NH_3 [33], and subsequent density measurements made by other workers [48, 49].

Electrophoretic measurements have demonstrated the presence of anionic charge at the droplet interface. The determined isoelectric point of the PDMS emulsion occurred between pH 2–3, which is consistent with that observed for silica spheres [48]. Zeta potential measurements of emulsion droplets assume that they behave as solid particles, in that no significant momentum transfer occurs across the the O/W interface in the moving droplet. This assumption is valid when a surfactant monolayer is present [50], but has not been established to be the case for the surfactant free PDMS system [48].

Increasing NH_3 concentration during the preparation stage leads to an increase in droplet size following enhanced coalescence of nucleation centres; this is a consequence of charge screening due to increased ionic strength. This process inevitably leads to a reduction in droplet number density.

PDMS emulsions have also been formed in ethanol-water solutions [33]. Increasing the ethanol volume fraction up to 0.5 leads to an increase in mean droplet size. At higher ethanol concentrations a single phase formed.

Molecular weight was found to be independent of ammonia concentration. Mass spectra showed the tetramer (Figure 3.1) to be the most abundant constituent, with a number-

averaged molecular weight of 310 g mol^{-}1 (4.2 repeat units). ^{1}H and ^{29}Si NMR spectra revealed the PDMS to be principally cyclic; the latter spectrum shows 88.6 % of the oil to consist of the tetrameric species, with an 11 % contribution from linear PDMS. Fewer than 1 % of the linear chains were ethoxy terminated [33, 36].

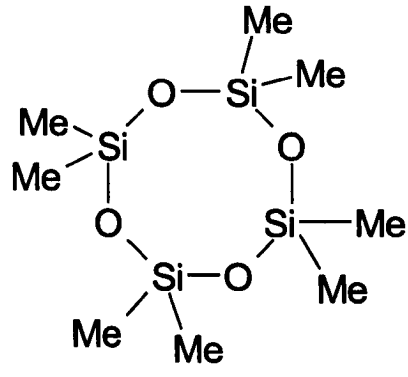

Figure 3.1: Octamethyltetrasiloxane was the most abundant oligomeric PDMS species produced by the surfactant-free emulsion polymerization under conditions of 1 % v/v NH_3 solution.

^{1}H NMR of PDMS emulsions formed in 40 % v/v ethanol showed the linear oligomer contribution to rise to 39.7 %, with 60.3 % cyclic oligomers; this reduction of cyclization was a consequence of improved solvency. The average molecular weight was unaffected however. Further increase of ethanol concentration lead to a predominance of linear oligomers at 85.6 %, while the tetrameric contribution fell to 13.6 %.

3.1.2 Cross-linked PDMS

Introduction of the cross-linking agent methyltriethoxysilane (MTES) during PDMS synthesis allows formation of particles that range from liquid to amorphous solid [51, 52]. Use of 3 aminopropyltriethoxysilane (APTES) can produce cationic particles in pH < 6; at higher pH the amine moiety remains deprotonated, and charge contribution derives from the anionically terminated linear PDMS [51].

PDMS oil, derived from 1 % v/v monomer and NH_3 regimes, becomes progressively more viscous with increasing MTES volume fractions, ϕ_{MTES}, up to 40 % due to enhanced cross-linking. Solid particles are produced with further increased MTES contribution. Particles formed exclusively from MTES are non-spherical and exhibit rough surfaces. Increases

in MTES contribution, relative to the total monomer volume fraction, also cause the particle size to decrease. If the MTES concentration begins to exceed that of the DMDES, particle size increases (Figure 3.2, reproduced from Reference [51]). Increasing ϕ_{MTES} leads to an increase in molecular weight [51, 52].

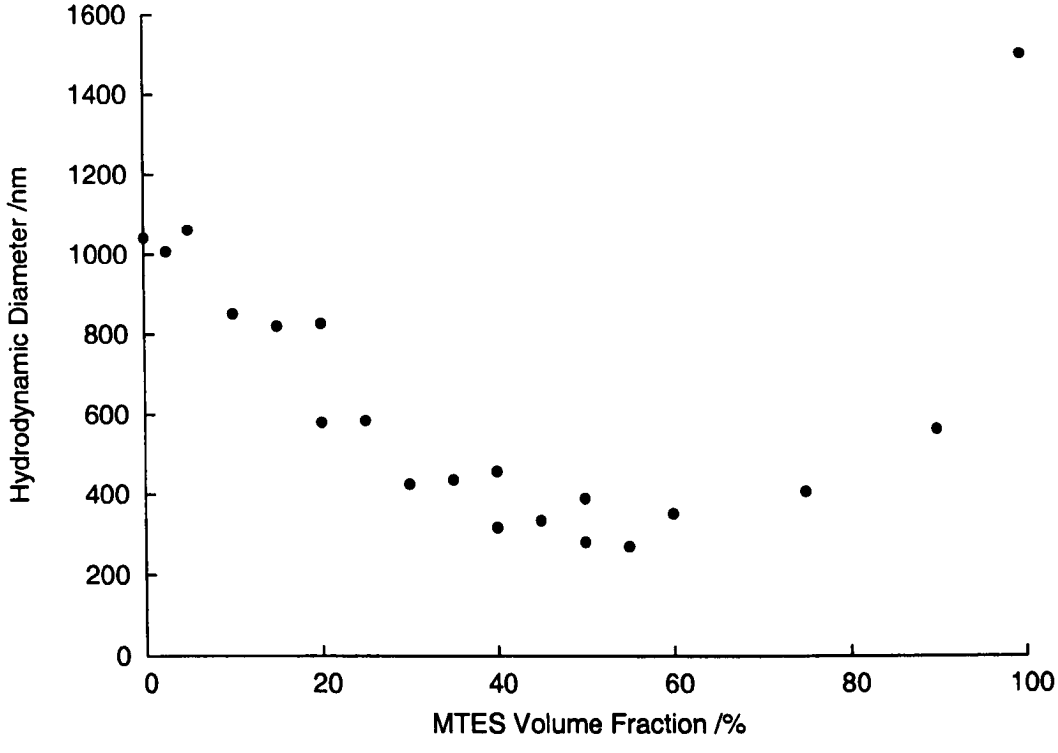

Figure 3.2: Droplet size, determined by PCS, as a function of MTES volume fraction with respect to the total monomer volume.

The decreasing particle size with increasing ϕ_{MTES} is a consequence of an enhanced rate of nucleation because the trifunctional MTES residues present three polymerizable loci. Increasing particle size with higher MTES concentrations occurs because the MTES contribution predominates in the formed oligomers; the oligomers then present more polar moieties, increased solubility, and a reduced nucleation rate.

In examined MTES regimes, mobility was found to decrease with increasing relative MTES volume fraction [52]. Increasing the trifunctional monomer contribution increases polymer branching, thereby reducing the conformational freedom of polymers, which restricts migration of anionically terminated linear oligomers to the particle-water interface.

Dispersions formed from 10 % total monomer and $\phi_{MTES} > 30$ % were observed to both cream and sediment. This behaviour was attributed to random polymerization that yielded a

wide distribution of oligomer molecular weights. Dialysis was observed to accelerate aggregation [52].

^{29}Si NMR of particles formed from ϕ_{MTES} of 20 % revealed the tetrameric oligomer to be the predominant species, corresponding to 48.7 % of the material. The difunctionally-derived linear contribution was increased to 37.7 %. For this MTES concentration trifunctional material constituted 6.3 % of the total. Increasing the MTES/DMDES ratio leads to an increased production of MTES-derived oligomers [52].

MTES-derived PDMS dispersions were only successfully formed in $\phi_{EtOH} < 0.6$. At higher ethanol concentrations a single phase persists. Increasing ethanol concentration in the polymerization conditions, up to the single phase threshold, causes larger particles to form, due to the suppression of nucleation by improved solvency. Addition of ethanol following formation, rather than using it as a co-solvent during the reaction, of the high MTES particles does not affect particle size. The presence of ethanol during particle formation acts to increase the ratio of trifunctional to difunctional material in the final particles, possibly as a consequence of improved partitioning of the monomer into the ethanol/water phase.

Dilution of particles, subsequent to their formation in ethanol and ammoniacal water, leads to a decrease in particle size. This is most pronounced if the initial ethanol concentration is $>$ ϕ_{EtOH} 0.5; under these conditions an apparent substructure is formed that collapses upon dilution with water.

PDMS formed in the presence of APTES exhibited increased size with monomer-relative volume fractions up to 20 %, whereas further increase to 50 % caused the size to decline [51]. Above 50 % APTES no droplets were observed. ^{29}Si NMR studies of APTES systems suggested that the APTES was not polymerized with the DMDES, but was instead incorporated as free monomer. Initial droplet size increase was caused by swelling, the decline in size at higher APTES concetrations may have been a consequence of PDMS solubility in the more hydrophilic monomer.

There is some uncertainty as to whether the MTES-derived PDMS dispersions actually constitute microgels. Microgels are defined as macroscopic structures that are intermediate between branched molecules and macroscopically cross-linked networks [53]; the

presence of such networks, as of writing, have not been determined in the PDMS systems. Nevertheless, MTES-derived PDMS materials swell in the presence of a suitable solvent, such as n-heptane, with a finite swelling limit that depends upon the extent of cross-linkage [51, 54, 48, 52]; this is indicative of microgel behaviour. With that consideration, the MTES-derived particles shall be described as microgels hereafter.

PDMS dispersions have also been prepared with TEOS as a cross-linking agent. In a 10 % v/v monomer in 1 % v/v NH_3 regime, TEOS volume fractions, relative to the total monomer volume, of 0.2, 0.4 and 0.6 formed an emulsion, a dispersion of gelatinous aggregates and a weak macrogel respectively [52].

In a 1 % v/v total monomer regime, stable dispersions formed up to 40 % ϕ_{TEOS}, while gelatinous aggregates formed with $\phi_{TEOS} >$ 40 % and no particles were visible when $\phi_{TEOS} > 0.6$ % as the formed oligomers were sufficiently soluble to prevent nucleation. The particles formed in this regime had similar hydrodynamic diameters to their MTES-derived analogues, but exhibited higher mobilities.

Nitrogen adsorption experiments made upon solid TEOS and MTES cross-linked material, with cross-linking volume fractions of 60 % in both cases, revealed a non-porous nature [52].

3.1.3 PDMS Dispersion Stability

PDMS droplet stability was long attributed solely to the presence of anionic groups at the O/W interface [33, 54, 51]. Hydrocarbon droplets, however, also exhibit negative charge when dispersed in aqueous media, derived from preferential adsorption of hydroxide ions at the interface: Zeta potentials (ζ) of 40 mV have been measured for *n*-heptane at 10^{-3} mol dm^{-3} NaCl at pH 7, while *n*-nonane and longer chained alkanes exhibited larger potentials [55]. Charge magnitude, both in cases of PDMS and hydrocarbons, is dependent upon pH and ionic strength. In contrast to the described PDMS systems, surfactant-free hydrocarbon droplets coalesce [48].

PDMS emulsions were formed from both distilled and unpurified (as received) monomers to assess any influence of impurity upon stability [48]; surface-active impurities have previ-

ously been observed in alkanes [56]. Little difference was observed between the two regimes, in fact the emulsions derived from purified monomer were slightly more stable to coalescence in the presence of 10^{-1} NaCl. The critical coagulation concentration (ccc) of NaCl with the emulsions was estimated to be between 10^{-1} and 10^{-2} mol dm^{-3}. Increases in droplet size caused a corresponding decrease in ccc as a consequence of increasing contact surface area. Upon isolation of the respective oil phases, no significant difference in surface tension was observed.

Comparison of measured mobilities, both for nucleated PDMS and various dispersed commercial PDMS oils, showed no significant difference, which suggests electrostatic repulsion does not solely account for the enhanced stability of the former case. All the examined PDMS oils had refractive indeces $\approx$ 1.4, suggesting similar Hamaker constants, which means stability can not be attributed to differing van der Waals attractions [48].

The enhanced stability may arise from the lower interfacial tension $\gamma_{O/W}$ exhibited by the nucleated PDMS and measured as 14.2 mN m^{-1}. Low interfacial tensions result in higher repulsive hydration forces. Methoxy-terminated PDMS $\gamma_{O/W}$ was 35.0 mN m^{-1}, while methyl terminated PDMS and n-heptane were 43.9 and 48.4 mN m^{-1} respectively. Hydroxy-terminated PDMS had a $\gamma_{O/W}$ value of 14.7 mN m^{-1}, which is similar to the synthesized PDMS. The difference in stability between the two forms may be attributed to the preferential interfacial adsorption of the linear groups in the latter case [48].

The formed low molecular weight PDMS exhibits surfactant properties. Absorption of n-heptane into PDMS droplets with minimum PDMS/heptane volume fractions of 0.25 yielded droplets that were resistant to coalescence. This was presumed to be a consequence of preferential PDMS adsorption at the O/W interface. Maximum packing of PDMS at the interface was determined to occur at a PDMS/heptane ϕ of 0.3, detected as a trend deviation in a $\gamma - \log(\phi)$ plot [48].

3.1.4 Silica Coated PDMS Microgels

Silica-shelled PDMS microgels have been prepared in a two step process developed by Goller [34]. Firstly the microgels were coated with a thin silica skin, precipitated from a

saturated silicate solution, and then subjected to Bogush seeded silica growth [57] to form thick shells. The seeded growth involves dispersing the microgel into an ethanol-ammonia solution, followed by slow addition of TEOS. Direct silica shell growth on the microgel is problematic because the Bogush process uses ethanol as a principle solvent, which dissolves the PDMS core. Goller demonstrated that the maximum survivable ethanol concentration for uncross-linked PDMS droplets is 40 % v/v. If the PDMS is formed from a 50-50 MTES-DMDES monomer mixture, the external ethanol concentration may be raised to 60 %. Increasing NH_3 concentration to 7.5 mol dm^{-3} allows silica to be successfully formed in 25 % ethanol [34]. Depending on both the extent of cross-linking and magnitude of the NH_3 concentration, a workable ethanol concentration in the range of 25 to 45 % was established.

Goller reported that to successfully shell the microgel it was first necessary to undertake the precipitation step from saturated sodium silicate solution. The suggested reason was that this layer prevented TEOS depletion by microgel absorption prior to shell formation. Given that solid shells have subsequently been grown on PDMS emulsions using mixtures of alkoxysilanes without this measure [35] (see Chapter 4), it seems more likely that the layer is required to render the microgel surface more compatible with silica growth.

Recently PDMS emulsions have been used as a core-material or template for various coated particles via shell growth [35] or particle adsorption [58, 59, 60, 61].

This chapter describes further investigation into the Goller method.

3.2 Experimental

3.2.1 PDMS Emulsion Synthesis

Emulsions were typically prepared in 1 % v/v NH_3 (0.181 mol dm^{-3}, from 35 wt%, Fisher) in deionized water. DMDES (97 %, Aldrich) and MTES (99 %, Aldrich) were purified with a neutral alumina column prior to use. The monomers (1 or 2 % v/v combined) were added to the basic solution and shaken for one minute, then aged for 24 hours. The dispersion was dialysed against deionized water, with 4 water changes per day, for two days.

3.2.2 Precipitation from Silicate Solution

DOWEX 50WX4-400 ion-exchange resin (Aldrich) was sequentially washed with hot water, 3N HCl (38 %, BDH) and distilled water. Sodium silicate solution (30 %, BDH) was diluted to 3 wt. % with water. The acid-washed resin was added in small quantities until the pH had dropped near to, but not below, 11 as determined by universal indicator paper. The silicate solution (100 ml) was pumped into a stirred PDMS microgel suspension (typically 230 ml, 1 vol. %) at a rate of 1 ml min^{-1} for 15 minutes and 0.5 ml min^{-1} thereafter. The pH was frequently measured with universal indicator paper and maintained in a range of 9.5–10 to enable silica precipitation. The suspension was left stirring for 12 hours and then dialysed against pure water with daily changes until the pH became constant.

3.2.3 Silica growth step

The dialysed dispersion (100 ml) was then added to a solution of ethanol (100 ml) and NH_3 (123 ml, 35 % solution, Fisher). TEOS (8 ml, 98 %, Aldrich) was then added at a rate of 1.2 ml hr^{-1}. The stirred dispersion was left for 12 hours and then dialysed.

3.3 Results and Discussion

The failure to shell low cross-linked microgels has been attributed to extensive swelling of the core material in the ethanolic conditions of the Stöber/Bogush process [34]. Microgel swelling as a function of ethanol concentration and extent of cross-linking had not been fully explored, so a series of microgels (0–70 % v/v MTES with respect to the total monomer volume fraction) were prepared. Maintaining constant microgel solution volume fractions of 40 %, water/ethanol mixtures were added to form a range of microgel solutions from 0–60 % ethanol. The microgel particle diameters were measured by PCS. Microgel size was monitored over several days in the cases of 0 and 30 % ethanol to ensure equilibrium had been reached; equilibrium was judged to have been achieved after one day in all cases. Each prepared ethanolic solution thereafter was left for at least this time prior to size measurement. Microgel particle volume was analysed as a function of cross-linker and ethanol

concentration (Figure 3.3).

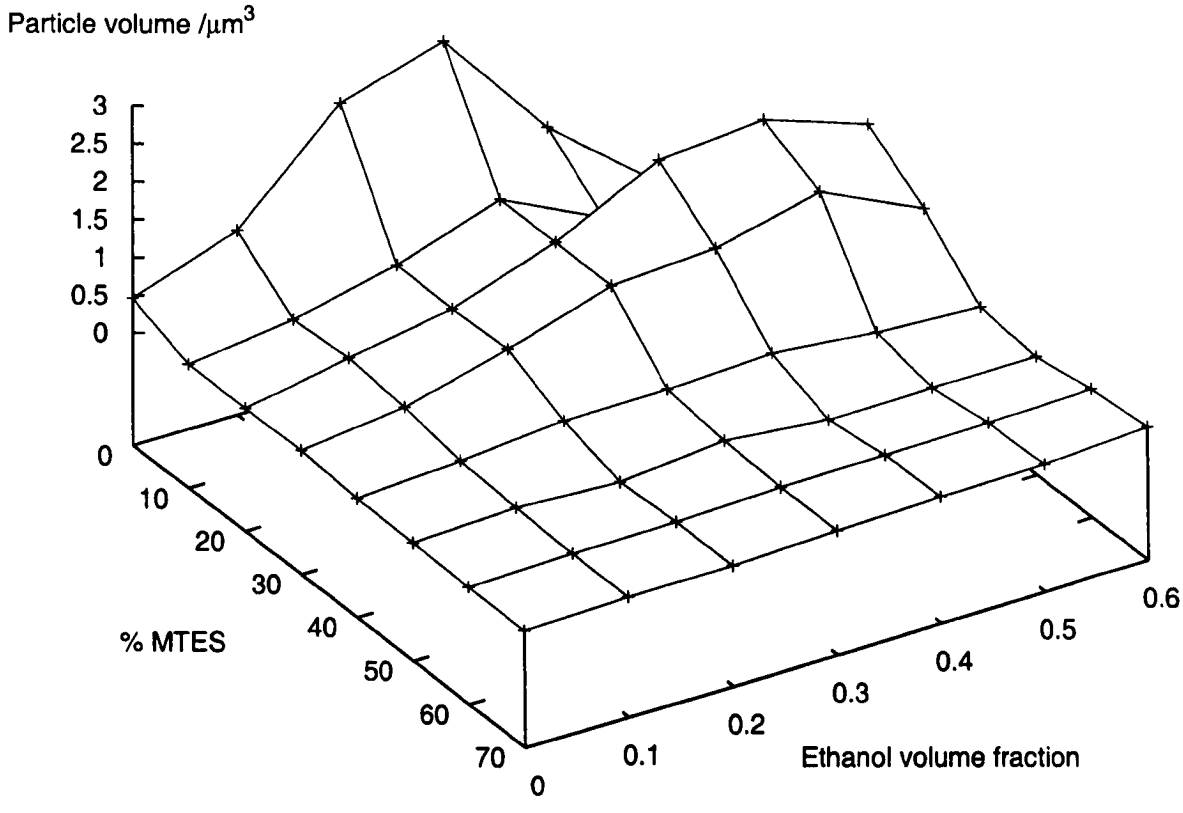

Figure 3.3: Effect of cross-linker and ethanol concentration on PDMS microgel volume

Extensive swelling was observed in 0–30 % microgels upon addition of ethanol. In the case of 0–10 % MTES a maximum size was reached at 30 % ethanol, thereafter the particle size decreased until after 40 % ethanol, at which point a single-phase system developed. In the cases of 20–30 % MTES a maximum size was achieved at 50 % ethanol. From 40–70 % MTES relatively little swelling was observed. The observation that successful core-shell particles could only be formed with MTES concentrations in excess of 60 % correlates with the swelling profiles exhibited by the microgels in ethanol. These data support the hypothesis that pronounced PDMS swelling by ethanol would occur in silica growth conditions, and may serve to disrupt the precipitated silicate layer and subsequent shell formation.

Decreasing particle size at higher ethanol concentrations may be attributed to dissolution of PDMS by the continuous phase; clearly, the swelling and solubilizing actions of ethanol are in competition at higher concentrations. The limited swelling observed in the 40+ %

MTES microgels is a consequence of the rigid nature of the formed microgel matrix. This behaviour has consequences for the use of such microgels for release of organic actives because the rigid structure may not be able to incorporate much material; also solubility of organic materials in PDMS decreases with increasing PDMS molecular weight [54].

Previously silica shells were grown upon PDMS microgel dispersions prepared from a 1 % total monomer volume fraction [34]. Initial experiments using dispersions derived from 2 % total monomer proved to be more successful, however, as the shelled particles were more numerous, discrete and less secondary material was produced (Figure 3.4). This improvement is probably a consequence of increasing the amount of interface available to the shelling process.

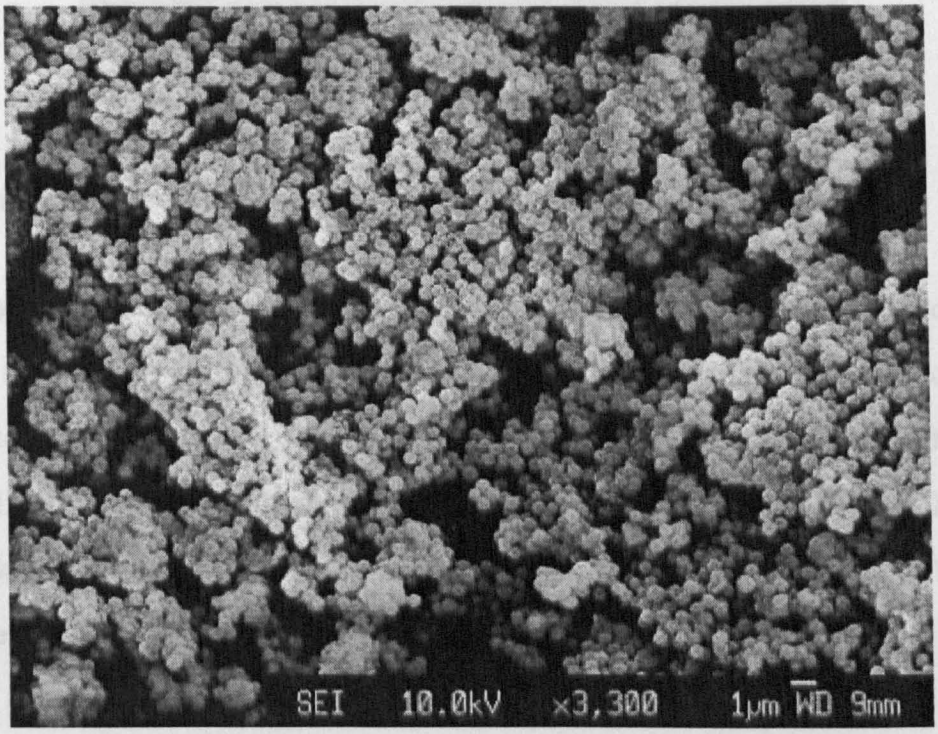

Figure 3.4: Silica-shelled microgel. The core material was a 60 % MTES-derived PDMS dispersion formed from 2 % v/v total monomer.

The swelling behaviour with ethanol related to MTES concentration, as depicted by Figure 3.3, suggested that microgels derived from MTES concentrations as low as 40 % may survive the ethanol concentration required by the shelling step. Indeed, microgels formed from both 50/50 and 40/60 MTES/DMDES were successfully shelled; Goller [34] had previously suggested that at least 60 % MTES is necessary. The particles were examined with SEM (Figure 3.5) and TEM using ultramicrotomy (Figure 3.6). Crushing the particles in a

pestle and mortar revealed broken shells under SEM (Figure 3.7). Using both techniques, the estimated shell thickness was 50–60 nm.

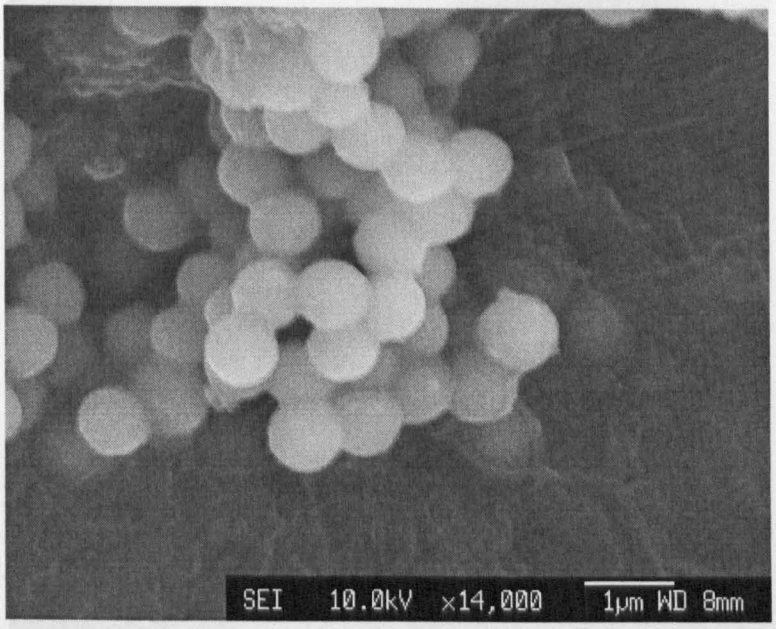

Figure 3.5: Silica-shelled PDMS particles. The core material was formed from 50 % MTES with a total monomer volume fraction of 2 % v/v.

Silica growth was attempted on skinned 30/70 MTES/DMDES. A cloudy solution formed and white flakes were observed. When examined under the optical microscope, silica-shelled resin particles were observed; these were smaller ion-exchange particles that had not been successfully separated from the dispersion (figure 3.8), but no shelled microgel particles were evident under SEM. The silica layer coating the resin particles proved to be brittle; they broke following gentle applied pressure on the slide cover-slip (figure 3.9).

3.3.1 Larger PDMS Microgels

The successfully shelled microgel particles had all been smaller than 1 μm in diameter. Larger particles may be formed under conditions of higher ionic strength, but at the expense of particle number density and available shelling interface. In an attempt to make larger particles, a range of dispersions with varying total monomer volume fractions and ratios were made. Although 5–10 % monomer yielded large droplets, dialysis caused separation into two phases: a creamed oil phase and solid sediment, which is consistent with the observations from previous work [52]. This is probably a consequence of different kinetics of hydrolysis

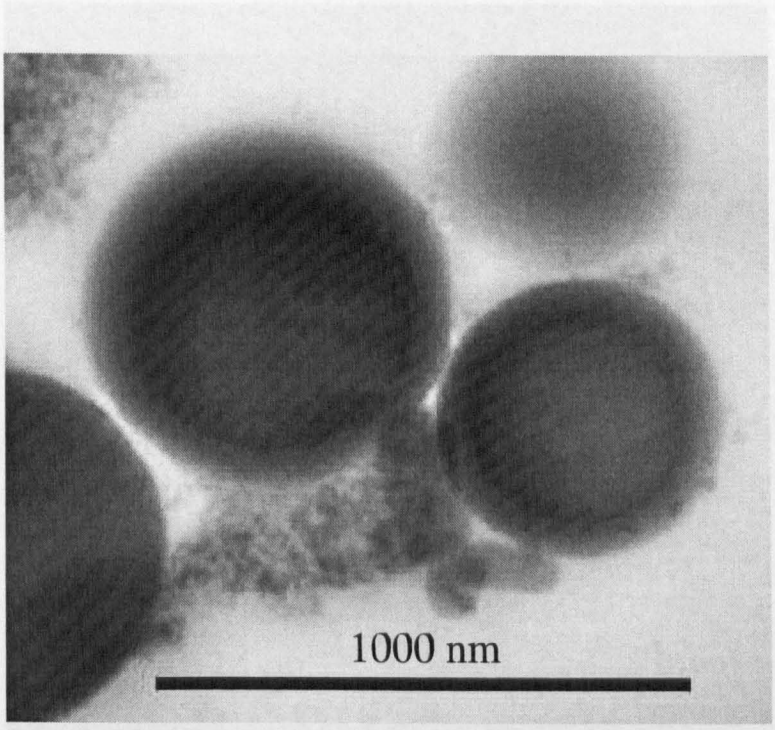

Figure 3.6: Silica-shelled microgel particle viewed with TEM following ultramicrotomy (shell thickness 50–60 nm)

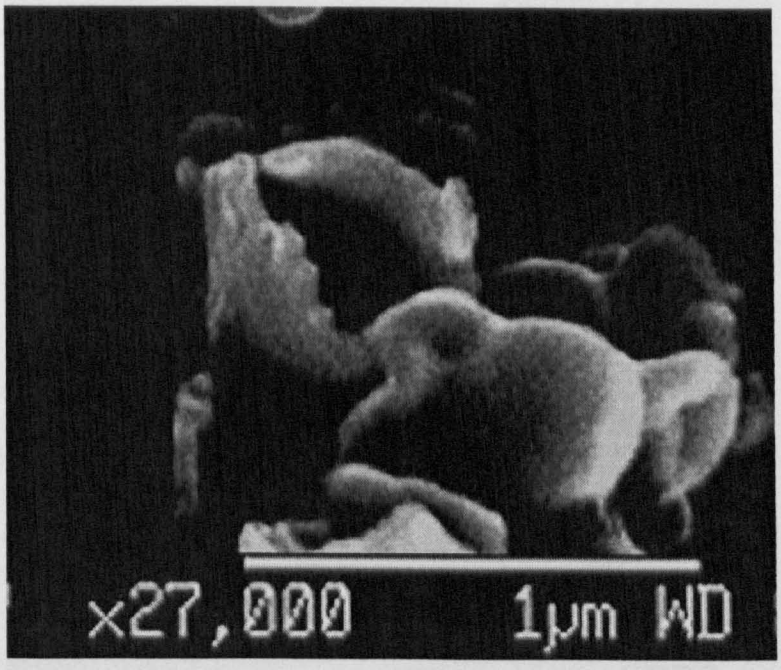

Figure 3.7: Broken silica-shell with absent core material (shell thickness 50–60 nm)

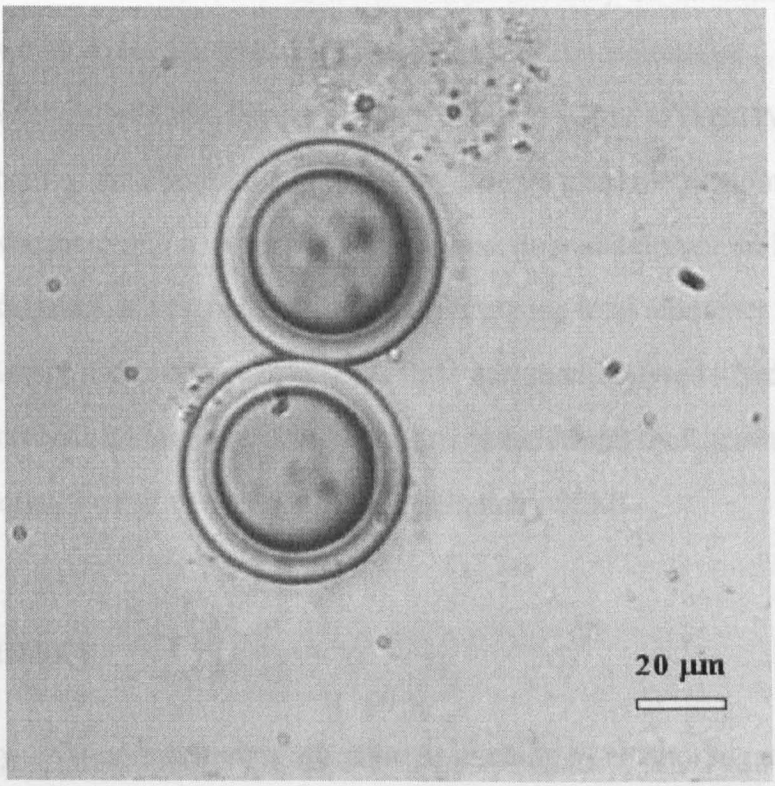

Figure 3.8: Optical micrograph of ion-exchange resin coated in silica

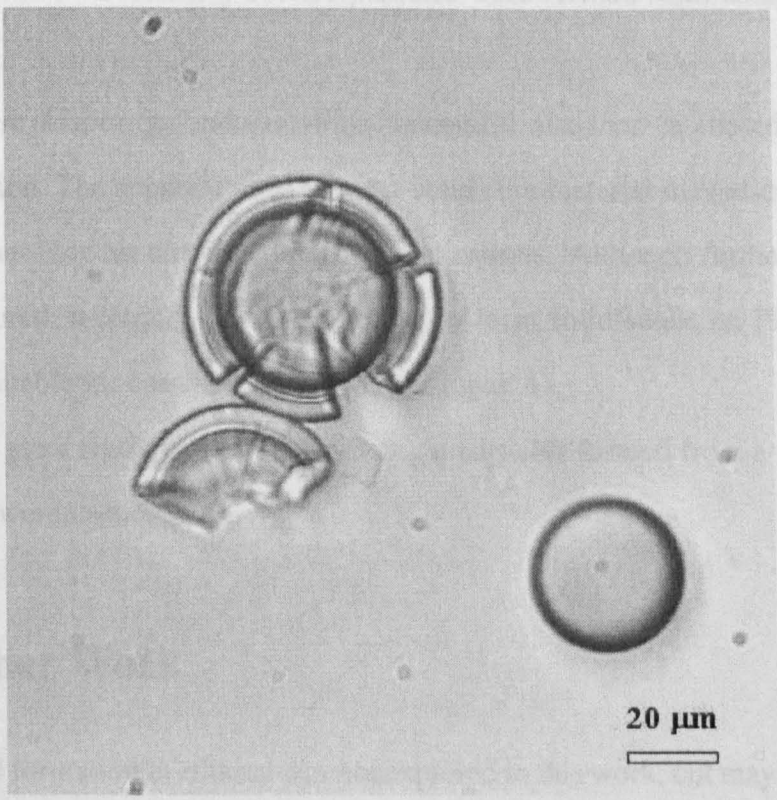

Figure 3.9: Ion-exchange resin particles with broken silica shells

and condensation for each monomer type; an effect that may be minimized at low total monomer concentration, but becomes significant at higher concentrations.

A PDMS seeded growth was then attempted. 1 vol. % 60/40 MTES/DMDES was used to make a microgel in the conventional way then, 6 hours after the monomer addition, the dispersion was decanted into a three-necked flask and slow addition of an MTES/DMDES mixture was undertaken at a rate of 0.8 ml hr^{-1} to bring the total monomer volume fraction to 6 %. The stirring dispersion was left overnight and then dialysed. Sedimentation was observed in the dialysis tubing. Following silica precipitation and shell growth, no successful silica-shelled particles were observed in this system under SEM.

3.4 Summary

Systematic study of the core materials' response to swelling by ethanol suggested that PDMS microgels derived from at least 40 % MTES cross-linker may be successfully shelled with silica by a Bogush-style method. The core material may be intermediate between a solid and a liquid, but the most successfuly shelled particles were formed from cores that tended to solid behaviour.

The procedure is laborious and not always successful, also there is limited opportunity for parallel production. The apparent need for near-solid core material may also restrict the usefulness of the particles for controlled release applications. Although further avenues could have been explored, a recently reported method to form solid shells on PDMS emulsions seemed more suitable for continued study [35] (Chapter 4).

Attempts to grow shells upon PDMS microgel particles formed from a two-step seeded growth method were unsuccessful.

3.5 Further Work

PDMS microgel formation in ethanol was not explored in this work, but may provide a useful core material. As detailed in Section 3.1.2, the nature of the formed microgel differs from that of microgels formed in absence of ethanol: a more swellable structure is formed. It is

possible that cores produced from such regimes may be more suitable for incorporation of active and subsequent shelling. It is important to establish if the microgel can be re-swollen with solvent following dilution-triggered collapse.

Further work into producing larger microgel particles is also of interest. The effects of a combined increase in ammonia and total monomer concentration has not been explored, and initial studies with uncross-linked PDMS suggest this may be a promising method (Chapter 4).

Use of an alternative initial precursor coating, rather than that precipitated from sodium silicate, could be considered. Silica shells have been grown upon solid particles, such as gold, using adsorbed poly(vinylpyrrolidone) to render the surface compatible for the Stöber process [62]. An adsorbed polymer layer may be less disrupted by any swelling of the PDMS core material in the ethanolic conditions required for silica growth, which may allow shell formation with less cross-linked templates.

The issue of surface compatibility with the Bogush silica growth warrants further consideration. It is likely that the silicate precipitation step creates a compatible surface, however it has not been established if this step would be successful if the microgel was first swollen with a solvent, such as ethanol or n-heptane. If silica can be precipitated onto a pre-swollen microgel, then use of 20 or 30 % MTES-derived PDMS dispersions may be explored. More significantly, if pre-swollen cores were unaffected by ethanol during the silica growth step, the Goller particles could have potential as a core-shell technology.

It is expected that shell thickness could be tuned using this method by varying the quantity of TEOS added in the shell growth step.

Chapter 4

Silica-Silicone Shelled PDMS

4.1 Introduction

Composite silicone-silica shells have recently been grown upon PDMS oil droplets [35, 36, 63]. PDMS oil droplets were prepared by the Obey-Vincent method [33], but not dialysed. They were then allowed to age 24, 48 or 72 hours before TEOS (0.018 mol dm^{-3}) was added with stirring. The TEOS undergoes condensation with hydrolysed DMDES or oligomers thereof to form a solid, yet elastic shell. 24 hour-old PDMS yielded the thickest shells, while 72 hour-old PDMS gave the thinnest. The shells were porous enough to allow dissolution of the oil core with ethanol.

Shell thickness was determined by first measuring the template droplet diameter by static light scattering (SLS) and then that of the particle diameter post-shelling. Systematic studies showed the shell thickness to be independent of TEOS concentration. Instead, DMDES concentration was attributed to be the predominant factor controlling shell thickness.

Upon drying three distinct particle morphologies were observed [35] that were related to the ratio of shell thickness to particle radius, h/R [36, 63]. Particles that remained spherical upon drying and TEM inspection were designated microspheres, and had $h/R > 0.23$. Particles occurring within the $0.23 > h/R > 0.05$ range presented a hemispherical morphology and were named as microcapsules. If $h/R < 0.05$, a collapsed and folded morphology was observed and described as a microballoon. Particle deformation was attributed to loss of core material upon drying [36]; the PDMS oligomers are known to be volatile [54].

Energy dispersive X-ray spectroscopy (EDX) of a range of Zoldesi particles that had been washed with ethanol to remove the PDMS core, revealed that the shells' Si/O ratio remained constant across the series, but the Si/C ratio declined with decreasing shell thickness signifying a lessening contribution from DMDES to the shell material.

^{29}Si Solid state NMR was also used to examine the ethanol-washed particles. The strongest contribution to the spectrum was identified as a cyclic tetramer that consisted of DMDES-derived units and one or more TEOS-derived unit (Figure 4.1). A strong Q_4 peak, corresponding to Si centres bound to four other Si atoms through siloxane bonds, was also present in the spectrum with a small Q_3 shoulder. These peaks represent contributions from TEOS residues alone and are found in silica particles [64]. As such, the shell material may be described as a TEOS cross-linked silica-silicone network. Shell density, as determined by sedimentation experiments in ethanol, was found to range from ~870–1050 kg m^3.

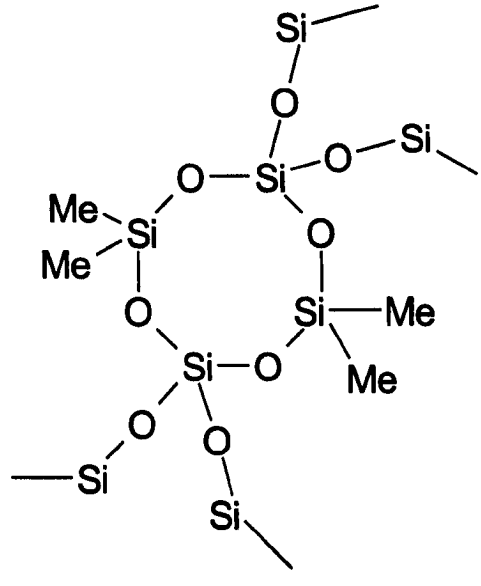

Figure 4.1: An example tetramer: a principal shell component, derived from DMDES and TEOS residues, as determined by solid state ^{29}Si NMR.

Dissolution of the core PDMS oil with ethanol demonstrated the shells' permeability to small molecules [35]. In addition ethanol-washed hollow particles were observed to uptake fluorescein-isothiocyanate from an ethanol solution and retain the dye for $\approx$ 2 minutes following solvent exchange with clean ethanol. This demonstrated the presence of pores with diameters of at least 1.1 nm in the shell [36, 63].

PDMS formation in the presence of surfactant leads to formation of smaller droplets by

enhancing the rate of solubilization of DMDES upon initial mixing, thereby increasing the number of nucleation centres [65]. Zoldesi and co-workers investigated the use of SDS, CTAB and Triton X in both PDMS and shell formation [63]. Cationic CTAB did reduce droplet size, but lead to increased polydispersity. SDS reduced emulsion size without substantial influence on size distribution, but thick shells could not be formed in the presence of the surfactant. Attempted Stöber silica growth on these SDS-stabilized particles lead to formation of a rough silica shell layer together with secondary nucleation. Shell growth on the Triton X stabilized particles was successful, and thick shells were observed.

The method developed by Zoldesi, and outlined above, provides core-shell particles of narrow size distribution whose shell thickness may be simply varied. The work presented in this chapter involves modifying the method to disconnect the shelling step from the core formation step, thereby providing scope for incorporation of active materials into the core by absorption. Different methods for altering shell thickness were also investigated, together with effects of varying the constituent shell monomers. A final aim was to consistently produce particles, of varying shell thicknesses, that were larger than 1 μm for analysis of mechanical strength by micromanipulation as this technique relies on optical microscopy.

4.2 Experimental

4.2.1 PDMS Emulsions

Emulsions were typically prepared in 1 or 2 % v/v dilutions of NH_3 (0.181 or 0.362 mol dm^{-3}, 35 wt%, Fisher) in deionized water. DMDES (97 %, Aldrich) was added to NH_3 solution in a 30 ml glass vial, and shaken with a Gallenkamp Spinmix at maximum setting for 1 minute.

4.2.2 Zoldesi Method

PDMS emulsions were formed and aged for a predetermined time before drop-wise addition of TEOS (0.018 mol dm^{-3}, 98 %, Aldrich) while stirred with a magnetic follower. Stirring continued for an hour, then the magnetic followers were removed and the dispersions left to stand for three days.

4.2.3 Secondary DMDES Method

PDMS emulsions were formed and aged for four days, with occasional agitation to prevent formation of a creamed phase if necessary. DMDES (0.023 mol dm^{-3}) and TEOS (0.018 mol dm^{-3}) were then added drop-wise to the emulsions with magnetic stirring, which was continued subsequently for an hour before removal of the follower. The dispersions were left to stand for three days.

4.2.4 Purification

Particle suspensions were diluted with INUTEC SP1 (donated by Orafti Non-Food), to form 0.1 wt. % solutions with respect to the surfactant, and were centrifuged three times at 500 g RCF in a Sorvall Legend T with removal of supernatant and washings with 0.1 wt. % surfactant solution. The particles were then stored in the INUTEC SP1 solution.

4.2.5 Microtomy

For purposes of microtomy, samples were centrifuged into ethanol three times. The sediment was scraped into microtome vials (Agar Scientific) and dried at 60 °C. Spurr's low-viscosity resin was prepared [66]: ERL 4206 (5.0 g, Agar Scientific), polypropylene glycol diglycidyl ether (3.0 g, DER 736, Agar Scientific), nonenyl succinic anhydride (13.0 g, NSA, Agar Scientific) and dimethylaminoethanol (0.2 g) were combined to form the liquid resin, which was added to the dried vials. The resin was then cured at 60 °C for 12 hours. The particles remained as sediment throughout the polymerization.

The resin blocks were sliced with a Diatome Ultra 45 diamond knife mounted on a MT-XL microtome (Ventana Medical Systems, USA). The resin stubs were retained, splutter-coated with palladium-platinum alloy, and examined with SEM.

4.3 The Zoldesi Method: Shell Thickness Controlled by the Time of TEOS Addition

4.3.1 System Purification

The successfully shelled systems all sediment, but with time the sediment becomes increasingly difficult to redisperse and solid residue forms, presumably due to the presence of residual monomer and NH_3. Zoldesi and co-workers typically centrifuged the particles into ethanol to remove the core material [35, 36, 63], a step that also removed coagulating agents. An alternative cleaning step was necessary to retain the PDMS core. Dispersions were centrifuged at 500 g RCF and washed with deionized water. The sediment formed in both cases could not be redispersed, even under sonication. Particle stabilization was therefore necessary for successful centrifugation.

INUTEC SP1 (Orafti Non-Food, Belgium), a hydrophobized inulin-derived polymeric surfactant, was then examined as a potential stabilizer. Inulin is a polysaccharide derived from chicory [67]. The surfactant concentration was fixed at 0.5 wt. % throughout a series of centrifugation experiments; this concentration is sufficient to stabilize 50/50 v/v O/W emulsions [68]. The particles were mixed with inulin solution and centrifuged at 300 g. The supernatant was extracted and three successive wash and centrifugation cycles were undertaken with successful redispersion on each occassion with 10 seconds of sonification.

Various inulin concentrations were then used to stabilize shelled PDMS systems. The lowest concentration tried, 0.1 wt. %, successfully stabilized the particles and that concentration was used in all subsequent purification proceedures.

Inulin-based surfactants have previously been shown to stabilize O/W emulsions and particles with lower surfactant concentrations than poly(ethylene oxide)-based surfactants [68, 69]. The surfactant stabilizes emulsions in high electrolyte concentrations (> 2 mol dm^{-3} NaCl or > 1 mol dm^{-3} $MgSO_4$) and at high temperature (50 °C), due to persistent hydration of fructose chains [68]. Experiments with INUTEC SP1 and polystyrene latices have shown the critical coagulation concentration of $CaCl_2$ to rise from 0.007 mol dm^{-3} to 4.3 mol dm^{-3} in the presence of 0.25 wt. % inulin surfactant [70].

4.3.2 Shelled Zoldesi Particles

Zoldesi particles were formed in conditions of 1 % NH_3, as described in Section 4.2.2, with TEOS addition delay times ranging from 25–96 hours. All delay times yielded particles. Bulk material was observed with the shortest delay time; discrete particles were observed in solution, but had thinner shells than expected (Figure 4.2). Thicker shells were evident with successive delay times (Figures 4.3 and 4.4). Under conditions of 2 % v/v DMDES and NH_3, particles were successfully formed without over-production of secondary material (Figure 4.5).

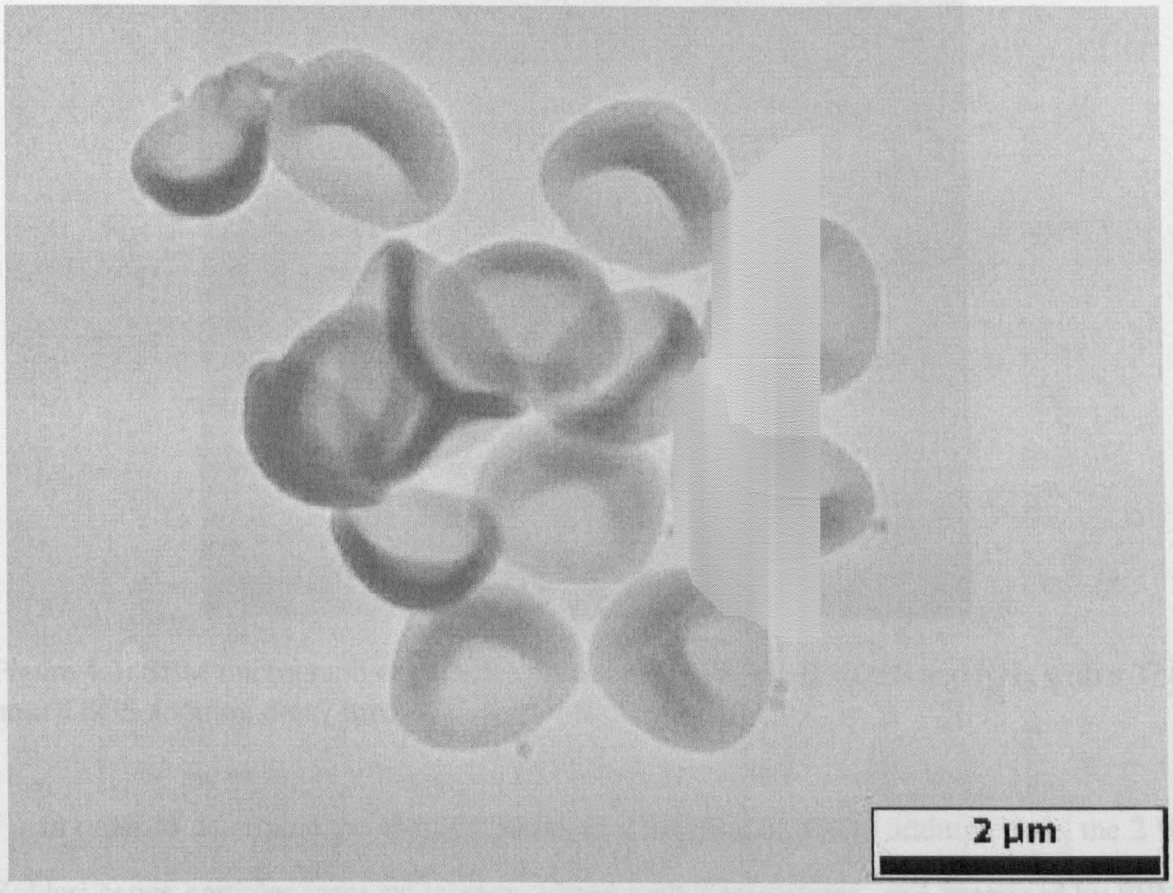

Figure 4.2: A TEM micrograph of Zoldesi particles produced from 1 % v/v DMDES and NH_3 with a TEOS addition delay time of 25 hours. The shells are thinner than expected, giving rise to a collapsed morphology, due to the production of secondary material. Small secondary particles are also present. The scale bar represents 2000 nm.

Image analysis of the micrographs using ImageJ [71] shows the particle size to remain roughly constant across the 1 % Zoldesi series and to show a slightly declining correlation in the 2 % series with TEOS addition delay time (Figure 4.6). All the particles had a collapsed hemispherical morphology, with the exception of the 25 hour 1 % class, which exhibited a

folded morpholgy consistent with a lower h/R, and as such the SEM measurements, based on chord lengths, may represent a slight overestimate of particle size. The standard deviation of the measurements (typically n =100 for each class) was less than 10 % in the 27–48 hour classes for the 1 % series and 24–44 hour classes in the 2 %. Longer addition time delays caused increases in polydispersity, which may be a consequence of creaming by the PDMS emulsion prior to shelling. Attempts to measure particle size with PCS were unsuccessful due to the presence of secondary material produced in the shelling step. The byproduct also remained in the dispersion following repeated centrifugation and washing.

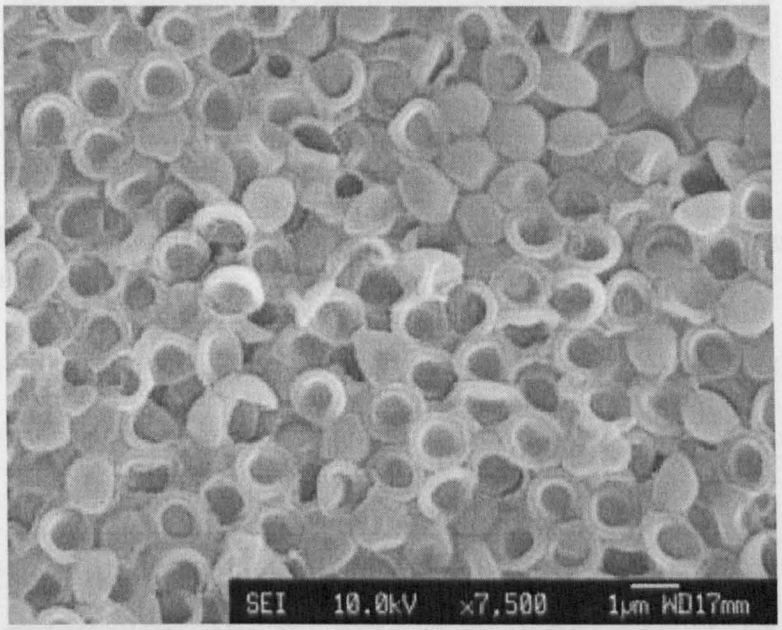

Figure 4.3: SEM micrograph of particles produced in 1 % v/v DMDES and NH_3 with a $27\frac{1}{2}$ hour TEOS addition delay time.

In order to determine the shell thickness as a function of TEOS addition time, the 2 % Zoldesi series particles were set in resin, sliced with a microtome, and examined by SEM (see Section 4.2.5). The shell thickness could then be directly measured from the micrographs. The resin was observed to have filled the particles (Figure 4.7). Some particles were observed to remain hollow (Figures 4.8 and 4.9). Apparent hollow particles were only observed in resin-set microtomed particles with shells of thickness 68 nm or less; the thicker shells were all resin filled. Zoldesi's EDX analysis had found a declining Si/C ratio with increasing TEOS addition delay time, while the Si/O ratio remained constant. It is possible, therefore, that the shells become denser, more glass-like and less permeable with increasing

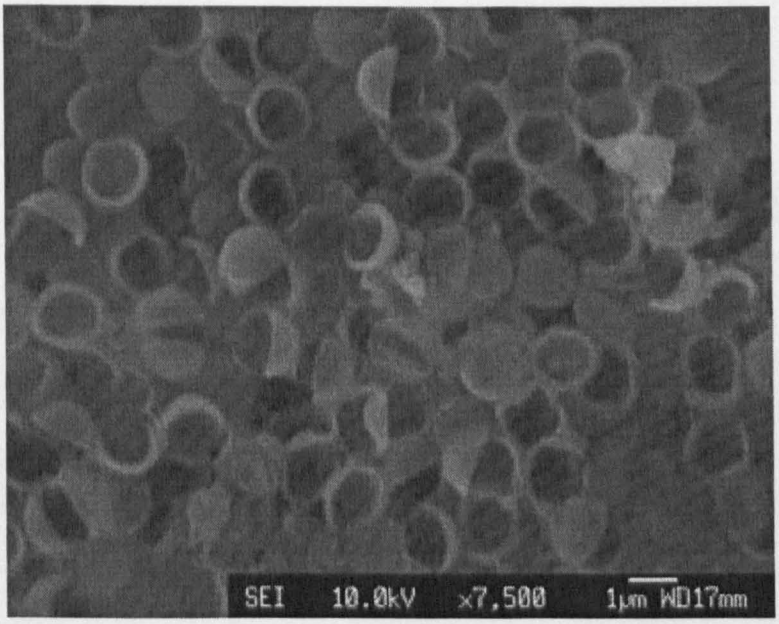

Figure 4.4: Zoldesi Method particles produced from 1 % v/v DMDES and NH_3 with a 48 hour TEOS addition delay time.

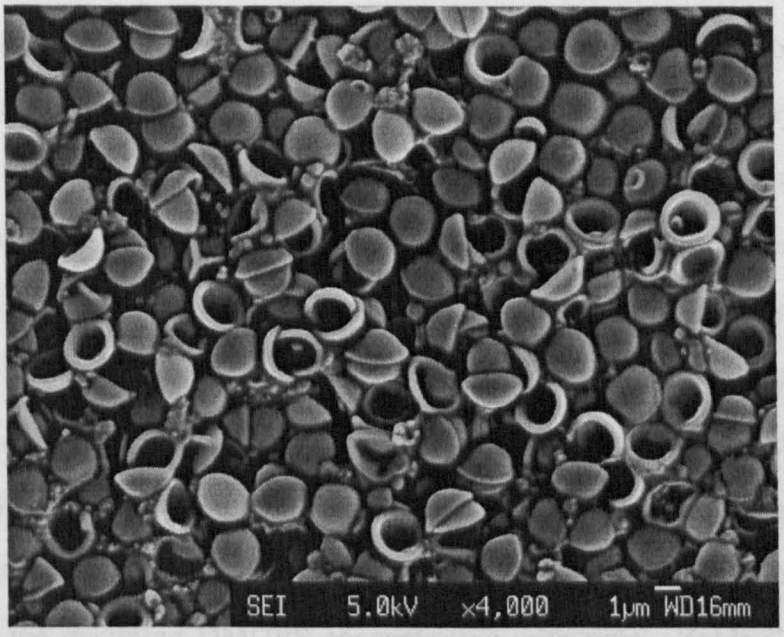

Figure 4.5: Zoldesi Method particles produced under conditions of 2 % v/v DMDES and NH_3 with a TEOS addition delay time of 24 hours.

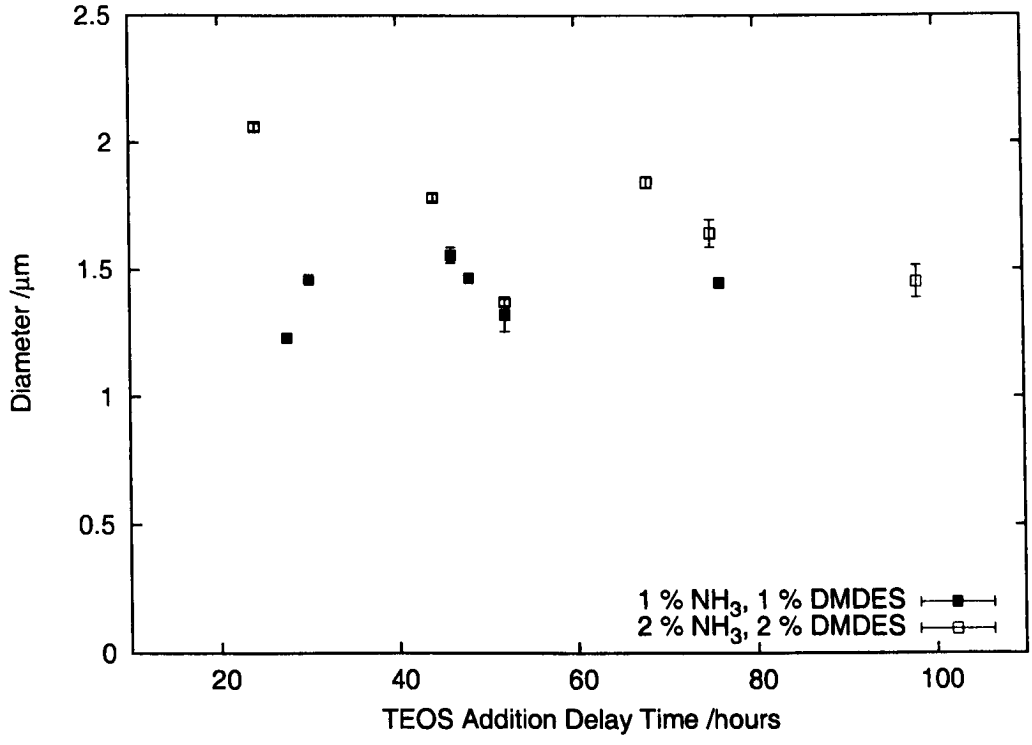

Figure 4.6: Particle size as a function of TEOS addition delay time.

delay times. Filled particles were however also observed in all cases (Figure 4.10) and the possiblity that the resin core had been displaced during microtomy should not be ignored.

Zoldesi's solution ^{29}Si NMR study showed that the DMDES monomer had been completely consumed after 96 hours, though a small quantity of doubly hydrolysed monomer was detected [63]. The microtomy results demonstrate that thin shells may still be grown after this time. Zoldesi had coalesced the 96 hour-old PDMS by centrifugation and then passed the derived oil through molecular sieves prior to NMR analysis, and it is therefore possible that some of the DMDES residue that could contribute to shell formation was lost to this process, leading to an overestimate of the extent of DMDES consumption.

Microtomy-determined shell thickness is plotted as a function of TEOS addition delay time in Figure 4.11. The presence of the shell does not explain the declining trend in overall particle size with TEOS addition delay time in the 2 % series. The size trend effectively correlates with the declining DMDES concentration with time. Zoldesi's EDX analysis showed the Si/C carbon ratio to decline with TEOS addition time, corresponding to a declining DMDES contribution to the shell material. It is possible that shells formed in conditions of ample DMDES are softer and more deformable, further exagerating the micrograph-based

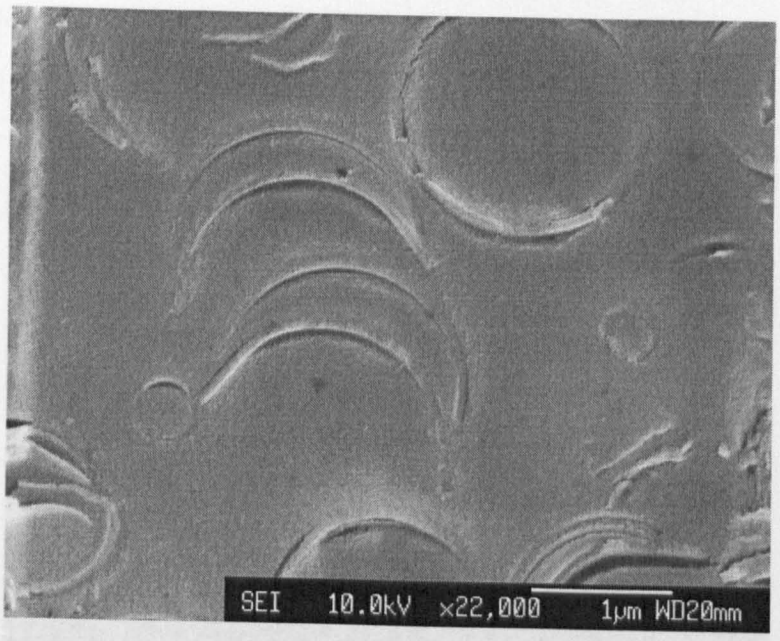

Figure 4.7: SEM micrograph of 2 % v/v DMDES and NH_3 derived Zoldesi particles formed with a 44 hour TEOS addition delay time. The resin has filled the particles. From a series of micrographs for this class, the shell thickness was estimated to be 84 nm with a standard deviation of 7 %.

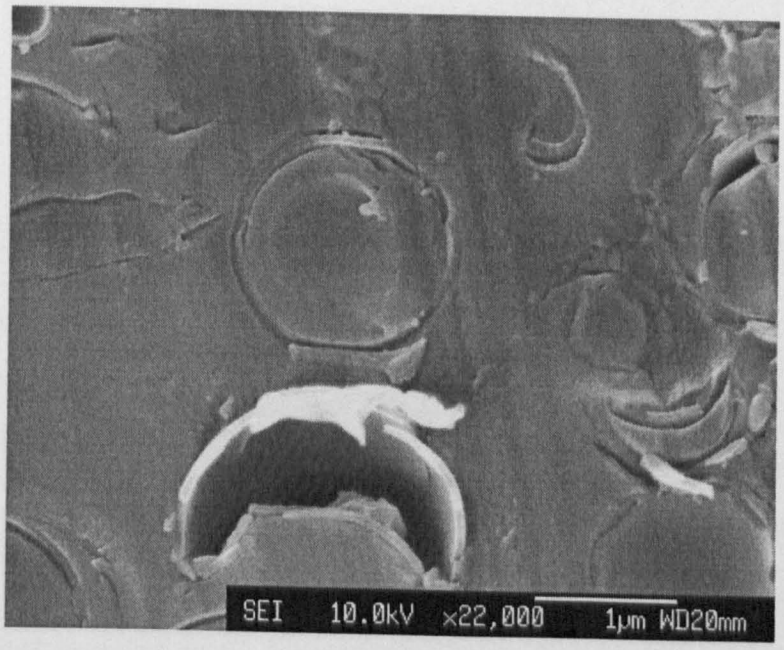

Figure 4.8: SEM micrograph of 2 % v/v DMDES and NH_3 Zoldesi particles formed with a TEOS addition delay time of 68 hours. The mean shell thickness was 68 nm with a standard deviation of 12 %.

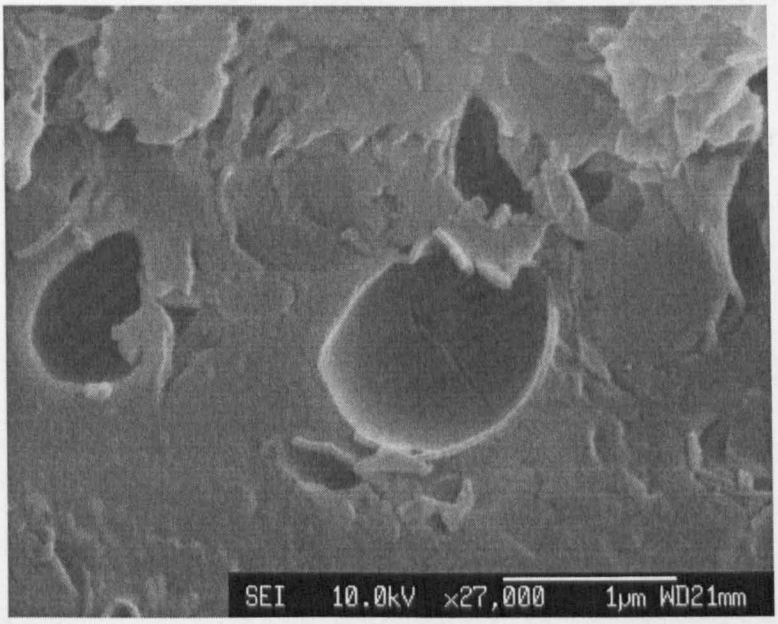

Figure 4.9: SEM micrograph of the 2 % Zoldesi class formed with a TEOS addition delay of 98 hours. The shell thickness was estimated to be 38 nm with a standard deviation of 5 %.

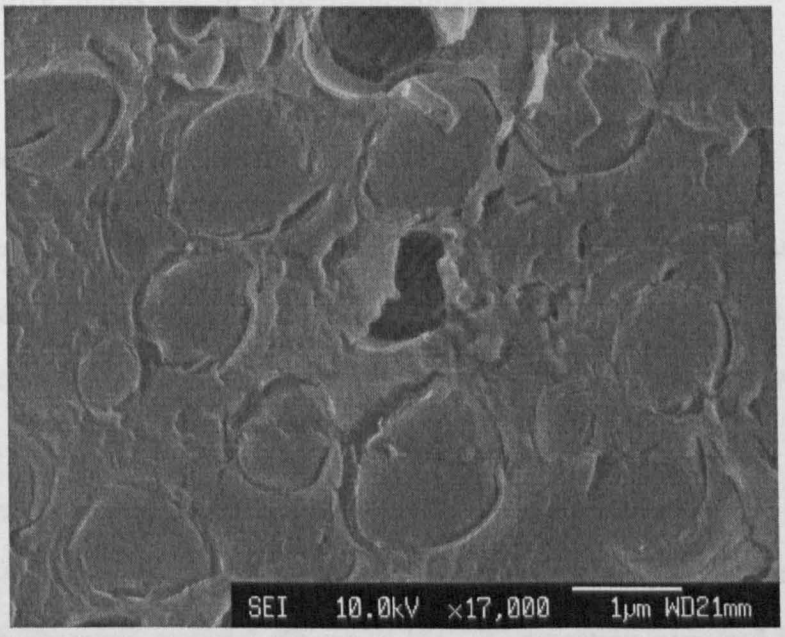

Figure 4.10: A further micrograph of the 98 hour 2 % Zoldesi class. Note the presence of both apparent hollow and filled particles.

size measurements. If TEOS absorption was responsible for the particle swelling, the opposite trend in particle size would be expected as, assuming the particle number density to remain constant, more PDMS interface is available with increasing time.

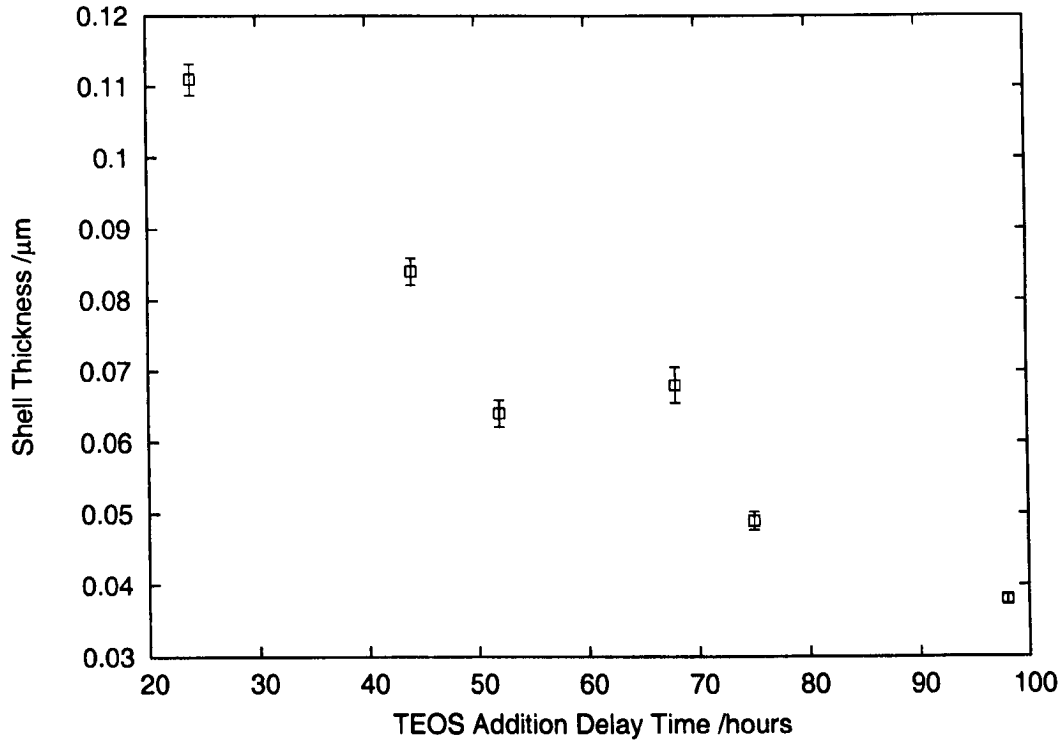

Figure 4.11: Shell thickness as a function of TEOS addition delay time. Error bars represent ± the standard error in this and all subsequent graphs.

Shell Growth on 6 Hour-old PDMS

1 and 2 % aqueous DMDES solutions in 1 % NH_3 were prepared and matured for 6 hours. It was hoped, with a shorter maturation time, more DMDES residue would be available for the shell formation to yield thicker shells. Attempts to follow the reaction with PCS proved unsuccessful as secondary material was produced.

SEM showed whole spherical particles for the 1 % system (Figure 4.13). Particles were present in the 2 % system, but these were embedded in an amorphous structure that accounted for most of the observed material (Figure 4.14). Aggregation occurred in both systems. The marked difference in observed structure between the two experiments may suggest a threshold DMDES residue concentration during the shelling step; above this concentration a bulk solid, in addition and detriment to shell material, is formed upon addition of TEOS.

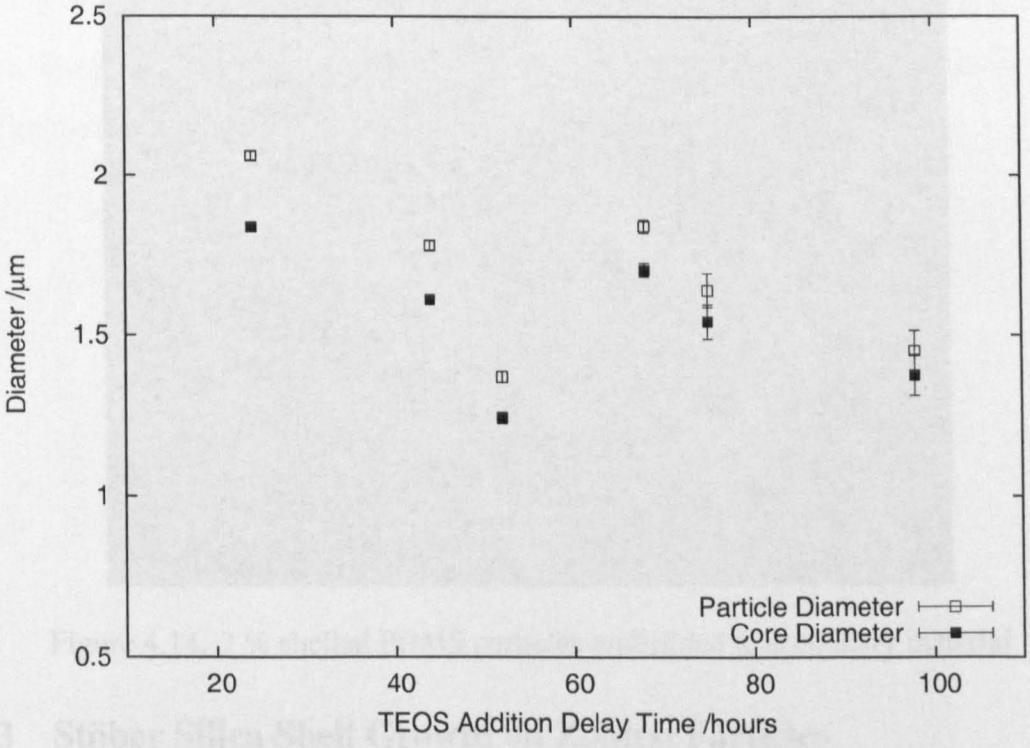

Figure 4.12: Particle and core diameters as a function of TEOS addition time

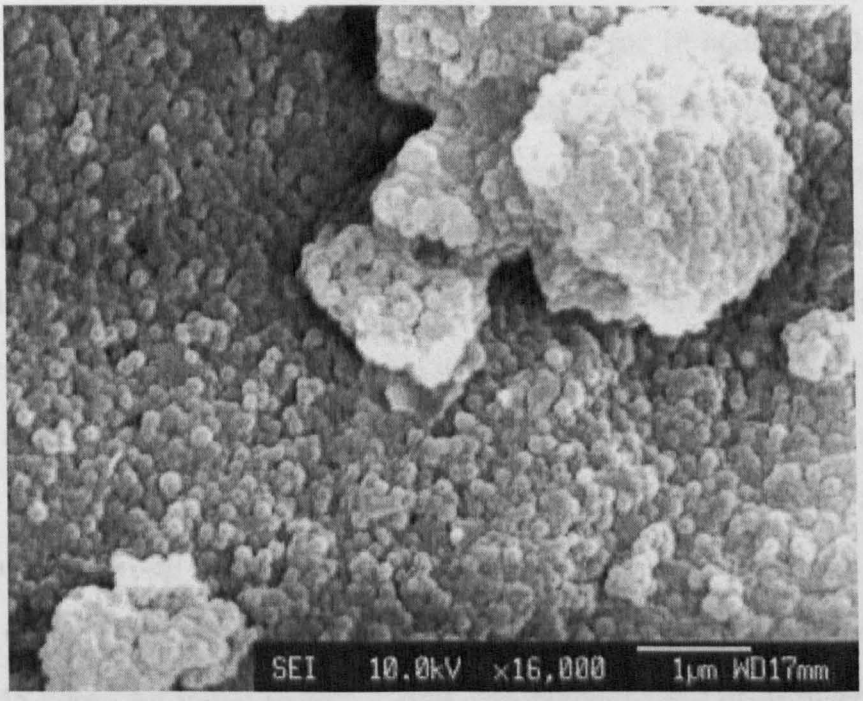

Figure 4.13: Silica-shelled PDMS from 1 % 6 hour-old core material

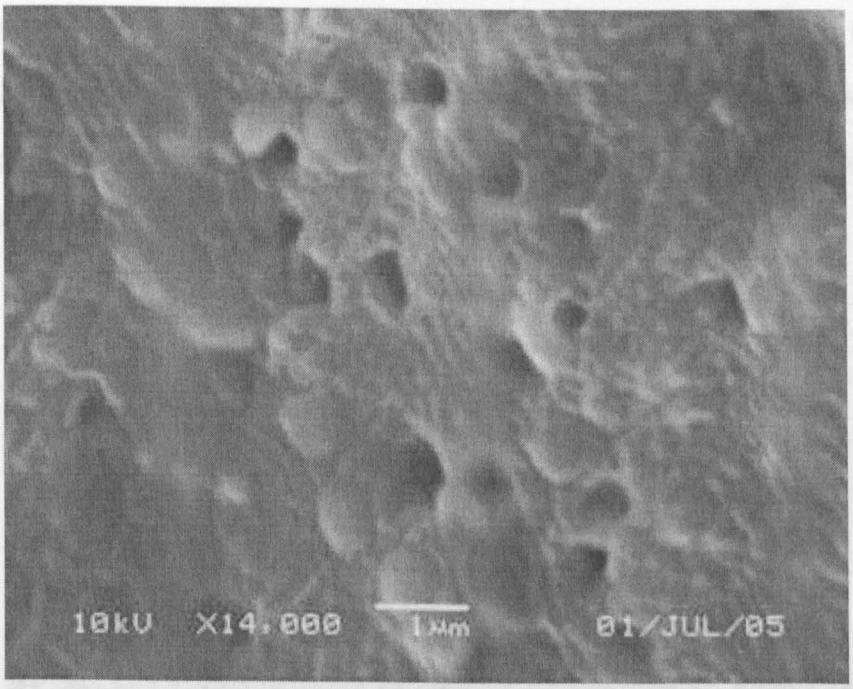

Figure 4.14: 2 % shelled PDMS particles embedded in secondary material

4.3.3 Stöber Silica Shell Growth on Zoldesi Particles

SEM micrographs reveal the shell material to be flexible. With the intention of forming a more rigid silica layer on the shell surface, shelled particles were subjected to a variation of the Stöber procedure described in Section 3.2.3.

A 2 wt. % PDMS oil emulsion was prepared, and left for 18 hours. TEOS (0.018 M) was added and the mixture stirred for two days. The resulting dispersion was split into two portions: the first was centrifuged into ethanol to remove the PDMS oil core and the second was subjected to Stöber growth. Initial centrifugation into ethanol yielded a frothy creamed layer and sediment, the former was probably a consequence of PDMS removal from the core. Following further centrifugation and washing with ethanol, only the sediment remained.

The unwashed particle dispersion (100 ml) was mixed with ethanol (100 ml) and NH_3 (123 ml, 7.6 M). TEOS (15 ml) was added at 1.2 ml hr^{-1}. This process was also repeated with the ethanol-dissolved hollow system.

The aim of these experiments was to further grow the formed shell both with and without the PDMS core. An initial shelled system was produced and centrifuged and washed with ethanol, which presented collapsed particles (Figures 4.15 and 4.16) when examined by SEM. The shell thicknesses estimated from these images were 75–100 nm.

Stöber growth on silica shells with PDMS cores was attempted. Both broken (Figure 4.17) and complete particles (Figure 4.18) were observed with SEM following this procedure. The particles appeared to be more rigid than in the previous system. From the broken particles, however, the shell thickness seemed similar.

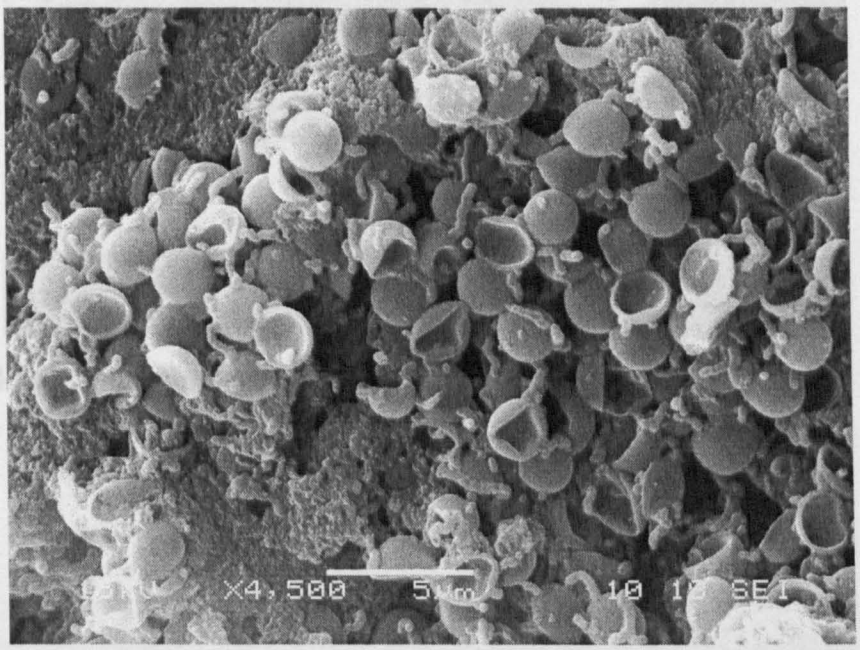

Figure 4.15: Hollow silica shells whose cores were dissolved with ethanol; note collapsed particles

Attempted silica shell growth on hollow cores yielded secondary silica because less water was present (Figure 4.19). Secondary material was also present in the other systems, but did not take a spherical form. The silica layer grown on the particles themselves formed an amorphous structure. It is possible that there was insufficient seed particle density for viable shell growth.

Attempted Stöber growth on PDMS containing core-shell systems will probably cause further PDMS extrusion into the continuous phase due to the presence of ethanol at a concentration that causes significant swelling in unshelled PDMS systems (see Section 3.3).

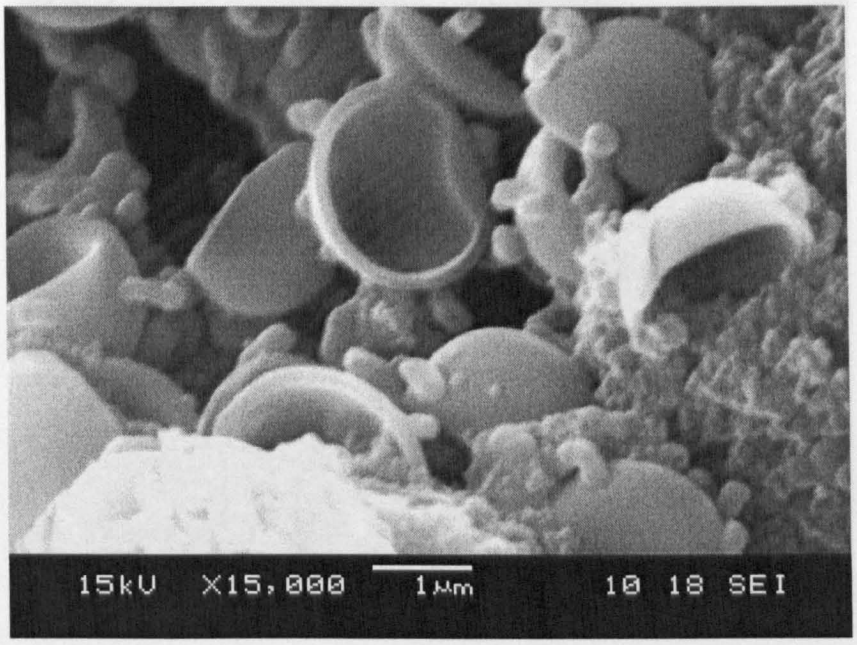

Figure 4.16: Hollow broken silica shells whose cores were dissolved with ethanol

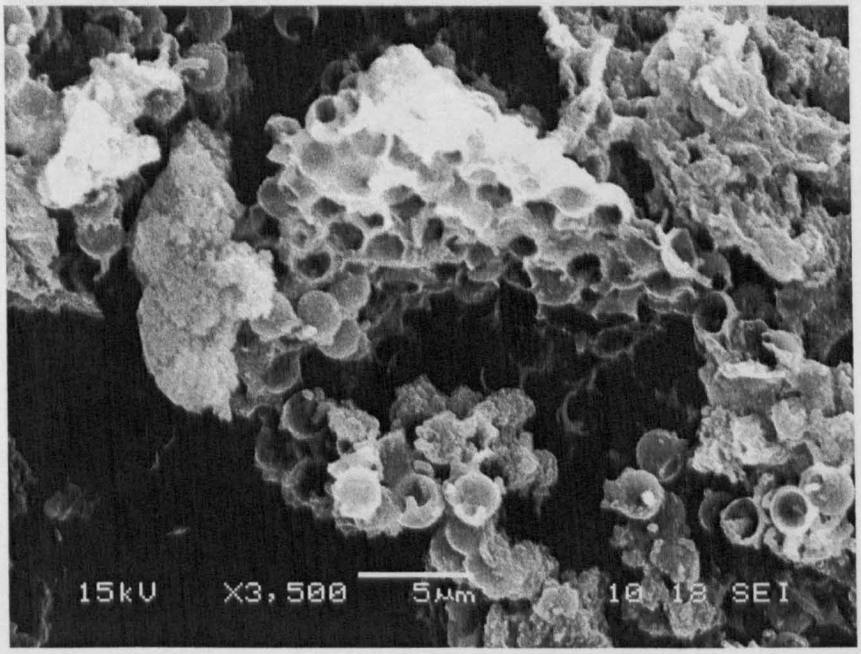

Figure 4.17: Stöber growth on silica shelled PDMS

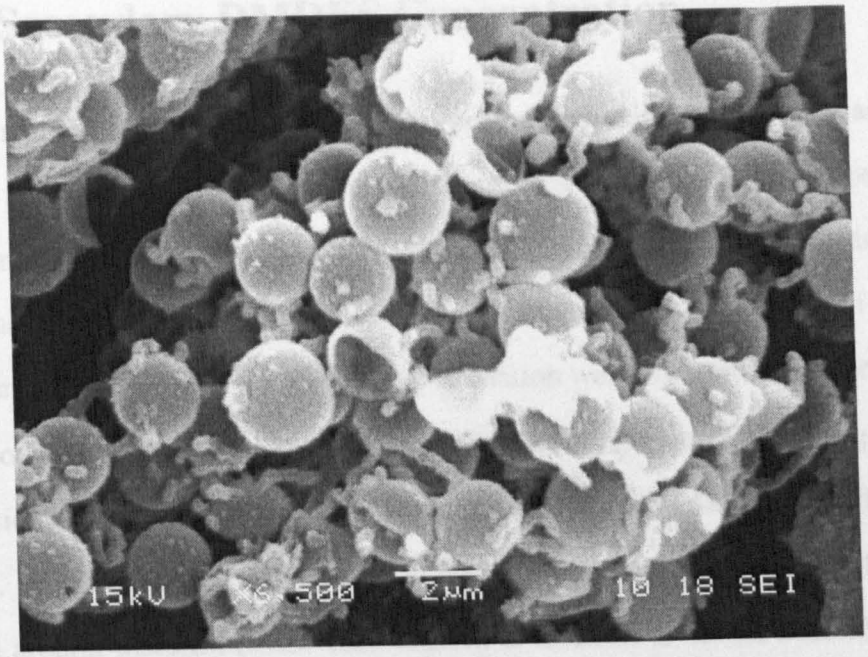

Figure 4.18: Stöber growth on silica shelled PDMS; note uncollapsed whole particles

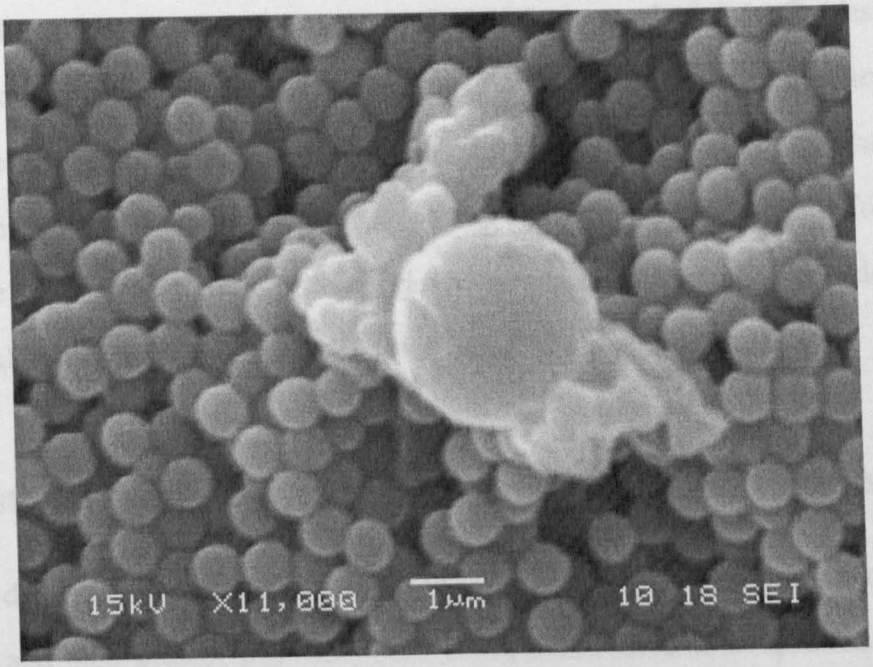

Figure 4.19: Attempted Stöber growth on hollow silica shells; note sub-micron secondary silica

4.4 Secondary DMDES Method: Shell Thickness Controlled by Secondary DMDES Concentration

The Zoldesi method forms core-shell particles with narrow size distributions and provides an avenue to control shell thickness. The shell formation, however, is time dependent upon the core formation step for provision of shell material, and as such provides little scope to incorporate active into the core prior to shelling. A modified form of the Zoldesi method was developed, and is presented here, whose shell formation was independent of core formation.

In the modified method, PDMS emulsions are allowed to mature, depleting the aqueous DMDES residue concentration, thereafter a secondary volume of DMDES is added together with TEOS. In effect the environment experienced by freshly prepared PDMS emulsions is recreated around mature PDMS. This method is referred to as the Secondary DMDES method hereafter. The secondary addition allows direct quantifiable study of the effect of DMDES and TEOS concentrations, and their respective ratios, on shell thickness. The method also allows use of alternative alkoxysilane shell monomers and, because the shelling step is discrete from core formation, provides scope for incorporation of actives.

A key difference between the Secondary DMDES approach and the Zoldesi Method is that, in the former case, the shell formation is independent of the core formation. Across a Zoldesi series the core diameter will vary, while it should remain constant in the Secondary DMDES series. If the shell formation occurs at the same rate as the emulsion formation, the final particle size across a Zoldesi series may be constant, whereas the Secondary DMDES method would yield particles whose diameter could vary with shell thickness.

4.4.1 Estimation of Appropriate Secondary DMDES Concentration

In order to determine a suitable secondary DMDES concentration, PDMS emulsions were formulated and their growth was monitored with photon correlation spectroscopy, PCS, at 25 °C (Figure 4.20). PDMS growth has previously been fitted by a variation of Equation 4.4.1 [36, 63], where d_t is droplet diameter as a function of time t, d_f is the final droplet diameter and $1/t_1$ is a fitting parameter.

$$d_t^3 = d_f^3 \left[1 - \exp\left(-\frac{t}{t_1}\right)\right] \tag{4.4.1}$$

If the reaction is assumed to go to completion, the depletion of DMDES may be predicted by Equation 4.4.2, in which V_t is monomer volume as a function of time and V_0 is the initial DMDES volume:

$$V_t = V_0 \left[\exp\left(-\frac{t}{t_1}\right)\right] \tag{4.4.2}$$

Equation 4.4.1 was fitted to the PDMS PCS data by non-linear least square analysis using R [72] to determine t_1 (Table 4.1). Substitution of volume by concentration in Equation 4.4.2, with use of the determined t_1 values from Table 4.1, allows the DMDES concentration as a function of time, M_t, to be estimated:

$$M_t = M_0 \left[\exp\left(-\frac{t}{t_1}\right)\right] \tag{4.4.3}$$

Table 4.1: Determined t_1 values from fits of Equation 4.4.1 to PCS measurements (Figure 4.20)

v/v NH_3 /%	v/v DMDES /%	t_1 /hours	V_t/V_f /%
1	1	39.2 ± 3	54 ± 4
1	2	14.6 ± 1.7	19 ± 2
2	2	15.0 ± 3.7	20 ± 5

The PDMS droplets prepared in 1 % v/v NH_3 had similar final droplet sizes, irrespective of the DMDES concentration, while the emulsion prepared with 2 % NH_3 consisted of larger droplets. This may be explained by the mechanism of droplet formation, which is thought to be analagous to that of Stöber silica formation [33]. In the Stöber process the reaction proceeds at a steady state as the reaction is limited by the first-order hydrolysis of TEOS [26]. Condensation of the hydrolysed monomer leads to formation of silica substructures that aggregate until there is sufficient surface charge to stabilize the nascent particle, which is determined by the ionic strength. Particle growth then continues by surface condensation of monomers or small oligomers. The number of nucleation centres relates to the monomer concentration, while the final particle size is determined by the ionic strength. Under conditions of 1 % NH_3, the 1 % and 2 % DMDES-derived PDMS droplet sizes are

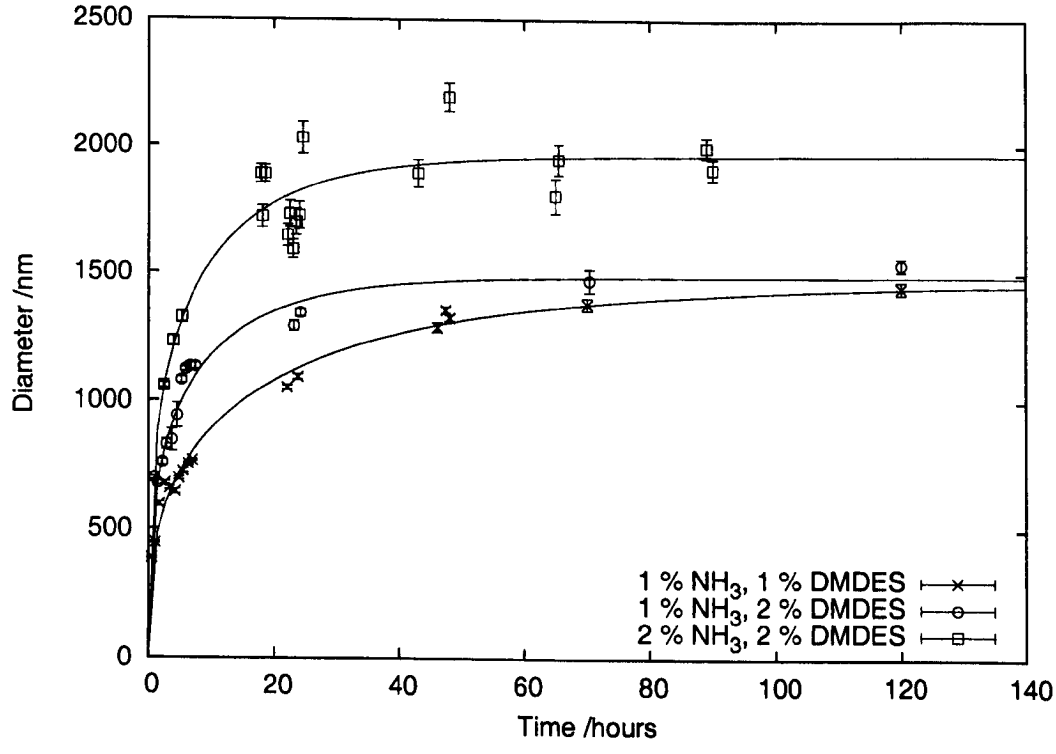

Figure 4.20: PDMS droplet diameter as a function of time. Equation 4.4.1 is fitted to the data.

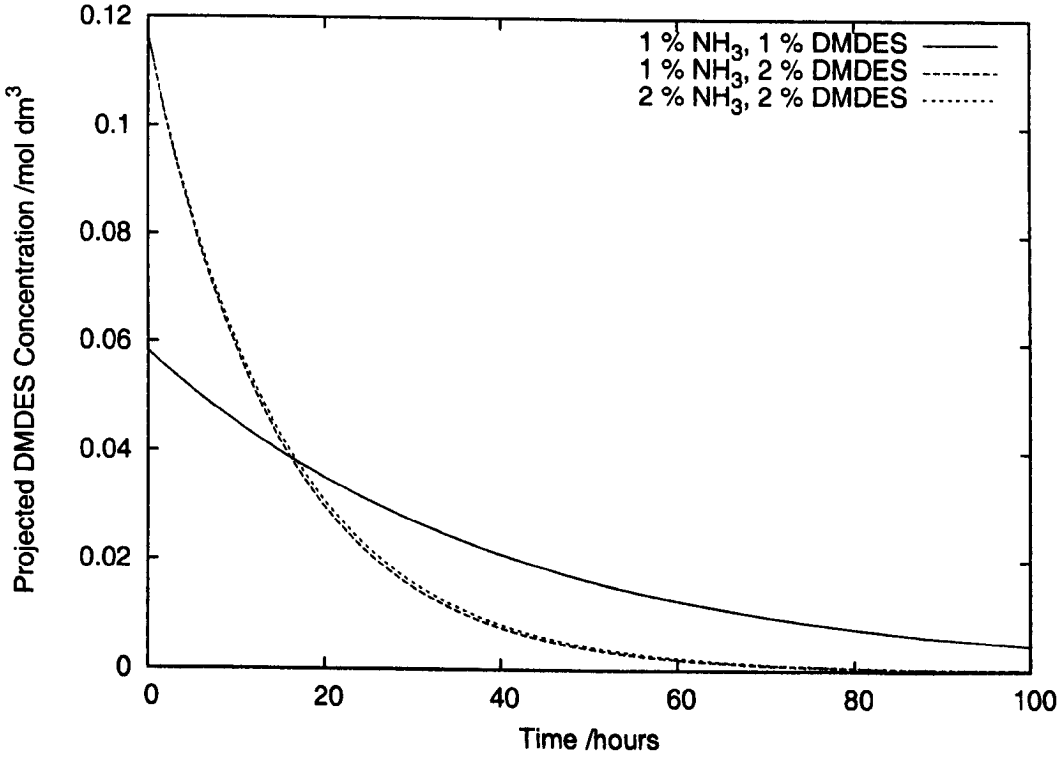

Figure 4.21: Projected DMDES Concentration during PDMS formation as a function of time

similar, despite the twofold increase in monomer concentration, because the droplet number density is increased rather than size.

Zoldesi determined t_1, using static light scattering data, for 1 % NH_3 and 1 % DMDES to be 45 ± 4.5 hours and 27 ± 2 for 2–6 % DMDES in corresponding NH_3 volume fractions, but did not determine t_1 for 2 % DMDES in 1 % NH_3 [63]. The 1 % DMDES/1 % NH_3 t_1 data is in reasonable agreement with the earlier work, however, the 2 %/2 % value is significantly smaller. Zoldesi reported final droplet sizes that are about 50 % smaller than those here determined in equivalent concentration regimes. Zoldesi reportedly used DMDES as revieved without further purification, while in this study the DMDES was passed through a neutral alumina column prior to use, which may contribute to the difference. t_1 may also be influenced by ambient temperature.

The 2 % DMDES and NH_3 derived PDMS PCS data is more scattered than the other regimes in Figure 4.20, however the determined t_1 values for both 2 % DMDES regimes are significantly similar. If $1/t_1$ is regarded as a rate constant, PDMS formation from 1 % DMDES in 1 % NH_3 seems to exhibit different kinetics from the other examined regimes.

The change in the constant relates to the DMDES concentration rather than that of the NH_3. DMDES concentration is most likely to affect the rate of hydrolysis and nucleation number density. Higher DMDES concentrations lead to formation of more surface area, which in turn increases the rate constant.

The aim of the PDMS study was to determine the unreacted DMDES concentration that is present 24 hours after PDMS growth was initiated. TEOS addition to this time regime tended to produce thickest shells with the Zoldesi method, and as such this concentration could be considered as an ideal starting secondary concentration. Inspection of the predicted DMDES concentration in Figure 4.21 indicated DMDES concentrations in the region of 0.02 mol dm^{-3} to be suitable for a 2 % regime. This concentration is almost equimolar with the TEOS addition. Less secondary material was produced in 1 % Zoldesi particles with TEOS addition times after ≈ 27 hours, which suggests use of 0.02–0.03 mol dm^{-3} DMDES for the 1 % regime.

4.4.2 Shell Growth on Mature PDMS

1 % and 2 % PDMS were prepared and allowed to mature for 11 days. A 1 % DMDES solution in 1 % NH_3 was made and added to an equivalent volume of 1 % PDMS, giving 0.5 % concentration of PDMS and DMDES at the start of the shelling process. The mixture was stirred continuously for three days. After this time a solid material had deposited on the stirrer, but the solution was clear. The process was repeated with 2 % PDMS, but stirring was only undertaken for the first hour following combination of core and shell solutions, whereafter the magnetic stirrer was removed. Successful core shell particles were observed with SEM. The dispersion sedimented. Aggregates then formed that could not be dispersed with sonication; no surfactant was added to prevent coagulation. SEM showed whole particles, indicating the shelling step was successful; some broken particles were also present (Figure 4.22). This method effectively disconnects the shelling step from the core synthesis.

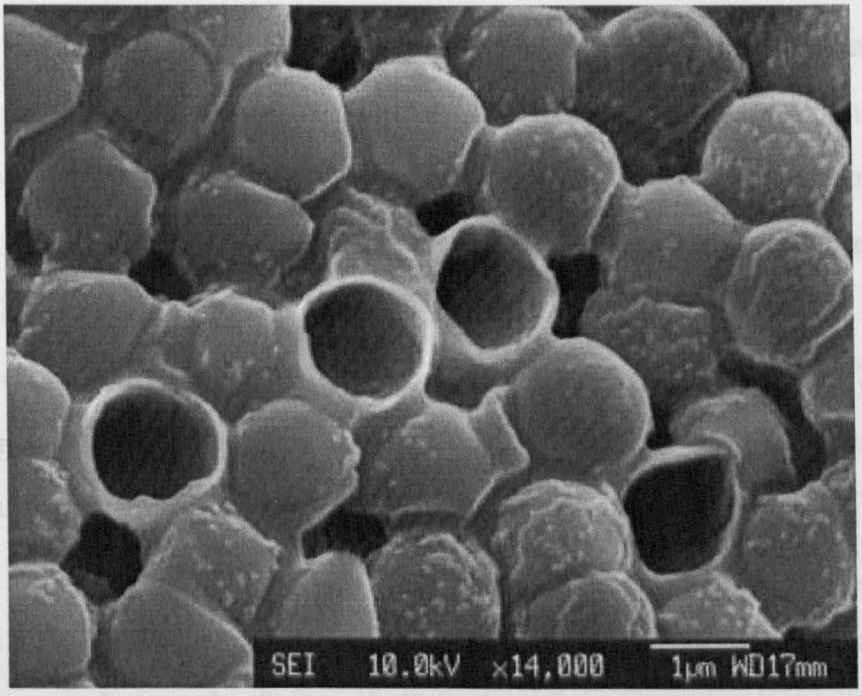

Figure 4.22: Shell growth on 11 day-old PDMS

Secondary DMDES systems were initially made by combining equal volumes of mature PDMS dispersions with freshly combined DMDES-ammoniacal solutions, which effectively halved the particle number density. Several of these systems were observed to aggregate during the shelling process. Calculation of the secondary DMDES concentration to estimated surface area ratios (see Page 62) showed successfully shelled systems were formed with

total monomer quantities of 6.5 mmol dm^{-3} m^{-2} or less. Aggregation was observed in systems with estimated ratios in excess of 7.0 mmol $dm^{-3}m^{-2}$. Direct addition of secondary DMDES and TEOS to the PDMS dispersion, without further dilution, allow shells to be formed at higher concentrations. The thickest observed shells were formed with DMDES concentrations of 15.3 mmol dm^{-3} m^{-2}.

Maturation times of 11 days, however, subject the maturing PDMS emulsions to creaming and coalescence. In order to reduce these factors a typical maturation time of 100 hours was adopted. Successful shells had been formed in this study following a delay time of 96 hours using the Zoldesi method, and there may still be a small contribution to shell growth from core-forming DMDES after 100 hours.

4.4.3 Control of Shell Thickness

Experiments were undertaken to vary the secondary addition DMDES concentration across a series of matured PDMS emulsions; this would directly determine the influence of this species upon shell thickness. The emulsions had been left to mature for 4 days. With increasing secondary DMDES concentration, increased shell thickness was observed in both the 1 % and 2 % regimes.

Hemispherical morphologies were prevalent in the 1 % regime (Figures 4.23 and 4.24). This morphology allows an estimate of the shell thickness, because the distance δ, as illustrated in Figure 4.25, could approximate to twice the shell thickness.

These δ values are plotted together with two microtomy measurements, which were made for the 1 % series (Figure 4.26), for comparrison (Figure 4.27). The microtomy measurements were made upon the thickest shells in the 1 % series, and correspond to $\approx$70 % of the value predicted by the δ measurement. Nevertheless, the δ values illustrate the increasing trend in shell thickness with secondary DMDES concentration.

Secondary DMDES Method particles produced in the 2 % v/v DMDES and NH_3 regime generally exhibited spherical uncollapsed morphologies for secondary DMDES concentrations in the range of 0.0058–0.0233 mol dm^{-3} (Figures 4.28 and 4.29). Above this concentration, however, collapsed hemispherical morphologies were observed (Figure 4.30). The

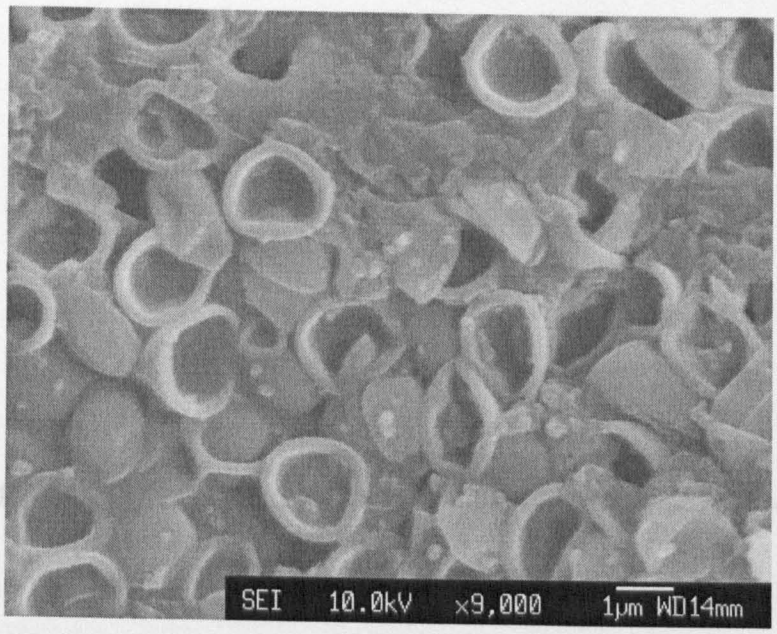

Figure 4.23: Shells formed by the Secondary DMDES method in the 1 % v/v DMDES and NH_3 series. The secondary DMDES concentration was 0.0175 mol dm^{-3}.

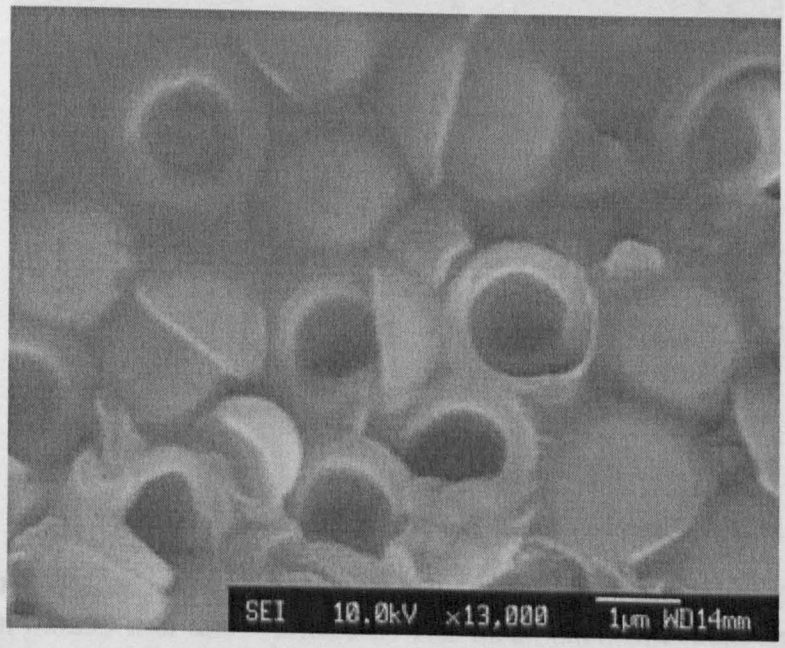

Figure 4.24: Thicker shells were produced, in the 1 % series, with a secondary DMDES concentration of 0.0233 mol $dm^{-}3$.

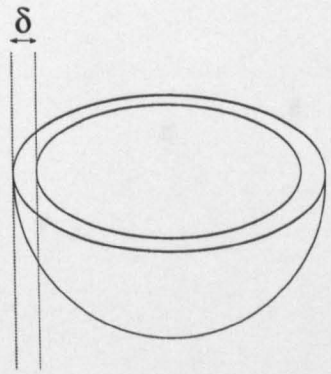

Figure 4.25: The δ estimate measurement on a collapsed particle

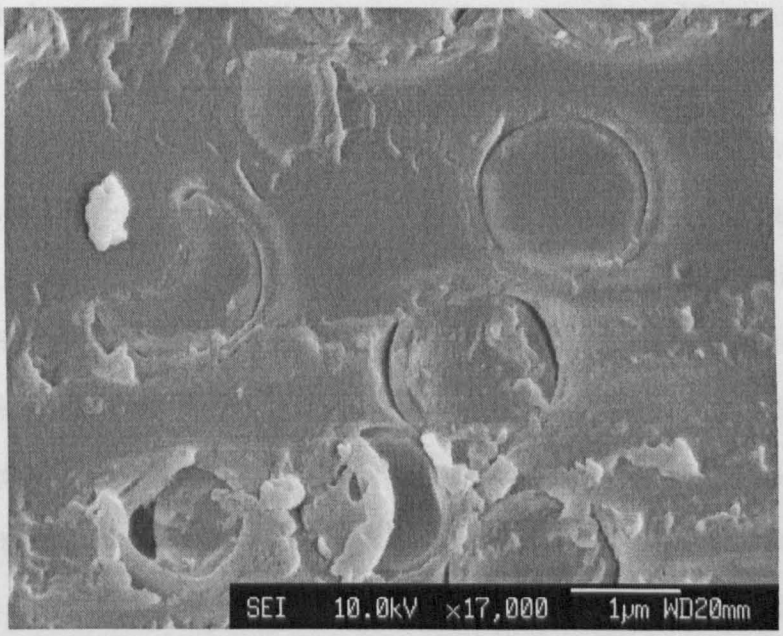

Figure 4.26: An SEM micrograph of microtomed 1 % Secondary DMDES particles with shells formed in 0.0233 mol dm^{-3} DMDES. The mean shell thickness for this class was determined as 113 nm with a standard deviation of 6 %.

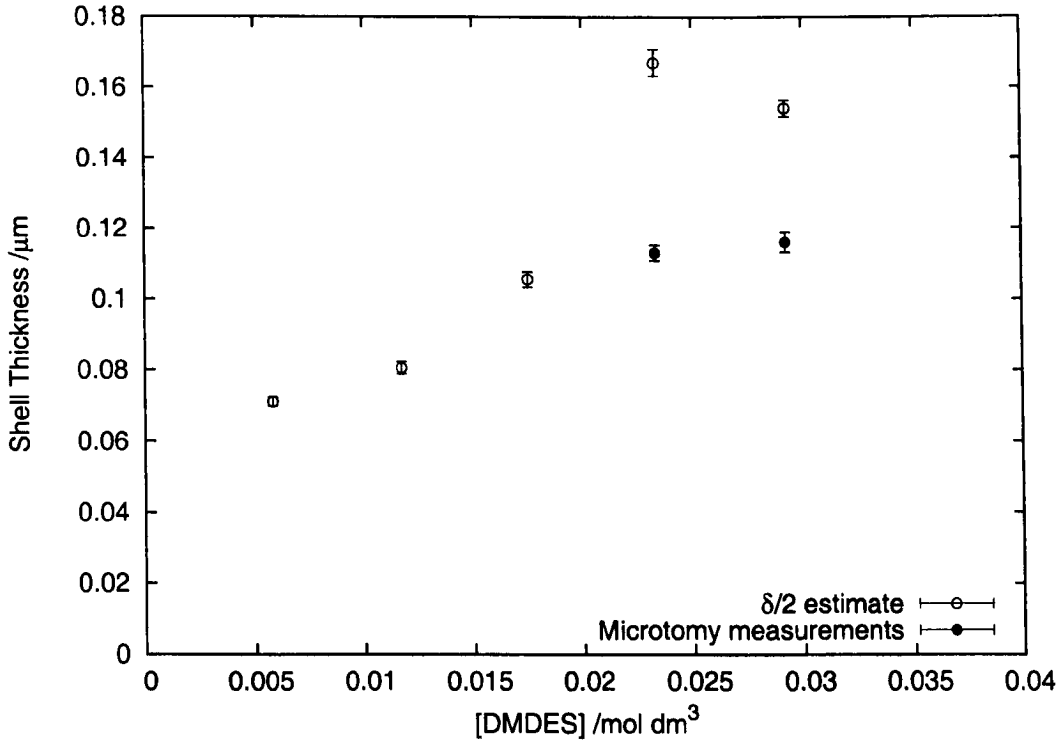

Figure 4.27: Shell thickness as a function of secondary DMDES concentration for a 1 % NH_3 1 % DMDES regime using SEM $\delta/2$ estimates (open circles, Figure 4.25) and microtomy (closed circles).

collapsed morphology signifies that the shells are thinner or that h/R is smaller due to increased particle size, or both.

When air-dried on a glass microscope slide, the Secondary DMDES particles were observed to form semi-ordered arrays (Figure 4.31), which is indicative of a narrow size distribution. Particle size measurements were made by image analysis of SEM micrographs (Figure 4.32). The SEM determined measurements were of similar magnitude to, though larger than, the PCS measurements made of the PDMS emulsion droplets. The 1 % regime exhibited little change in droplet diameter across the series, while particle size in the 2 % regime increased with increasing secondary DMDES concentration. This size increase correlates with increasing secondary DMDES concentration and may be a consequence of monomer absorption or formation of more deformable shells, but not of creaming of the initial droplets, as the series was equally matured prior to shelling.

The 2 % Secondary DMDES particles were subjected to microtomy and examined by SEM (Figures 4.33 and 4.34). Shell thickness was found to increase with increasing secondary DMDES concentration up to 0.0233 mol dm^{-3}, and to decline with further increase

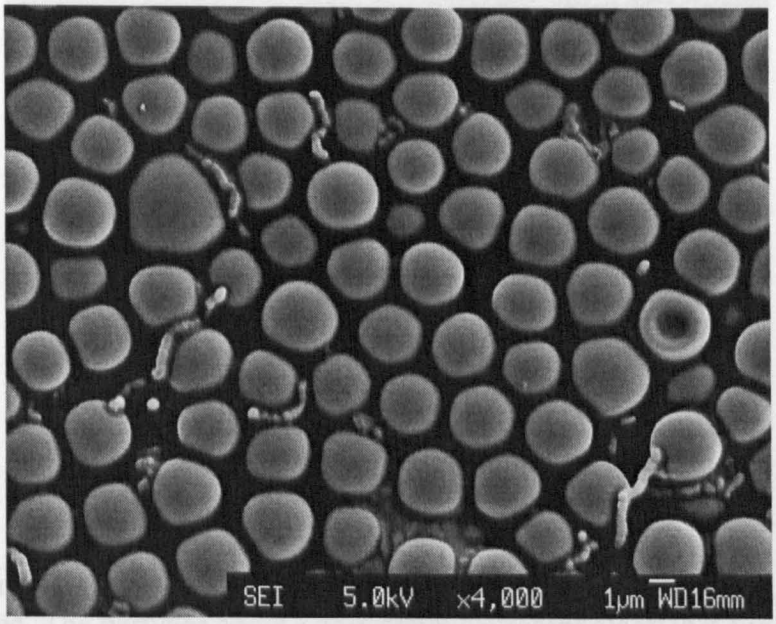

Figure 4.28: Shells formed in the 2 % v/v DMDES /NH3 series. The secondary DMDES concentration was 0.0117 mol dm^{-3}.

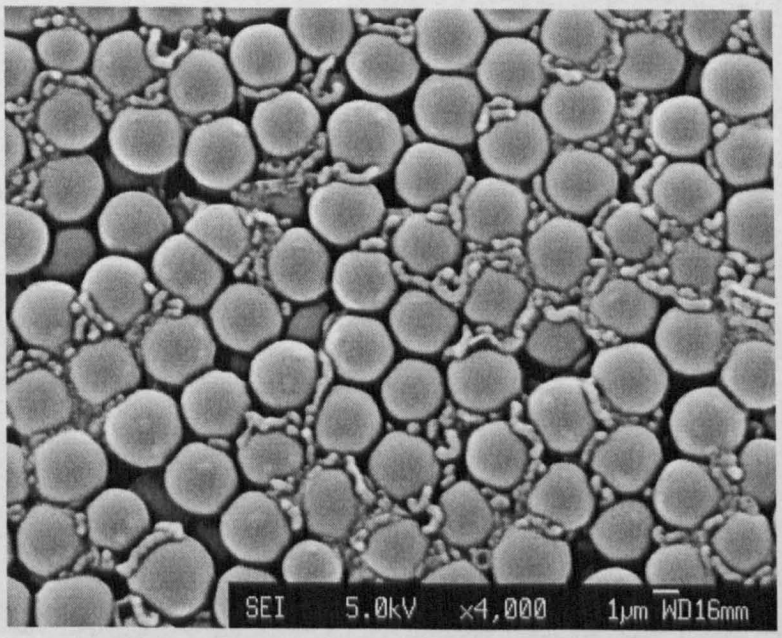

Figure 4.29: 2 % series shells formed with a secondary DMDES concentration of 0.0233 mol dm^{-3}. The particles typically exhibit a spherical morphology.

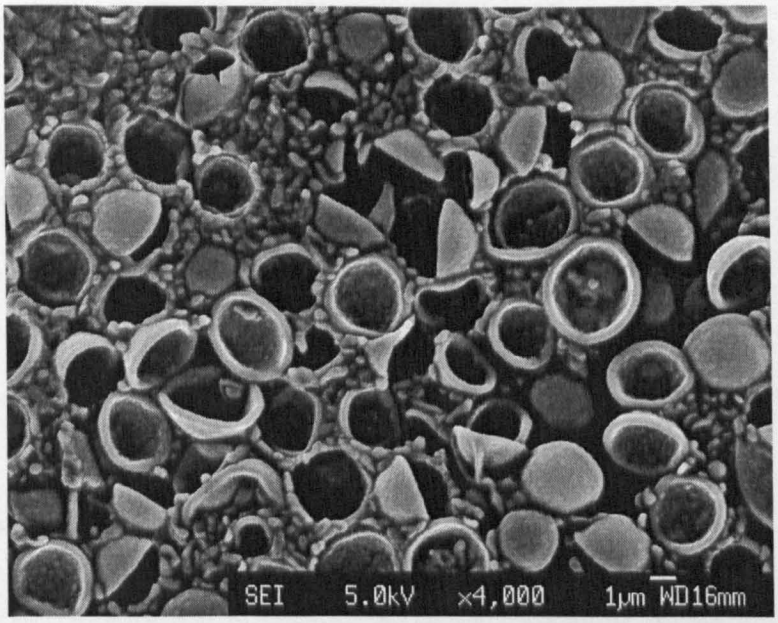

Figure 4.30: Particles formed with a secondary DMDES concentration of 0.0350 mol dm^{-3} in the 2 % regime. The particles adopt a hemispherical morphology that suggests their shells are thinner or have a lower h/R than those observed with lower secondary DMDES concentrations (Figures 4.28 and 4.29).

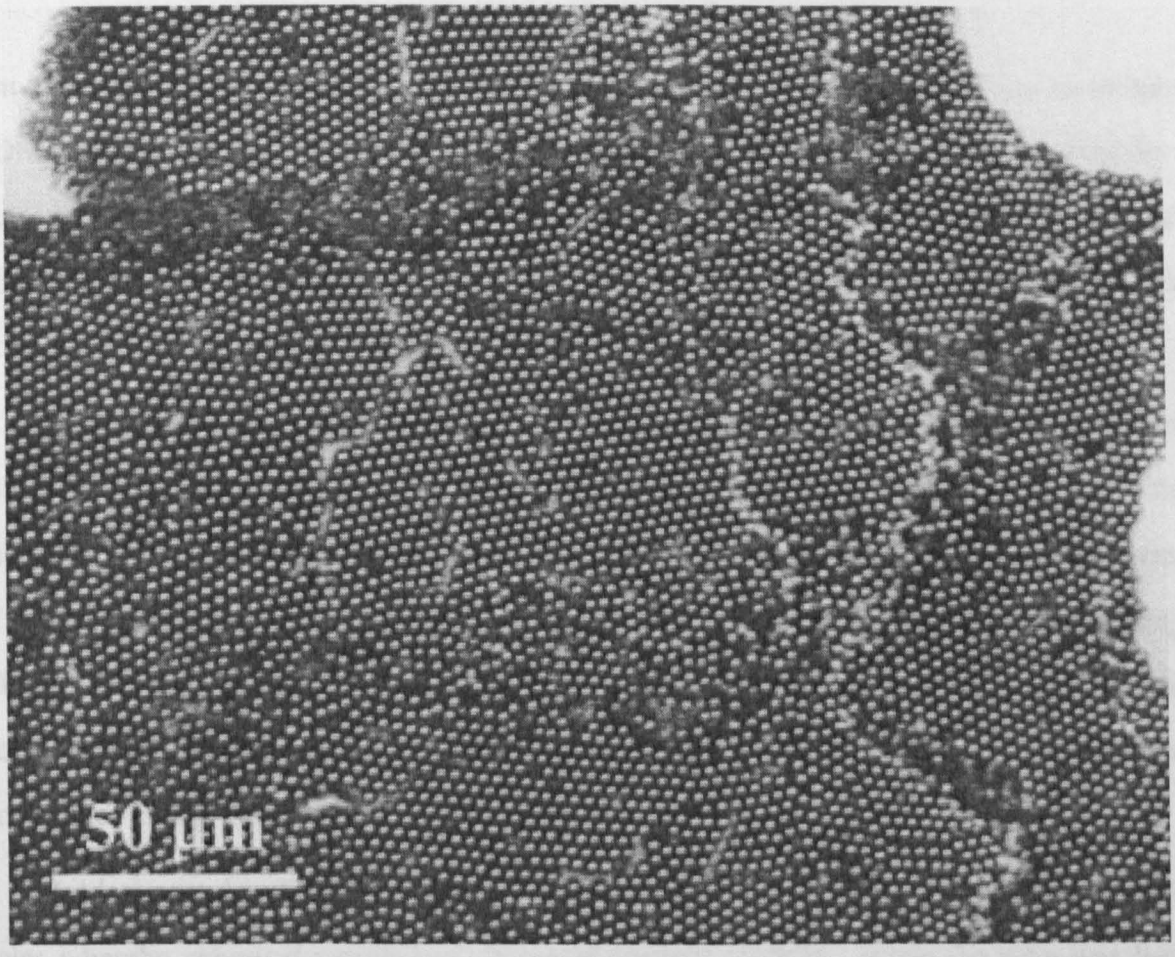

Figure 4.31: Optical micrograph of a 2 % Secondary DMDES system dried onto a glass slide

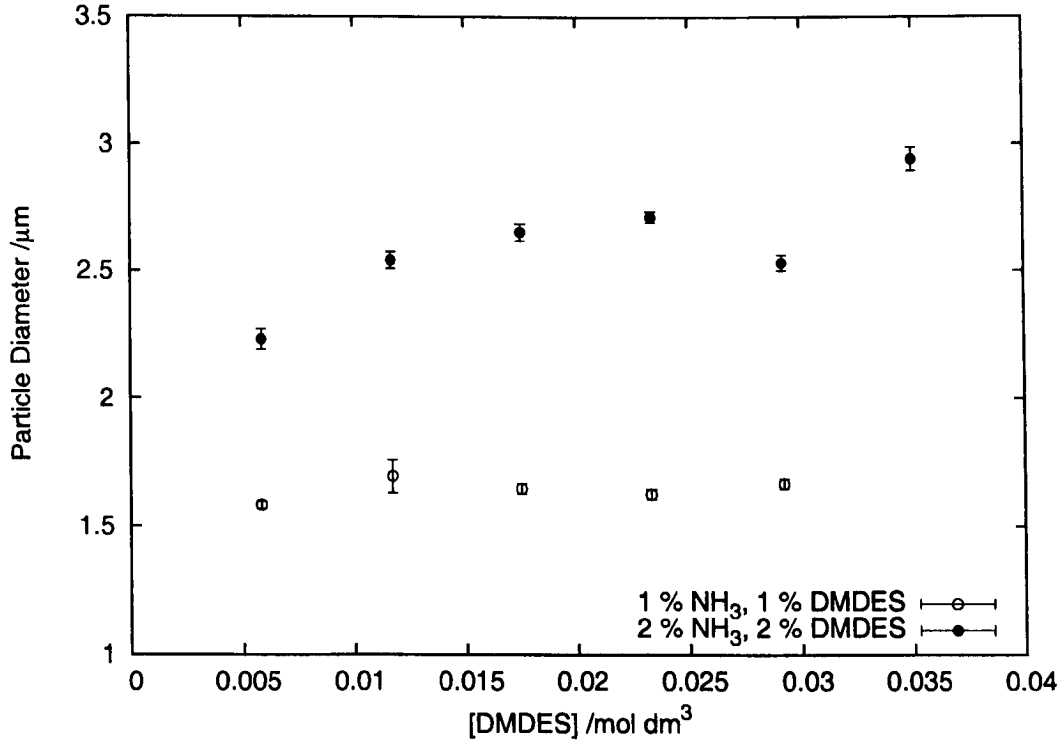

Figure 4.32: Particle size as a function of secondary DMDES concentration for both 1 % and 2 % v/v DMDES and NH_3 regimes.

in concentration (Figure 4.35). As already mentioned, the particles formed in secondary DMDES concentrations ≥ 0.029 mol dm^{-3} adopted a hemispherical morphology upon drying, while shells formed in lower concentrations were uncollapsed. These results seem to indicate a threshold DMDES concentration above which shell growth is less efficient, which may relate to the availability of surface area that may be polymerized upon.

As with the 2 % Zoldesi Method particles, the apparent change in particle size across the 2 % Secondary DMDES series can not be attributed solely to the presence of a shell; the increase in size across the series mirrors the trend observed for the derived core diameter (Figure 4.36). The 2 % Zoldesi series exhibited a declining particle size with increasing TEOS addition time (Figure 4.6), but the situation is analogous to the particle-size trend exhibited by the 2 % Secondary DMDES regime as, in both cases, particle size increase correlates to unpolymerized DMDES concentration.

Zoldesi postulated a relationship between h/R and the morphology exhibited by particles whereby spherical morphology occurred for $h/R > 0.23$. When the ratio was less, hemispherical morphologies were observed [36]. The determined thicknesses of the $\geq$

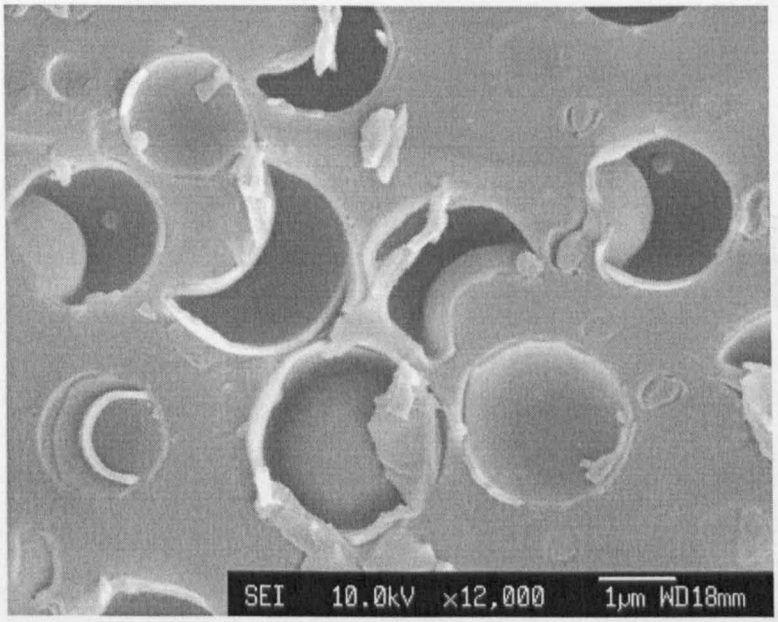

Figure 4.33: An SEM micrograph of microtomed 2 % Secondary DMDES particles formed with a secondary DMDES concentration of 0.0117 mol dm^{-3}. The mean shell thickness was determined to be 84 nm with a standard deviation of 7 %.

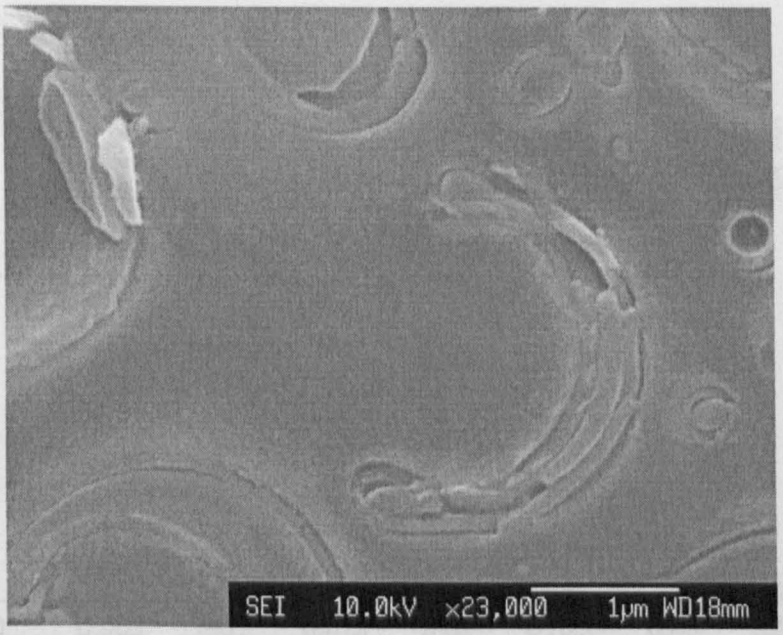

Figure 4.34: Microtomed 2 % Secondary DMDES particles formed with a shell DMDES concentration of 0.0233 mol dm^{-3}. The mean shell thickness was determined as 120 nm with a standard deviation of 17.5 %.

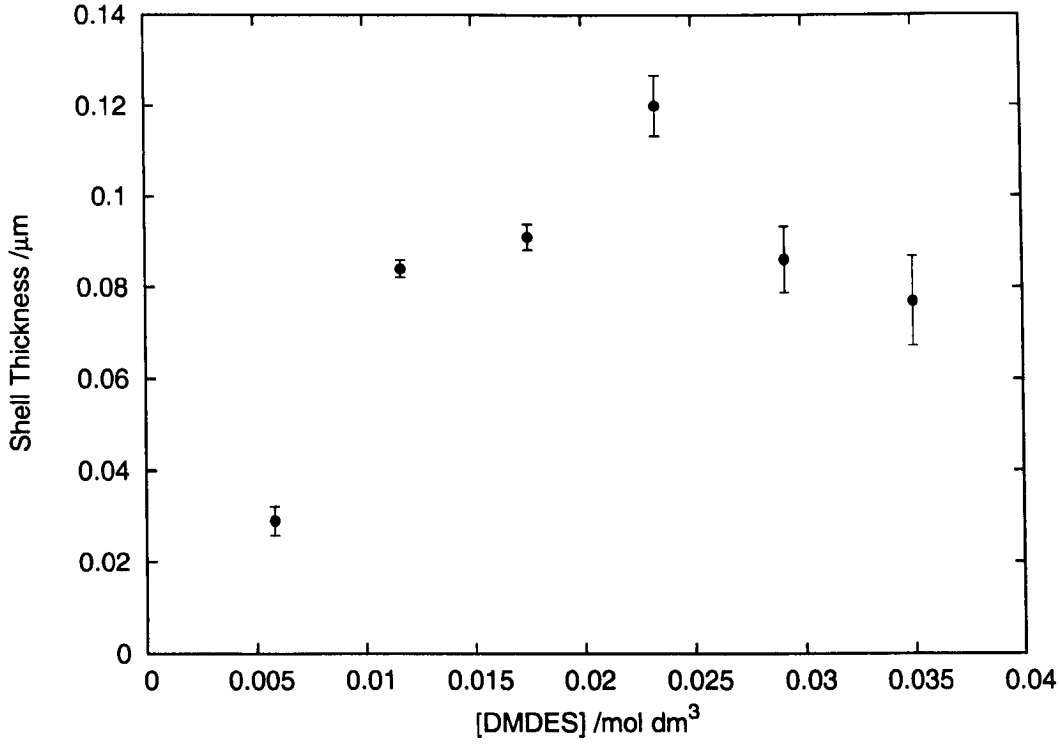

Figure 4.35: Shell thickness, determined by microtomy, as a function of secondary DMDES concentration

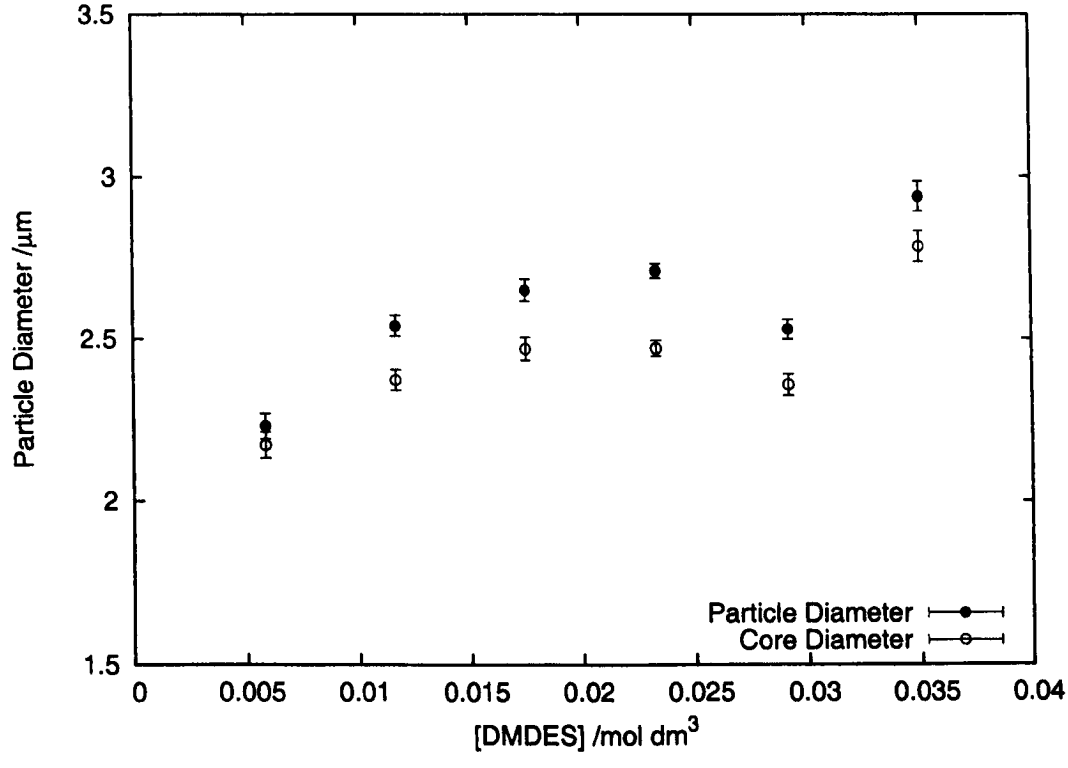

Figure 4.36: Particle and core diameters as a function of secondary DMDES concentration. Core diameter was calculated by subtraction of twice the microtomy-determined shell thickness from the total particle size.

0.029 mol dm^{-3} Secondary DMDES particles, which exhibited hemispherical morphology, were larger than lower concentration particles that displayed spherical morphology. Inspection of h/R as a function of secondary DMDES concentration (Figure 4.37) for the 2 % regime reveals h/R for the higher concentrations to be of similar magnitude to those lower concentrations that exhibit spherical morphology. Also, surprisingly, all of the h/R ratios across the series are less than the threshold ratio determined by Zoldesi.

The Zoldesi Method particles made in this study had all adopted non-spherical morphologies, as did the 1 % Secondary DMDES series, and are consistent with Zoldesi's results. The 2 % Secondary DMDES particles' deviation from the suggested trend, at least up to 0.0233 mol dm^{-3}, suggests a non-equivalence in the shell materials made by the two methods in the 2 % regime. This difference may relate to the extent of cross-linking within the shell, which may be influenced by the concentration ratio of DMDES to TEOS.

The DMDES in the Zoldesi method is typically extensively hydrolysed upon addition of TEOS, whereas in the Secondary DMDES method this is not the case because the two monomers are typically added concurrently. This means that, depending on the relative rates of hydrolysis, the quantities of readily polymerizable shell material in the Secondary DMDES method may not be analogous to those experienced by emulsion droplets shelled under Zoldesi conditions.

Monomer to Surface Area Ratio

The difference in surface area available for shelling between 1 % and 2 % DMDES regimes can be estimated using the ratio of maximum PDMS droplet diameter for each regime as empirically determined by PCS:

$$d_{2\%} \approx \frac{4}{3} d_{1\%} \tag{4.4.4}$$

The number of PDMS droplets, N_{TOT}, of diameter d may be estimated from the total PDMS volume V_{TOT}:

$$N_{TOT} = \frac{6V_{TOT}}{\pi d^3} \tag{4.4.5}$$

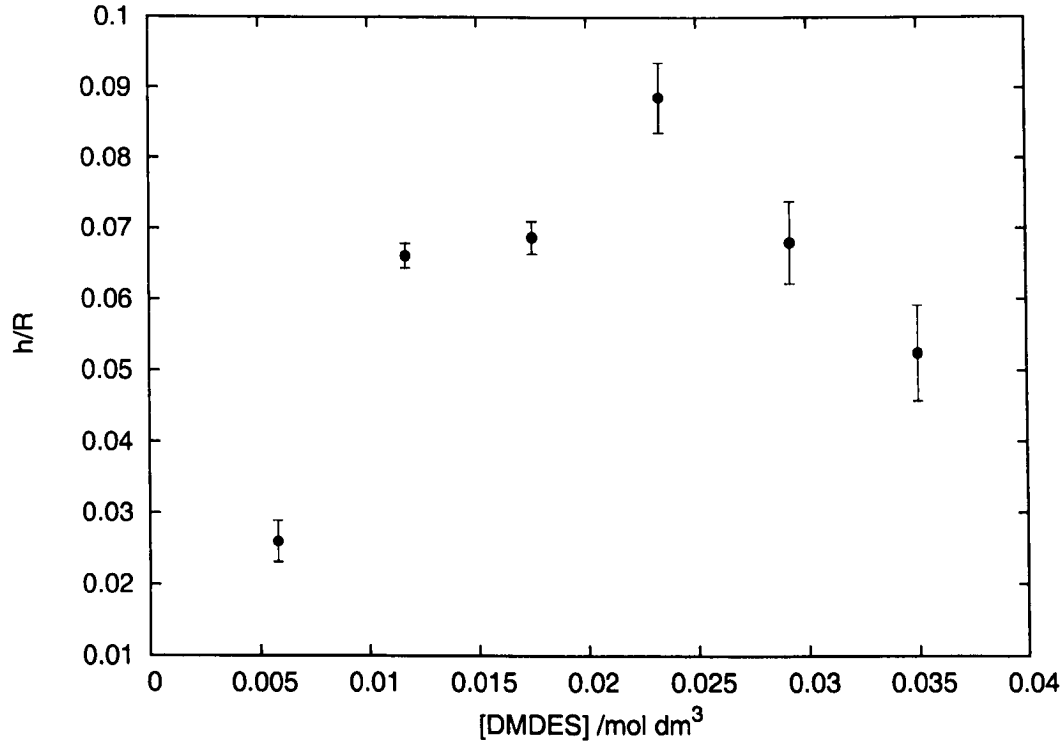

Figure 4.37: h/R as a function of secondary DMDES concentration for the 2 % regime

Combining Equation 4.4.5 with Equation 4.4.6 allows the total surface area, A_{TOT}, to be calculated in terms of V_{TOT} and d:

$$A_{TOT} = N_{TOT}\pi d^2 = \frac{6V_{TOT}}{d} \tag{4.4.6}$$

Using the approximate relationship in Equation 4.4.4, $A_{2\%}$ may be estimated in terms of $V_{1\%}$ and $d_{1\%}$:

$$A_{2\%} \approx \frac{9V_{1\%}}{d} \approx \frac{3}{2}A_{1\%} \tag{4.4.7}$$

Given that a 2 % DMDES-2 % NH_3 regime provides approximately 50 % more surface area for shelling than the 1 % regime, thicker shells could be expected in the 1 % regime for equivalent concentrations of secondary DMDES. With the consideration that the δ estimates represent an overestimate of shell thickness, thicker shells are not generally observed in the 1 % regime, which indicates the 2 % regime's shelling step may be more efficient.

4.5 Quench Method: Shell Thickness Determined by Shell Reaction Quench Time

An obvious approach for controlling shell thickness in both the Zoldesi and Secondary DMDES methods is to vary the shell formation time. This may be achieved by dialysis or centrifugation into fresh solvent. The latter method was selected for this study, because the quench time is more quantifiable. As discussed in Section 4.3.1, it was necessary to use INUTEC SP1 to stabilize the particles during centrifugation. A 1 % v/v DMDES and NH_3 PDMS series was made, allowed to mature for 100 hours, and then subjected to Secondary DMDES swelling. Classes were then quenched after shell maturation times in the range 15–69 hours. With increasing quench time the proportion of particles adopting hemispherical morphologies (Figure 4.38) declined (Figure 4.39). Image analysis of micrographs showed little variation of particle size across the series (Figure 4.40), which is consistent with the other 1 % PDMS systems.

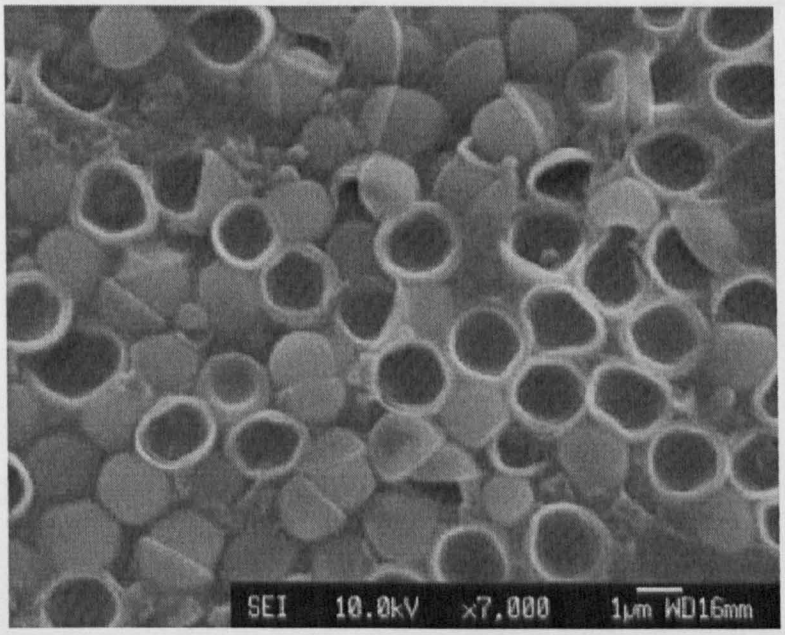

Figure 4.38: 1 % Secondary DMDES particles whose shell growth was arrested after 15 hours.

The quenched series was subjected to microtomy (Figures 4.41 and 4.42), which revealed an increase in shell thickness with quench time (Figure 4.43).

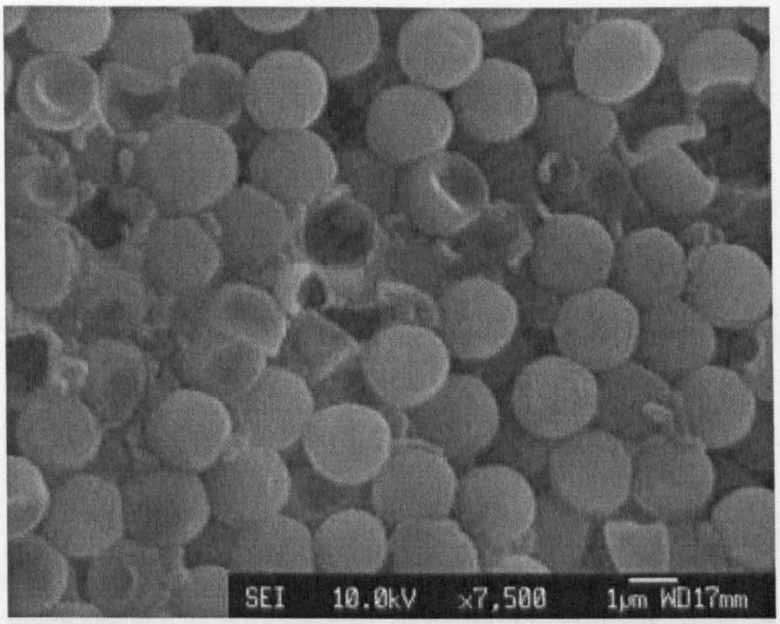

Figure 4.39: 1 % Secondary DMDES particles formed with a shell quench time of 69 hours.

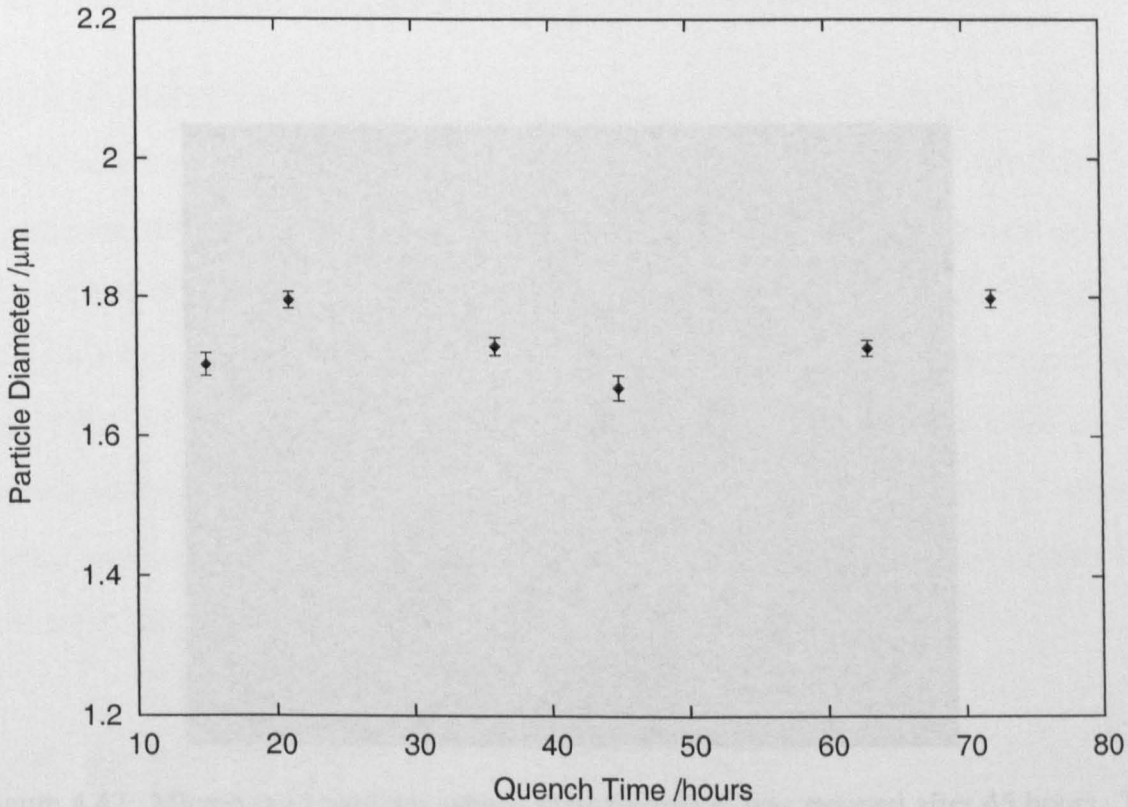

Figure 4.40: Particle size as a function of quench time

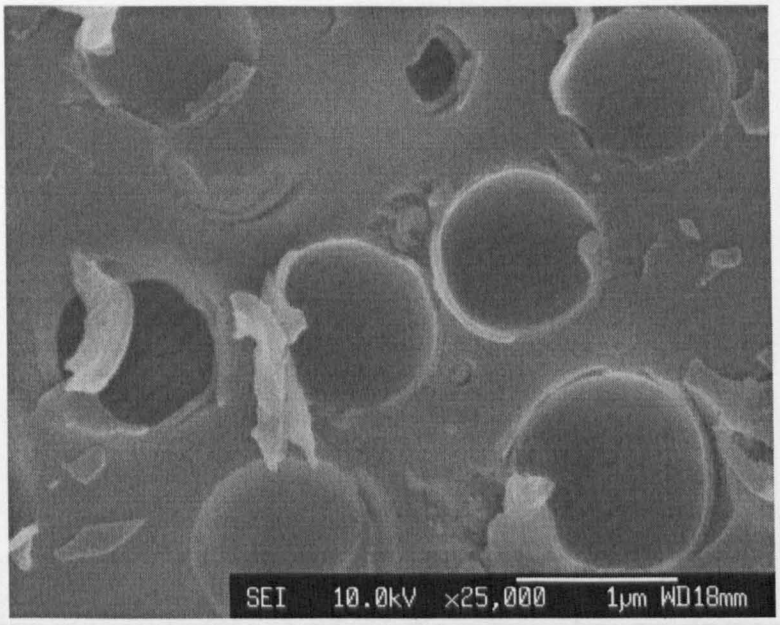

Figure 4.41: An SEM of microtomed 1 % particles whose shell growth was quenched after 15 hours. The mean shell thickness for this class was determined as 53 nm with a standard deviation of 11 %.

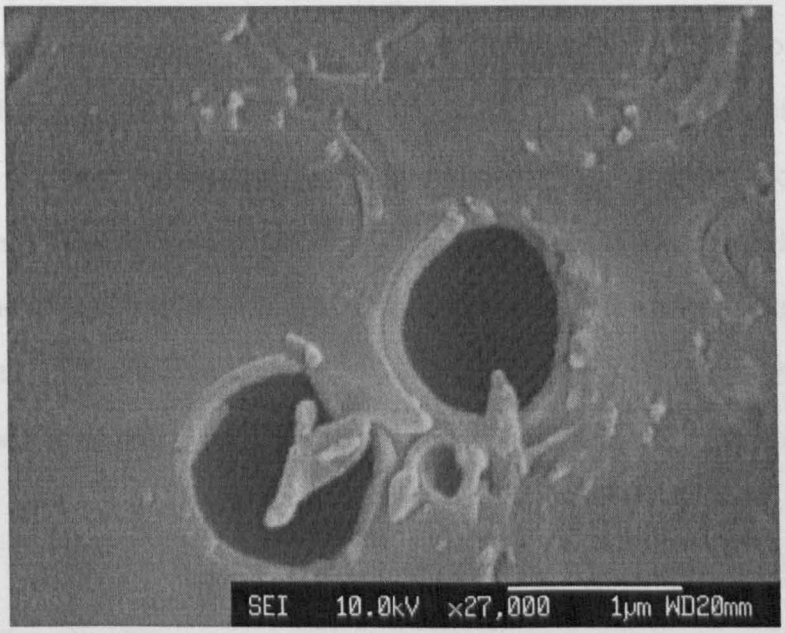

Figure 4.42: Microtomed particles whose shell formation was stopped after 45 hours. The mean class shell thickness was determined to be 102 nm with a standard deviation of 6 %

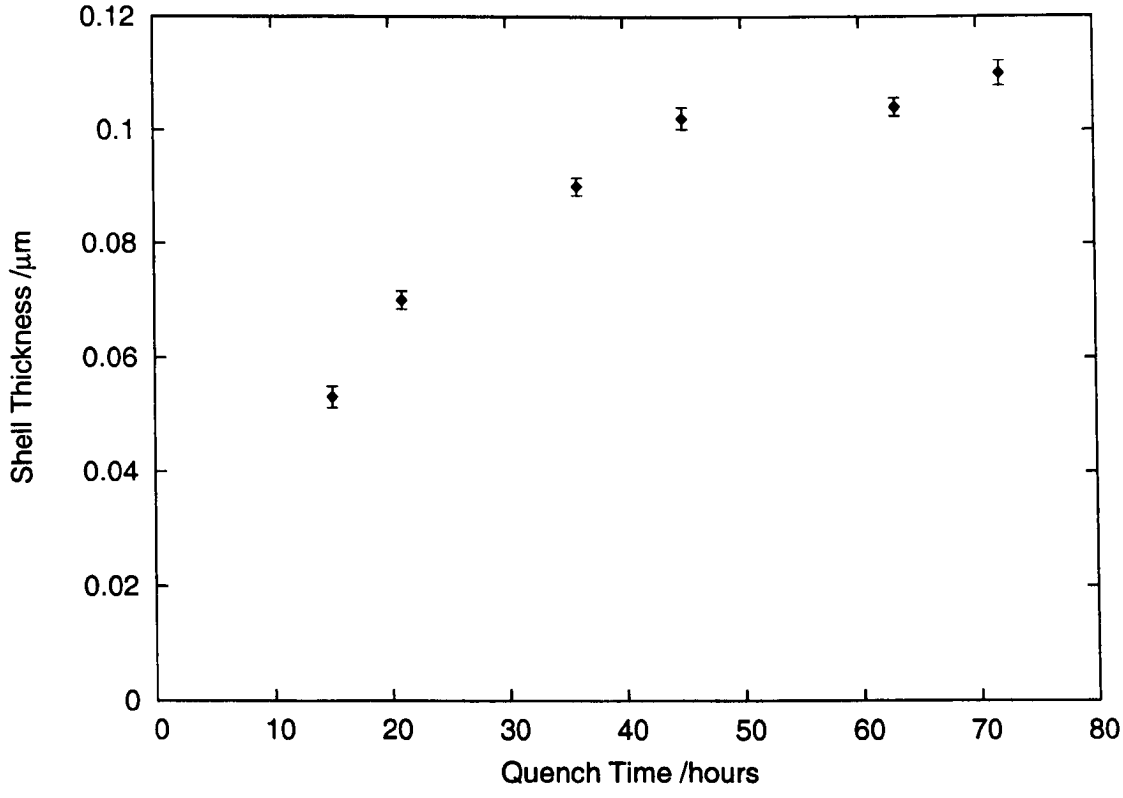

Figure 4.43: Shell thickness as a function of quench time

4.6 The Effect of Changing TEOS Concentration

A 2 % v/v DMDES and NH_3 PDMS emulsion series was made and matured for 100 hours. Shells were formed using the Secondary DMDES method. The TEOS concentration was varied from 0.0090–0.0202 mol dm^{-3}, while the secondary DMDES concentration remained fixed at 0.0233 mol dm^{-3} across the series. The lowest TEOS concentration yielded particles that uniformly adopted a hemispherical morphology upon drying, particles formed under high TEOS concentration adopted a spherical morphology, and intermediate TEOS concentrations produced particles in which both morphologies were present; the ratio of spherical to hemispherical morphology increased with increasing TEOS concentration (Figures 4.44, 4.45 and 4.46).

4.7 MTES Shells

In addition to forming shells from DMDES and TEOS, three different 2 % series were made that used an additional trifunctional shell monomer, methyltriethoxysilane (MTES), to de-

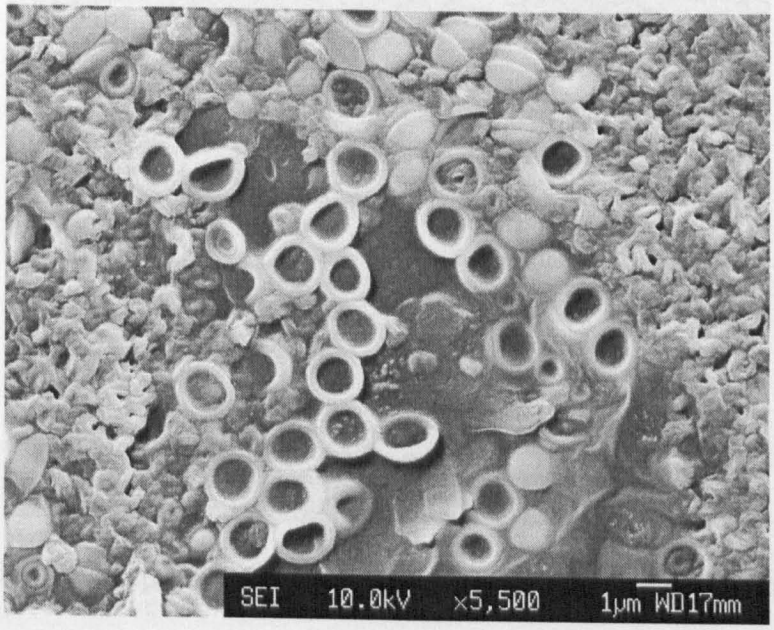

Figure 4.44: 2 % Secondary DMDES particles formed in the presence of 0.0090 mol dm^{-3} adopted hemispherical morphology upon drying.

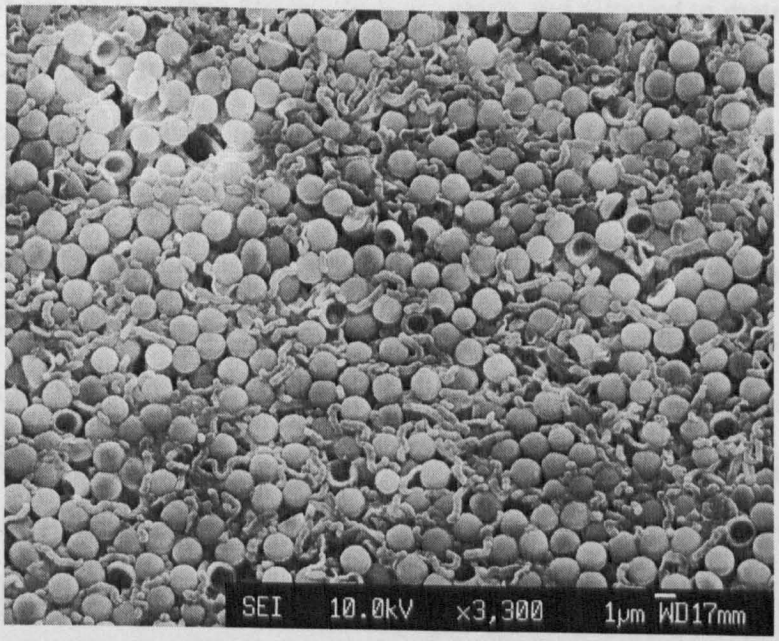

Figure 4.45: Both spherical and hemispherical morphologies were observed in the particle class formed in 0.0157 mol dm^{-3} TEOS. The spherical morphology predominates in this case.

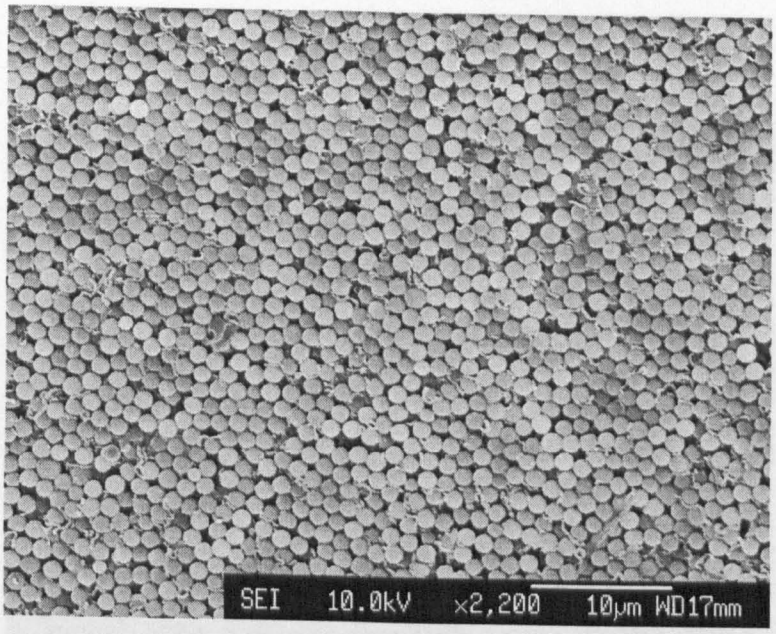

Figure 4.46: Uniformly spherical particles were produced from 0.0202 mol dm^{-3} TEOS

termine the monomer's effect upon shell strength.

4.7.1 Zoldesi Method with MTES

2 % v/v DMDES and NH_3 PDMS emulsions were made and allowed to mature for 27 hours, whereupon TEOS/MTES mixtures were added, with a fixed total shell monomer volume fraction comparable to that used in previous experiments: 0.8 %. The TEOS/MTES concentration ratio range was 0–6.25. Particles formed with TEOS/MTES ranging from 0–0.89 yielded particles with very thin shells that seemed to adopt a microballoon morphology (Figure 4.47), however a hemispherical morphology is present in the particle classes formed with TEOS/MTES ratios $\geq$ 1.49 (Figure 4.48). Particles formed with a shell ratios $\geq$ 2.68 were observed under SEM to have developed rough nodular surfaces. Some spherical morphology was also observed with TEOS/MTES ratio of 6.25 (Figure 4.49). It is clear that substitution of TEOS by MTES leads to the formation of thinner shells. The trifunctional nature of MTES means that it has less cross-linking potential than TEOS, but it may also disrupt formation of the princpal shell tetramer.

MTES-TEOS shells were also formed by the Secondary DMDES method using the same concentration ratios with similar results.

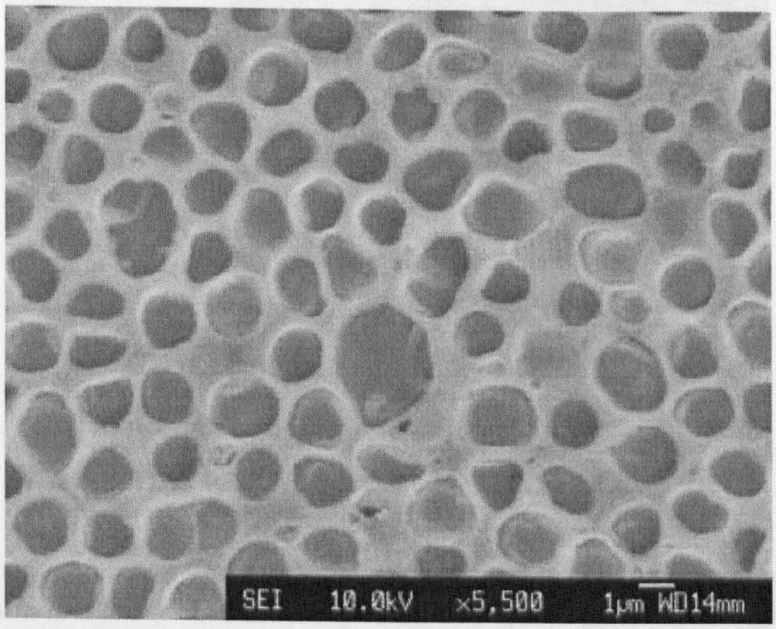

Figure 4.47: Particles formed with a TEOS/MTES shell monomer ratio of 0.89 adopted a collapsed microballoon morphology upon drying. Charging is evident around the particles.

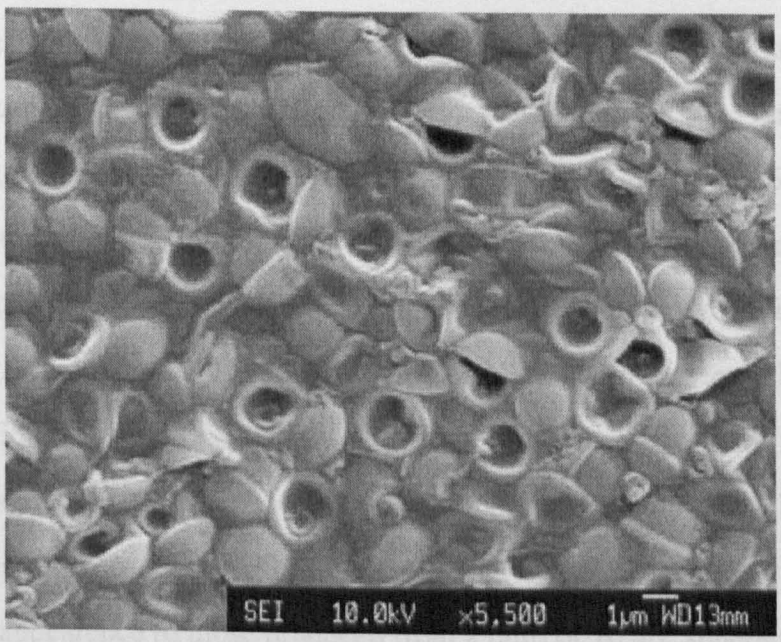

Figure 4.48: Declining MTES concentration leads to thicker shells and hemispherical morphology. The TEOS/MTES ratio was 1.49.

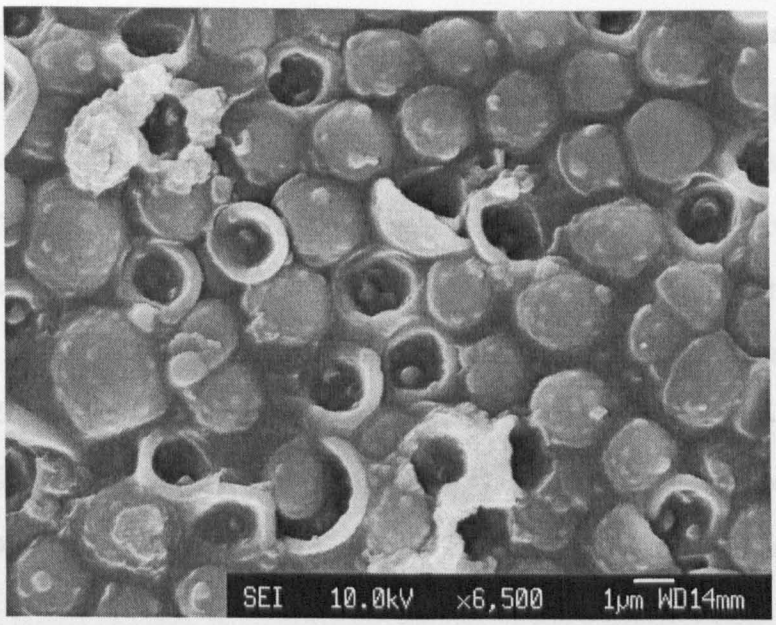

Figure 4.49: Particles whose shells were formed from a TEOS/MTES ratio of 6.25 exhibited a combination of spherical and hemispherical morphology. Nodular growths were also present on the shell surfaces.

4.7.2 Secondary DMDES/MTES Method

To determine the effect of replacing the DMDES shell component with MTES it was necessary to use the Secondary DMDES method. Mixtures of DMDES and MTES were made with both a fixed TEOS concentration and total shell monomer volume fraction of 0.8 %. Shells were made with DMDES/MTES molar concentration ratios in the range 10.45–1.16. Pronounced aggregation was observed with the DMDES/MTES ratio of 1.16, so lower ratios were not attempted. Particles formed with a DMDES/MTES ratio of 10.45 generally adopted a spherical morphology, a significant amount of a granular secondary material was also produced (Figure 4.50). Increasing the concentration of MTES with respect to DMDES to give a DMDES/MTES concentration ratio of 4.65 lead to formation of particles that appeared to be softer and adopted a generally hemispherical morphology (Figure 4.51). Further increase of MTES concentration to a DMDES/MTES ratio $\geq$ 2.71 lead to formation of particles that were similar in appearence to those produced from a ratio of 10.45: spherical morphologies were observed (Figure 4.52).

The effect of replacing DMDES shell monomer with MTES initially has little affect upon the formed shell, but increasing the MTES concentration leads to formation of softer

shells, but, surprisingly, with further substitution firmer shells are again produced up to a concentration ratio of 1.16 which destabilizes the dispersion. A possible explanation is that the MTES at low concentration has little influence on the shell material, possibly because it is consumed forming secondary material and makes little contribution to the shell directly, but higher concentrations relative to the DMDES act to disrupt tetramer formation, leading to a more open gel-like structure. The recurrence of less deformable shells with further increased MTES concentration may be a consequence of enhanced cross-linking density. The destabilized classes indicate a threshold level of DMDES is necessary to form the shells, and shells cannot be made purely from MTES and TEOS without further modification of this method.

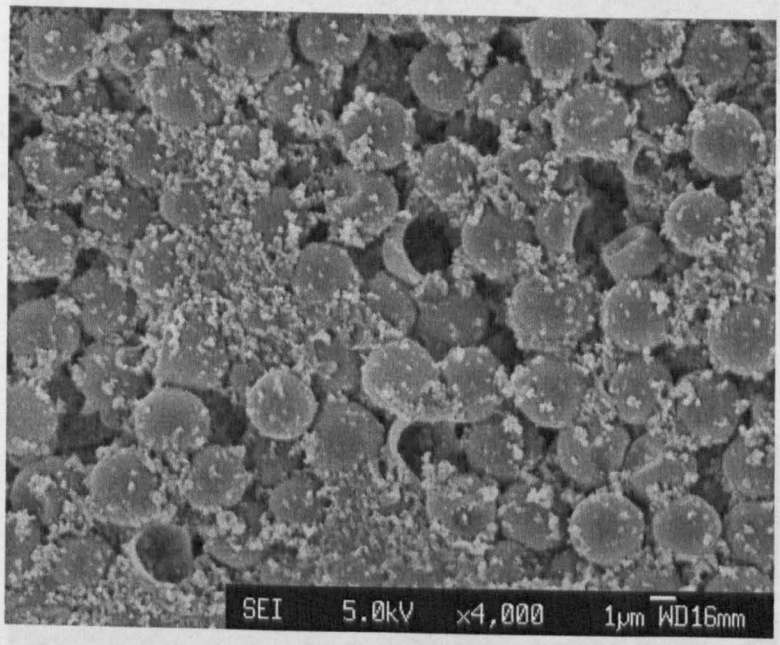

Figure 4.50: Secondary DMDES/MTES particles formed with a DMDES/MTES concentration ratio of 10.45. The particles adopt a generally spherical morphology. Granular secondary material is present.

4.8 Summary

The Zoldesi method to control shell thickness depends upon the concentration of unpolymerized DMDES from the PDMS core formation step, which is gradually consumed over a period of days. Addition of TEOS causes the formation of a cross-linked hybrid silica-silicone shell. The shell thickness is determined by the time that elapses between PDMS

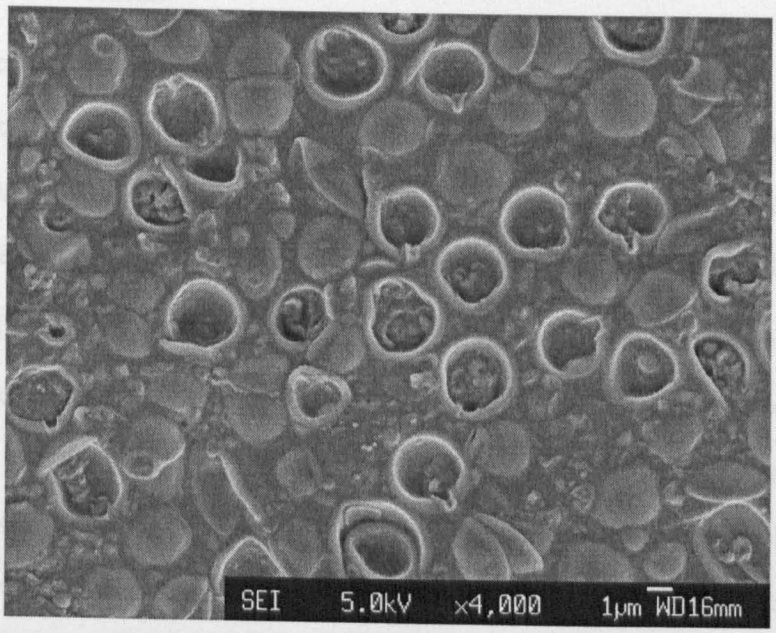

Figure 4.51: Secondary DMDES/MTES particles formed with a DMDES/MTES ratio of 4.65. The particles appear softer and have generally formed hemispherical morphologies.

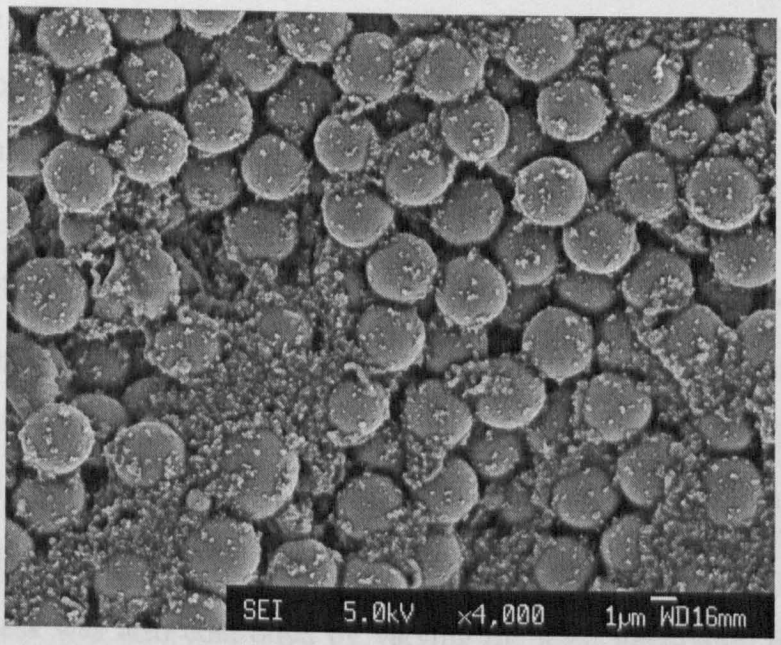

Figure 4.52: Secondary DMDES/MTES particles formed with a DMDES/MTES ratio of 1.74 yielded particles similar to those produced with a ratio 0f 10.45 (Figure 4.50)

core formation and TEOS addition. Attempts to further thicken the shell by Stöber silica growth proved unsuccessful.

The produced particles were found to be unstable to sedimentation and coagulated with time. The particles could be centrifuged and redispersed into ethanol, which dissolved the core material, but not into water. It was necessary to add a polymeric surfactant, INUTEC SP1, to the dispersions to stabilize them and thereby retain the core material.

If thick shells are required, there is little scope to incorporate an active agent into the core. A modified method was developed that disconnected the shell formation step from the core formation. Addition of a combination of DMDES and TEOS to matured PDMS lead to formation of shells whose thickness, as determined by microtomy and SEM, depended on the secondary DMDES concentration. The correlation between shell thickness and DMDES concentration persisted up to a threshold value, beyond which thinner shells and quantities of secondary material were produced. It is hypothesized that this threshold concentration relates to the available interfacial area, increasing particle density may allow use of higher shell monomer concentrations and hence provide thicker shells. Reduction of particle density by dilution leads to pronounced formation of secondary material and aggregation. Shells produced above the threshold DMDES concentration adopted collapsed morphology, while thinner shells formed below this concentration remained spherical. This suggests DMDES concentration may also influence shell hardness.

Particle size was dictated by the size of the emulsion template, which was determined by the initial DMDES concentration. Droplet growth could be fitted by a first order rate equation, although the relatively high NH_3 concentration may have created pseudo first order conditions. A different rate profile was observed under 1 % v/v DMDES and NH_3 conditions, while 2 % DMDES/1 % NH_3 and 2 % DMDES and NH_3 revealed similar profiles. This difference relates to the quantity of DMDES rather than NH_3.

Shell thickness was also controlled by varying the shell maturation time. The shell growth step was arrested by quenching, whereupon a positive correlation between shell thickness and maturation time was determined by microtomy.

Zoldesi had determined no effect of TEOS concentration on shell thickness, however, in-

spection by SEM showed an apparent trend in particle morphology with TEOS concentration that suggests harder shells may form with high TEOS/DMDES ratios.

Substitution of TEOS by MTES lead to formation of particles with nodular surfaces at high TEOS/MTES ratios, while increasing MTES lead to formation of thinner and apparently softer shells: a consequence of the reduced cross-linking potential of MTES.

Substitution of secondary DMDES by MTES at high DMDES/MTES ratios leads to apparent shell softening, however, further increase of MTES concentration leads to a return to spherical morphology suggestive of firmer shells: perhaps a consequence of enhanced cross-linking density. Below a threshold DMDES/MTES ratio bulk material is produced.

The Zoldesi method and methods derived from it are both simple and yield relatively thick shells. Particles were formed in a suitable size range for micromanipulation study, and shell thicknesses were determined by microtomy.

4.9 Future Work

The Secondary DMDES method revealed an apparent DMDES concentration threshold above which thinner shells were produced. Further study of the influence of droplet template surface area upon the magnitude of this concentration would be of interest as manipulation of these conditions could lead to the formation of thicker shells. Such variation in surface area could be brought about through use of a surfactant or varying primary DMDES concentration.

Further work to enhance shell thickness would be of interest, combined with efforts, such as slow monomer addition, to reduce secondary nucleation. Alternative mixing regimes could also be considered. A second shell growth step could be attempted, either another DMDES-TEOS derived layer or an alternative material such as calcium carbonate, if a more rigid or brittle structure is required. Alternatively, functionalization of the shell surface could allow polymer grafting, or site-specific polymerization.

The influence of TEOS and MTES on cross-linking density in the shell material could be explored by EDX or shell density measurements, to determine if there is scope for tuning shell hardness. The porosity of the silica-silicone shells has not been quantified. Mercury

porosimetry could be undertaken across various series to determine the effects, if any, of varying TEOS/DMDES ratio or inclusion of MTES.

Chapter 5

Micromanipulator

5.1 Introduction

Many techniques have been developed to study the mechanical properties of microcapsules and cells. Some methods are indirect: the capsule populations are subjected to shear or compression. The extent of disruption may then be assessed by the measurement of released amounts of quantifiable material [73, 74, 75] or by direct inspection of deformation using SEM [76]; clearly the latter detection method is only suitable for particles that are not deformed upon drying. Variables imposed by shearing apparatus that are difficult to quantify, such as the process hydrodynamics, or even polydispersity within the sample population, can complicate analysis of results.

Direct methods are typically applied to individual particles. An early technique was micropipette aspiration, which was used to measure the elastic properties of microcapsules [77] and cells [78], though no measurement of microcapsule bursting strength could be made.

In general direct methods to probe particle mechanical properties involve compression, or indentation [79], to determine applied force as a function of deformation. Particle strength can be assessed on a basis of breaking force or the force required to deform a particle to a certain extent [80].

In compression studies, a particle is typically positioned in proximity to a probe-mounted force transducer. A micromanipulation technique that used two flat-ended optical fibres, one attached to a micromanipulator and the other to a force transducer, was used to measure the

bursting strength of mammalian cells. This apparatus was also used to investigate microcapsules [81], though it has since been superseded by micromanipulation rigs that deploy a probe-mounted force transducer to compress particles against a slide surface [82] (and see Section 5.2.1).

The micromanipulation technique allows simultaneous measurement of applied force and particle deformation. In addition to experimentation upon dried microcapsules, the technique has been used to compress microcapsules in water [83, 84]. While the method depends upon optical microscopes to position target particles beneath the probe, a minimum practical size limit of ≈ 1 μm is imposed. A modified rig was developed that, when combined with the an environmental scanning electron microscope, allowed examination of both hydrated and dried sub-micron particles [85].

Atomic Force Microscopy (AFM) has also been used to measure microcapsule [86, 87], and cell strength through compression [88], in combination with optical or confocal microscopy to allow simultaneous deformation analysis. The same technique has also been used in conjunction with Reflection Interference Contrast Microscopy, which is a technique that uses constructive or destructive interference patterns of monochromatic light to determine capsule shape [89].

Various direct methods are also available to measure small forces, such as optical [90, 91] and magnetic tweezers [92], though these are limited to pN regimes [93].

Use of direct methods can allow determination of mechanical properties in addition to the breaking force. Compression and release of particles can reveal hysteresis in force-deformation curves, to demonstrate regimes of elastic and plastic deformation [83]. Modelling the force-deformation data, through treatment of a capsule as an elastic air-filled sphere [94], a leaking sphere [88], or a sphere filled with incompressible fluid [95] has allowed determination of the particle-wall Young's Modulus. The most sophisticated models compute the geometries of a hollow sphere as it is compressed, including additional deformation at the compression loci, in combination with constitutive equations that account for the relationship between stress and strain [96, 95]. Most models, however, assume the particles possess a thin membrane, but for shell thickness/particle ratios (h/R) above 5 % it is

necessary to compute the 3D wall deformation [95]. A far simpler approach relies on analysis of the linear relationship between force and compression that may occur during small particle deformation [89].

5.2 Method

5.2.1 The Micromanipulation Rig

Particle bursting forces were investigated using a micromanipulation technique developed by Zhibing Zhang and co-workers [82]. The micromanipulation rig (Figure 5.1) consisted of a fine glass probe that was glued to a force transducer input, which was in turn mounted on a three-dimensional micromanipulator that could be programmed to deploy the probe at a specified speed. The glass probe was formed from 1.0 mm borosilicate capillary tube (Harvard Apparatus Ltd) that had been heated and drawn. Half of the drawn tube was mounted on a Microforge (Narishige Co., Japan), which consists of a filament arranged in front of a transverse microscope. The drawn capillary was clamped and brought into proximity with the filament, which was heated and raised to meet the capillary tip (Figure 5.2). The filament was then pulled away from the now molten tube, further drawing it into a finer tip. The probe tip is then subjected to a micropipette grinder (Narishige Co.) to ensure an even surface.

The probe array was positioned perpendicularly above the stage of an inverted microscope. Samples were deposited on sections of borosilicate glass slide, which where then placed on the stage. The feeds from the microscope-mounted camera and an additional transverse camera were combined in a splittable view on a monitor, which allow individual particles to be precisely positioned below the glass probe prior to an experimental run. During the experiment the micromanipulator was lowered under computer control and the output transducer voltage was sampled using a PC data acquisition board. A maximum threshold voltage was set beyond which the array descent would be halted to prevent transducer damage by exceeding tolerance.

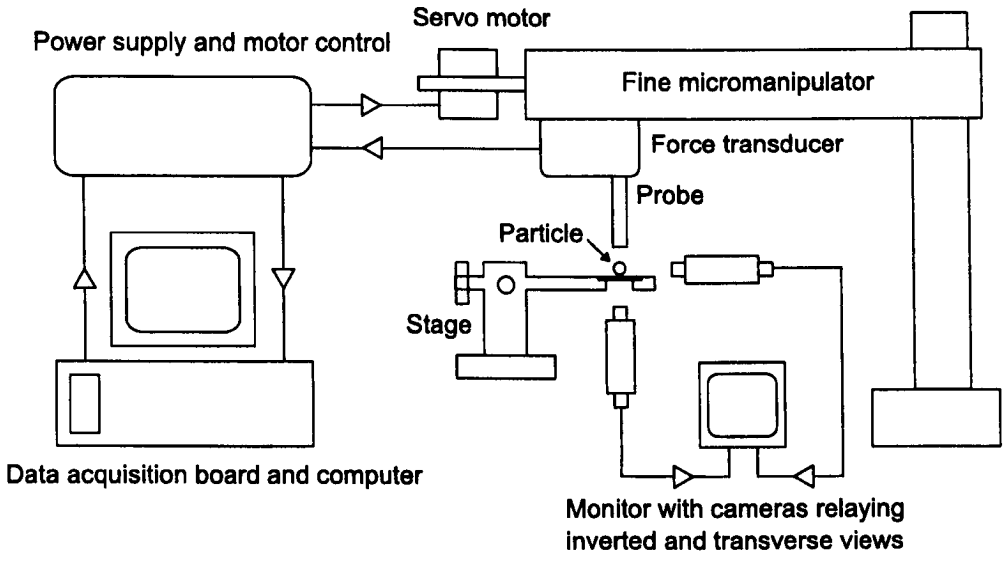

Figure 5.1: A schematic of the micromanipulation rig

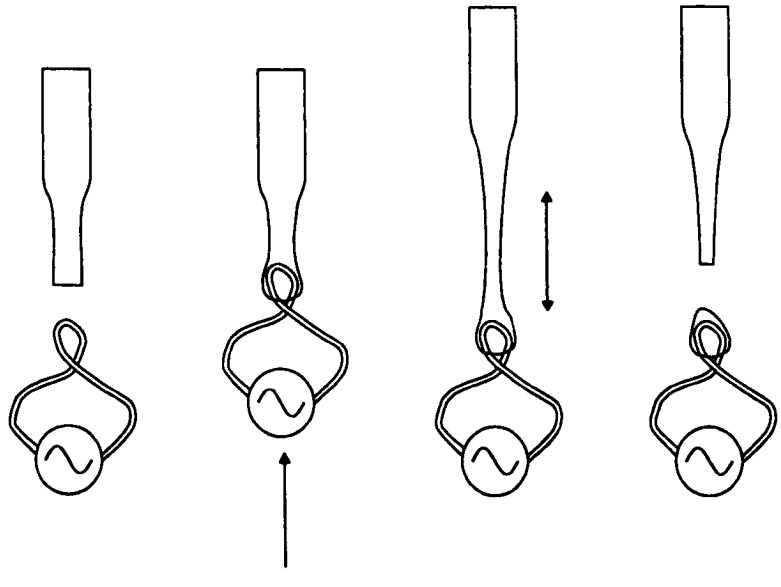

Figure 5.2: The drawn glass probe brought into proximity with a stage-mounted filament. The filament is heated and raised to meet the probe tip, which it melts. The molten probe tip is drawn and breaks to yield a finer tip.

5.2.2 The Experiment

An aliquot of each studied dispersion was diluted to 1 % of its initial concentration. A drop of the diluted dispersion was then placed on a portion of microscope slide. Initial experiments were attempted while the droplet persisted, but the particles were so small that their rapid Brownian motion prevented them from being accurately placed beneath the probe. All experiments thereafter were carried out on slides whose samples had been air dried. The individual slides were placed on the microscope stage and manovered with the stage's translational controls so that the discrete, stationary particles could be positioned directly beneath the probe. The probe tip was then manually lowered to a safe distance above the particle, ensuring no clash between the probe and the slide surface could occur. Probe descent was then initiated and controlled by computer. Descent proceeded until the cutoff voltage was reached. The probe was then withdrawn by computer control. The probe tip was regularly cleaned by a fine tissue twist moistened with acetone. At least 20 repeat runs were attempted for each particle class in each examined series.

5.3 Results and Discussion

5.3.1 Force Transducer Sensitivity

In these experiments a Cambridge Technology Series 400A 0.05 g force transducer system was used, which was the most sensitive commercially available. Prior to probe attachment, it was necessary to determine the transducer sensitivity (the force per volt). To achieve this the masses of small weights, formed from paper and Blu-tak, were measured with a four-figure balance. The transducer was inverted and secured to a bench top. The weights were applied to the transducer and the output voltage was recorded from a voltmeter. A plot of applied load against voltage gives a linear relationship whose gradient is the sensitivity (Figure 5.3). The determined value for this transducer was 58.2 $\mu NV^{-1} \pm 2.7$ %.

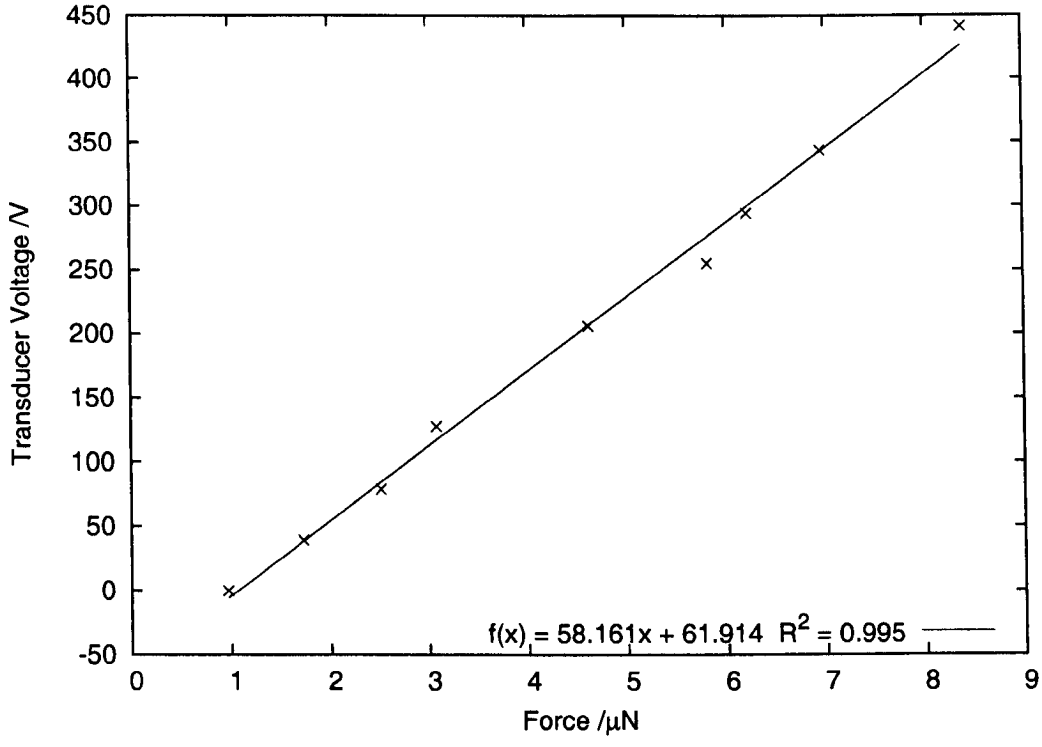

Figure 5.3: Transducer sensitivity determination

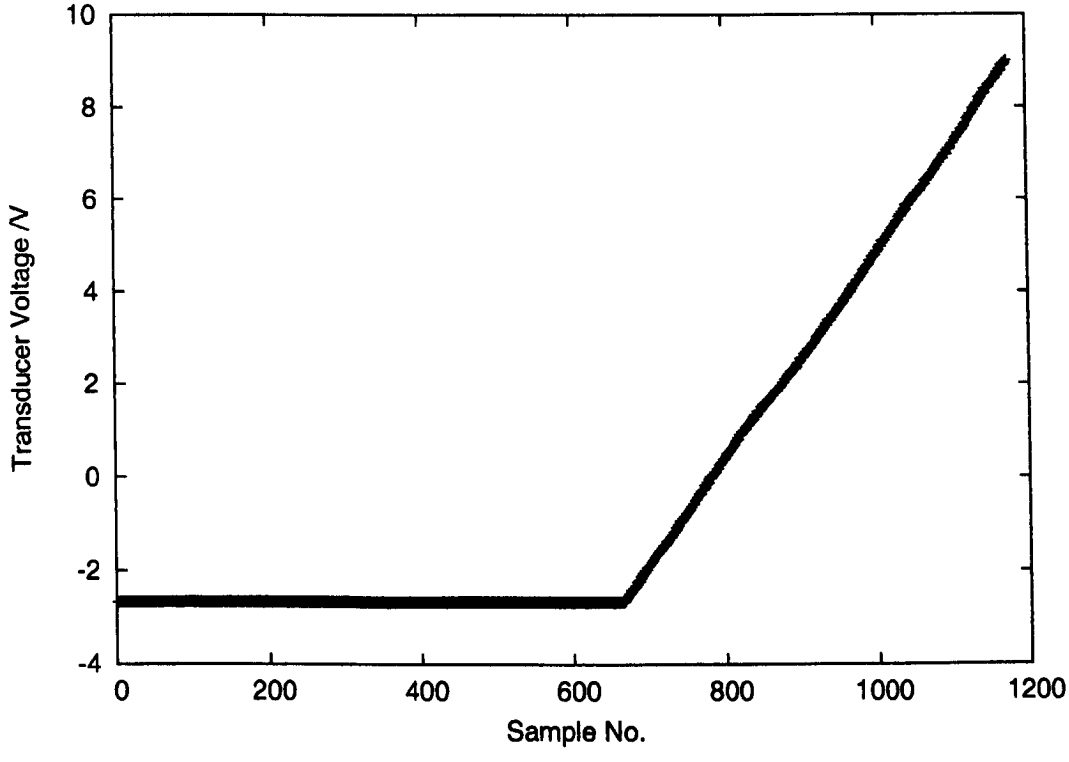

Figure 5.4: Raw transducer data recorded from probe depression upon an empty slide. The zero-gradient region occurs as the probe moves through air, while the non-zero region is generated as the probe is impeded by the slide.

5.3.2 Probe Compliance

During probe depression onto a surface there may be some compression or movement within the probe array. It is necessary to determine the probe compliance so that it may be factored into the data analysis. Probe compliance was determined by monitoring the voltage output from the transducer as the probe was lowered, under computer control, and pressed to tolerance onto a clean glass microscope slide. A plot of transducer voltage against sample number, n, shows a $\frac{dV}{dn} = 0$ region, corresponding to the probe moving through air, and a $\frac{dV}{dn} \neq 0$ region corresponding to contact with the slide (Figure 5.4). Compliance, C in μm/μN, is given by equation 5.3.1.

$$C = \frac{t_a v_p}{S} \left(\frac{dV}{dn} \right)_a^{-1} \tag{5.3.1}$$

t_a is the acquisition time in seconds, v_p is the probe velocity in μms^{-1}, S is the sensitivity in μNV^{-1}, while $\left(\frac{dV}{dn}\right)_a$ is the average of non-zero gradients from multiple probe depressions onto an empty slide (Figure 5.5). The compliance determined for the principal probe array used in this study was 0.015 μm/μN $\pm$ 4.5 %.

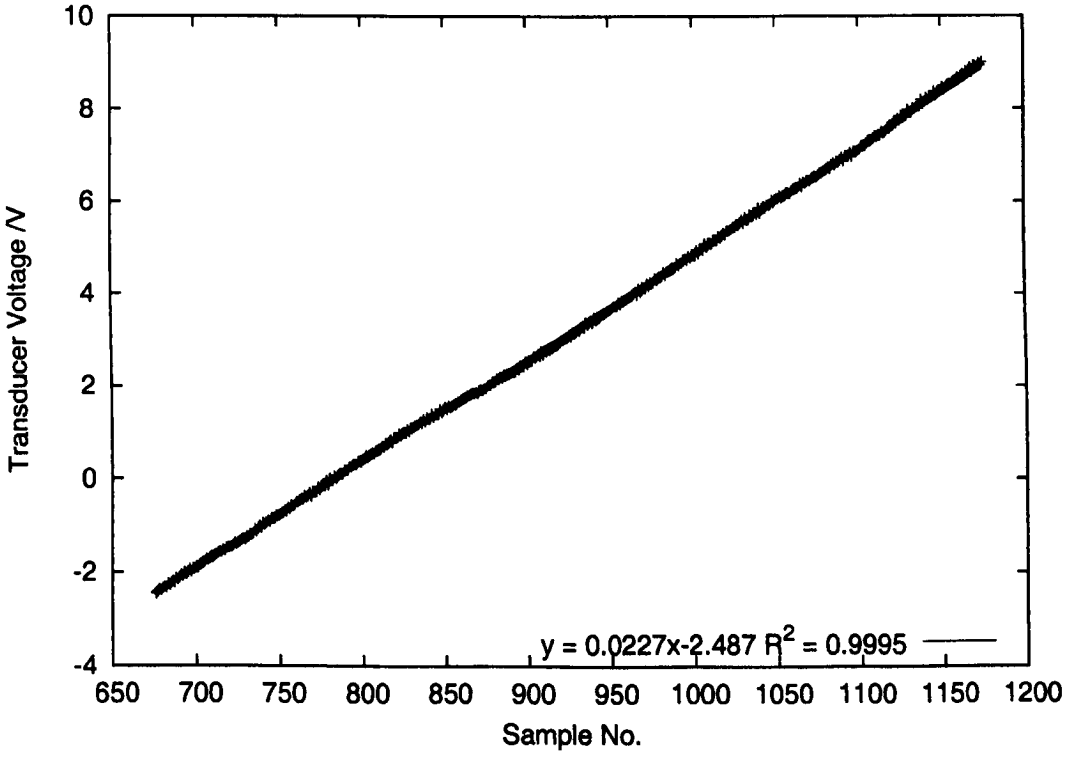

Figure 5.5: Example compliance data

5.3.3 Data Analysis

The experimental raw data consists of transducer voltage corresponding to sample number. As with the compliance experiment, a plot of voltage against sample number reveals an initial zero gradient corresponding to unhindered probe descent. When the probe comes into contact with the particle there is a corresponding increase in voltage until the particle bursts, resulting in a sharp drop or discontinuity (Figure 5.6). The voltage then briefly returns to its unhindered value until it meets the slide surface or particle remnants adhered to it, whereupon the voltage climbs sharply.

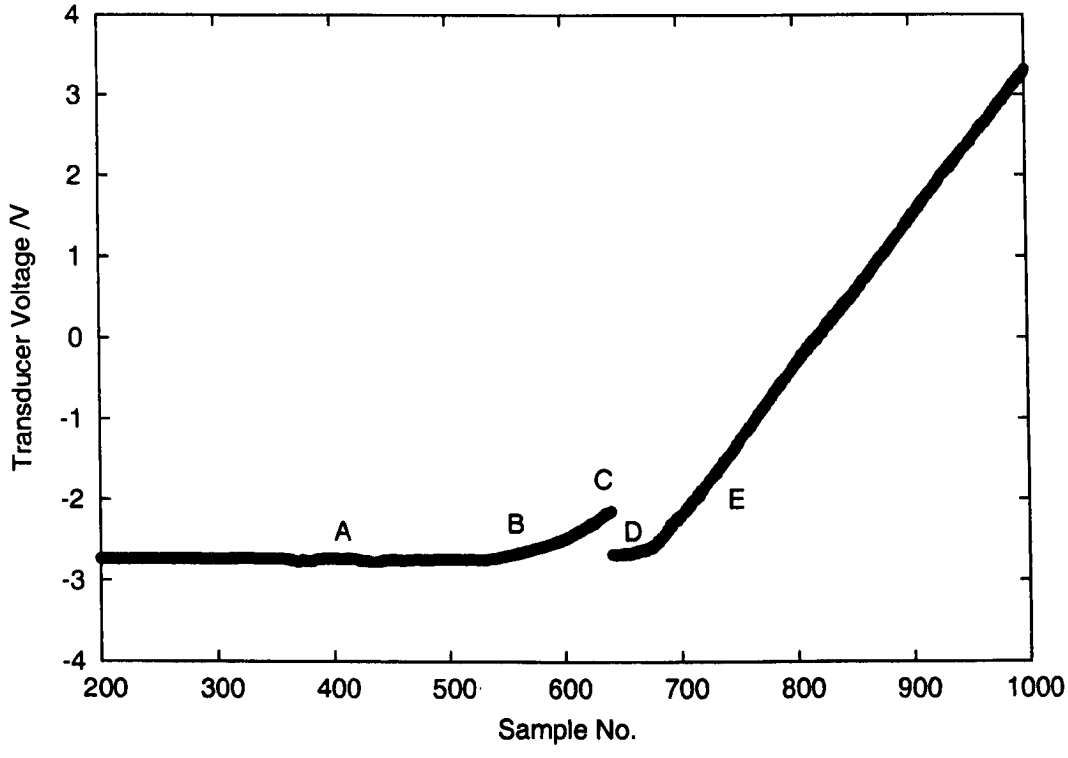

Figure 5.6: Example raw data from a particle compression experiment; this is a particle produced by the secondary DMDES method. The probe is unhindered in region A, meets resistance from the particle at B, which breaks at C. At D the probe is unhindered until it nears the slide surface before E.

A base-point voltage, V_b and sample number, n_b, corresponding to the moment immediately prior to the probe's contact with the particle is determined by inspection of the plotted raw data: in Figure 5.6 this is the point from which the voltage begins to climb in region B. The inverted sample rate was set at 0.019 s, which allows the elapsed time, t_i, at any given

sample number, n_i, to be calculated:

$$t_i = n_i - n_b + 0.019(i - b) \tag{5.3.2}$$

The probe's raw displacement, s_i, is calculated using the known v_p (1 μms^{-1}):

$$s_i = v_p t_i \tag{5.3.3}$$

The applied force is calculated using the sensitivity, S, and the transducer voltage:

$$F_i = SV_i \tag{5.3.4}$$

The raw displacement may then be corrected for probe deformation during the experiment using the determined compliance:

$$s_{ci} = s_i - (F_i C) \tag{5.3.5}$$

Calculation of these parameters allows a plot of force against probe displacement from the point of initial contact with the particle until the probe presses onto the slide surface (Figure 5.7). The breaking force may then be determined for the individual particle, together with the extent of particle deformation at that point.

If more than one particle was present under the probe, then multiple breaking points are observed in the force/displacement plot (Figure 5.8).

The shape of the curve, prior to rupture, may be explained through consideration of the two main contributions to the force profile [97]. Compression of a hollow capsule is resisted by an elastic response, F_{elast}, from the wall material [89, 97]:

$$F_{\text{elast}} = \frac{Eh^2 x}{R(1-\sigma)\sqrt{[6(1+\sigma)]}} \tag{5.3.6}$$

Where E is the Young's Modulus, h is the shell thickness, x is the displacement, R is the capsule radius and σ is the Poisson ratio: the ratio of strain perpendicular to the applied stress to

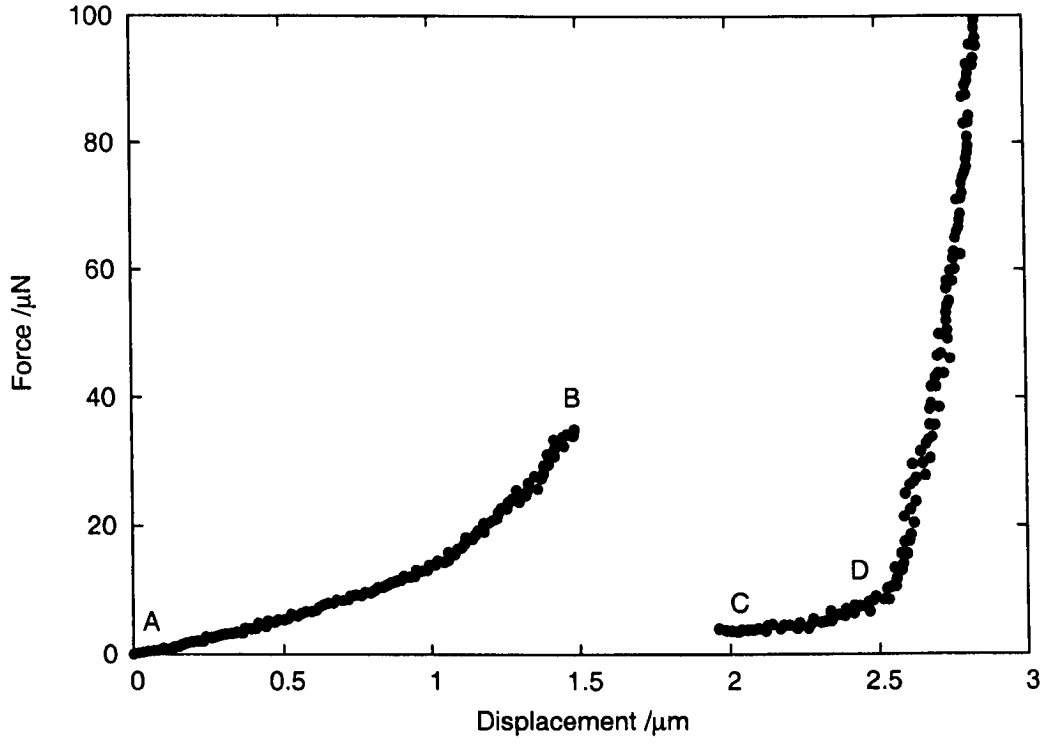

Figure 5.7: Processed data from a particle compression experiment using a particle produced by the secondary DMDES method. The probe meets the particle at point A, the applied force builds until the particle breaks at point B. The probe meets no resistance until C when it begins to compress the particle debris. At D the probe connects with the slide surface. The displacement from point A to point D serves as an estimate for the particle size.

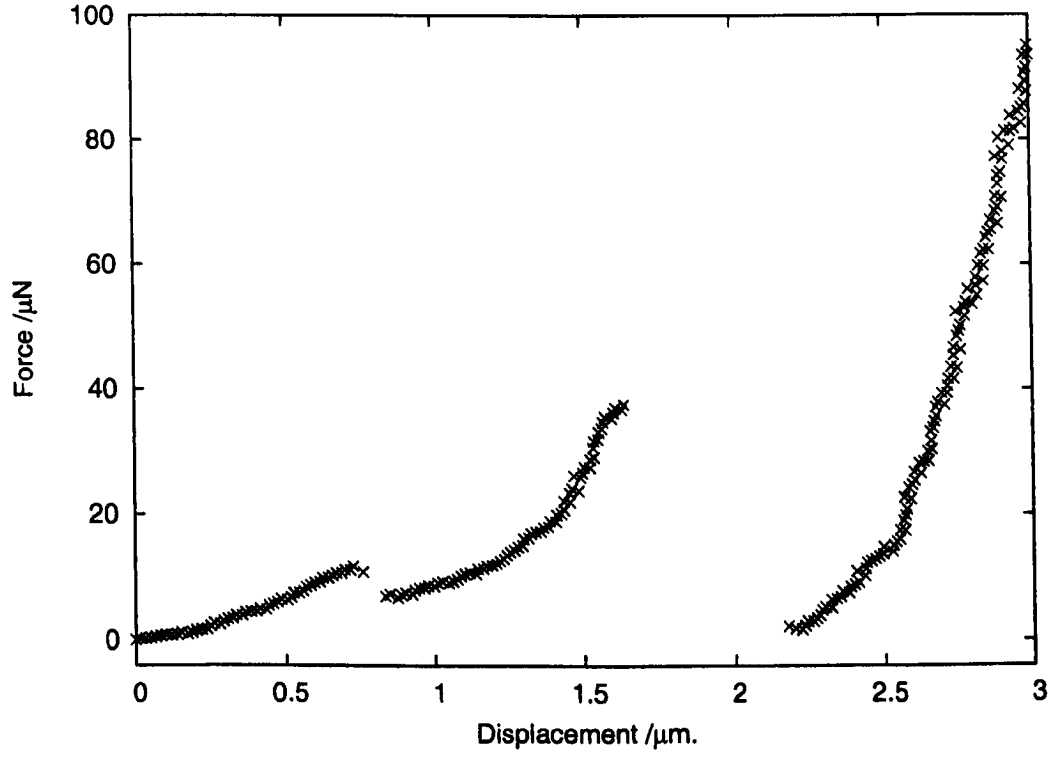

Figure 5.8: Multiple peaks show the presence of more than one particle

the strain parallel to that stress, or, more simply, a measure of a material's tendency to bulge during compression. The σ value is unknown, but can be assumed to be $\frac{1}{3}$ for a compressible polymeric material [79, 89, 97, 63]. Incorporating this value for σ into Equation 5.3.6 gives:

$$F_{\text{elast}} \simeq \frac{2}{3}\frac{Eh^2x}{R} \tag{5.3.7}$$

If the capsule wall is impermeable to the incompressible core material, at least on the compression timescale, an additional restoring force arises due to capsule stretching to maintain a constant volume [89, 97]:

$$F_{\text{volume}} \simeq \frac{2}{3}\frac{\pi Ehx^3}{R^2} \tag{5.3.8}$$

The deformation at which the linear relationship is succeeded by the cubic regime may be determined by balancing the two terms:

$$x_{\text{cross.}} \approx \left(\frac{hR}{\pi}\right)^{\frac{1}{2}} \tag{5.3.9}$$

Figure 5.9 is a plot of the two force contributions.

5.3.4 The Examined Particles

Five types of particle series were examined with the micromanipulation technique:

Zoldesi Shell thickness controlled by delaying the time of TEOS addition following core PDMS formation (see section 4.3)

Secondary DMDES Shell thickness controlled by the concentration of a secondary addition of DMDES (see section 4.4). The Secondary DMDES method consisted of two series: particles formed in 1 % and 2 % aqueous NH_3 environments respectively.

Varying TEOS Shells formed with fixed DMDES, but varying TEOS, concentrations (see section 4.6)

Shell Quench Shell thickness controlled by shelling step quench time (see section 4.5)

MTES Shell Shells formed from varying DMDES/MTES compositions (see section 4.7)

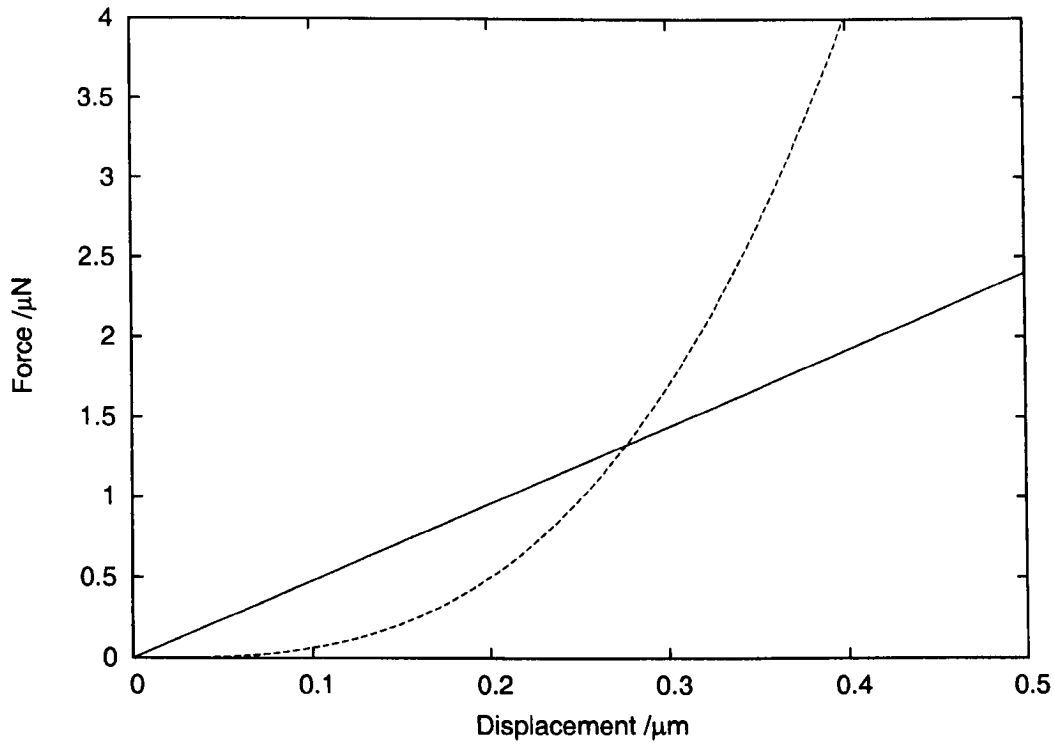

Figure 5.9: The linear elastic (Equation 5.3.7) and cubic volume-constraint (Equation 5.3.8) contributions to the force-deformation profile. For the purposes of illustration, E, h and R were assumed to be 1000 MPa, 0.12 and 2 μm respectively, which approximate measurements made in this study.

5.3.5 Particle Compression: Zoldesi Particles

Five classes in this Zoldesi series yielded curves with breaking peaks, such as in Figure 5.10. Comparisons of force-deformation curves obtained from the micromanipulation measurements with the force contributions described in Section 5.3.3 and illustrated in Figure 5.9, show both linear and cubic regimes in the force-deformation profile, which indicates the shell material is impermeable to the core during compression. Furthermore, analysis of the linear regimes in each force-displacement plot allows estimation of E.

Surprisingly, no breaking force could be determined for Zoldesi Method particles that had been formed with a TEOS addition time of 24 hours, which are the thickest shells of the series. Representative force/displacement data for this particle class is shown in Figure 5.11. The plot shows that the force climbed as the probe tip met the particle, but no clear breaking peak is apparent before the probe connected with the slide surface. Prior to probe contact with the slide, an apparent cubic regime is observed, again suggesting shell impermeability. It is possible that the shell did not rupture until immediately prior to the probe's contact

with the slide, which suggests substantial compressive deformation. Breakage effectively muffled by high compression has been observed in other polymer-shelled systems with high h/R ratios using this technique [80]. Though this particular class represents the highest h/R ratio in the examined Zoldesi series (approximately 11 % based upon microtomy and SEM measurements) particles with higher h/R ratios yielded measurable breaking forces (see Section 5.3.6).

During contact with the slide surface, the probe tip was observed to drift on the feed from the inverted microscope. This suggests that the probe surface was not quite parallel with the slide surface. It is possible that some particles may have been insufficiently compressed, or displaced, prior to the probe's leading edge reaching slide surface (Figure 5.12); subsequent rupture could then be masked by the probe-slide contact force profile.

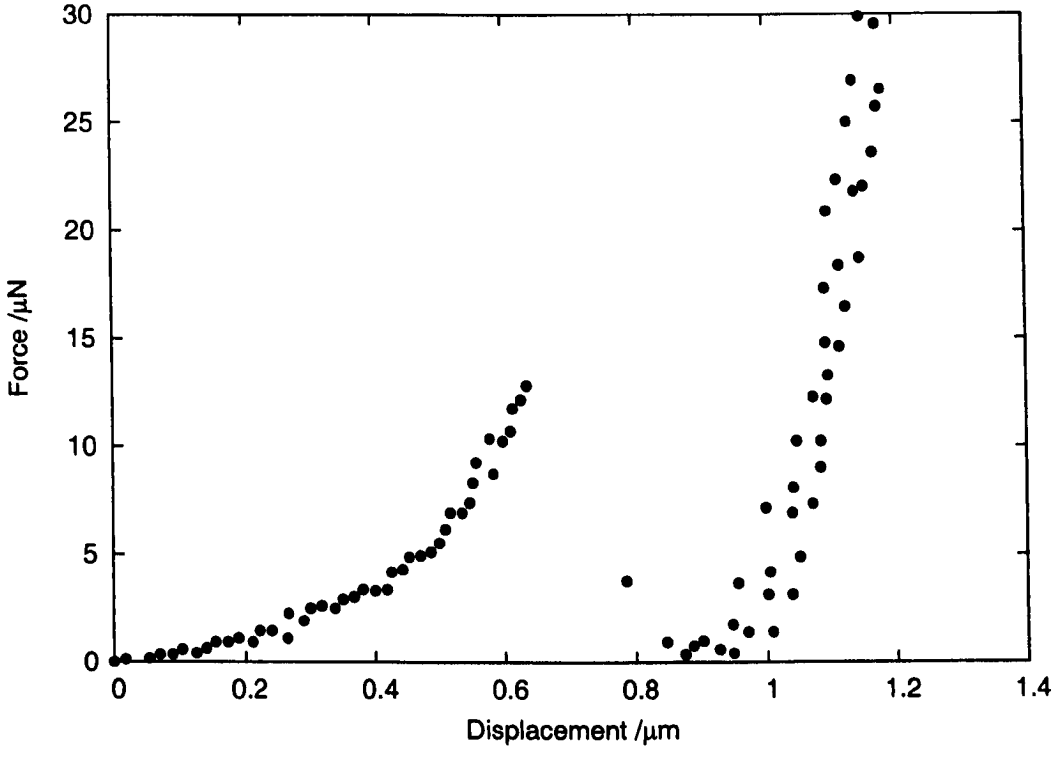

Figure 5.10: A representative force-displacement profile for the Zoldesi series. An initial linear relationship is observed that is succeeded by a cubic trend prior to rupture.

For a probe inclination angle of θ, the gap b between the slide and the probe plane along the adjacent dimension a may be calculated by

$$b = a\tan\theta \tag{5.3.10}$$

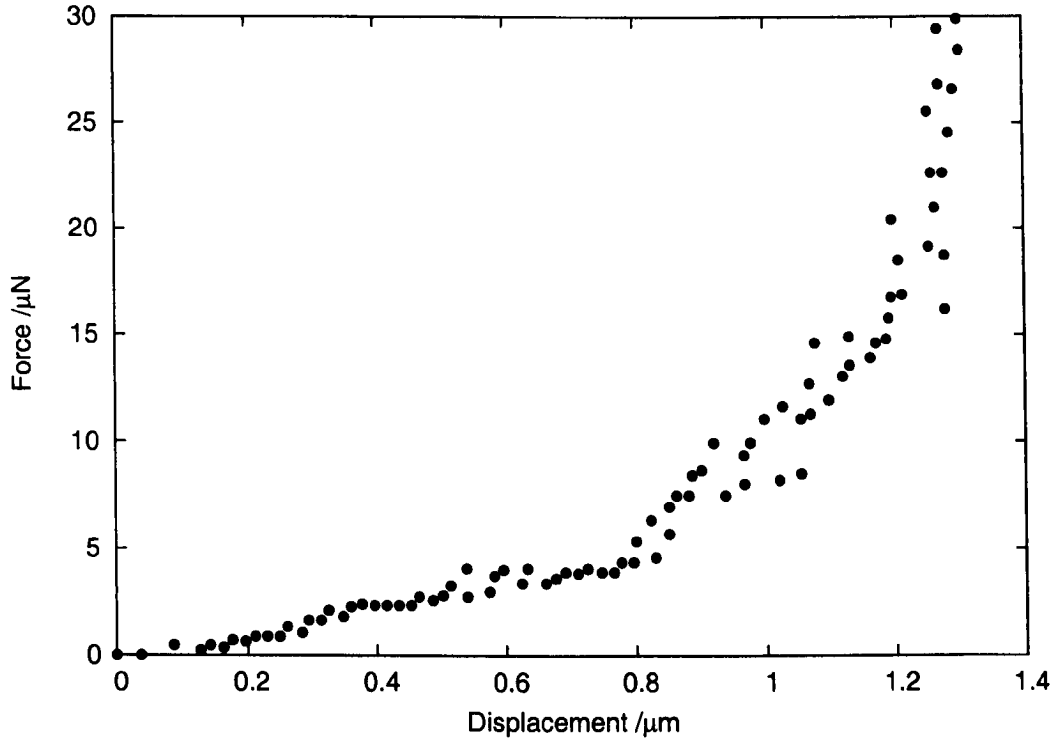

Figure 5.11: A force-displacement profile for the thickest-shelled of the Zoldesi series. No clear breaking force was observed for this particle class prior to the probes contact with the slide. Both the linear and cubic relationships are apparent.

Figure 5.13 shows the effect of varying θ on the plane separation b along an adjacent distance a corresponding to the probe tip diameter, which was estimated to be 20 μm. For small values of θ the centre of the probe would correspond to an a value of 10 μm, where a θ deviation of 1° would result in a gap of 175 nm at point of contact. To minimize the gap at probe-slide contact at the compression locus, the leading edge of the probe was determined, and all particles were consistently placed near it prior to their experimental run, rather than in the centre (Figure 5.14). Despite these measures, a breaking force was still not be determined for the thickest Zoldesi system.

Compression of the Zoldesi Method particles revealed a declining trend in breaking force relative to TEOS addition delay time (Figure 5.15). With increasing delay time, the shell thickness decreases (Figure 4.11, Page 42). At 68 hours there is a deviation from the apparent trends in both Figure 5.15 and Figure 4.11, which signifies an anomalous shell thickness rather than an anomalous breaking force. When breaking force is plotted against shell thickness, as determined by microtomy, there is an apparent linear correlation (Figure 5.16).

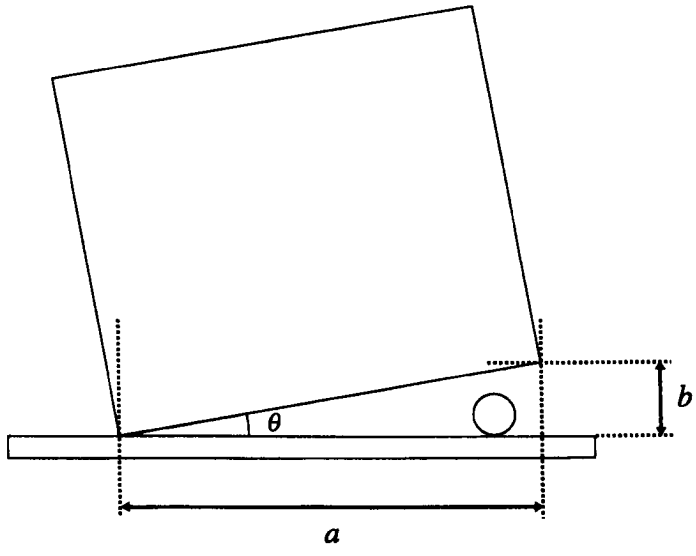

Figure 5.12: An inclination of angle θ gives a gap of height db at a distance da from the point of initial contact

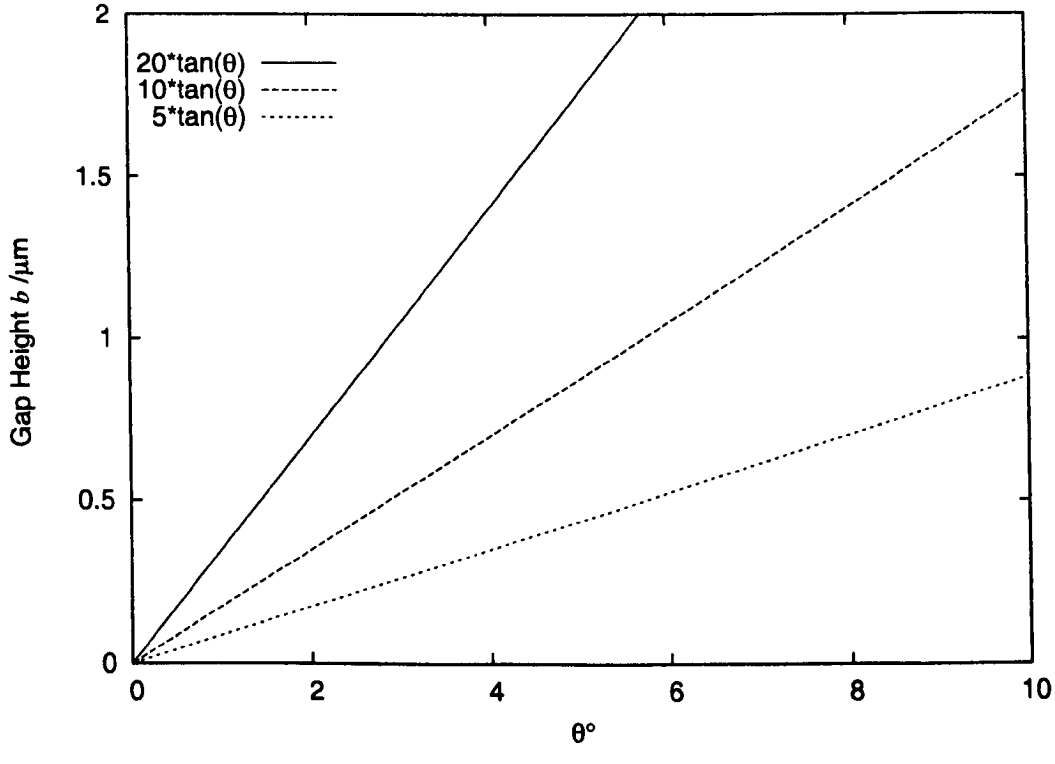

Figure 5.13: A plot of gap height b as a function of probe angle θ for various values of a

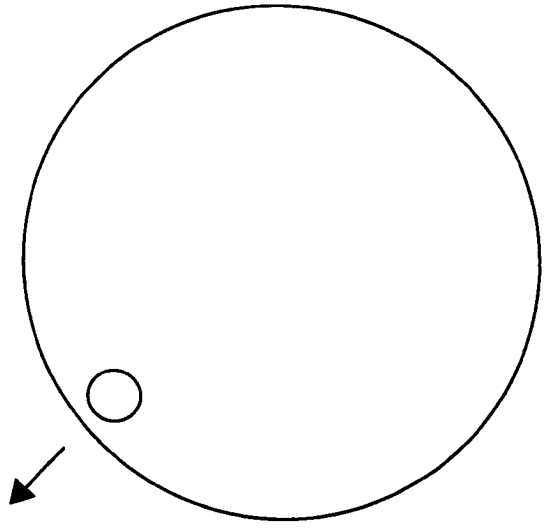

Figure 5.14: The particle is positioned under the leading edge of the probe to determine the sweet spot. Illustrated as viewed with the inverted microscope. The arrow indicates the drift direction.

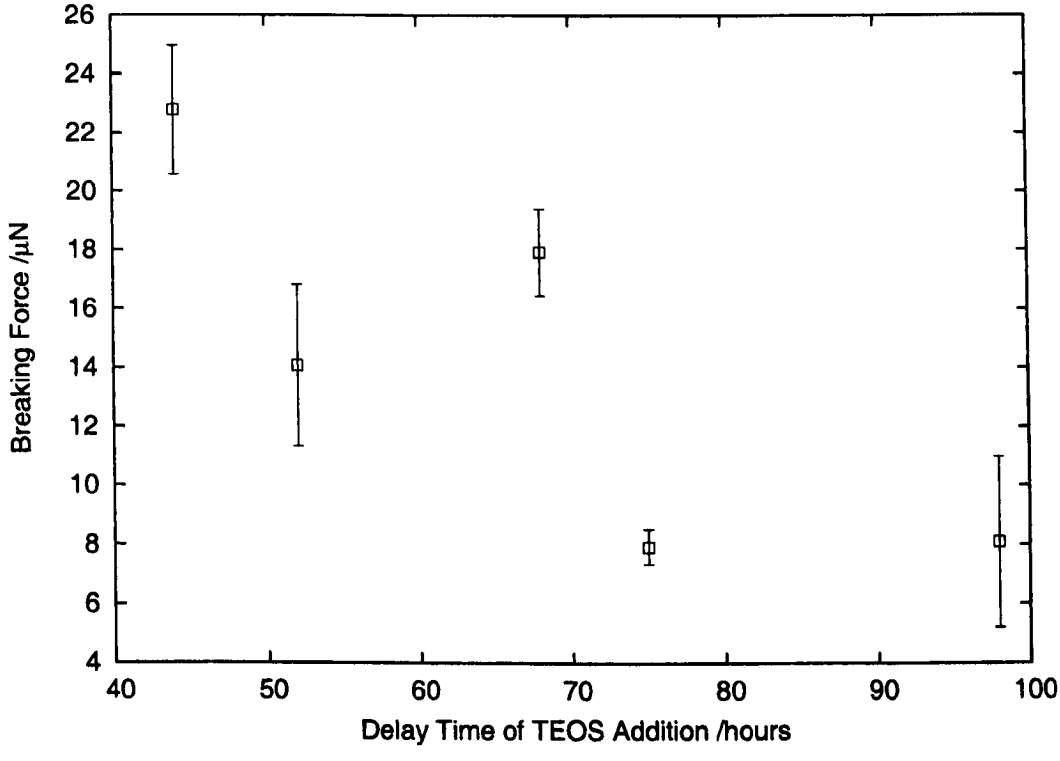

Figure 5.15: Breaking force results from a series of particles produced by the Zoldesi method. Delay Time refers to the time of TEOS addition following initiation of PDMS formation. The declining trend should correspond with thinning shells with time. Error bars correspond to the standard error in the data in this and all succeeding graphs.

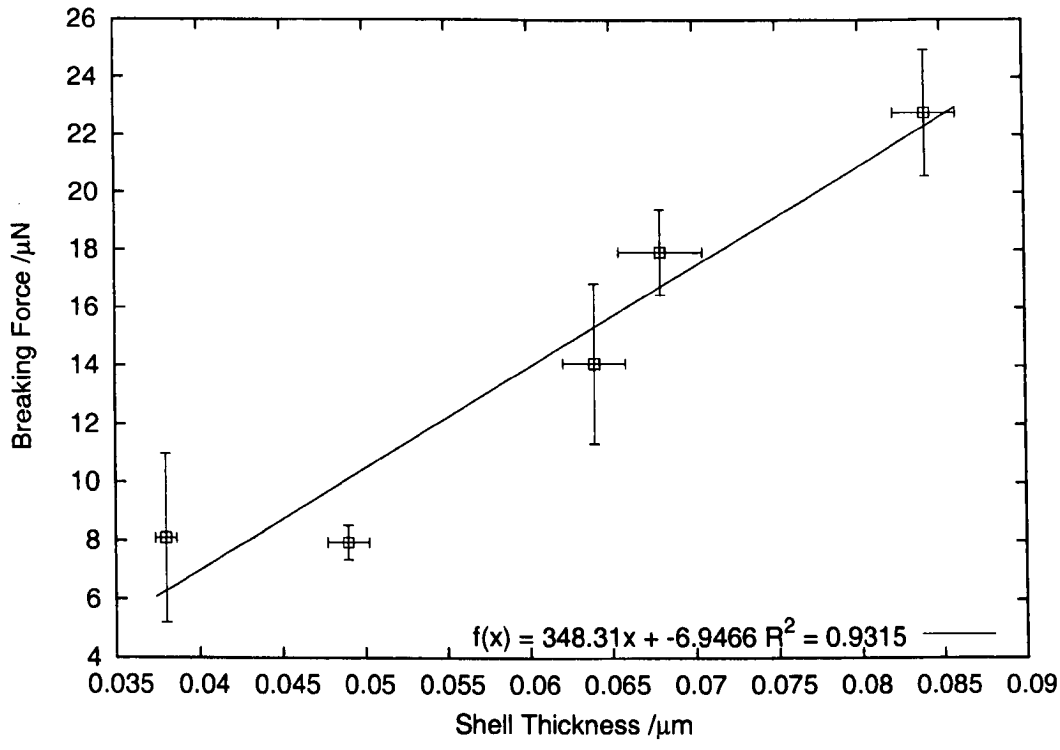

Figure 5.16: Breaking force data from the Zoldesi series correlated to shell thickness as determined by microtomy

Maximum probe displacement is a measure of the distance travelled by the probe from the point of contact with the particle until the point of contact with the slide. This measurement can be used to estimate particle size, with the corollary that probe inclination could impose an error. Figure 5.17 plots the particle diameters for the Zoldesi series as determined by the maximum probe displacement, with the inclusion of SEM measurements for comparison. The displacement measurements record smaller values than their SEM equivalents. This is not surprising, as the SEM samples tended to be in a dessicated and, on occasion, hemispherical state that could lead to an overestimate of size. In contrast, the probed samples, though air dried, were observed to release liquid as they burst. Though they appeared spherical, their may have been some oblate deformation due to gravity, the extent of which would depend on shell elasticity, thickness and particle size. Combined with possible systematic error due to probe inclination, the probe displacement measurements could be regarded as underestimates. Though the magnitudes of the size measurements vary between the two methods, the general relative trend in size with addition time is reproduced, most notably with the deviation at 68 hours in both cases. Though breaking force and shell thickness did

show a linear correlation (Figure 5.16), this trend does not account for the effect of varying particle size across the series. Plotting breaking force against the h/R ratio, using radii determined from probe displacement measurements, shows little correlation (Figure 5.19). A plot of the same variables, but this time using SEM data for the radii, shows an increase in breaking force with thickness/size ratio (Figure 5.20). The improved correlation in this new plot does not necessarily indicate that the SEM measurements are more reliable than those determined by probe displacement.

Particle breaking compression may be calculated by dividing the probe displacement at breaking point by particle size. The breaking compression declines with a linear correlation with increasing TEOS addition delay time, which corresponds to decreasing shell thickness (Figure 5.21). Relating the breaking compression with the h/R ratio shows an increasing trend that seems to plateau (Figure 5.22).

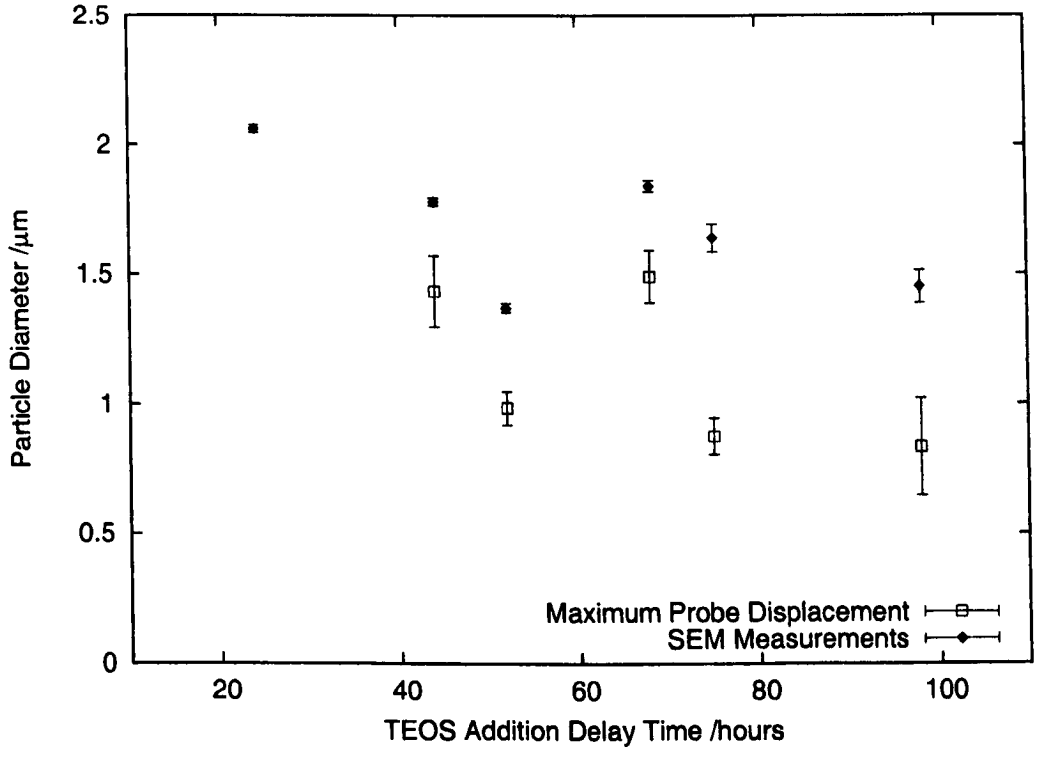

Figure 5.17: Particle sizes for the Zoldesi method series as determined by maximum probe displacement (closed diamonds). SEM measurements are included for comparison (open squares).

Young's modulus (E) values were calculated for each compressed particle using the relationship described by Equation 5.3.7 and a least squares analysis of the linear region for

small deformations $< x_{cross}$ (Equation 5.3.9). The E values were calculated using R values determined by the maximum probe displacement for each compressed particle and also using the average R for each class as determined by SEM. Comparison of E values determined for each particle class in the examined Zoldesi series shows a decrease in E with shell thickness (Figure 5.18). This suggests that the shell material is stiffest in the class with the thinnest shells. The variation in E may also account for the breaking compression trend observed in Figure 5.22.

Considering the E values calculated using the maximum probe displacement in isolation, an argument could be made that only the thinnest shelled system is substantially stiffer, while little correlation between shell thickness and E can be determined for the remaining classes. A more pronounced correlation is evident from the SEM data.

This declining trend implies the nature of the shell material varies across the series. It should be recalled that shell thickness is effectively controlled by the concentration of DMDES residue in the aqueous phase upon addition of TEOS, which acts to cross-link the silicone shell. Zoldesi observed no effect on varying TEOS concentration on shell thickness [36], however, EDX studies showed an apparent increase in cross-linking density with declining levels of DMDES [63]. The thin shells in this case correspond to relatively low DMDES/TEOS ratios, which may promote more extensive cross-linking with a consequential increase in E. Zoldesi determined an E value $\approx$ 100 MPa for particles with shells formed at a single TEOS addition delay time of 20 hours (in 2 % NH_3 and in the presence of Triton X surfactant), which corresponds to a higher DMDES/TEOS concentration ratio than examined in this series [63]. On that basis, and considering the declining trend in E with DMDES/TEOS ratio observed here, these results may be consistent with Zoldesi's value. Zoldesi's E value was determined using shells formed by a quench method. If declining levels of DMDES cause a cross-linking density gradient across the shell thickness, a quenched sample could provide a less cross-linked shell with a lower E.

The E value that corresponds to the thinnest shell in the series approaches that which divides polymers from porous ceramics $\approx$ 10 GPa; all subsequent E values in the series are representative of polymer materials [98]. If cross-linking density is influenced by the

DMDES/TEOS concentration ratio, the decline in DMDES concentration as the shells are grown may cause the shell to be increasingly cross-linked towards the external surface.

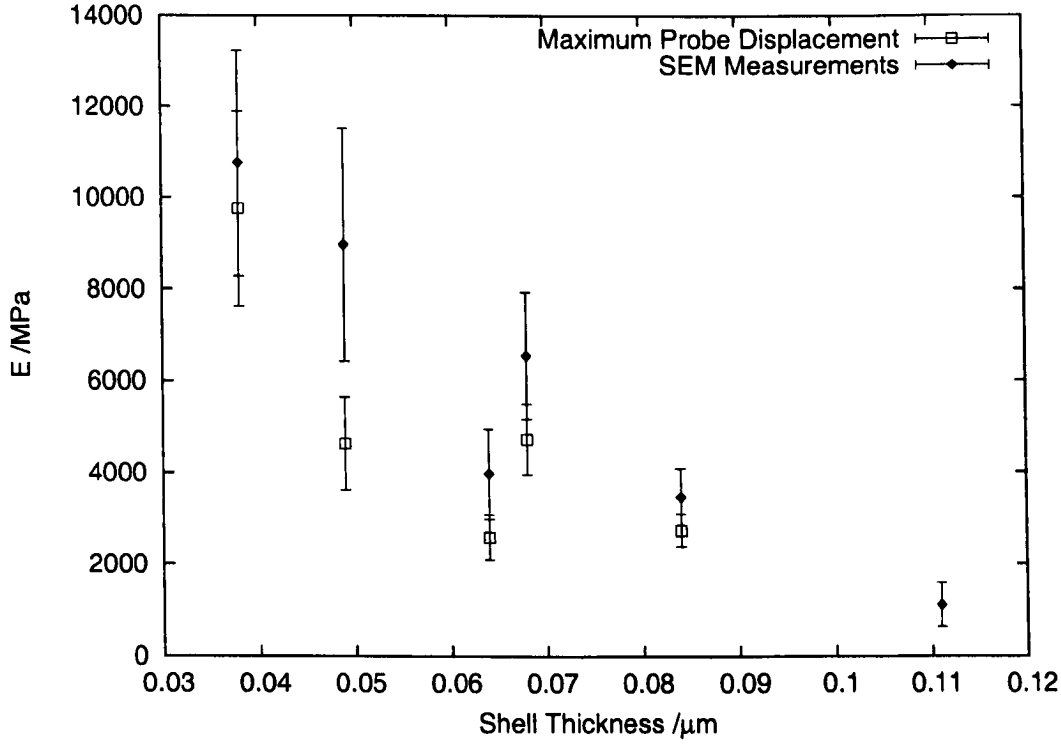

Figure 5.18: The Young's Modulus decreases with increasing shell thickness in the Zoldesi series. The Young's modulus is plotted as calculated using maximum probe displacement measurements (open squares) and SEM measurements (closed diamonds).

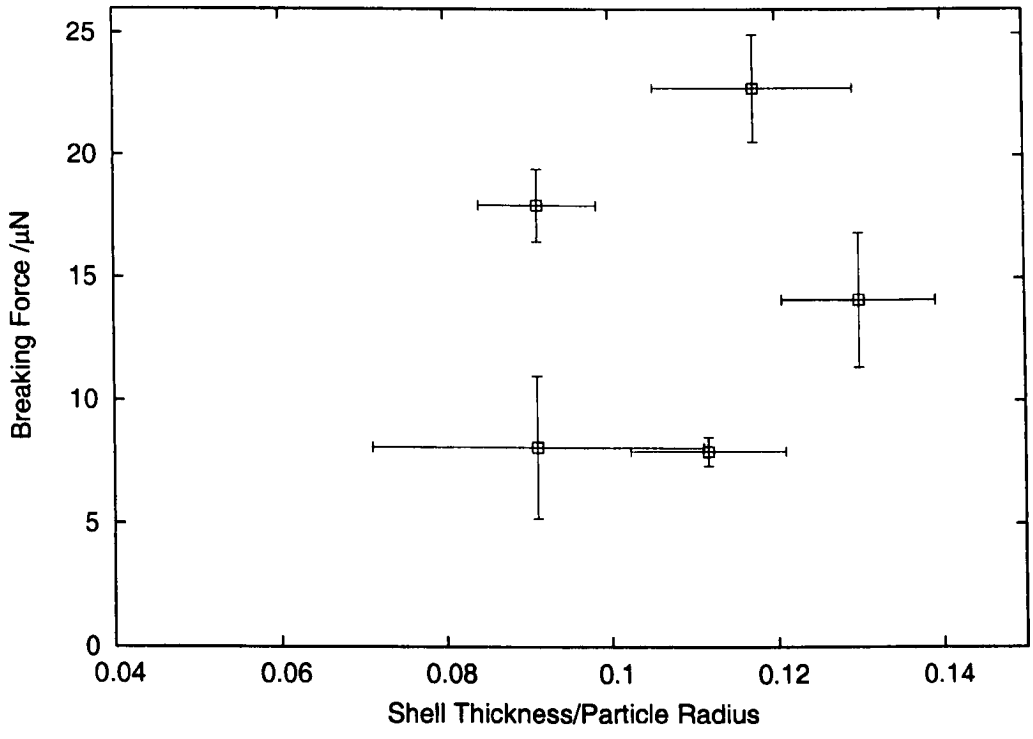

Figure 5.19: Breaking force plotted against the h/R ratio as determined by maximum probe displacement

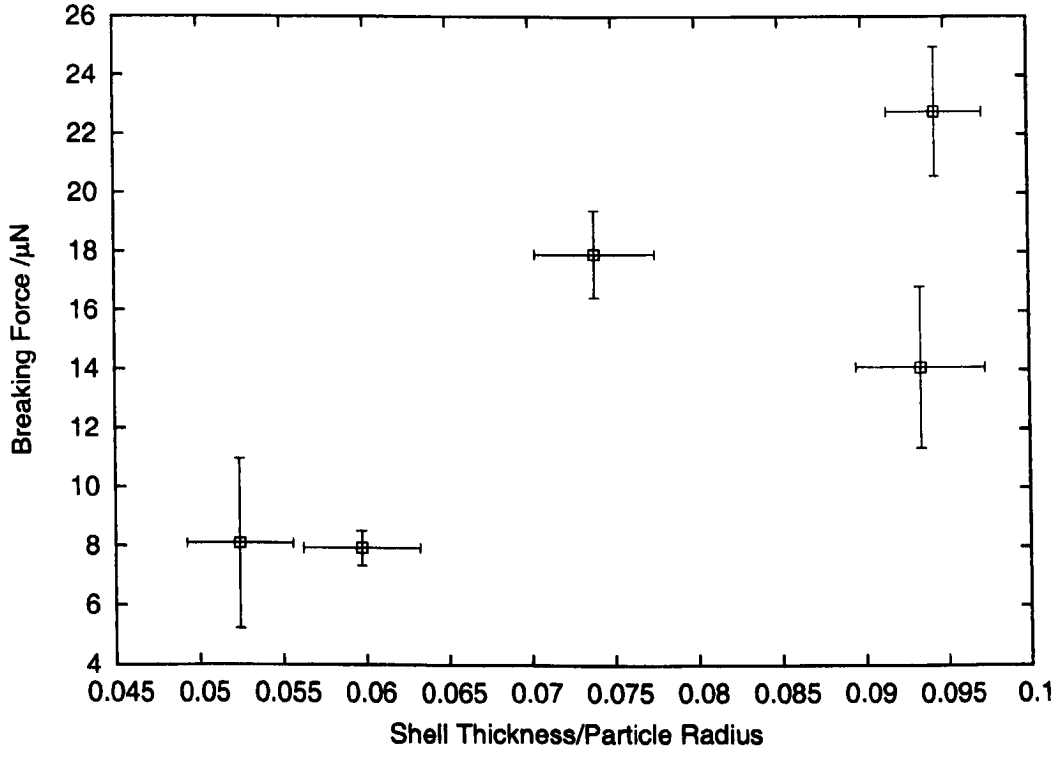

Figure 5.20: Breaking force correlated to the h/R ratio as determined from SEM measurements

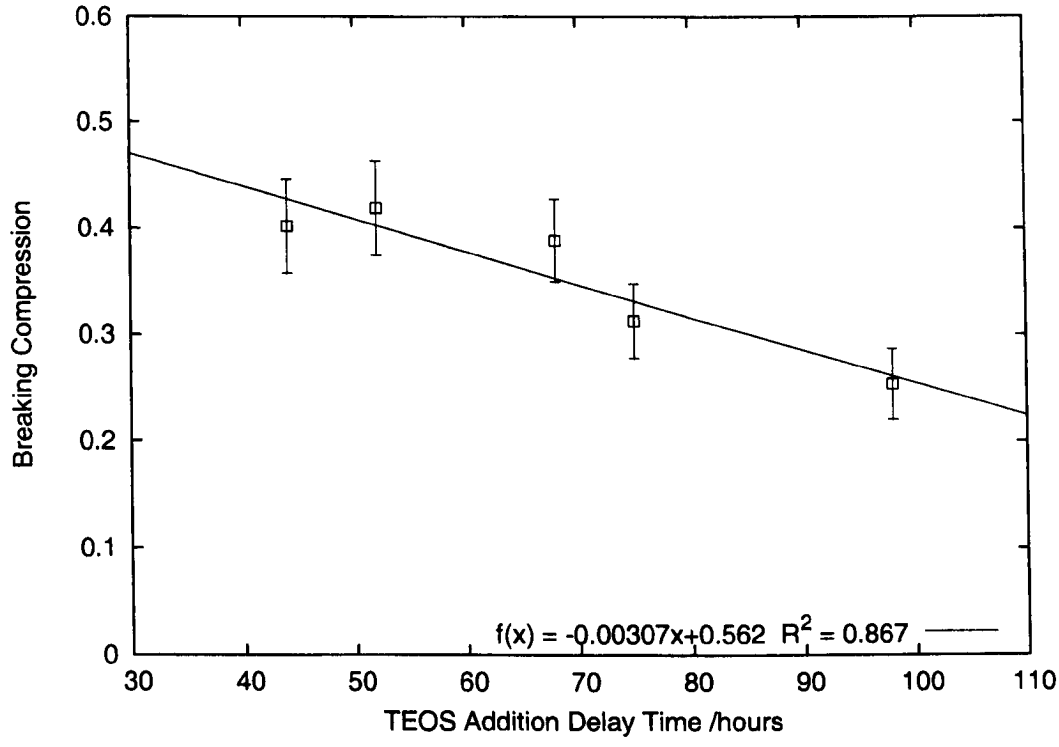

Figure 5.21: Breaking compression data from the Zoldesi series shows a declining linear correlation with TEOS addition time

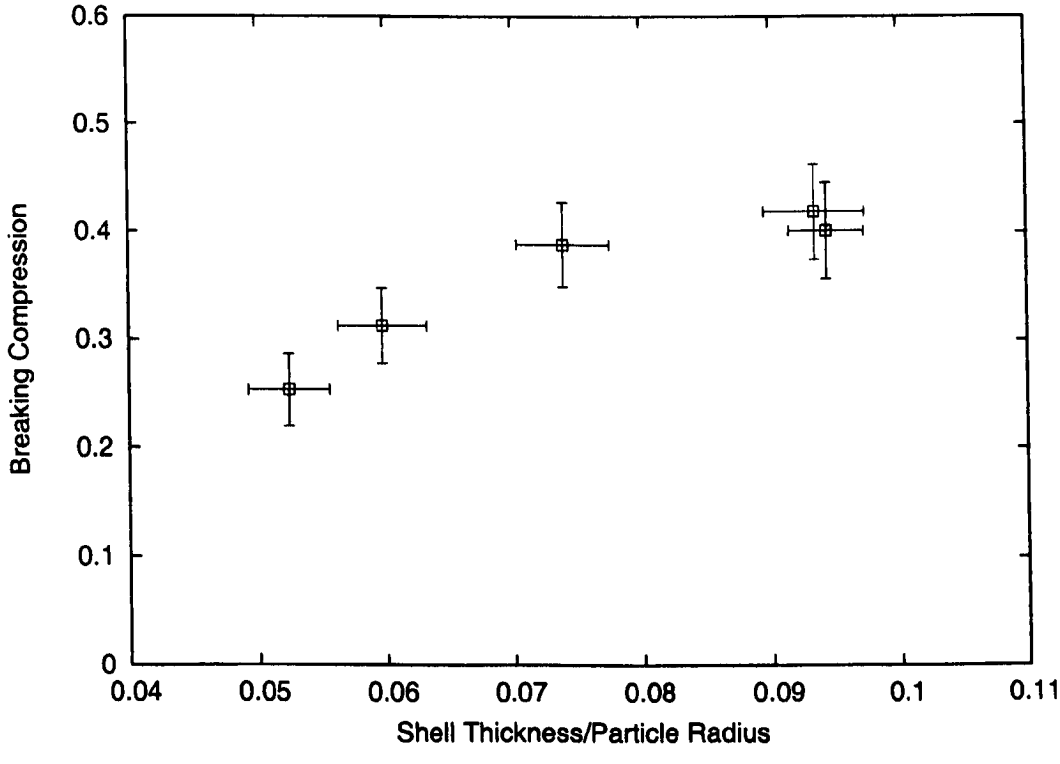

Figure 5.22: Breaking compression plotted against the h/R ratio shows increasing trend that plateaus

5.3.6 Particle Compression: Secondary DMDES Particles

The Secondary DMDES Method controls shell thickness through selection of appropriate DMDES/TEOS concentrations. Unlike the Zoldesi method, the PDMS cores are allowed to mature so that the aqueous DMDES residue concentration declines. A mixture of DMDES and TEOS is then added to form the shell: this is the secondary DMDES addition. Two series were investigated, one that was prepared in 1 % NH_3, the other at 2 % (see Section 4.4.1). Only two of the five classes in the the 1 % NH_3 series exhibited measureable breaking forces. Breaking forces for five classes in the 2 % series were measured.

Compressing Secondary DMDES particles, formed in 2 % NH_3 to rupture revealed an apparent linear trend with increasing secondary DMDES concentration, until after 0.025 mol dm^{-3} whereupon the breaking force was observed to drop (Figure 5.23). No compression measurements were made for the 0.029 mol dm^{-3} class. Shell thickness measurements showed that shells formed in 2 % NH_3 and in excess of 0.025 mol dm^{-3} DMDES tended to be thinner, probably due to enhanced formation of a secondary material (see Section 4.4.3).

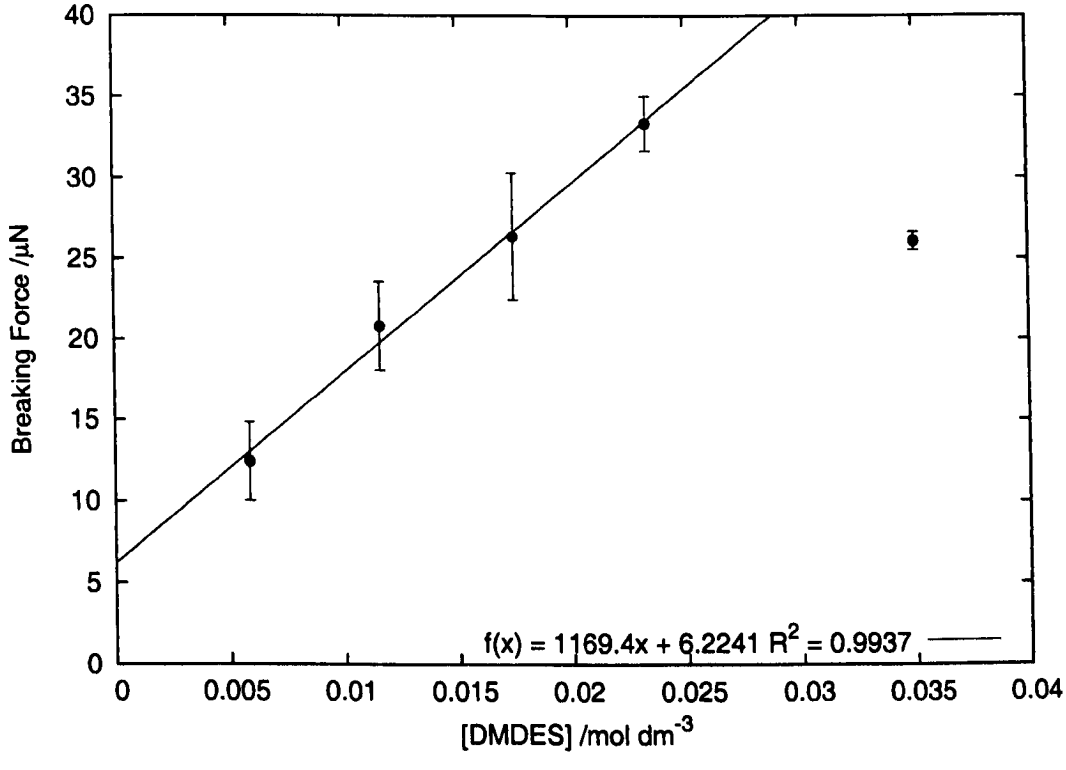

Figure 5.23: Breaking force data for a series of particles prepared by the Secondary DMDES method. The first four data points have an apparent linear relationship.

Plotting breaking force directly against shell thickness reveals an apparent linear cor-

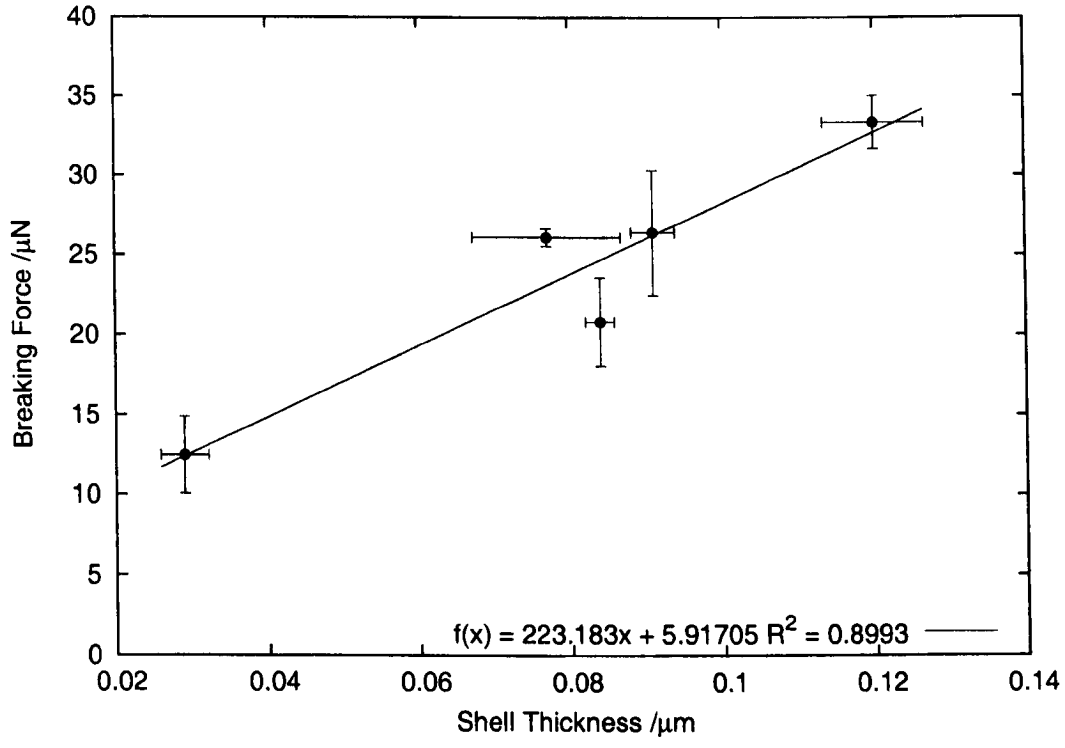

Figure 5.24: Breaking force data for the Secondary DMDES particles correlated to their shell thickness as determined by microtomy

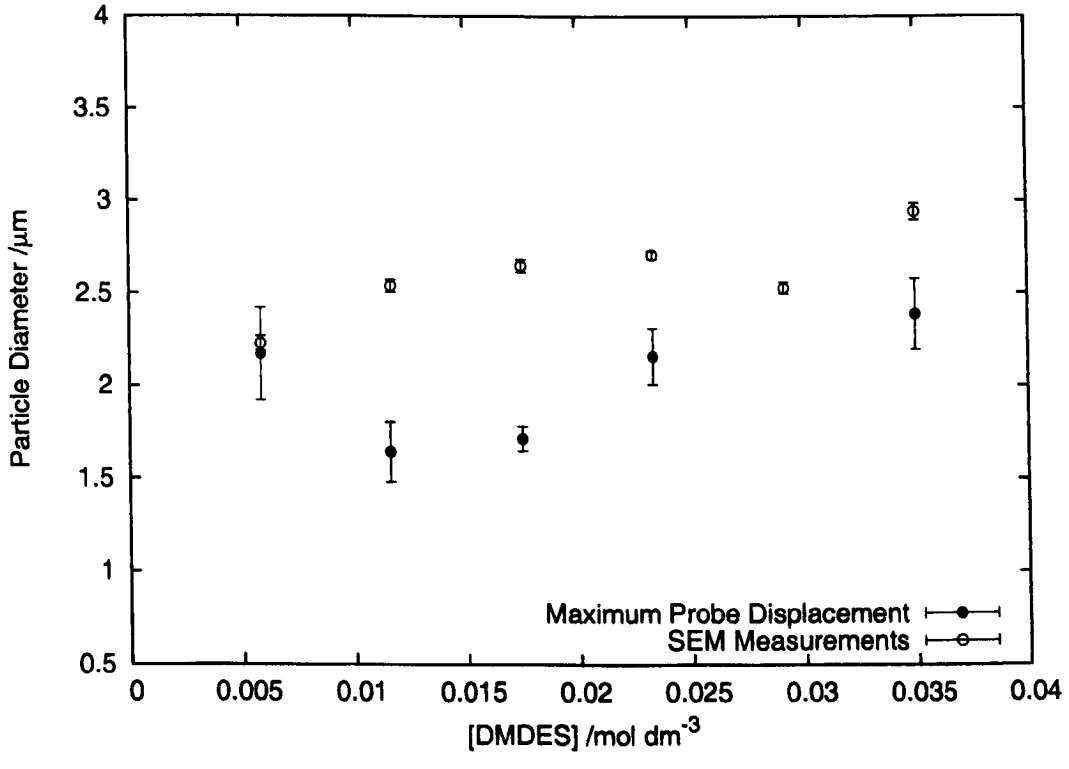

Figure 5.25: Secondary DMDES particle sizes determined by maximum probe displacement and SEM measurements (2 % NH_3 system).

relation for all five data points (Figure 5.24). Comparison of particle sizes determined by maximum probe displacement and SEM shows that, as for the Zoldesi particles, probe displacement gives smaller values (Figure 5.25). Unlike the Zoldesi particles, however, the two methods show different trend profiles. Inspection of the SEM micrographs shows the particles to be less deformed than in the Zoldesi case, and as such the SEM measurements are more reliable (see section 4.4). Breaking force was found to increase with h/R ratios, both for probe displacement (Figure 5.26) and SEM measurements (Figure 5.27), though the latter analysis had an improved linear correlation.

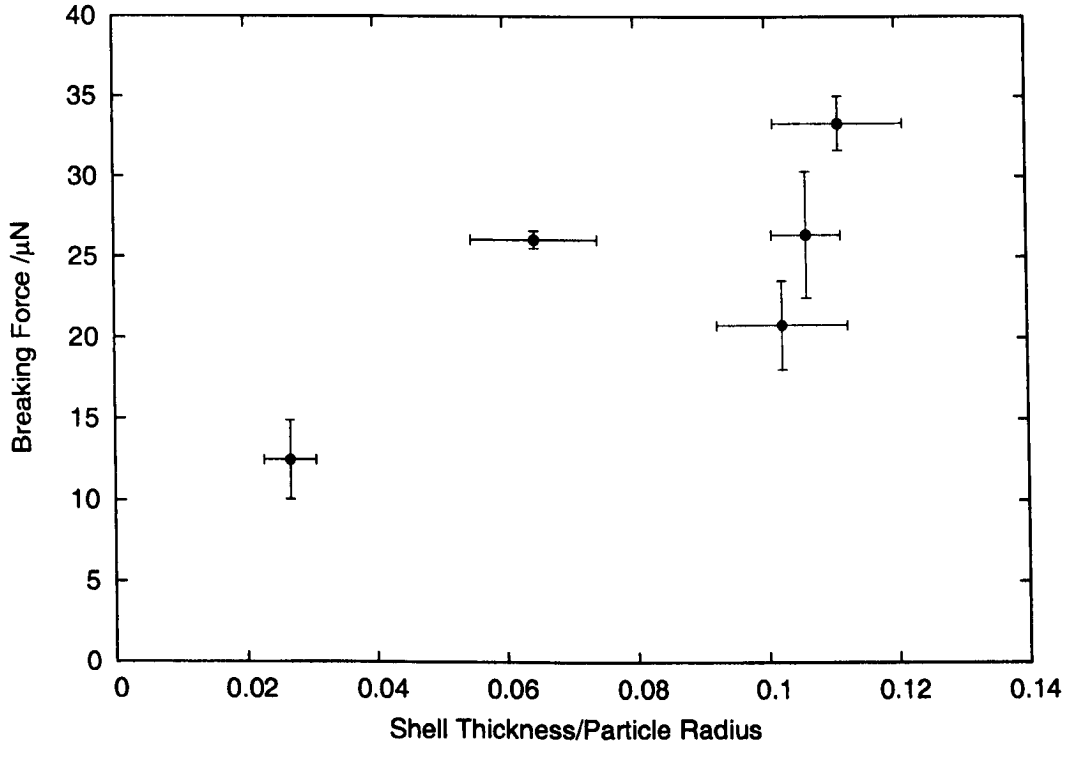

Figure 5.26: Breaking force plotted against the h/R ratio as determined from the maximum probe displacement

Inspection of breaking compression with increasing secondary DMDES concentration shows little variation across the series until the 0.035 mol dm^{-3} class, which has a higher breaking compression (Figure 5.28). Though this was the highest DMDES concentration of the series, the shells were not the thickest. The increase in breaking compression may relate to a reduction in cross-linking density within the shell leading to enhanced elasticity. A plot of breaking compression against h/R ratio for the series shows the high breaking compression measured for the high DMDES particle class does not relate to its h/R (Figure 5.32).

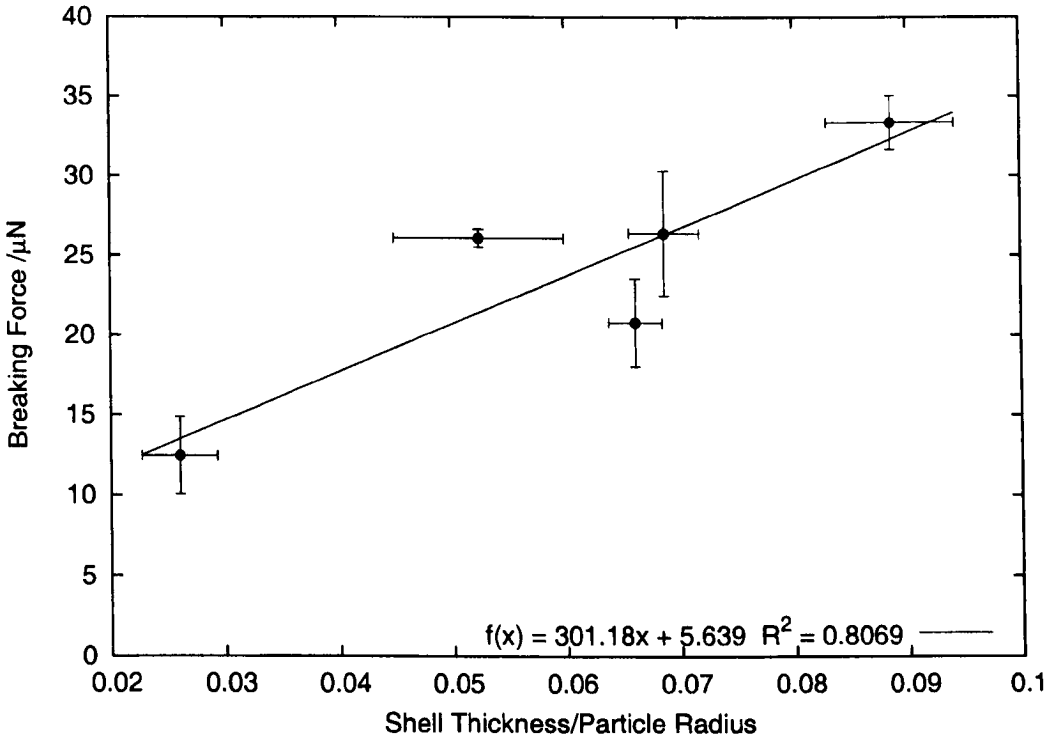

Figure 5.27: Breaking force correlated to the h/R ratio as determined from SEM measurements

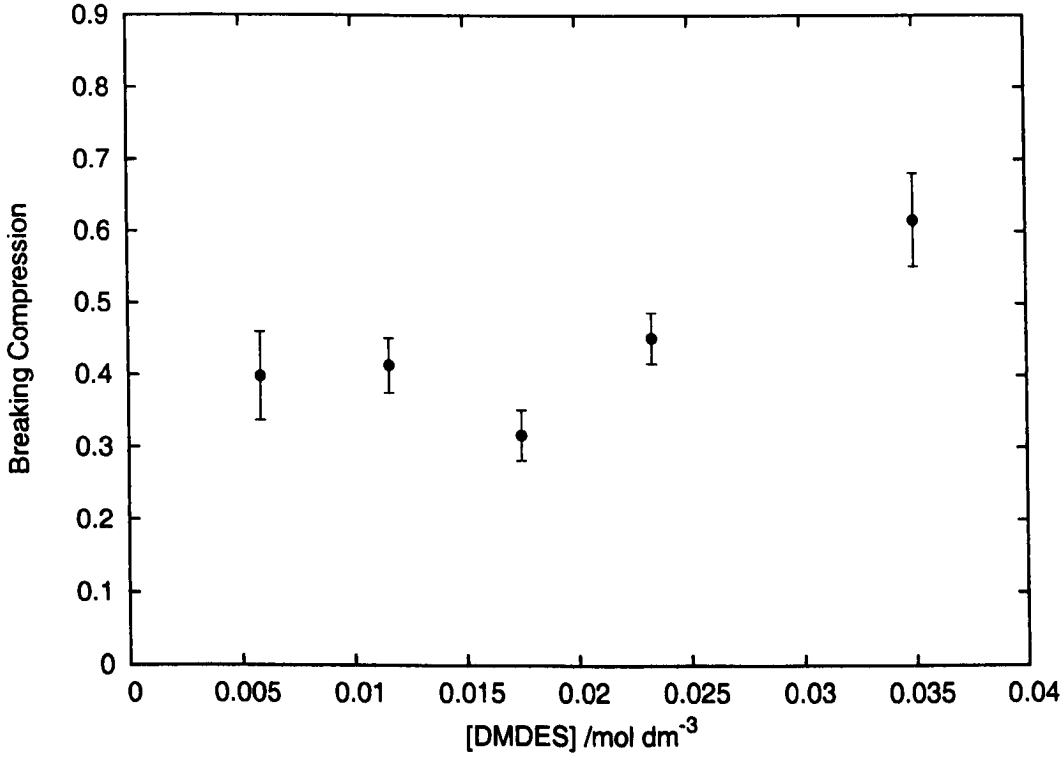

Figure 5.28: Breaking compression against secondary DMDES concentration

A comparative plot of the breaking force data for both Secondary DMDES series relative to their respective h/R ratios does not reveal a consistent trend between the two series (Figure 5.29). The 1 % NH_3 classes have a much lower breaking force than would be predicted from the linear trend suggested by the 2 % data. No equivalent thickness/radius ratio was made in the 2 % series, however. It is possible that beyond a threshold ratio the particles are more readily ruptured due to enhanced strain at the shell exterior [80]. Alternatively, formation of PDMS emulsions in conditions of 1 % NH_3 and 1 % DMDES have been shown to exhibit different growth rate constants to those formed at higher concentrations (Section 4.4.1, it is therefore possible that this change in kinetics may influence the shell formation leading to variation in cross-linking density.

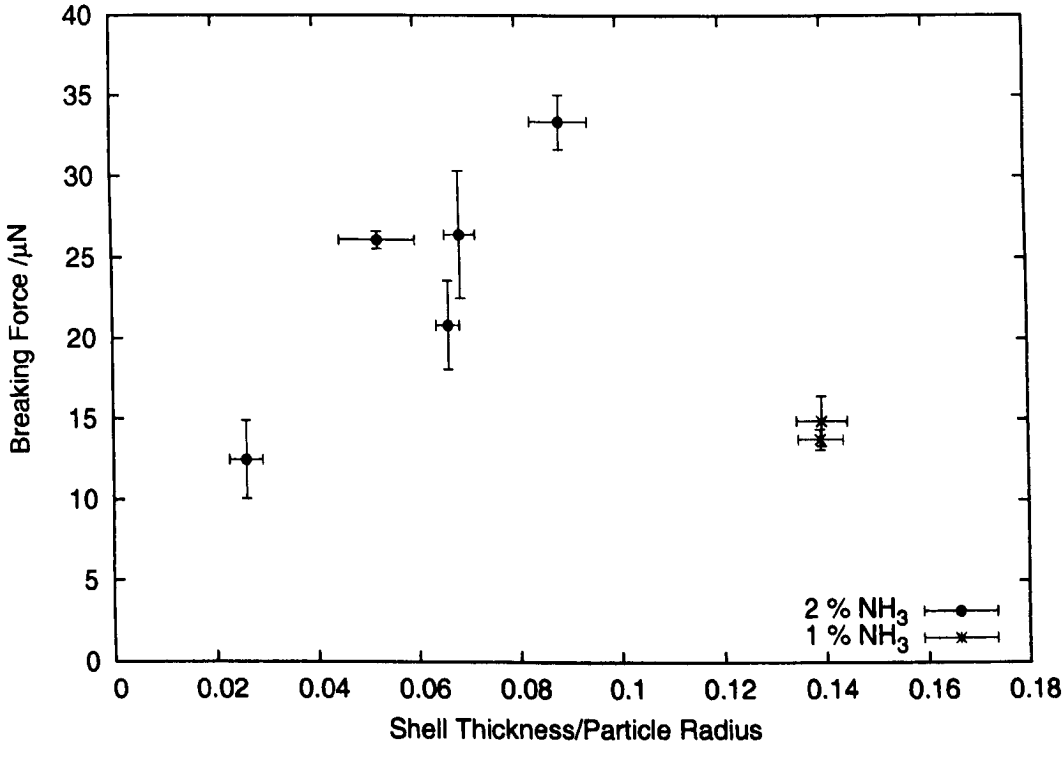

Figure 5.29: Combined data correlating breaking force against respective h/R for both Secondary DMDES series.

Plotting the breaking forces of the Zoldesi series and the 2 % NH_3 Secondary DMDES series with their respective shell thicknesses reveal a linear correlation (Figure 5.30), the correlation, however, does not persist upon plotting their respective breaking forces against the h/R ratio (Figure 5.31). The separation is less marked than that of the 1 % and 2 % Secondary DMDES series. The examined Zoldesi series was prepared in 2 % NH_3, however,

so an improved correlation would be expected.

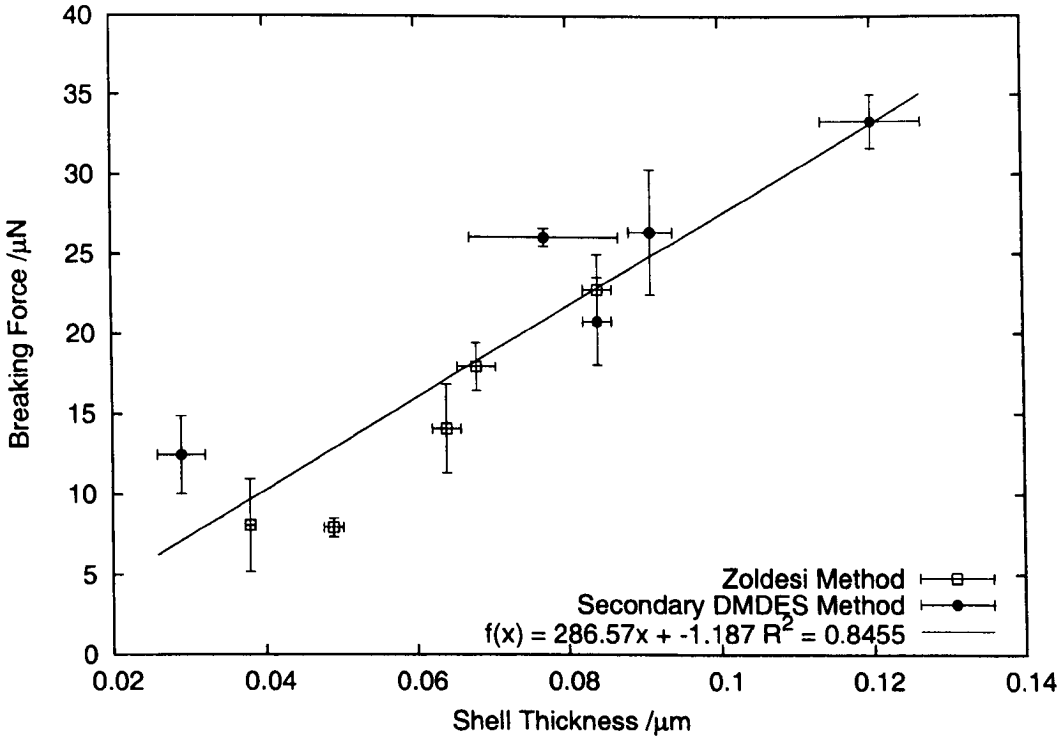

Figure 5.30: Combined data from the Zoldesi (open squares) and Secondary DMDES (closed circles) particles correlated with their shell thicknesses. There is an apparent linear relationship.

While the Zoldesi series exhibited an increasing trend in breaking compression with h/R ratio, the Secondary DMDES series shows no such correlation, further suggesting the non-equivalence of the two series.

Young's modulus, E, values are plotted as a function of secondary DMDES/TEOS ratio concentration in Figure 5.33. The lowest DMDES/TEOS ratio corresponds to the thinnest shell in the series and, as for the Zoldesi series, exhibits a Young's modulus that is considerably larger than those measured for the other classes. For the secondary DMDES system, higher DMDES/TEOS ratios do not seem to correspond with a declining trend in E, instead they seem to fluctuate around a base line value. The E values are substantially larger than Zoldesi's value of approximately 100 MPa [63], even at high DMDES/TEOS ratio, but are similar to those measured for the Zoldesi system studied here (Section 5.3.5).

E values were also determined for the two classes from the 1 % NH_3 Secondary DMDES series that yielded measurable force-displacement profiles (Table 5.1). These values were

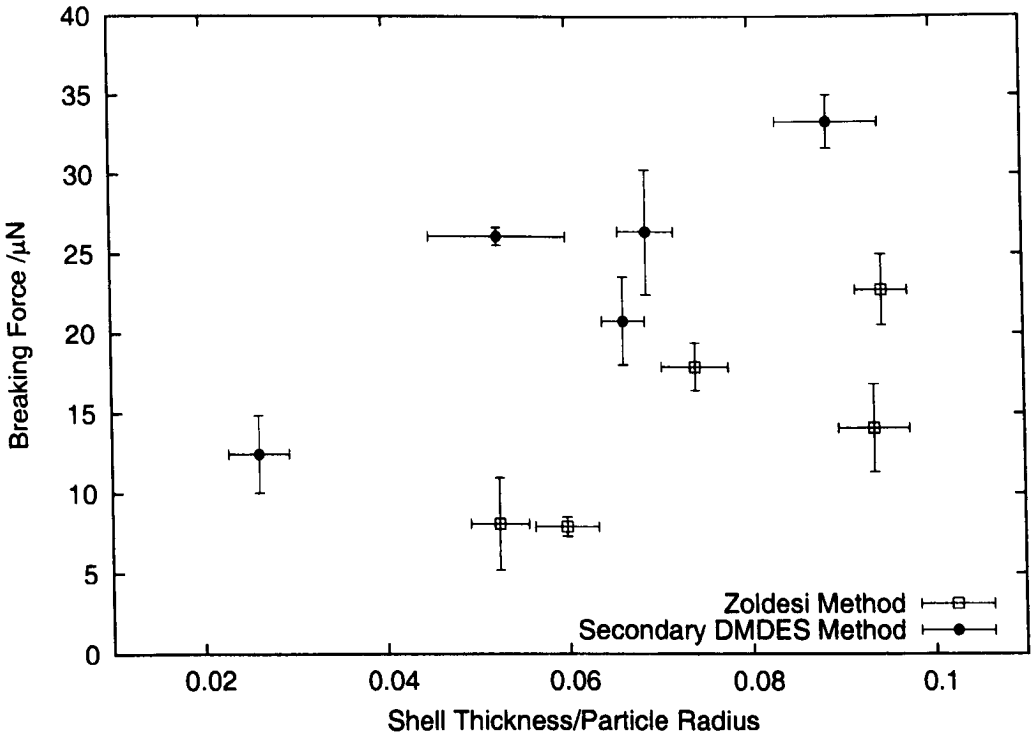

Figure 5.31: Combined data for breaking force against respective h/R ratios for both the Zoldesi and Secondary DMDES Methods, using SEM size measurements.

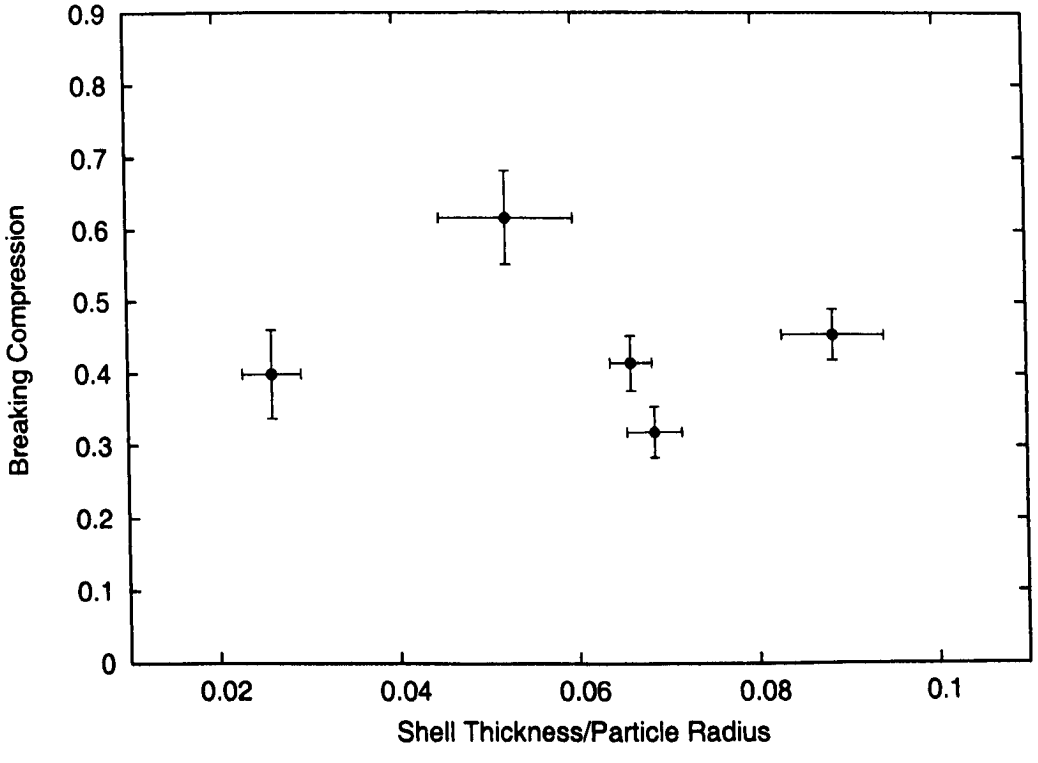

Figure 5.32: Breaking compression against h/R ratio

lower than those measured in the 2 % NH_3-2 % DMDES regime, which suggests the low DMDES concentration may influence cross-linking density in the shell. Also the lower E may explain the apparent deviation of the 1 % system from the breaking force trend established for the 2 % particles (Figure 5.29).

Table 5.1: Young's modulus values determined for Secondary DMDES particles prepared in 1 % NH_3. E_{SEM} is the Young's modulus determined using SEM size measurements, while E_{probe} is determined using the maximum probe displacement.

DMDES/TEOS Ratio	E_{SEM} /MPa	E_{probe} /MPa
1.30	1800 ±270	1130 ±140
1.62	1220 ±230	774 ±99

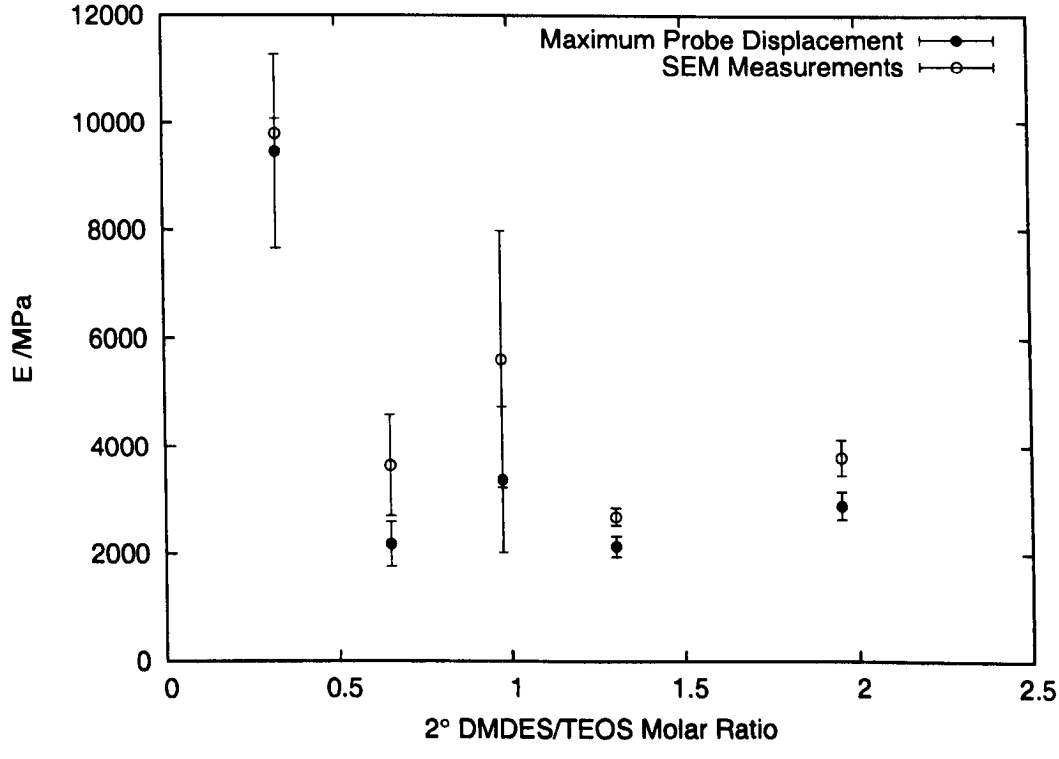

Figure 5.33: The Young's Modulus plotted as a function of secondary DMDES/TEOS concentration ratio. The Young's modulus is plotted as calculated using both maximum probe displacement measurements (closed circles) and SEM measurements (open circles).

5.3.7 The Shell Quench Method

Particles in this series had been formed under identical conditions in 1 % NH_3 using the Secondary DMDES method, but the shelling step had been quenched by dilution and centrifugation to remove the ammonia. The longer the shelling step was allowed to proceed, the thicker the formed shells. Unfortunately no breaking forces could be determined for the four initial particle classes in the series, corresponding to the thinnest and medium thickest shells. This reproduces the behaviour observed for the 1 % NH_3 secondary DMDES series.

5.3.8 Varying TEOS Method

A secondary DMDES particle series was made to determine the effect of varying TEOS concentration during shell formation. Compression of these particles showed little variation across the series with increasing TEOS concentration (Figure 5.34). Both maximum probe displacement and SEM measurements showed particle size to drop across the series (Figure 5.35). Both methods reveal a similar trend, though once again the SEM measurements are larger than those from the probe displacement. Breaking force shows no apparent correlation with increasing TEOS concentration (Figure 5.36).

Young's modulus values for the series are plotted as a function of secondary DMDES/TEOS ratio in Figure 5.37. No microtomy measurements were made for this series, so a constant shell thickness corresponding to that of equivalent 1 % Secondary DMDES particles was assumed for the calculation. In general increasing the TEOS concentration with respect to that of the secondary DMDES (lowering the DMDES/TEOS ratio) had little effect upon the E values, which is consitant with the breaking force behaviour already observed. The low DMDES/TEOS regime that gave E values near to that of pourous ceramic did not feature in this series. The results suggest that shells formed in conditions above a certain DMDES/TEOS ratio achieve a consistant effective Young's modulus that is representative for polymers. The secondary DMDES series data in Figure 5.33 suggests a threashold ratio ≈ 0.5.

Inspection of SEM micrographs reveals a change in particle morphology across the series, with the shell material appearing to soften as the TEOS concentration was reduced

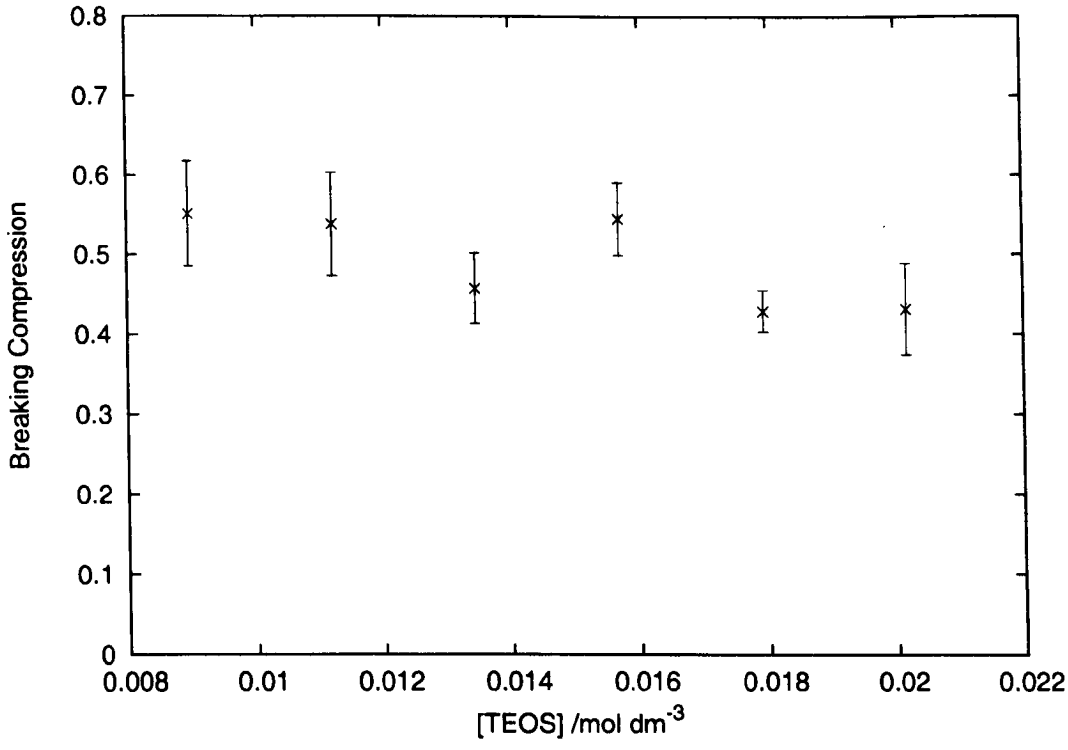

Figure 5.34: Breaking compression shows no real correlation with TEOS concentration

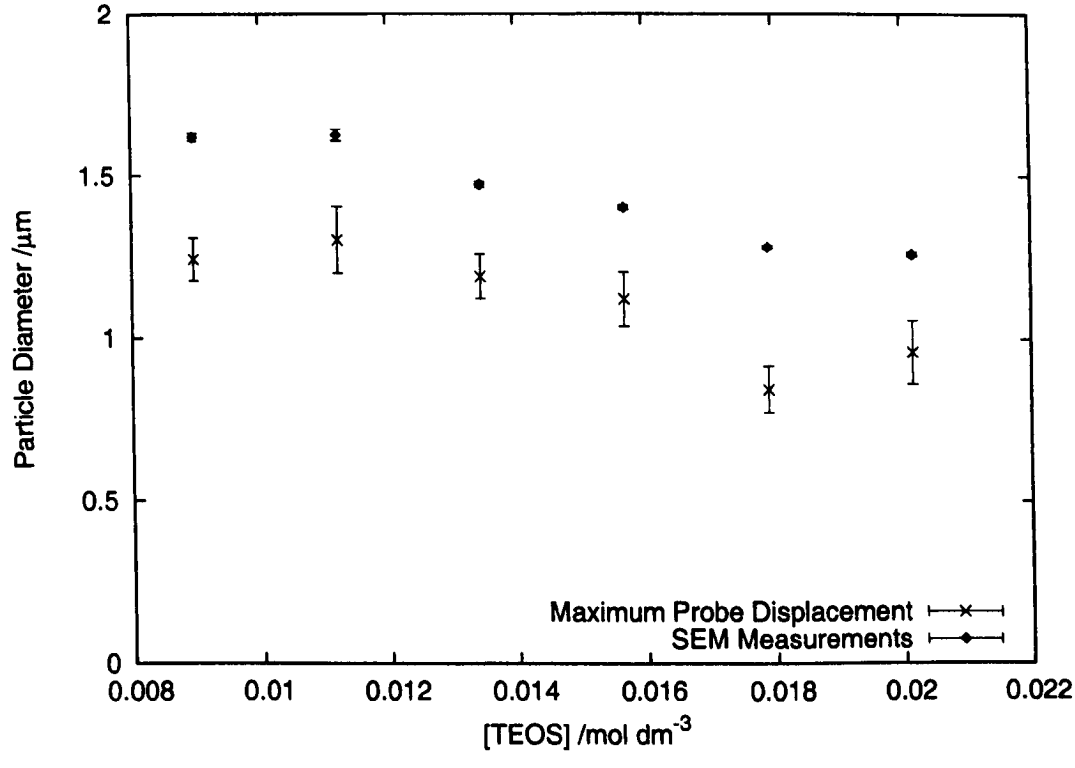

Figure 5.35: Maximum probe displacement against TEOS concentration

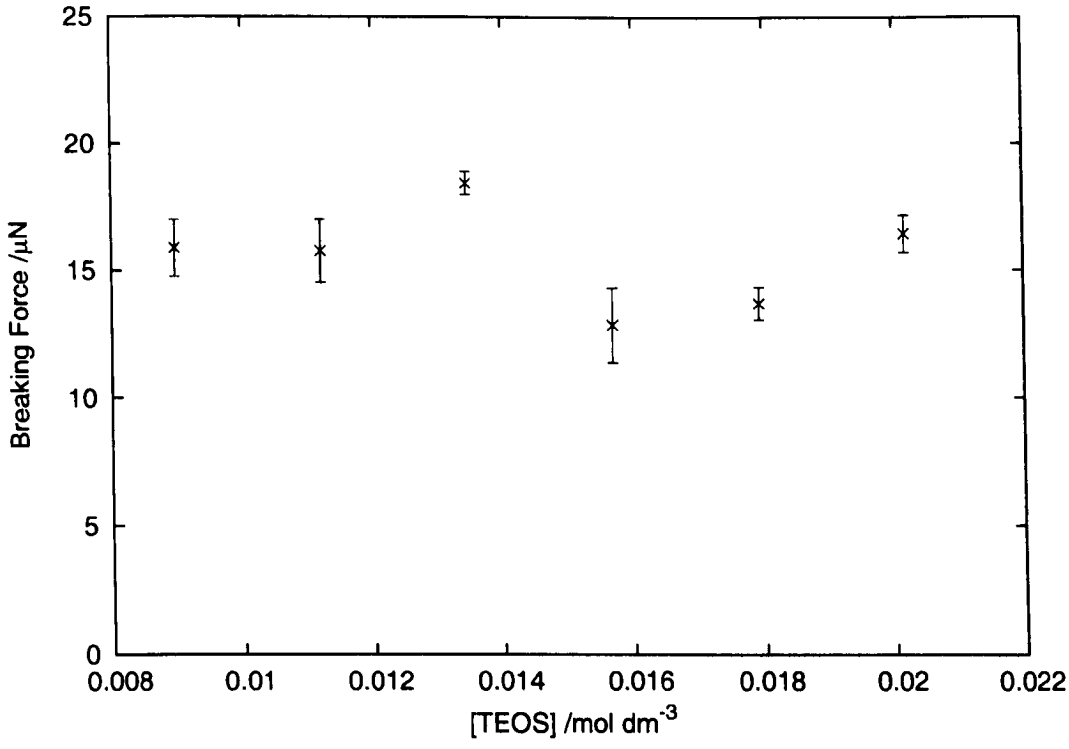

Figure 5.36: Breaking Force shows no apparent correlation to TEOS concentration

(see Section 4.6). The lack of correlation observed between the determined E and the DMDES/TEOS concentration does not reflect qualitative SEM observation. This discrepancy suggests the assumption that shell thickness remained constant across the series may be wrong.

The Varying TEOS series was formed in 1 % NH_3 conditions, and the calculated E values are consistant with those determined for the secondary DMDES series formed in similar conditions.

5.3.9 MTES Shell

A particle series was made, based on the 2 % Secondary DMDES method, that used MTES, DMDES and TEOS as shell monomers (see section 4.7). The TEOS concentration was fixed, and the total combined volume of DMDES and MTES was kept constant, while the ratio of MTES to DMDES was varied across the series.

Particle size as a function of MTES/DMDES ratio is plotted in Figure 5.38. All of the particle classes in the series, bar one, yielded measurable force-deformation profiles. In SEM

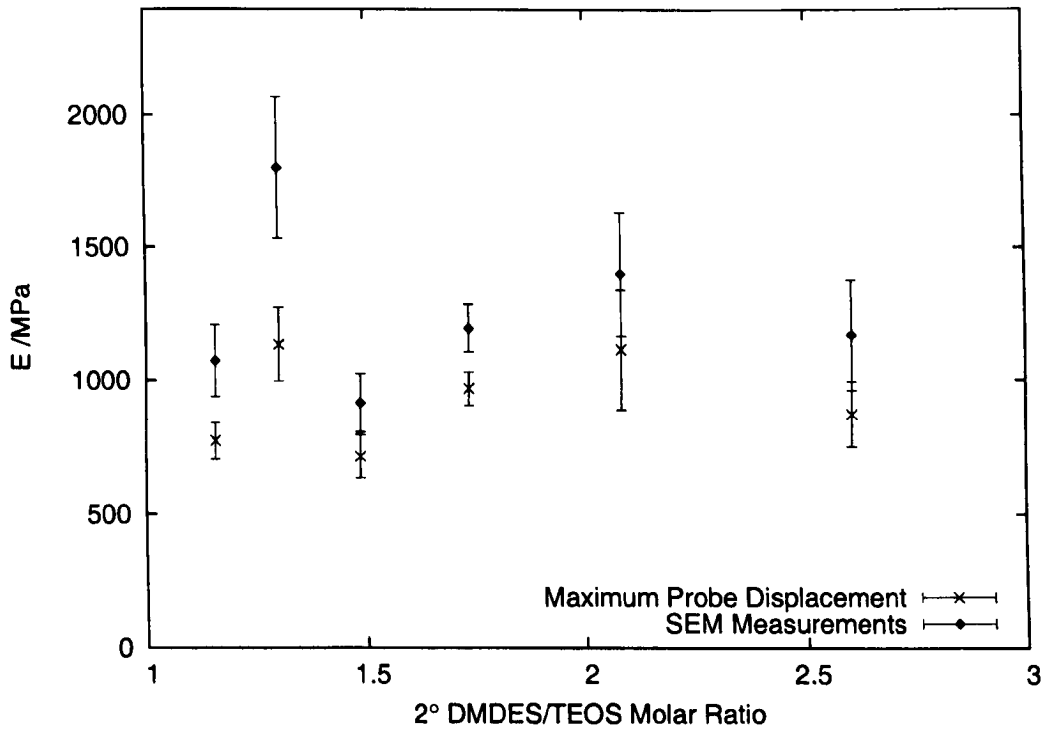

Figure 5.37: Young's Modulus values plotted as a function of secondary DMDES/TEOS concentration ratio. E values are calculated using size measurements determined using maximum probe displacement (crosses) and SEM (filled diamonds).

micrographs the missing class (0.022 MTES/DMDES) appears to be in a soft and collapsed state, while all the other classes in the series appear are typically spherical and uncollapsed.

A declining trend in breaking force with MTES/DMDES ratio is plotted in Figure 5.39, while little variation in breaking compression is observed across the series (Figure 5.40). The determined Young's moduli for the series show a decline with increasing MTES/DMDES ratio, which is most pronounced in the SEM-based values. These data support the qualitative observation that addition of MTES serves to soften the shells, possibly because it competes with TEOS to cross-link the DMDES residues and its trifunctionality acts to reduce cross-linking density.

5.3.10 Particle Drying

The use of air-dried samples, rather than samples in solution, raises the issue that the PDMS core material may leak or evaporate from the particles with time. A sample from the Secondary DMDES series was left to air-dry on a slide for 96 hours to investigate drying effects

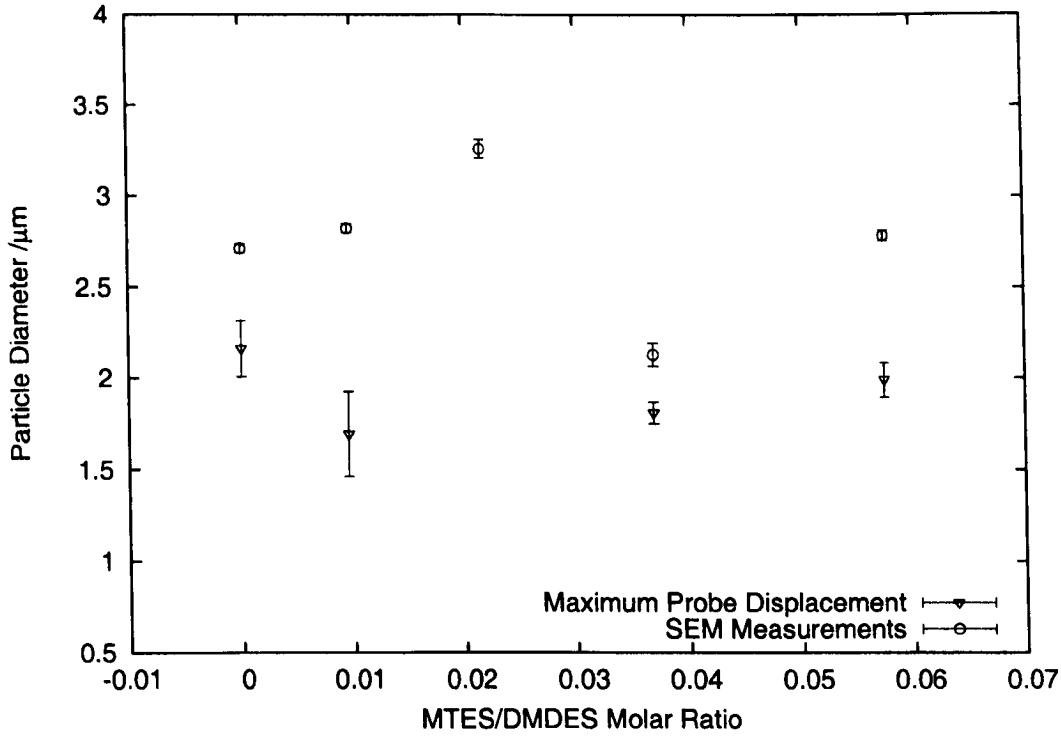

Figure 5.38: Particle size as determined by maximum probe displacement and SEM

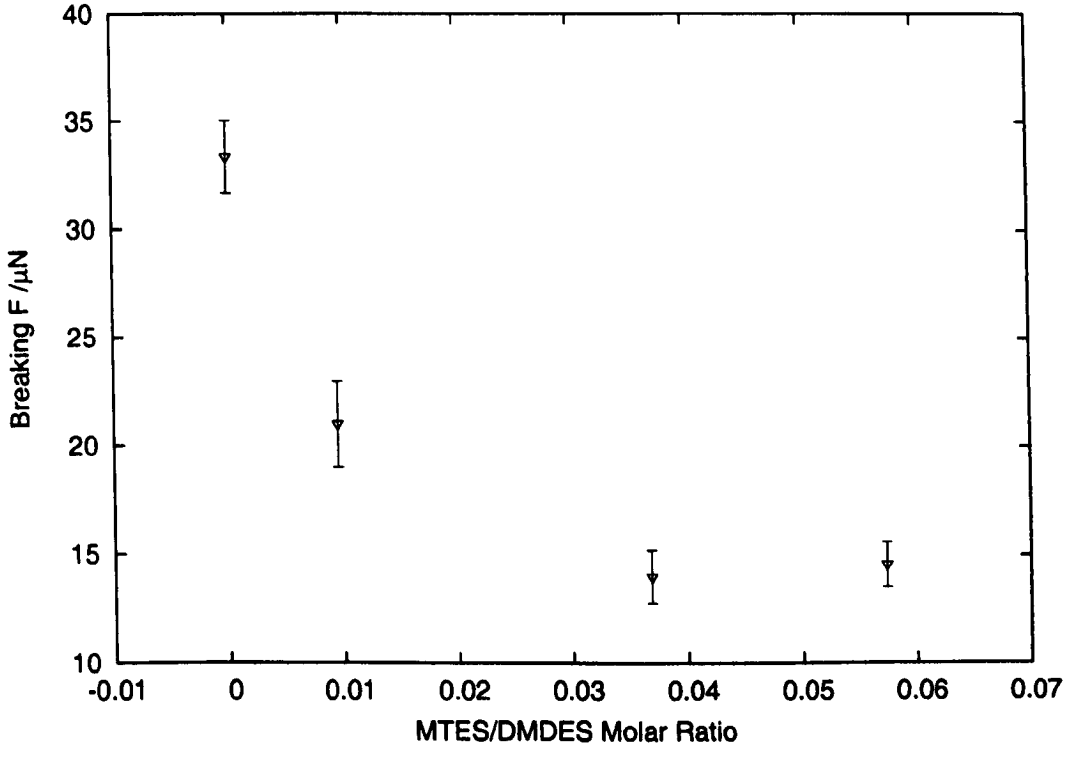

Figure 5.39: Breaking force as a function of MTES/DMDES molar ratio

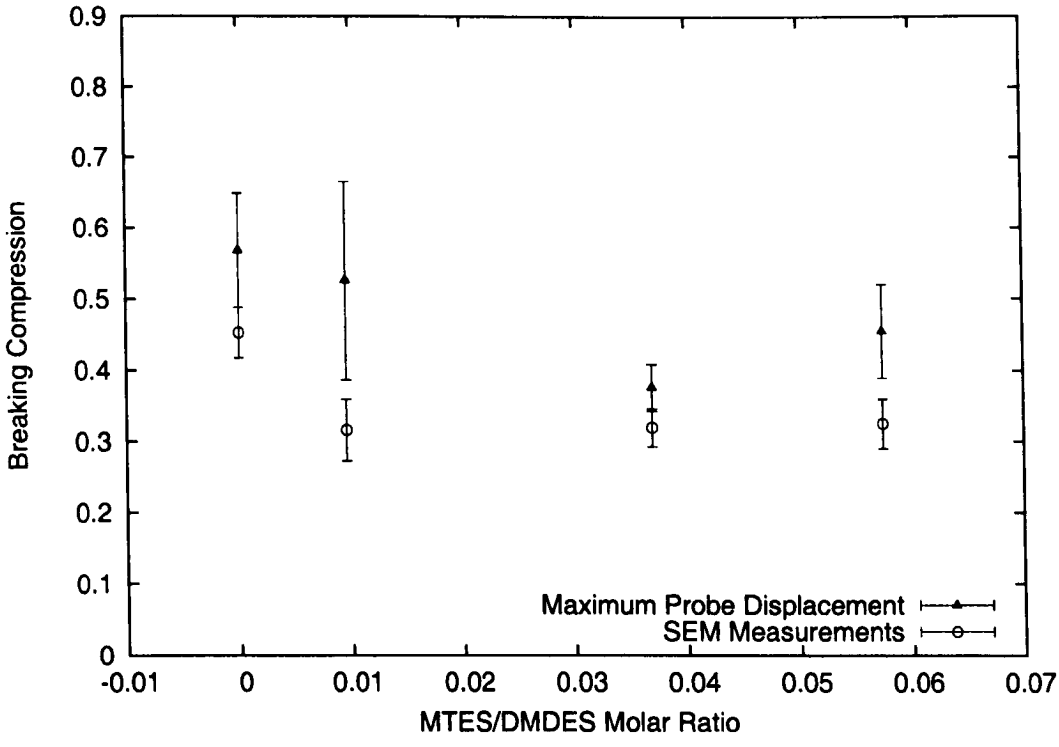

Figure 5.40: Breaking compression as a function of MTES/DMDES molar ratio

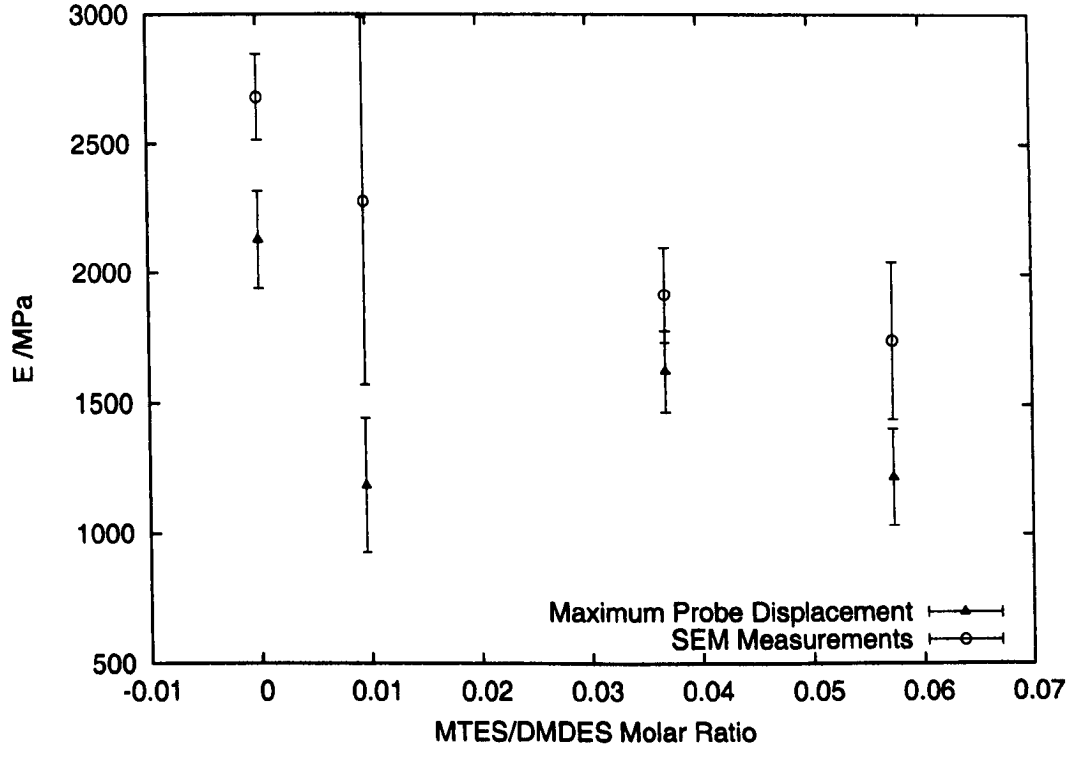

Figure 5.41: The shells' Young's moduli as a function of MTES/DMDES molar ratio

on compression behaviour. Upon compression, the dried particles were observed to rupture and release oil, together with measurable breaking forces (Table 5.2).

To statistically compare the fresh and 4 day-old sample the raw data was analysed with the Wilcoxan Rank Test using R [72], after first checking the variances were not significantly different using F-tests. The Wilcoxan test is preferable to a two-tailed t-test if the sample distribution is non-normal or skewed by the presence of outliers [99].

Comparison of the breaking force means with a Wilcoxan Rank Test gives a p-value of 57 % that they are the same. Similar comparrison of the mean breaking displacements give a p-value of 100 % for the Wilcoxan Rank Test. Lastly the compression means give a Wilcoxan p-value of 76 %. The four-day drying period, therefore, had no significant effect for the particles. In addition, the determined Young's modulus for the fresh and dried systems were similar when determined using both SEM and maximum probe displacement.

It is important to note, however, that the 4-day dried samples had the thickest shells of the Secondary DMDES series, and as such provide little basis for ascribing similar integrity to thinner shells.

Table 5.2: Comparison of freshly dried particles with those that had been dried for 98 hours

Measurement	Freshly dried	98 hour Sample
Breaking F /μN	33 ± 2	30 ± 3
Breaking disp. /μm	1.2 ± 0.1	1.3 ± 0.1
Max probe disp. /μm	2.1 ± 0.2	2.2 ± 0.2
Breaking Compression	0.57 ± 0.01	0.61 ± 0.04
E_{SEM} /MPa	2700 ± 170	2900 ± 300
E_{probe} /MPa	2100 ± 190	2300 ± 210

5.4 Summary

The DMDES/TEOS concentration ratio has an apparent consequence for the Young's modulus. In series prepared by both the Zoldesi and Secondary DMDES methods, low DMDES/TEOS ratios with low absolute DMDES concentrations gave rise to high E shells in the region of 10 GPa. Higher DMDES/TEOS ratios formed shells with E values typically in the region of 1-3 GPa, and no apparent trend between E and monomer ratio was observed in the latter

regime, although the assumption of constant shell thickness across the examined series may have obscured a correlation. If a shell material with a consistent E is required, the best approach to control shell thickness may be the Quench method. DMDES concentration also has an influence on cross-linking density: particles prepared in conditions of 1 % DMDES and 1 % NH_3 had lower E values than their 2 % counterparts.

Positive linear correlations were observed between shell thickness and breaking force. Though, particularly in the case of the Zoldesi series, a less marked correlation was observed between breaking force and h/R. Linear empirical trends were also observed for breaking force against DMDES concentration in the case of the 2 % Secondary DMDES series, and between breaking compression and TEOS addition delay time in the Zoldesi series. No apparent correlation was observed between breaking compression and DMDES concentration was observed in the Secondary DMDES series, though there was an increasing trend towards a plateau in the relationship for the Zoldesi series, which may be a consequence of variation in E.

Inconsistencies in the formation of the PDMS core-shell systems may account for deviations from or fluctuations about expected behaviour. Such inconsistencies include reaction time, rate of mixing, extent of dispersion and dissolution of the monomer, and production of secondary material. Creaming of the PDMS phase prior to shelling may also broaden any size distribution.

Particle drying had no apparent effect on shell integrity in the thickest shell system. All particles retained their oil cores upon brief drying, and the oil was observed to be rapidly released upon shell rupture. The force deformation curves were consistent with particles whose shells are impermeable to their core material, at least over the compression time scale.

5.5 Further Work

The breaking forces associated with particles with diameters in the region of 1 micron or less tended not to be detected by the force transducer. The use of optical microscopes to position the particle beneath the probe impose an optical size limit upon the particles used, and suitable placement beneath the probe is complicated as a result. Also, if a system comprises

a broad size distribution then only the section of the distribution that exceeds a certain size may be successfully measured. Alternative AFM based techniques, or micromanipulation using ESEM could be considered to investigate the MTES-based particles and their shells.

The necessity to restrict particle movement by drying in order to reliably compress them raises a further issue, as core material may be lost in the process. Use of a polyelectrolyte coating on the glass slide surface, such as polyethyleneimine, may promote particle adhesion to the slide surface to allow compression under water [89]. The presence of the INUTEC surfactant may interfere with such a step, though the sample dilution may be sufficient to deplete the adsorbed surfactant concentration.

The apparent high Young's moduli observed in systems with low DMDES/TEOS molar ratio suggest an approach to making more rigid shells. Further investigation of this concentration regime would therefore be of interest, possibly in a two step process involving formation of both high and low E shells in the same particle.

Furthermore, a direct investigation of the cross-linking density in the shells would be useful. Solid state ^{29}Si NMR can be used to identify Si atoms bonded through siloxane bonds to four other Si atoms, which corresponds to TEOS-derived cross-linking units, whose signal strength may be compared to those of Si atoms residing in environments with fewer such bonds in the same sample. Such an investigation would be complicated by the presence of the observed silicone-silica secondary material, which persists after repeated centrifugation.

The possibility that a gradient in cross-linking density across the shell thickness arises due to declining DMDES/TEOS ratio could possibly be explored with neutron scattering. If the cross-linking density has an effect upon surface roughness, high Q small angle neutron scattering would be able to distinguish between rough and smooth surfaces [100] and could be used to compare, for example, shells formed from a quenched method that could conceivably be uniformly cross-linked unlike shells formed from a complete reaction.

The breaking forces measured here derive from anisotropic pressure. An alternative isotropic application of pressure would also be of interest, for instance to determine the suitability of particles for use under conditions of high pressure. To this end the particles could be subjected to increasing pressure in an isothermal pressure vessel. As an indirect method,

such an investigation would require a suitable chemical marker to be contained in the core material to determine the extent of particle rupture. A direct method could be devised using a small-volume pressure cell that allows observation of the subject particles.

The effect of core swelling with solvent upon shell strength has not yet been determined for this system: initial attempted micromanipulation experiments were unsuccessful. Another useful variable to explore would be that of the effect of cross-linking density within the core, as this may engender additional strength to the particle.

Chapter 6

Incorporation of Material

6.1 Introduction

PDMS emulsions and microgels may be swollen by a variety of organic solvents, which provides a means to incorporate an active material. Successive encapsulation using methods described in Chapter 4 would then form a core-shell particle.

Previously swelling of PDMS dispersions was brought about by direct combination with organic solvents [54, 48, 52]. The solvent diffuses into the dispersed phase until its chemical potential equalizes between the dispersed and continuous phases. While it is not necessary to mix the solvent into the continuous phase, the absorption of solvent can enhance creaming or sedimentation and may bring the formed, concentrated dispersion in proximity to any immiscible solvent phase leading to coalescence and polydispersity. Stirring or agitation by tumbling prevents this occurrence [54]. Pronounced swelling may cause coalescence if the surface stabilizing groups are sufficiently diluted.

If the PDMS is sufficiently cross-linked to form a gel network within the particle, swelling establishes an elastic restoring force that acts against the osmotic driving force. Also, the magnitude of the restoring force increases as swelling progresses. This effect increases the internal solvent chemical potential so that, at equilibrium, the microgel volume is less significantly increased than that of its less cross-linked counterparts. Studies with varying MTES volume fractions showed that pronounced swelling is observed in PDMS dispersions derived from 0–40 % MTES (with respect to the total monomer volume fraction), while MTES vol-

ume fractions in excess of 40 % yield particles whose swelling is limited. Swelling studies with n-heptane showed 1 % v/v PDMS dispersions, derived from 10 % MTES, to be swollen to 30 times their initial volume, which suggests that $\approx$ 97 % of the swollen droplet volume was heptane. Swelling of PDMS particles that were derived from 60 % MTES to equilibrium revealed 35 % of the droplet volume to be heptane [54].

PCS studies of PDMS emulsion swelling revealed the size distribution to remain monodisperse initially, but to broaden if allowed to cream. Emulsions swollen by toluene, styrene and 1,1,1-trichloroethane were found to be less stable to coalescence than dispersions swollen with alkanes [54]. Polar solvents and high molecular weight non-polar solvents were less effective swelling agents.

An effectivity series has been established for various solvents' swelling action on PDMS dispersions [54]: 1,1,1-Trichloroethane > toluene > styrene > cyclohexane > n-heptane > n-octane > DMDES > n-octanol > n-dodecane > n-hexadecane > n-decanol > PDMS. The solubility in water, with the exception of n-octane, decreases as the series is descended, which suggests this factor to be more significant than solubility in PDMS. n-Octanol is more water-soluble than toluene, but its presence below n-heptane in the series may relate to a significantly low solubility in PDMS, although this has not been determined. Mobilities of PDMS emulsions swollen to different extents, up to 10 % ϕ_{PDMS} were used to calculate their respective zeta potentials [54]. Surface charge density was found to be unaffected by extent of swelling, indicating a preferential occupancy of PDMS at the droplet water interface. Although the presence of a charge stabilization mechanism may now be in doubt [48] (see section 3.1.3), stability is derived from a consistant PDMS presence at the interface.

Uptake of Sudan Yellow dye into PDMS dispersions has previously been attempted [54]. One method used n-heptane, diethylether and toluene as vector solvents. Dye-loaded solvent was added drop-wise to stirred PDMS dispersions over a 24 hour period. Another attempt involved dissolution of the dye into DMDES monomer that was then used to form a PDMS dispersion. Both methods proved unsuccessful as the systems broke down upon dialysis and no dispersed dye was observed. In the presence of $\geq$ 60 % v/v ethanol PDMS is sufficently soluable that no dispersed phase is formed, however dilution by water following polymer-

ization leads to precipitation [33]. Sudan Yellow was successfully incorporated into PDMS dispersions by first dissolving the dye in an ethanol-water solution, forming PDMS as a single phase, and then precipitating the dispersion. The quality of the formed dispersions were not reported [54].

This chapter describes attempts to incorporate dye into PDMS dispersions prior to a shelling step to form core-shell particles.

6.2 Results and Discussion

6.2.1 PDMS Swelling with n-Heptane

PDMS emulsions derived from 1 % v/v DMDES in 1 % v/v NH_3 were prepared and monitored with PCS prior to swelling: measurements were undertaken for two weeks. A mature PDMS emulsion was split into 6 aliquots. Portions of n-heptane were added to each aliquot. The n-heptane formed a layer on top of the aqueous dispersion and was gradually absorbed into the emulsion droplets. Each dispersion was sampled at intervals, ensuring that the n-heptane layer was undisturbed, and subjected to PCS; samples were returned to the swelling environment following each measurement. Droplet size was observed to increase in the presence of the n-heptane, with the most pronounced increase in the presence of the largest n-heptane addition (Figure 6.1).

6.2.2 Shell Growth on Heptane-swollen PDMS

2 % PDMS emulsions in 1 % NH_3 were made and allowed to mature for three days. Sufficient n-heptane was added to give a PDMS/heptane volume ratio of 1. The dispersion were then tumbled for four days to allow swelling and then shelled by addition of DMDES (0.023 mol dm^{-3}) and TEOS (0.018 mol dm^{-3}) with stirring for one hour followed by three days of maturation time.

A soft solid residue was observed to form at the air-water interface. Swelling the PDMS droplets with n-heptane enhanced their creaming rate, and, as a result, a creamed phase formed rapidly during the shell maturation stage, which acted as a sink for the shell monomers.

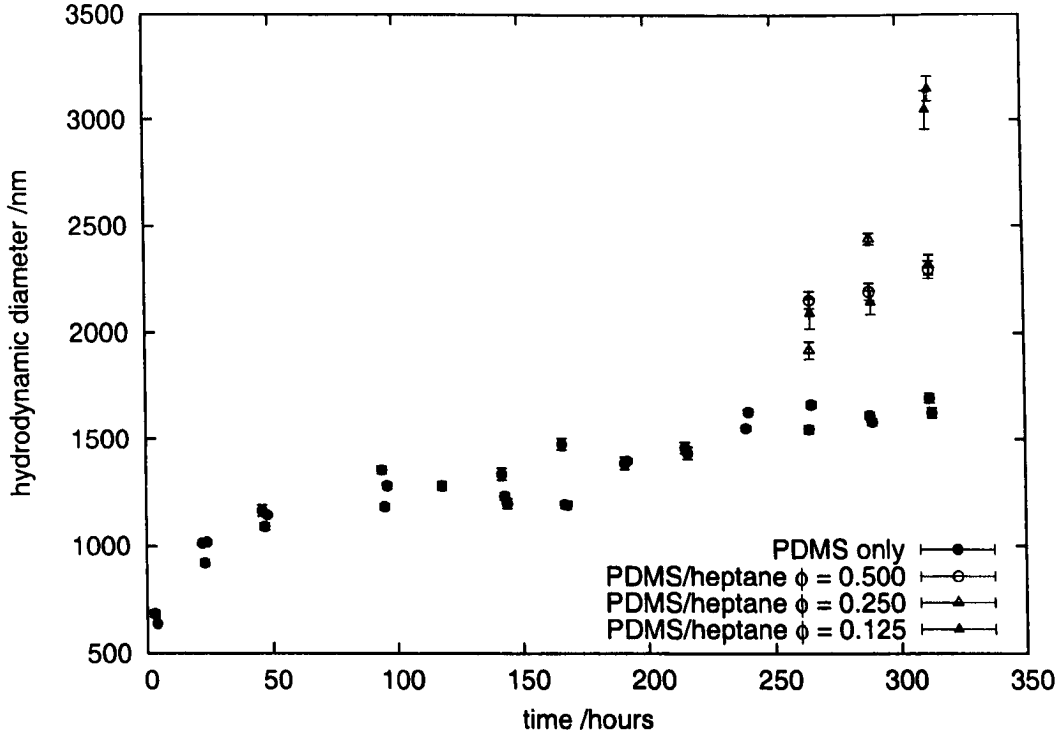

Figure 6.1: PDMS droplet growth with time and in the presence of n-heptane

Under SEM, collapsed shelled particles were observed in addition to a substantial amount of secondary material (Figure 6.2).

The experiment was repeated with PDMS microgels derived from 30/70 v/v MTES/DMDES and the dispersions were continually tumbled throughout the shell maturation stage. Aggregation was observed in all such experiments however, following centrifugation into INUTEC SP1 solution, the particles could be redispersed. Under SEM smoothly shelled particles were observed, but the size distribution was broader than that of unswollen regimes (Figure 6.3 and 6.4). The particles were observed to form a collapsed morphology, which shows the core material exuded through the shell upon drying. Tumbling during the shell maturation step reduced the extent of secondary material formation.

6.2.3 Ethanol-swelled PDMS

As discussed in Chapter 3, ethanol also swells PDMS. Because it is miscible with water, the three phase complication posed by combination of n-heptane and PDMS emulsions upon creaming does not apply to an ethanol-water-PDMS system. Ethanol does however increase

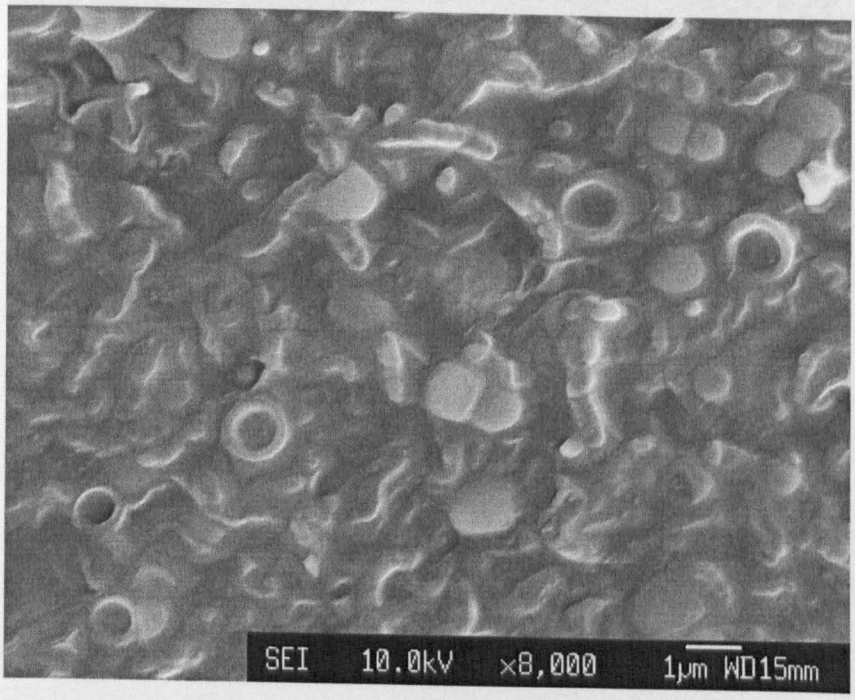

Figure 6.2: Shelled PDMS emulsion droplets whose cores had been swollen with n-heptane prior to the shelling process.

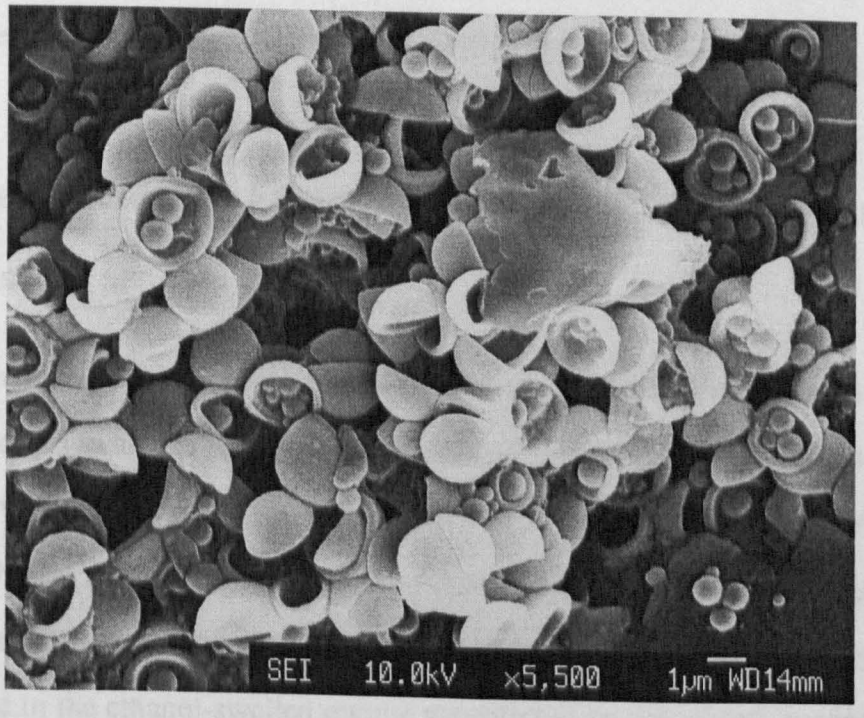

Figure 6.3: Shelled particles derived from PDMS microgels swollen with n-heptane

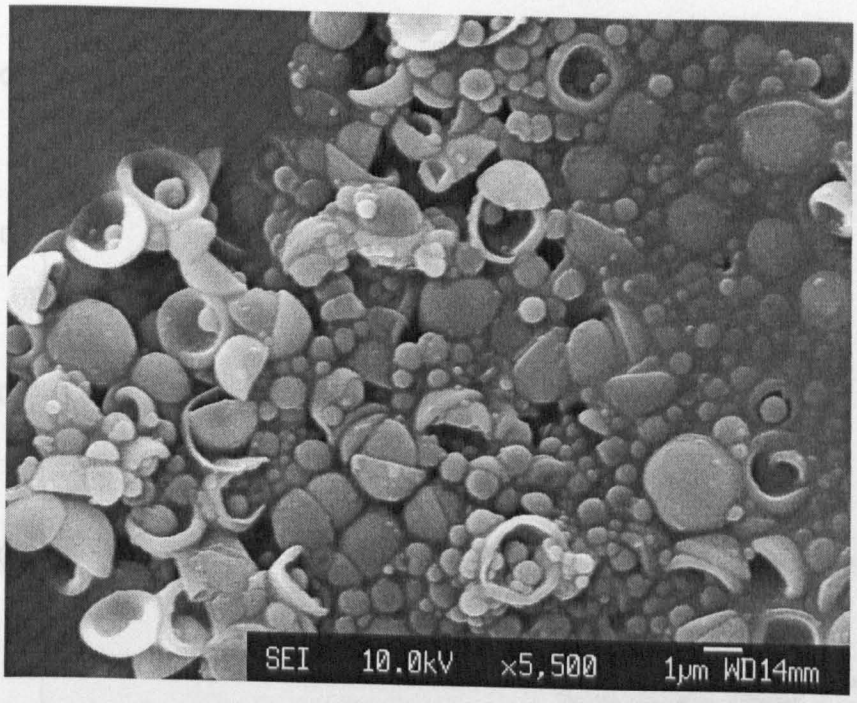

Figure 6.4: Shelled microgel derived from 30/70 MTES/DMDES

the solubility of the alkoxysilanes in water, which may have implications for the shell structure: it may be more porous or flexible. Two PDMS emulsions were made: 1 % PDMS; and a 1 % PDMS microgel formed from 30/70 DMDES and MTES. The emulsions were matured, and then diluted to 70 % v/v concentration by ethanol. Droplet sizes in both swollen and unswollen states were monitored with PCS (Figures 6.5 and 6.6).

6.2.4 Shell Growth on Ethanol-swollen PDMS Emulsions and Microgels

PDMS dispersions that were swollen in 30 % ethanol were subjected to shelling. Aggregation was observed in all shelled systems, presumably due to the presence of ethanol. Under SEM, no particles were evident for uncross-linked PDMS systems. Particles were observed in the cross-linked regimes; in comparison to unswollen shelled microgels (Figure 6.7), the particles presented a rough morphology, but appeared to be of a similar size (Figure 6.8). The shell material in the ethanol-swollen regime appeared to be crenulated, suggesting that the shell is thin and that the particle have undergone collapse upon drying as a result of ethanol and core material loss. In conditions of higher secondary DMDES concentration, similarly

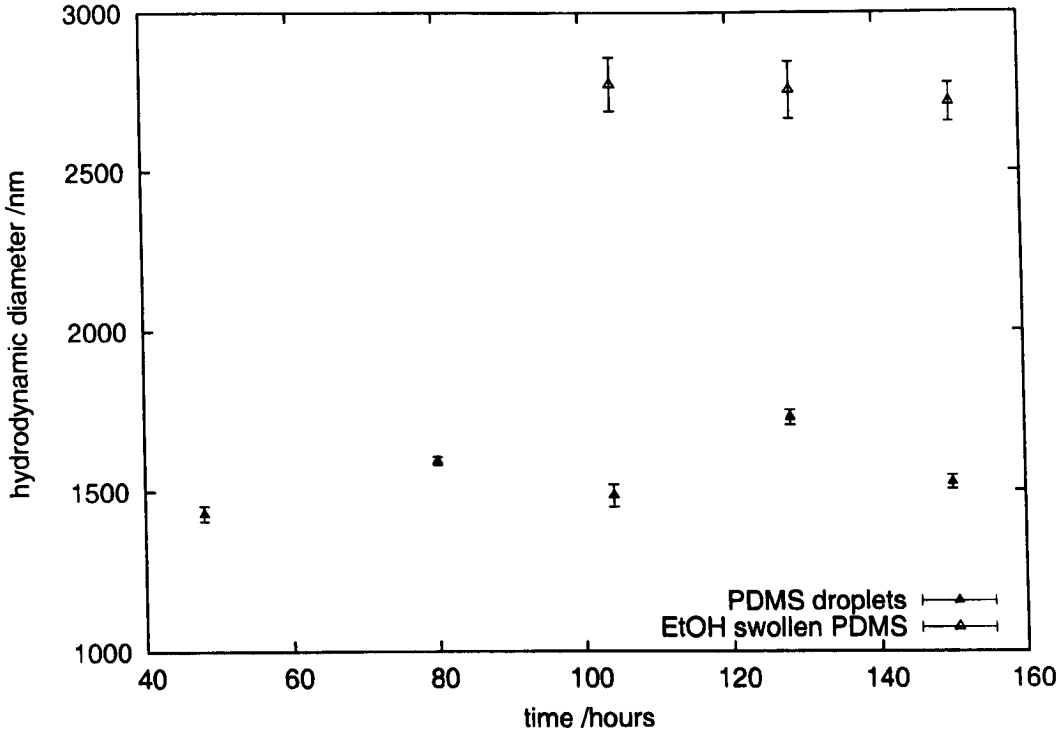

Figure 6.5: PDMS droplet growth with time and in the presence of ethanol

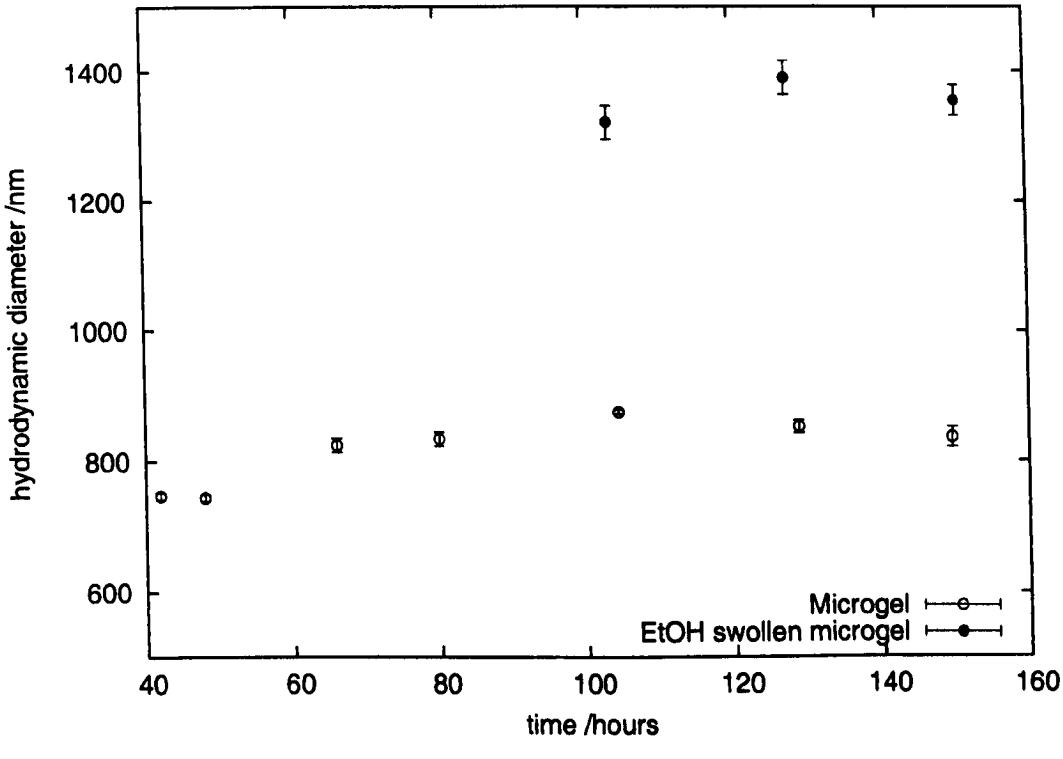

Figure 6.6: Growth of a PDMS microgel, derived from 30/70 MTES/DMDES, with time and in the presence of ethanol

sized particles were observed, but these featured adsorbed secondary particles (Figure 6.9).

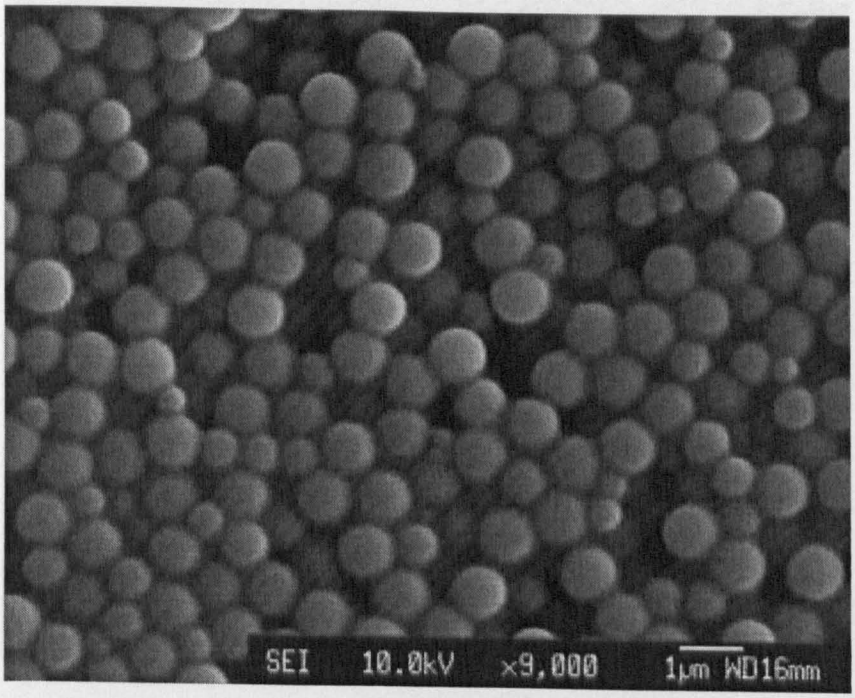

Figure 6.7: Unswollen shelled PDMS microgel

6.3 Absorption of Dye into PDMS Emulsions and Microgels

Two principle methods of dye incorporation into shelled PDMS were considered. Dye-loaded DMDES could be used to form PDMS and shelled by the Zoldesi method; or a dye loaded vector solvent could be absorbed into a PDMS emulsion or microgel and then shelled.

6.3.1 PDMS Formation from Dye-loaded DMDES

DMDES loaded with 4-nitroanisol (1 wt. %) was mixed with NH_3 solution (2 %), using a Gallenkamp Spinmix, for 40 seconds and then left to stand for 24 hours. A yellow turbid emulsion formed.

TEOS (0.018 M final concentration) was added to the emulsion, stirred for 1 hour and left to stand for three days. An aggregated dispersion formed. Surprisingly, centrifugation yielded a white sediment and a yellow supernatant. A PDMS emulsion was made using the

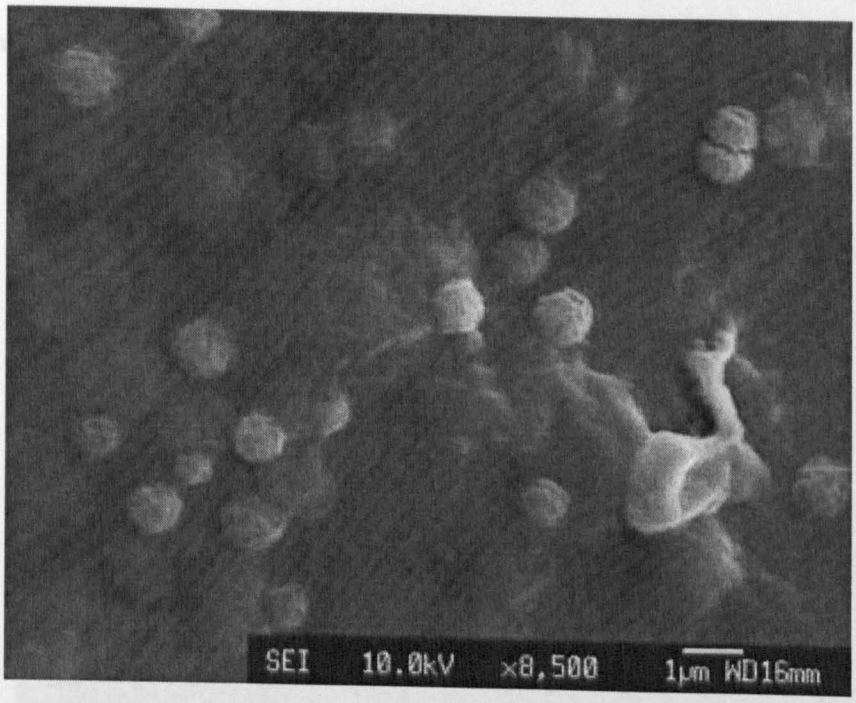

Figure 6.8: Shelled ethanol-swollen microgel with 0.015 mol dm^{-3} secondary DMDES. The particles adopt a crenellated morphology.

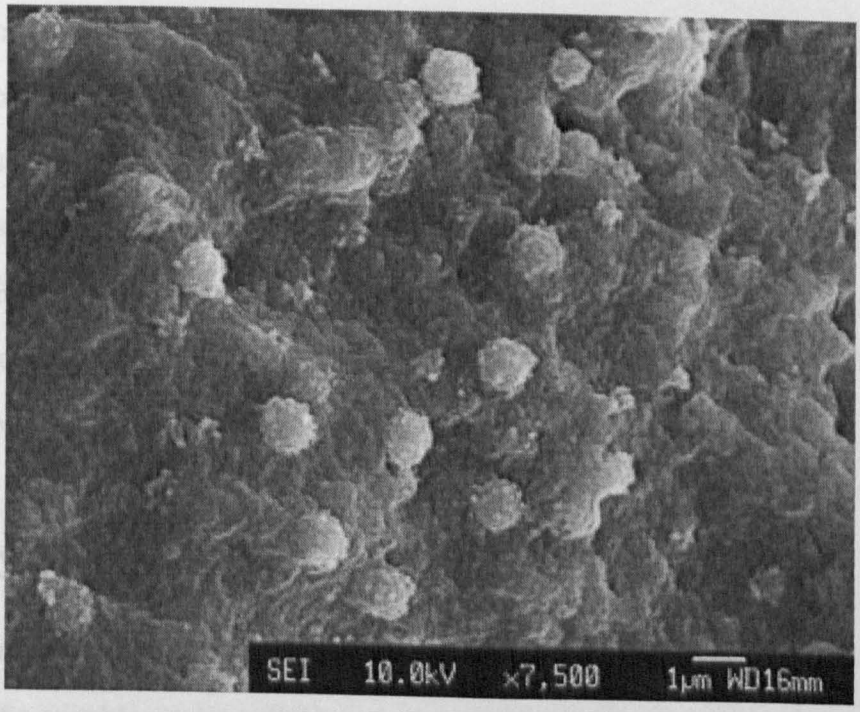

Figure 6.9: Shelled ethanol-swollen microgel with 0.029 mol dm^{-3} secondary DMDES. The particles may adopt a crenellated morphology, but this is obscured by a layer of adsorbed secondary material.

dye-loaded DMDES, but this time remained unshelled and was allowed to cream over three days. The creamed PDMS layer was white, while the aqueous phase was golden.

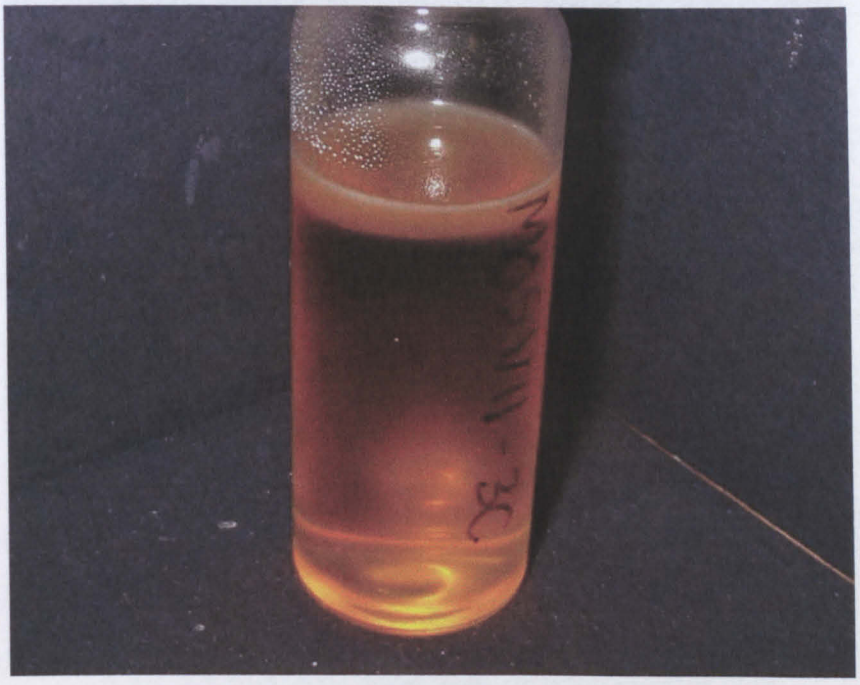

Figure 6.10: A PDMS emulsion formed from DMDES loaded with 4-nitroanisol. A white creamed layer formed on standing, while the solution turned yellow-gold.

Solid 4-nitroanisol was added to both a 2 % NH_3 solution and to water. After 1 hour the NH_3 solution took on a golden colour, while the ammonia-free solution remained colourless with no visual evidence of dissolution (Figure 6.11). 4-Nitroanisol may undergo nucleophilic substitution by hydroxide ions to give either 4-methoxyphenol or 4-nitrophenol (Figure 6.13). Both the functional groups interact with the aromatic π electron system, and can support ipso substitution (Figure 6.12). A similar photocatalysed reaction of 4-nitroanisol has been observed in water-benzene or water-cyclohexane mixtures [101].

6.3.2 Dye Adsorption with a Vector Solvent

A limitation on the dye-loaded DMDES approach is the solubility of material in DMDES. Selection of a suitable vector solvent can remove this limitation, although the method could still be subject to the same pH issues. Various vector solvents and dyes were considered. Attempts were made to dissolve Sudan II and Sudan III in n-heptane, hexadecane, toluene and DMDES. 1 wt. % mixtures were not completely solubilized. Chloroform, however,

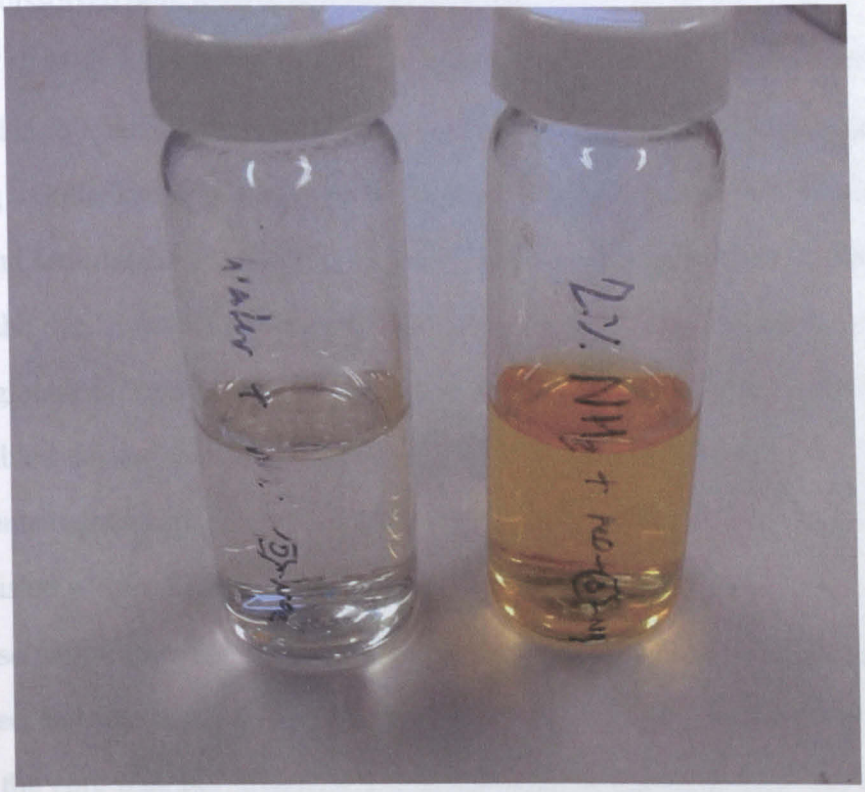

Figure 6.11: 4-nitroanisol remained undissolved in deionized water (left), but was partially soluble in ammonia solution (right).

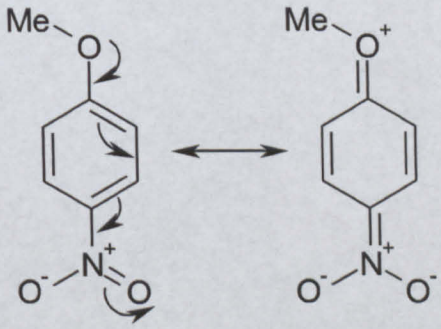

Figure 6.12: Resonance form of 4-nitroanisol

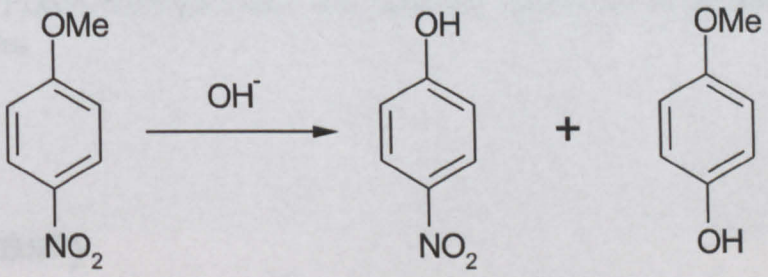

Figure 6.13: Possible nucleophilic substitution of either the methoxy or nitro group on 4-nitroanisol by hydroxide ions.

successfully dissolved both dyes at this concentration.

Sudan III (0.75 g, Aldrich, 90 %) was dissolved in chloroform to form a 1 wt. % solution and then added to a series of PDMS emulsions and microgels. Each dispersion was then shaken using a Gallenkamp Spinmix and then placed on a rotor for 4 days. All the emulsions turned red and sedimented on standing, which indicated successful uptake of both the chloroform and the dye. Some dark liquid droplets were also present, these were dye-saturated chloroform globules (Figure 6.14). The dispersions were then subjected to shelling and continually tumbled during shell maturation. Aggregates formed, but these were redispersed following centrifugation into INUTEC SP1 solution. The sediment was red, indicating that the dye persisted within the particles.

SEM observation revealed the formed shells to be smooth. None of the dispersions were monodisperse, but the size distribution seemed to narrow with an increasing MTES contribution to the core material (Figures 6.15 and 6.16). It is possible that the more viscous MTES-derived PDMS was more resistant to coalescence in its swollen state.

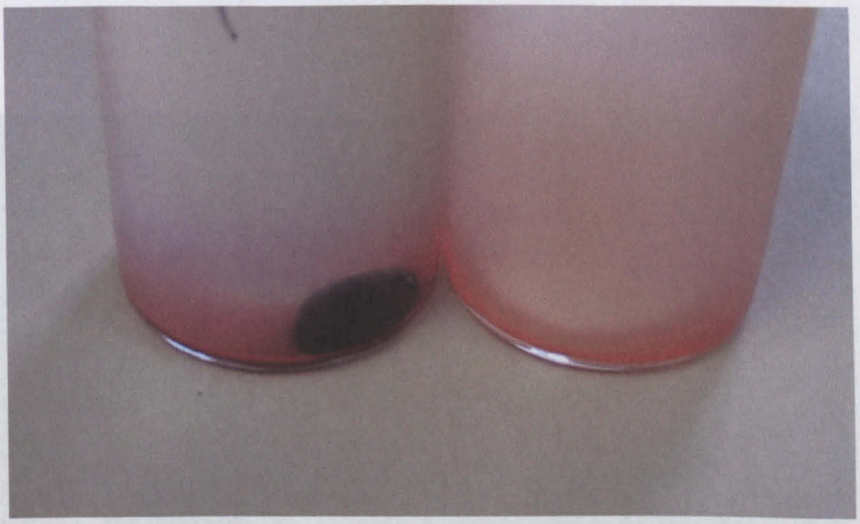

Figure 6.14: A PDMS microgel (left) and emulsion (right) following absorption of dye-loaded chloroform

6.4 Summary

PDMS microgel dispersions were shelled following core swelling with ethanol, n-heptane and chloroform. All the regimes were observed to aggregate during the shelling process, even

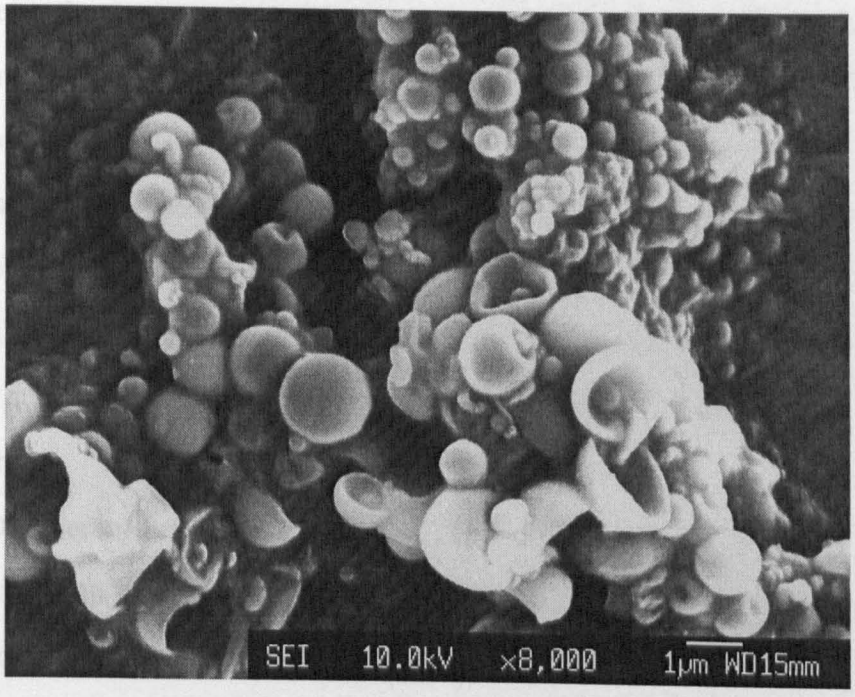

Figure 6.15: Shelled PDMS microgel that had absorbed Sudan III in chloroform prior to shelling. The core material was formed from 70/30 v/v DMDES/MTES.

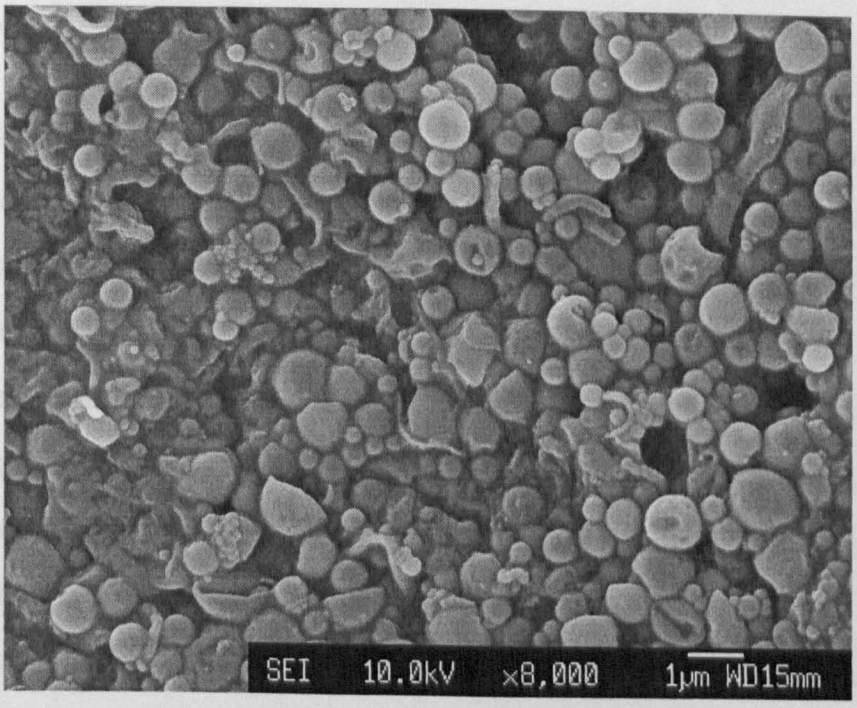

Figure 6.16: Shelled PDMS microgel. The core had been swollen with Sundan III in chloroform and was formed from 60/40 v/v DMDES/MTES.

if tumbled. n-Heptane dispersions that were not tumbled during shell maturation formed a soft solid layer at the water-heptane interface; this was an apparent consequence of monomer-absorption into the organic phase. Chloroform and n-heptane-swelled dispersions could be redispersed following centrifugation into INUTEC SP1 surfactant solution.

The ethanol-swelled particles were embedded in secondary material, and were observed to form crenellated structures under SEM. Smooth shells were formed upon chloroform and heptane-swollen dispersions. The crenellated nature of the shells formed in the ethanol systems may be attributed to the enhanced solubility of alkoxysilane-derived oligomers in the continuous phase.

While PDMS emulsions could be formed from 4-nitroanisol-loaded DMDES, the dye did not partition into the PDMS phase. Instead, the basic emulsion forming environment rendered the dye water-soluble, possibly due to nucleophilic substitution by hydroxide.

Absorption of dye-loaded solvent proved a more successful method to incorporate dye, as solubility in DMDES is not an issue. Use of MTES cross-linker improved the quality of the final shelled particles, which may be attributed to an enhanced stability to coalescence.

6.5 Further Work

PDMS swelling enhanced density effects so that sedimented or creamed phases formed. This process can enhance polydispersity and also lead to formation of secondary material. Selection of a vector solvent, or use of a mixture of solvents, of similar density to water could reduce these effects, as may use of smaller initial template droplets.

A significant issue posed by the shelled PDMS system is the limiting effect of high pH on the nature of potential active constituents. Use of dialysis to lower the pH prior to swelling followed by addition of NH_3 during the shelling step could be explored. Such a study could determine if the PDMS core extends any protection to contained active.

UV spectroscopy has previously been used to measure diffusion of dye through polymer shells [102] and could be similarly used for shelled PDMS dispersions.

The effects of swelling and presence of the dye during shell formation may also warrant investigation. It would be useful to determine if dye is trapped within the shell, and whether

shell thickness and Young's modulus is affected.

The dye incorporation studies typically involved dye concentrations of 1 wt. % in solvent. Extensively swollen PDMS emulsions may have solvent volume fractions nearing 97 %, however no attempt to shell such emulsions has as yet been attempted. Non-ionic surfactants could be used to prepare sub-micron PDMS droplets, which may then be swelled up to 1 micron, rather than attempting to shell droplets swollen to 3 μm. Unless the presence of PDMS microgel can demonstrably strengthen the particle, the core material should primarily consist of active material.

Chapter 7

W/O Capsules

7.1 Introduction

PDMS emulsions or microgels are unsuitable media for salts and some polar molecules. An aqueous core/solid shell system, derived from W/O emulsions, was investigated for applications that would involve such species.

Silica-coated emulsion droplets have previously been formed by interfacial sol-gel reactions [28, 29]. Ammoniacal $CaCl_2$ brine has been emulsified into kerosene or n-hexadecane in the presence of a surfactant to form a W/O emulsion. TEOS or MTES, added to the organic continuous phase, condensed at the oil-water interface to form a membrane that is thought to thicken until no further interaction between the monomer and the aqueous phase is possible. An advantage of this approach is that the active constituent is present in the core phase from the outset and does not have to be subsequently absorbed.

TEGOPREN 7008, from Degussa, is an alkyl- and polyether-modified siloxane comb polymer (Figure 7.1). Its molecular weight is > 10,000 Da. Previous workers have postulated that alkoxysilanes may condense with the hydroxy-terminated polyether moieties to form a cross-linked network [28]. This surfactant shall subsequently be referred to as TEGOPREN.

The formation of a membrane at an oil-water interface, following the condensation of alkoxysilane mixtures, has been studied by a rheological technique that measures the interfacial shear elasticity and viscosity [29]. Mixtures of TEOS and DMDES were found to both adsorb faster and form films that exhibit more elasticity than mixtures of MTES and

DMDES. Also, adsorption rate was found to relate to the nature of the continuous phase. Increasing aliphatic chain length was found to decrease the rate of adsorption.

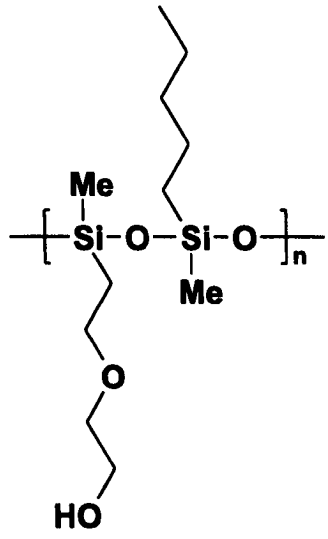

Figure 7.1: TEGOPREN monomer

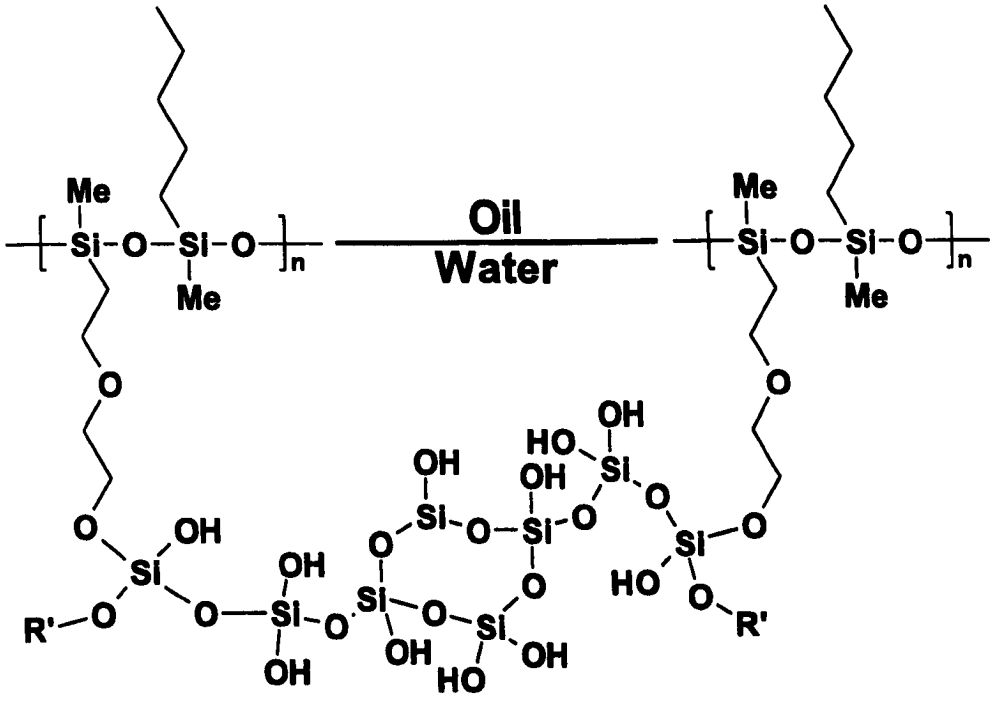

Figure 7.2: TEGOPREN cross-linked with silica at the oil-water interface

7.2 Experimental

Hexadecane with dissolved TEGOPREN 7008 (1 wt. %) was sheared by a Silverson LR4T mixer, at 3000 RPM, as an aqueous phase, e.g.NH_3 (1 % v/v), was added to give a total aqueous volume fraction of 20 %. The dispersion was left under shear for 30 minutes before adding TEOS (typically 20 g dm^{-3}). The emulsion was further sheared for 5 minutes and left to stand for 24 hours.

7.3 Results and Discussion

Initially silica shell formation at the oil-water interface of W/O emulsions brought about by catalysed hydrolysis of alkoxysilanes was investigated.

7.3.1 Water-in-Oil Emulsions

Hexadecane

Hexadecane was principally used as the continuous oil phase because it is non-volatile (it has a vapour pressure less than 1 Pa at room temperature), immiscible with water, and chemically inert. It boils at 286.3 °C and is less dense (0.773 kg dm^{-3}) than water [103].

7.3.2 SPAN 80 Stabilized W/O Emulsion

A 20/80 v/v W/O emulsion stabilized by sorbitan monooleate (SPAN 80, 1 wt. %, Figure 7.3) was made. The aqueous phase was 1 % v/v ammonia. First the SPAN 80-hexadecane mixture was mixed at 1000 rpm, then the aqueous phase was added and mixing continued for 30 minutes. A cream-coloured emulsion was formed (Figure 7.4). The emulsion was observed to phase separate on standing, with a clear aqueous bottom layer and a sedimented emulsion-in-hexadecane top layer.

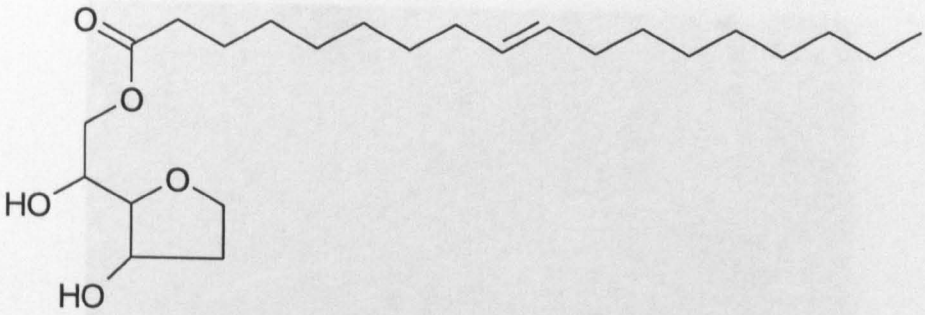

Figure 7.3: SPAN 80

Silica Shell Growth on a SPAN 80 W/O Emulsion

The emulsion was added to the TEOS and the mixture was homogenized at 1000 rpm for 5 minutes. The TEOS volume fraction (ϕ_{Si}) was 90 % (840 g dm^{-3}) and the emulsion volume fraction (ϕ_E) was 10 %, based on the method reported by Kaneva [29]. A cloudy mixture formed. Sedimentation was observed. Under a microscope spherical droplets were observed; some were ruptured and seemed to reveal a silica membrane (Figure 7.5). Long-term stability of these systems was not monitored.

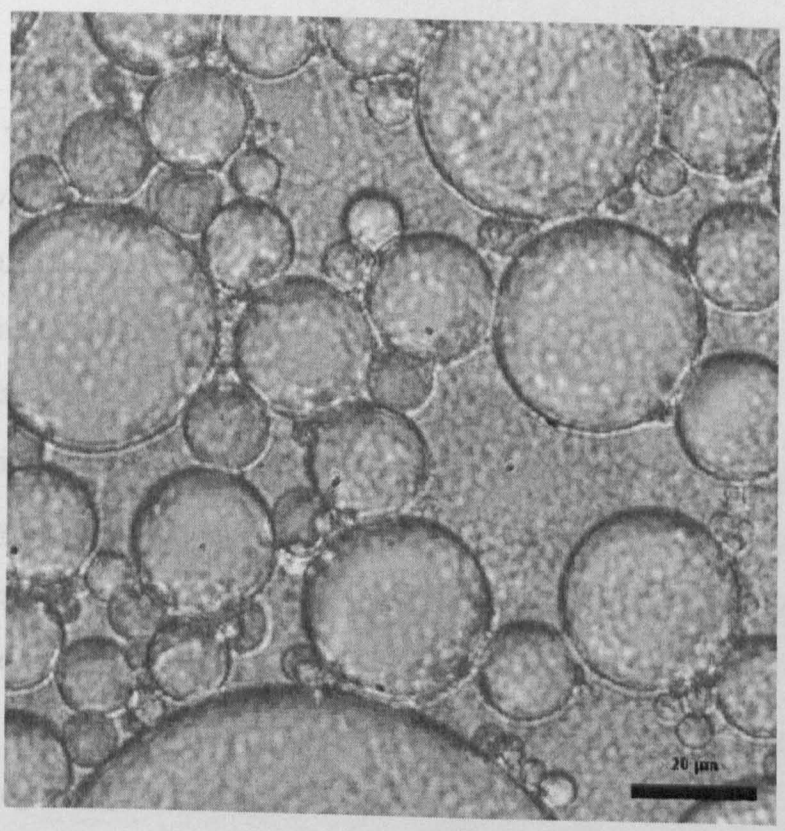

Figure 7.4: W/O emulsion stabilized by SPAN 80

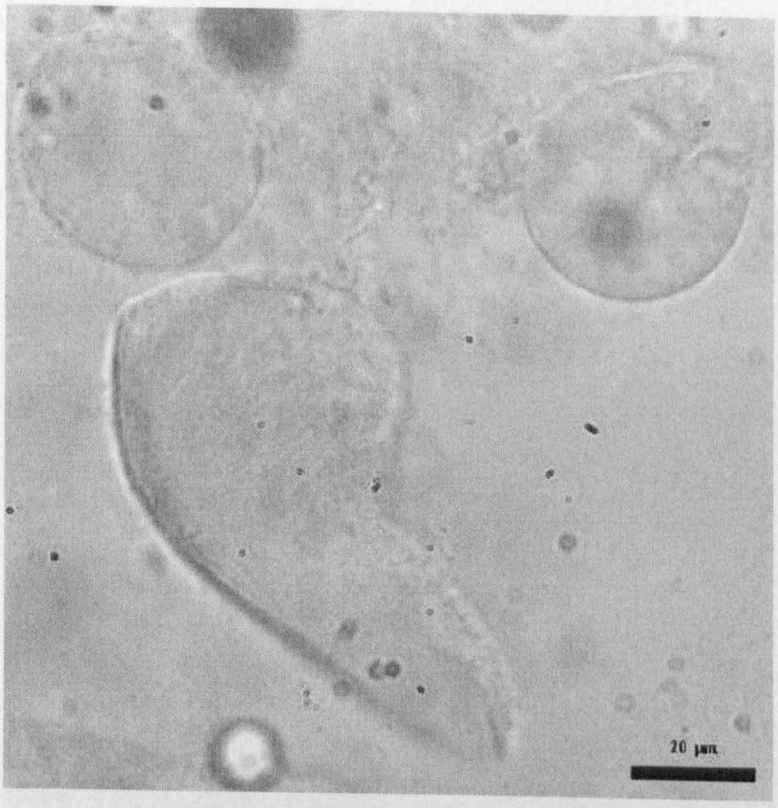

Figure 7.5: Ruptured droplets revealing a silica skin

7.3.3 W/O Emulsions Stabilized by TEGOPREN 7008

20/80 v/v W/O emulsions were prepared stabilized with TEGOPREN 7008. The aqueous phase was 1% v/v ammonia and the oil phase was hexadecane. The TEGOPREN 7008 concentration was set to 1 wt. %. The TEGOPREN was dissolved in the hexadecane with stirring. The aqueous phase was added to the mixture and stirring continued for a further 30 minutes. A white emulsion formed and sedimented on standing, but did not breakdown to form an aqueous layer.

Silica membranes were then grown on the emulsion droplets as before, but with different alkoxysilane regimes: TEOS; 80/20 v/v TEOS/MTES; and MTES. The emulsion and the silica-skinned regimes all sedimented upon standing; they were all redispersed with gentle shaking, apart from the pure MTES regime, which required more vigorous shaking. When inspected under the microscope after 24 hours, all the shelled systems were observed to be in a state of collapse (Figure 7.6, 7.7).

The particle collapse observed in the above systems may be a consequence of the high alkoxysilane volume fraction, which may increase osmotic pressure inside the droplets. Ini-

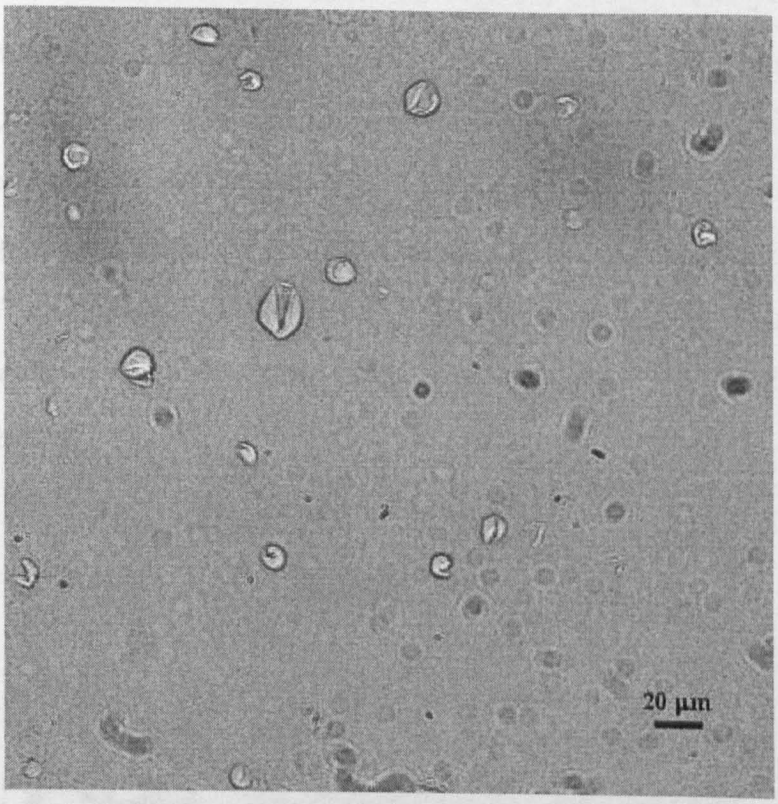

Figure 7.6: Optical micrograph of ruptured W/O capsules with TEOS-derived skins

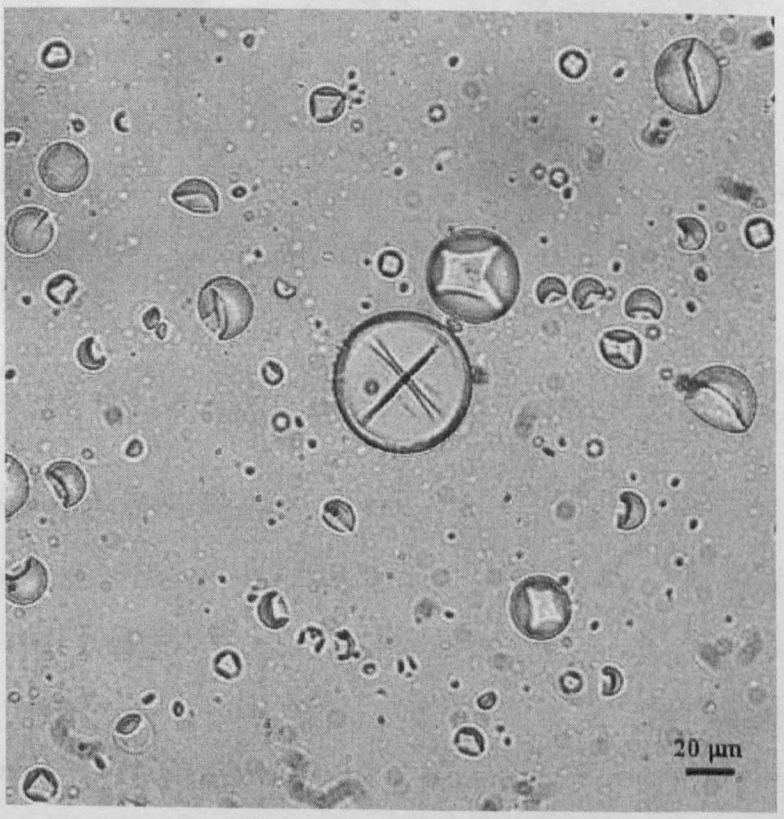

Figure 7.7: Optical micrograph of ruptured W/O capsules with MTES-derived skins

tial work with this system used much lower alkoxysilane volume fractions than those reported by Kaneva [29], typically 0.5–20 g dm^{-3} of emulsion [28]. Here the emulsion was made as before, but the TEOS monomer (corresponding to 20 g dm^{-3}) was added to the emulsion with further stirring at the same speed for 5 minutes. The system was not observed to exhibit total particle collapse in the bulk and was observed to be intact after 5 months (Figure 7.8). When examined by optical microscopy, the membrane-coated droplets were observed to crenellate, split open and disgorge a droplet when in proximity to the oil/air interface (Figure 7.9).

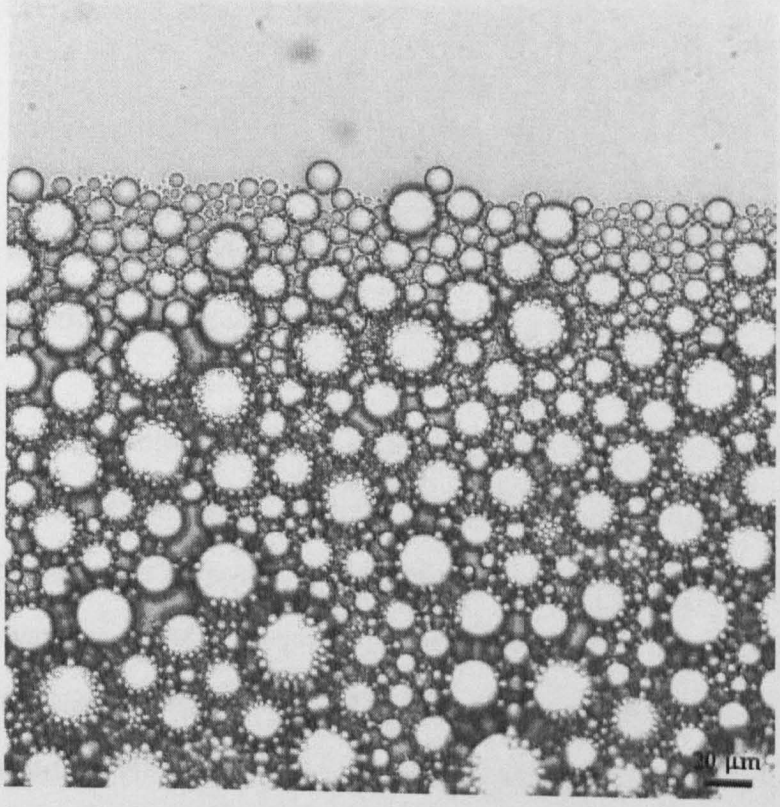

Figure 7.8: Optical micrograph of silica-skinned capsules prepared with a TEOS concentration of 20 g dm^{-3}. No particle collapse was observed in the bulk dispersion.

An emulsion was made without a silica shell to observe the behaviour of droplets at the oil boundary on the microscope slide surface. The droplets were observed to shrink, and then vanish over a period of five minutes (Figure 7.10, 7.11). The focal plane of the microscope was raised and lowered at this time to ensure that the droplets were not just moving out of focus, but the spreading hexadecane was too thin in this region to allow such motion. It seemed that the emulsion droplets were evaporating, which suggests that water was evaporating from the capsules too, thereby causing the crenellation. When too little

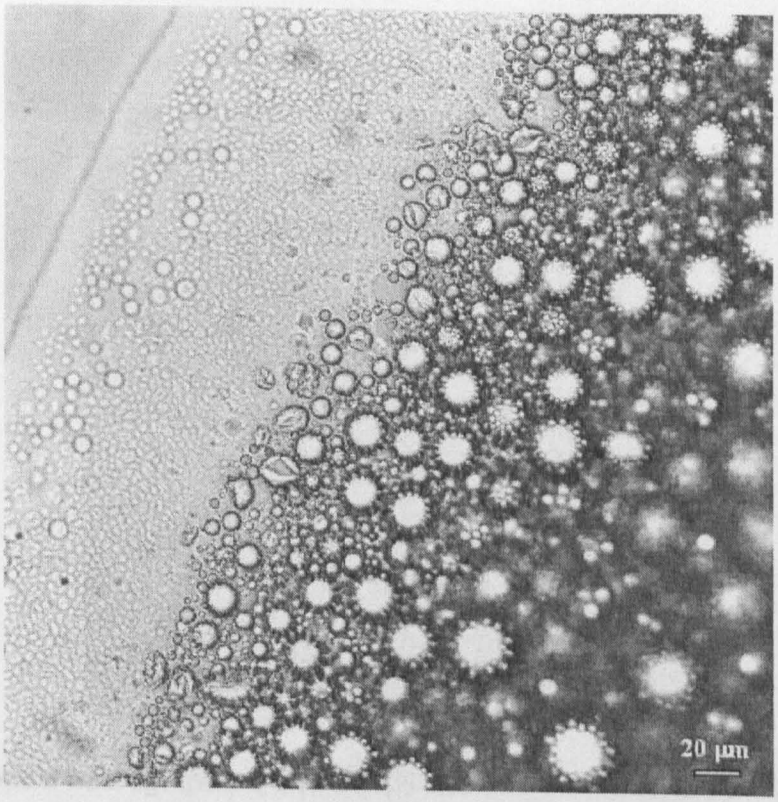

Figure 7.9: Optical micrograph of capsules rupturing at the hexadecane boundary

water remained in the core to support the silica membrane, it was torn, allowing remaining water to escape to the oil boundary where it continued to evaporate (Figure 7.12). That the capsules did not exhibit this behaviour in the bulk, even after many months, suggests that the observed effect was due to either a warming effect from the microscope lamp, proximity of the capsules to the air/oil interface—or both. The crenellation behaviour was not observed in the silica-skinned systems immediately after their preparation, instead they exhibited the emulsion-like vanishing, crenellation was typically observed after an hour's maturation time.

7.3.4 Alternative Sol-Gel Regimes

Use of catalyst in the organic phase of the TEGOPREN systems was investigated. A small quantity of glacial acetic acid was shaken with hexadecane, but it would not mix and phase separation occurred. Octanoic acid, however, was soluble in the hexadecane, but it formed an emulsion when shaken with water.

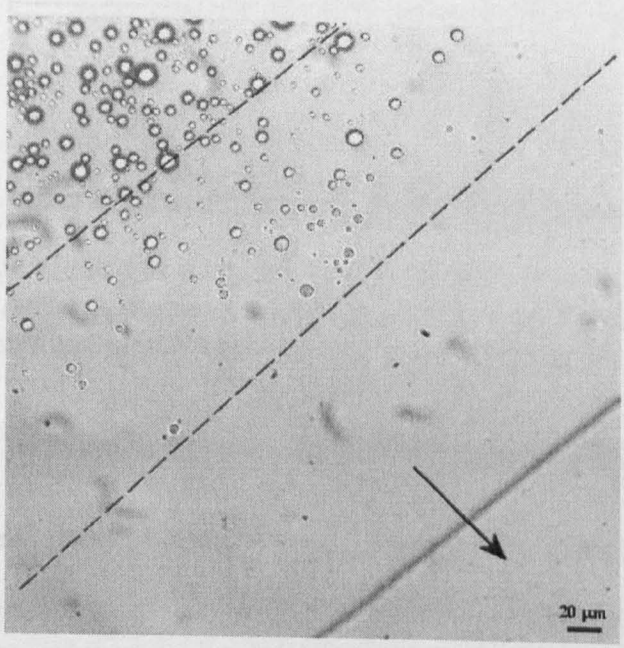

Figure 7.10: Optical micrograph a TEGOPREN stabilized W/O emulsion. The dashed lines show the region where the droplets evaporated from, the arrow indicates the direction of hexadecane boundary movement

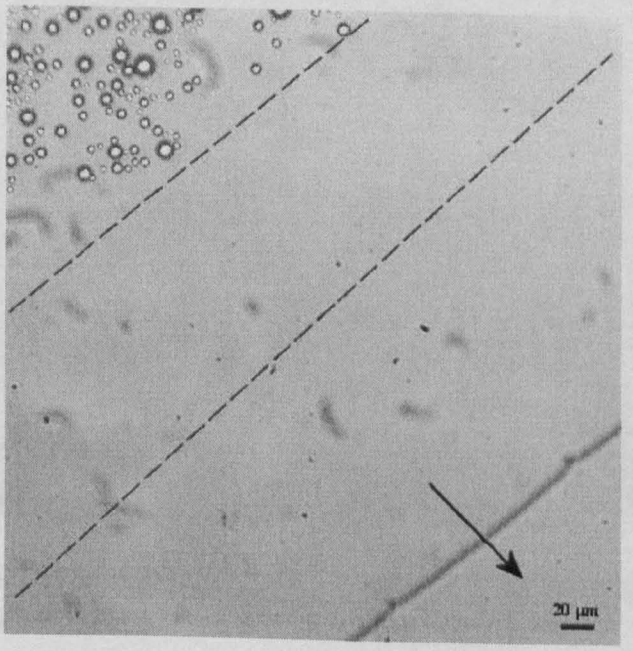

Figure 7.11: Optical micrograph of the drying W/O emulsion (figure 7.10) after 5 minutes

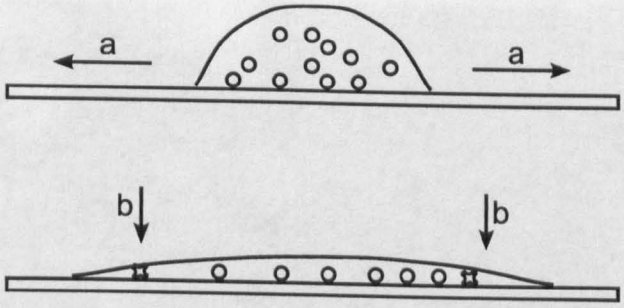

Figure 7.12: Schematic of the spreading hexadecane droplet on a microscope slide surface, without a cover-slip. Arrow **a** shows the direction of hexadecane boundary movement. Arrows **b** indicate the boundary region where crenellations are observed.

Acid Hydrolysis of TEOS using Octanoic Acid in the Organic Phase

For each system a new standard emulsion was prepared that consisted of 20/80 v/v water/hexadecane stabilized by 1 wt. % TEGOPREN 7008, and then TEOS was added with stirring for 5 minutes.

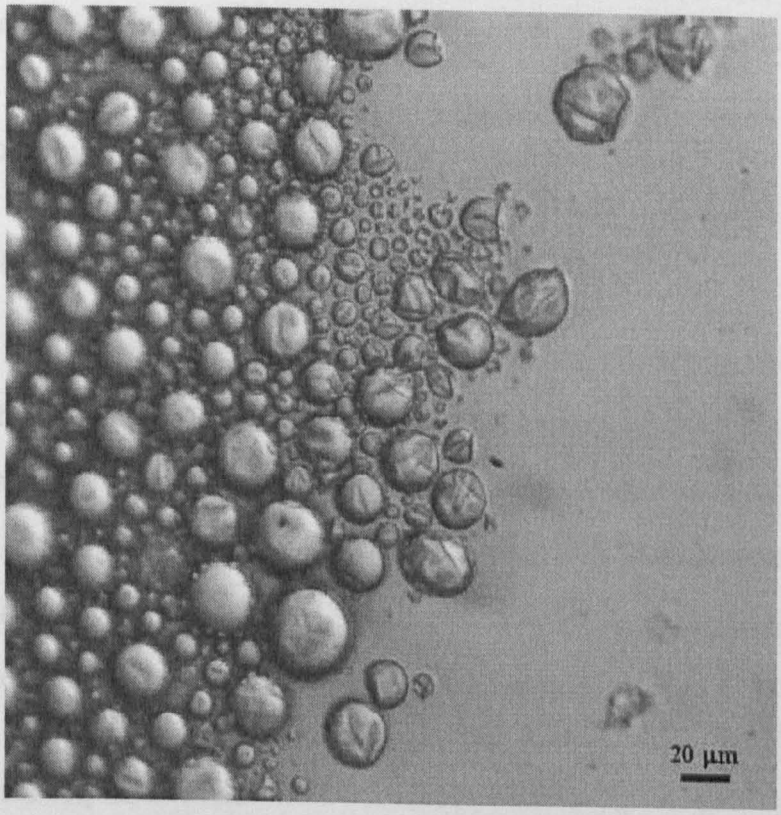

Figure 7.13: Capsules whose skin formation was catalysed by octanoic acid in the hexadecane phase. Age 24 hours.

The non-spherical capsules could possibly be a consequence of particle coalescence, suggesting some fluidity in the shells of this system—or that fluid from ruptured capsules

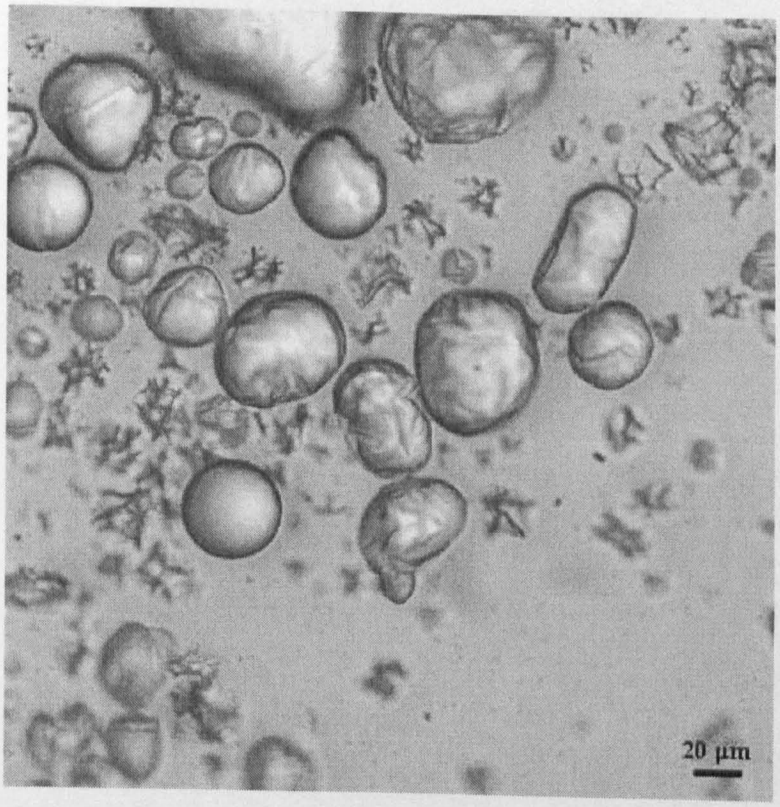

Figure 7.14: Capsules whose skins formation was catalysed by octanoic acid. Age two weeks.

had coalesced to form larger droplets and then formed a membrane.

Weak Acid in the Aqueous Phase

The use of acids in the aqueous phase was investigated because it was hoped that the alkoxysilanes would be hydrolysed under such conditions to form charged precursors that would be slow to condense, thereby increasing shell precursor uptake into the droplet. Acetic acid (200 ppm) used in place of ammonia. Initially a system with similar behaviour to that of the typical ammonia regime was formed, but after ageing for 10 days large numbers of non-spherical capsules and crenellations were observed in the bulk (Figure 7.15).

Strong Acid in the Aqueous Phase

Skinned droplets were also formed using 1 % v/v HCl in the aqueous phase. A system similar to the ammonia regimes was observed, which was still stable after a week, unlike the other acid systems. Crenulation still occurred at the the oil boundary of the microscope slide, but no water droplets were observed to disgorge. The capsules at the oil boundary were observed

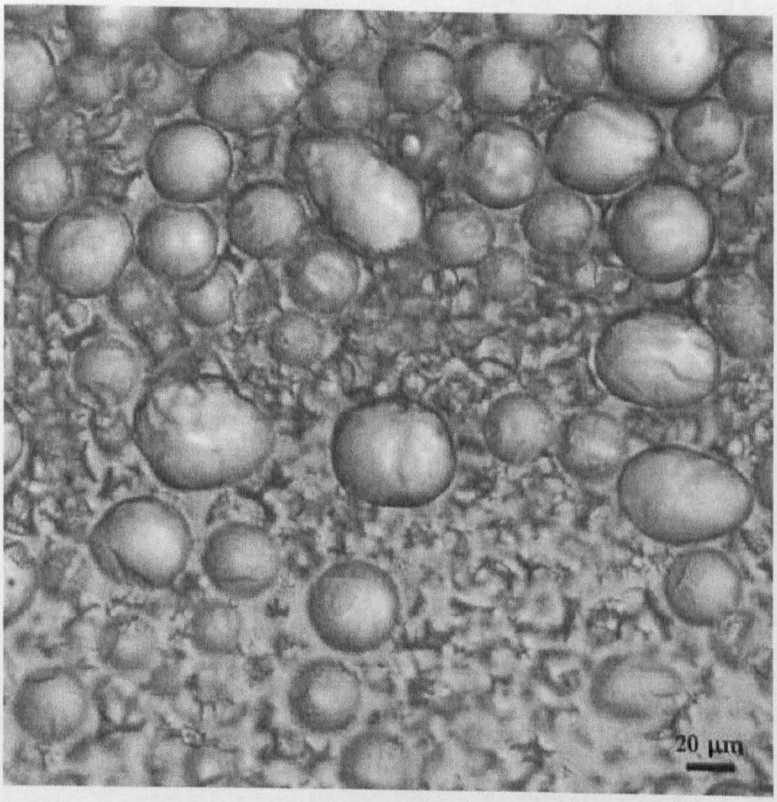

Figure 7.15: Droplets whose skin formation was catalysed by acetic acid.

to crenulate within the first minute of being placed on the microscope stage, whereas the ammonia system did not begin to crenulate until after 3 minutes. Use of HCl does not seem to convey any advantage to the system. The HCl system, like the other acid systems, did not seem to disgorge secondary droplets upon tearing of the silica skin (Figure 7.16). It is not clear why the disgorging effect is observed in the ammonia system and not in the HCl one. The skin coalescence observed in the organic acid-catalysed regime, but not in the HCl system, may be a consequence of acid adsorption at the interface leading to incorporation in the skin.

7.3.5 W/O Emulsions Stabilized by a SPAN 80/TEGOPREN Blend

The incorporation of a co-surfactant was investigated to determine if reduced TEGOPREN cross-linking would prolong monomer uptake into the aqueous phase. The total surfactant concentration was maintained at 1 wt. %. Because capsules had been observed in SPAN 80 systems, it was decided to use SPAN 80 as the co-surfactant. Also, a lower aqueous volume fraction (10 % v/v) was used, as SPAN 80 had not stabilized 20 % v/v previously.

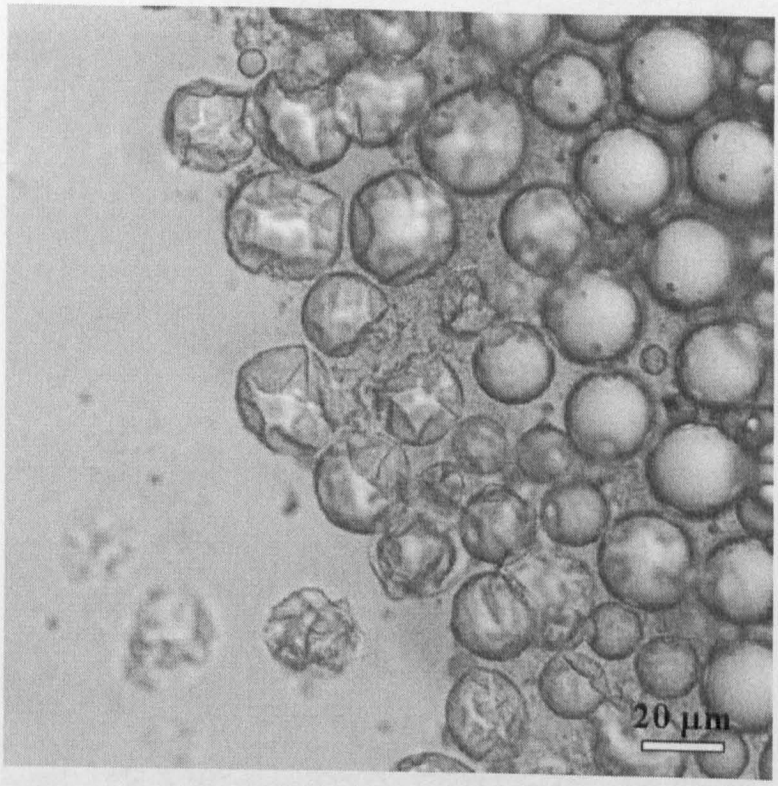

Figure 7.16: Capsules formed with 1 % HCl as a catalyst in the aqueous phase.

Skinned droplets stabilized by 75/25 wt/wt SPAN 80/TEGOPREN 7008 exhibited extremely rapid sedimentation due to particle aggregation (Figure 7.17). Either the SPAN 80 provided insufficient steric stabilization, or the low levels of TEGOPREN promoted bridging flocculation. The flocculated structure was broken-up on a microscope slide by applying gentle pressure to the cover-slip, this also ruptured some of the capsules (Figure 7.18). Phase separation was observed in the 50/50 TEGOPREN-SPAN blend. The 25/75 SPAN 80/TEGOPREN regime exhibited crenellations, but this system was the most similar to the original TEGOPREN systems.

7.3.6 Particle Stabilized Systems

W/O emulsions may be stabilized by hydrophobic silica particles, which adsorb at the oil-water interface creating a dense film that acts as a barrier to droplet coalescence [104]. Additional stability may also arise from the formation of a three-dimensional particle network in the continuous phase. Successful W/O emulsions have previously been formed using hydrophobic fumed silica [105]. W/O emulsions are typically formed after hydrophobic silica

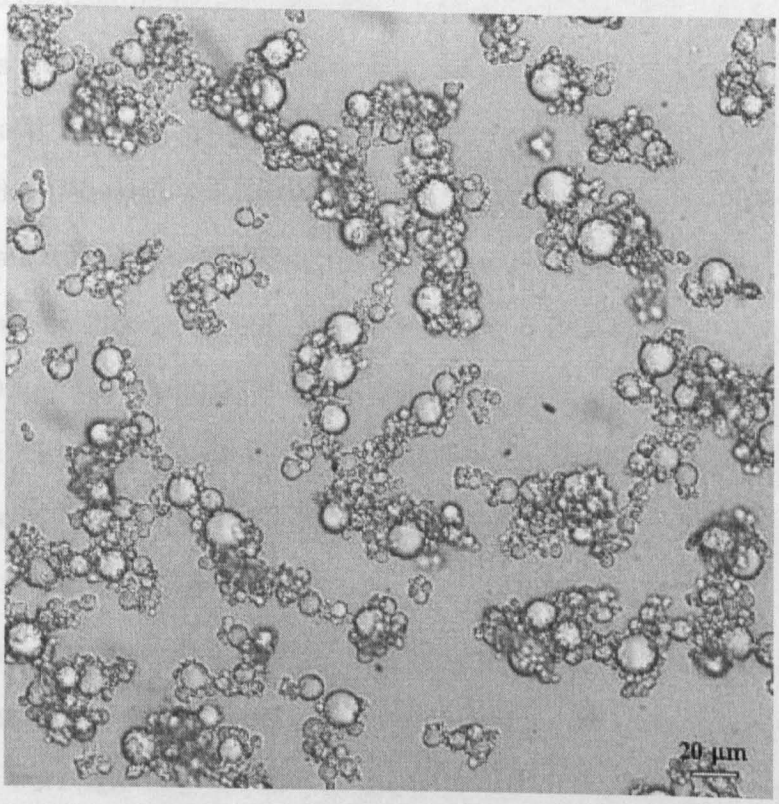

Figure 7.17: Flocculated skinned system derived from a 75/25 SPAN 80/TEGOPREN 7008-stabilized emulsion

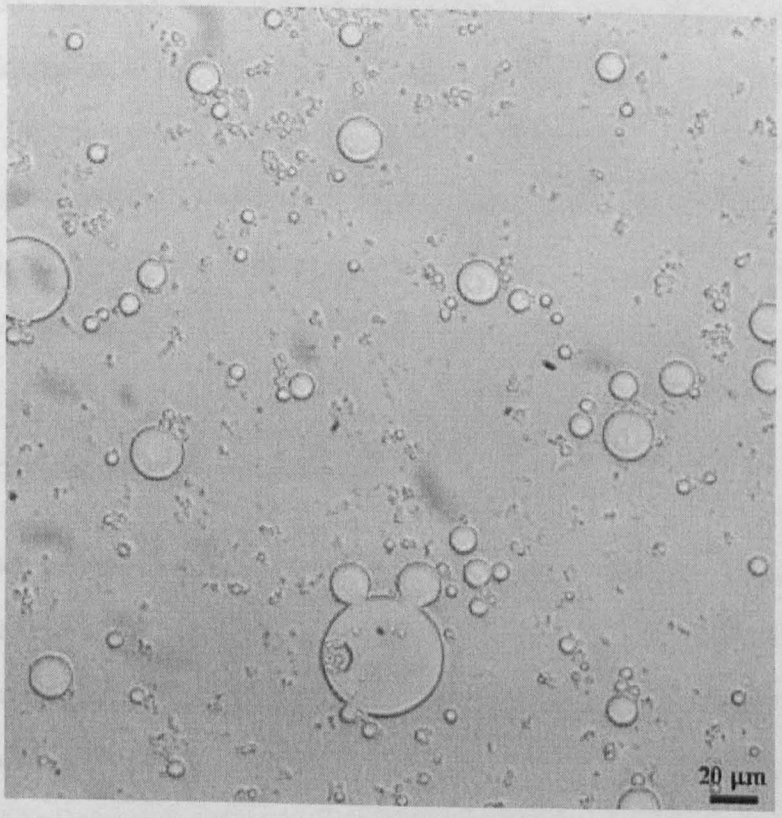

Figure 7.18: The capsules shown in Figure 7.17 squashed with a cover-slip

is dispersed into the continuous oil phase prior to addition of water.

Experiments were undertaken to form W/O emulsions containing NH_3 in the aqueous phase and then add TEOS to the hexadecane phase to form silica at the interface. HDK H30 hydrophobic silica (Wacker) was dispersed (1 wt. %) into hexadecane with sonication. 1 % aqueous ammonia was added with shear.

When sheared at 4000 RPM, a polydisperse emulsion with many droplets of diameter greater than 100 μm was produced. Further shear at 5000 RPM for 5 minutes yielded smaller droplets (Figure 7.19). Using 5 wt % HDK H30 silica as a stabilizer yielded an emulsion with smaller droplets still (Figure 7.20). The 5 wt. % system was also resistant to sedimentaion because the silica formed a supportive gel network around the water droplets.

Crenellations were observed in the capsules upon evaporation of the aqueous phase, suggesting that the silica has formed a gel layer at the interface. Silica particle-stabilized systems containing HCl were also successfully prepared. In an attempt to grow silica at the interfaces of particle-stabilized W/O emulsions (containing 1 % ammonia), TEOS was added to the hexadecane phase. The particle-stabilized emulsion was a dense white paste prior to the addition of TEOS, so further homogenization at 6000 RPM with subsequent sonication for 5 minutes was undertaken to ensure adequate mixing of the TEOS. Crenulated capsules were observed under the microscope, but because this behaviour was observed in the absence of TEOS for particle-stabilized systems the extent of silica formation at the interface is uncertain. The crenulated capsules seem to be smoother (Figure 7.21) than the TEOS free systems (Figure 7.20), which suggests the nature of the interface has changed.

Dilution of Particle-stabilized Emulsions

If particles posses suitable wetting properties at an interface they are said to be irreversibly adsorbed, unlike traditional surfactants whose occupancy at an interface is in dynamic equilibrium with occupancy in the bulk [105, 104]. A consequence in the differing behaviour of the two systems may be observed following dilution. In the case of traditional surfactants, dilution may lead to formation of larger emulsion droplets as the surfactant concentration is reduced to the extent that it can no longer maintain a large surface area. In the case of

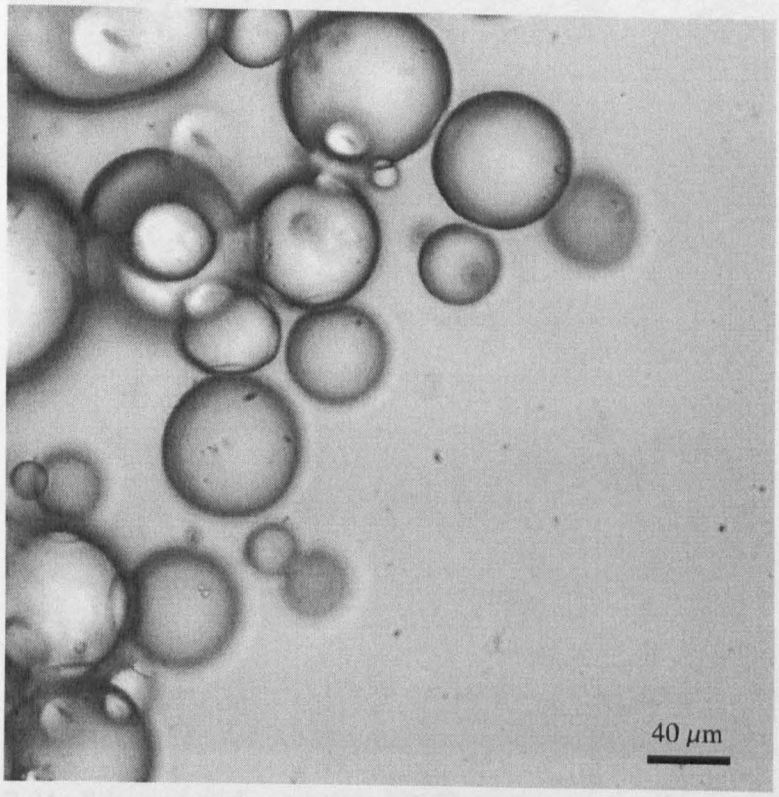

Figure 7.19: W/O emulsion stabilized by 1 wt. % hydrophobic silica particles

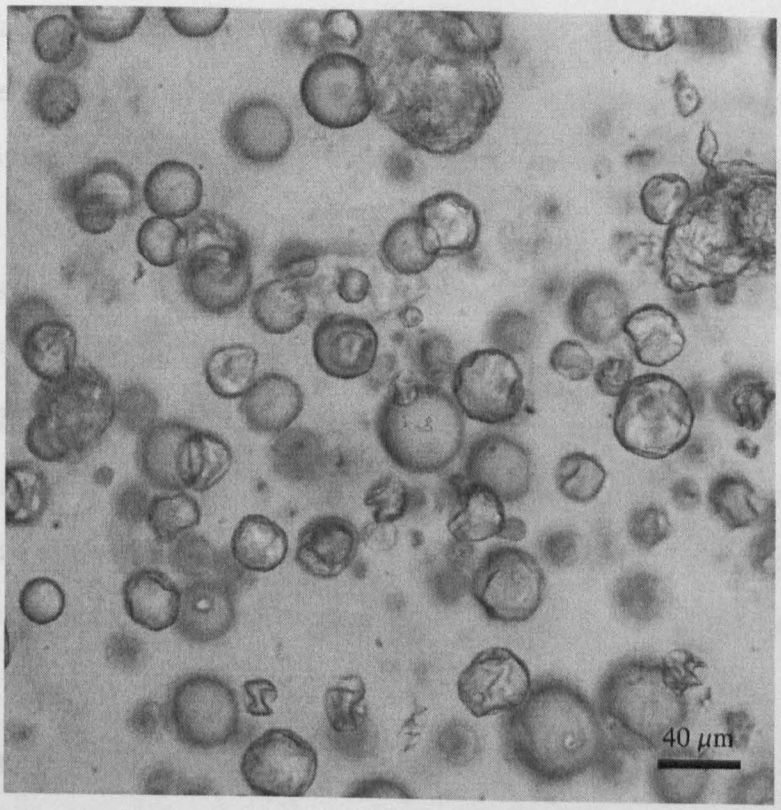

Figure 7.20: W/O emulsion stabilized by 5 wt. % hydrophobic silica particles with crenulations evident

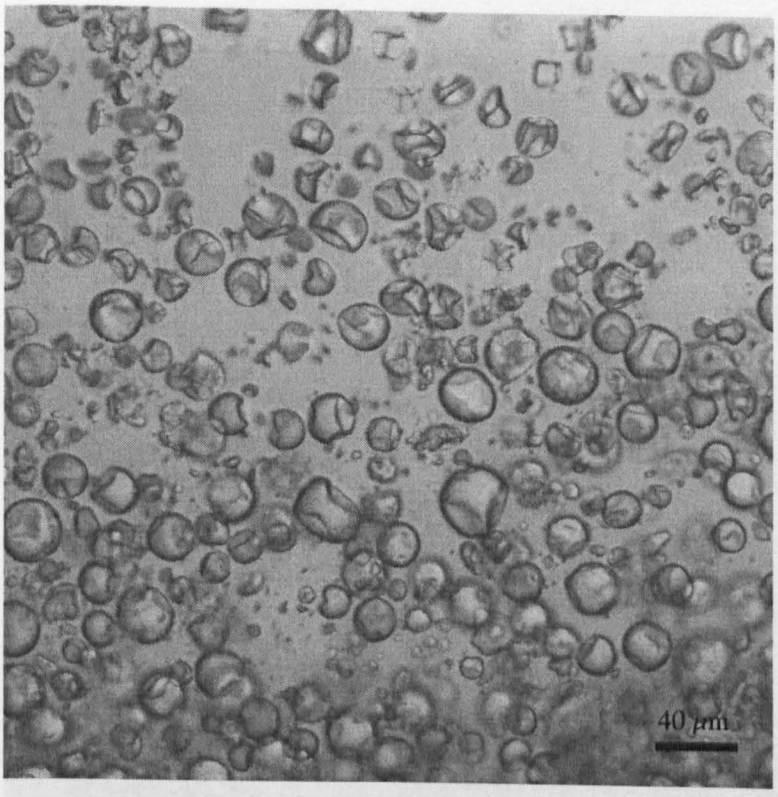

Figure 7.21: Silica particle-stabilized W/O NH_3 system with added TEOS

particle stabilizers, dilution is not so significant because the particle concentration at the emulsion interface remains constant. The silica stabilized systems were diluted with hexadecane to observe this behaviour first-hand. Though the diluted systems were no longer resistant to sedimentation, as the supportive silica gel network was dispersed, there was no obvious change in the size of the emulsion droplets.

The systems were also exposed to increasing external TEOS concentrations ranging from 10–75 vol % (Figures 7.22, 7.23 and 7.24). Interdroplet silica was observed in all cases. In the case of the 75 % TEOS, particle collapse was also observed (Figure 7.24). It is probable that initial silica formation occurred at the droplet interface, and that the ethanol produced as a consequence allowed further localized dissolution of TEOS. Following sedimentation water may have exuded into the interdroplet spaces causing further silica formation.

7.3.7 Centrifugation Study: Dispersions into Water

In order to investigate external shell growth in the silica-shelled systems through exploitation of surface chemistry, and to conduct osmotic pressure experiments, it is necessary to transfer

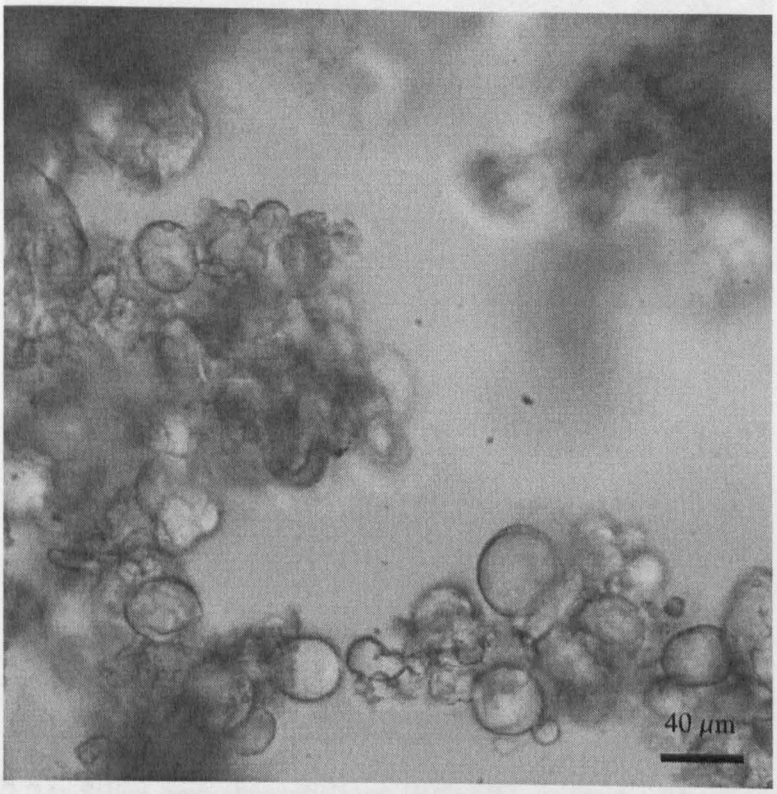

Figure 7.22: Silica particle-stabilized W/O NH_3 system with added TEOS

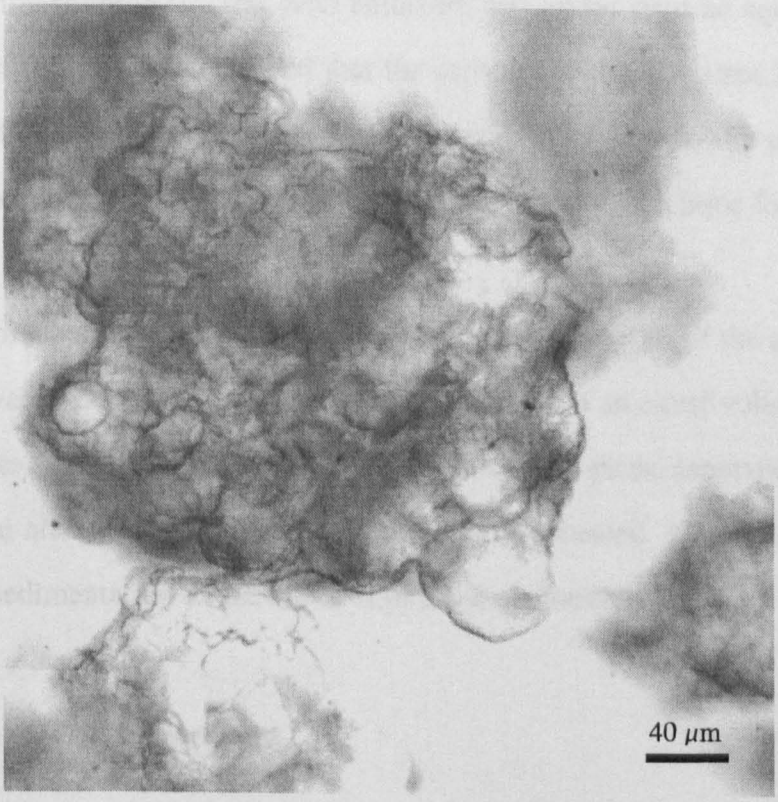

Figure 7.23: Silica particle-stabilized W/O NH_3 system with added TEOS

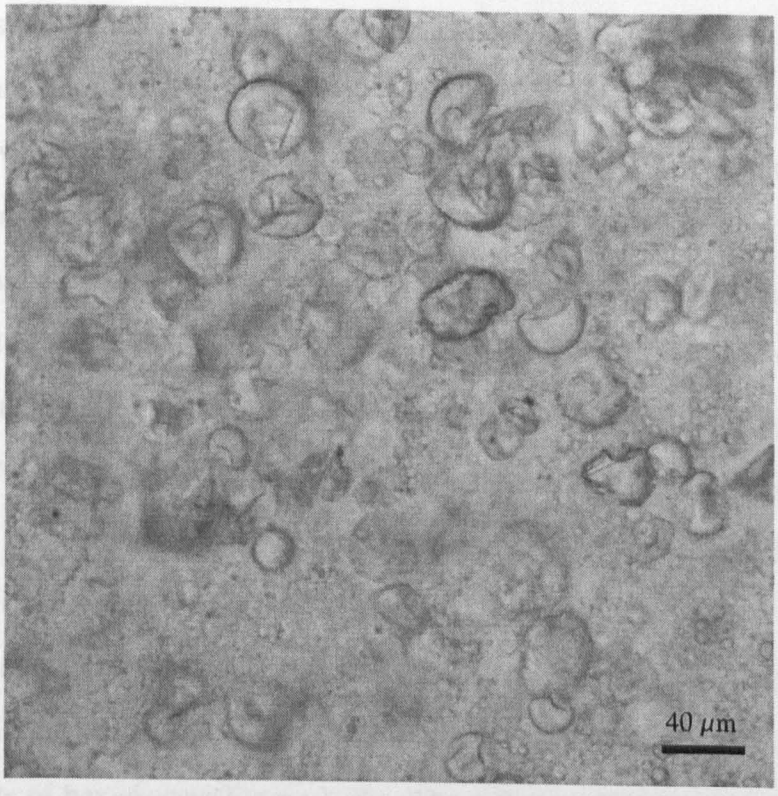

Figure 7.24: Silica particle-stabilized W/O NH_3 system with added TEOS

the capsules to an aqueous continuous phase. Centrifugation has previously been used to achieve such a transition [12]. The W/O emulsion was added onto an aqueous surfactant system and then centrifuged. Provided that the capsules are denser than the non-aqueous phase, they are forced into the aqueous phase to be stabilized there by the surfactant. Water is denser than hexadecane, so centrifugation is an appropriate technique for use with these systems.

Initial experiments were undertaken to determine the behaviour of the ammonia regime capsules with water. 5 ml of the dispersion was shaken with an equal volume of deionized water, then left to stand. A foamy emulsion formed. Limited phase separation was observed to have occurred after 4 days. The gross emulsion still persisted. No obvious transition of capsules to, or sedimentation in, the aqueous phase was observed.

Centrifugation: CTAB Experiment

Cetyltrimethylammonium bromide (CTAB) was initially used as a surfactant in the aqueous phase. The skinned emulsion was centrifuged with 0.5 and 1 wt % CTAB solutions at 145

RCF. The emulsions underwent rapid sedimentation and formed a cake that was driven into the aqueous phase (Figure 7.25). The aqueous phase was retained together with some of the emulsion-cake, which was readily redispersed with gentle shaking. In contrast with the W/O systems, the formed emulsion was observed to cream. This suggests that oil was drawn into the aqueous phase along with the capsules, and remained associated with them. The CTAB surfactant could act to stabilize the surface bound oil. Various droplet morphologies were observed under the microscope. Some capsules were apparently contained in larger hexadecane droplets (Figure 7.26) and some were observed seemingly separated from the hexadecane and freely floating in the aqueous phase. The majority of the freely floating capsules had smaller particles within (Figure 7.27). This might indicate that some of the hexadecane was forced through the particle skin during centrifugation. As the continuous aqueous phase evaporated from the slide, isolated capsules were observed to crenulate, as did those inside the small pockets of hexadecane(Figure 7.28). The different CTAB concentrations seemed to have little effect upon the formation of the sediment cake.

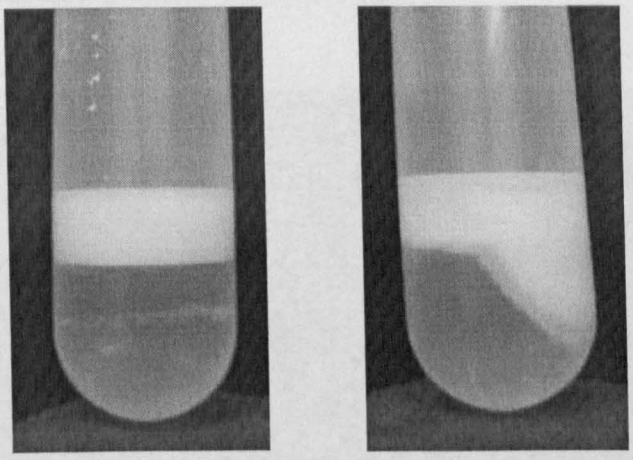

Figure 7.25: Centrifuge experiment: The left-hand tube is pre-centrifugation, with an emulsion top layer. The right tube is post-centrifugation and the emulsion layer has been displaced into the aqueous layer.

Influence of TEGOPREN Concentration

Five systems, based on the standard ammonia regime, with varying TEGOPREN 7008 concentrations were made. These systems were centrifuged into water, with 1 ml emulsion to 5 ml water, without any surfactant in the aqueous phase in order to see if residual TEGOPREN

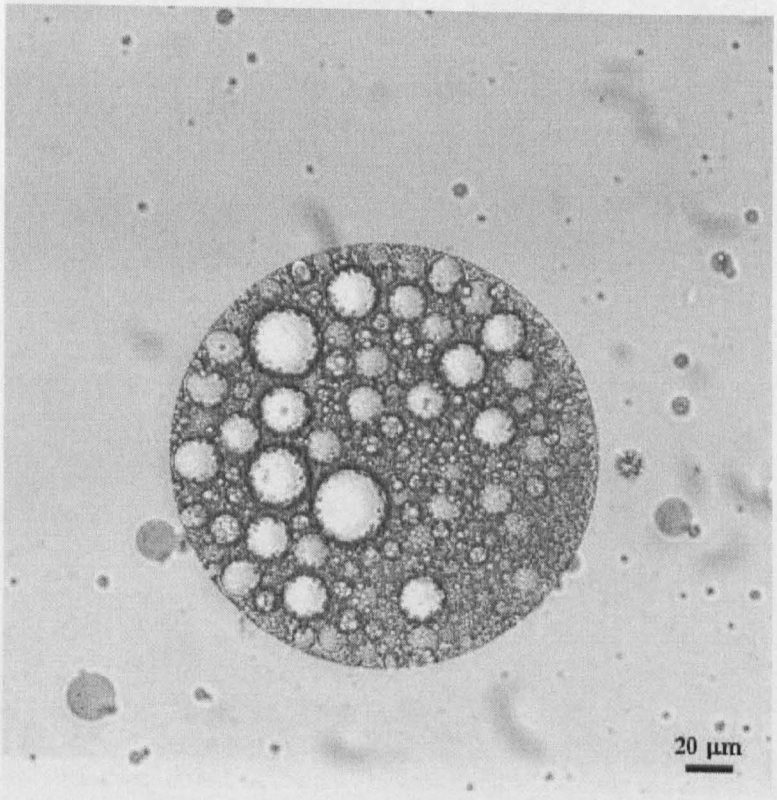

Figure 7.26: Skinned capsules contained in a large hexadecane droplet that is, in turn, in 1 % aq. CTAB. Free floating capsules are also present.

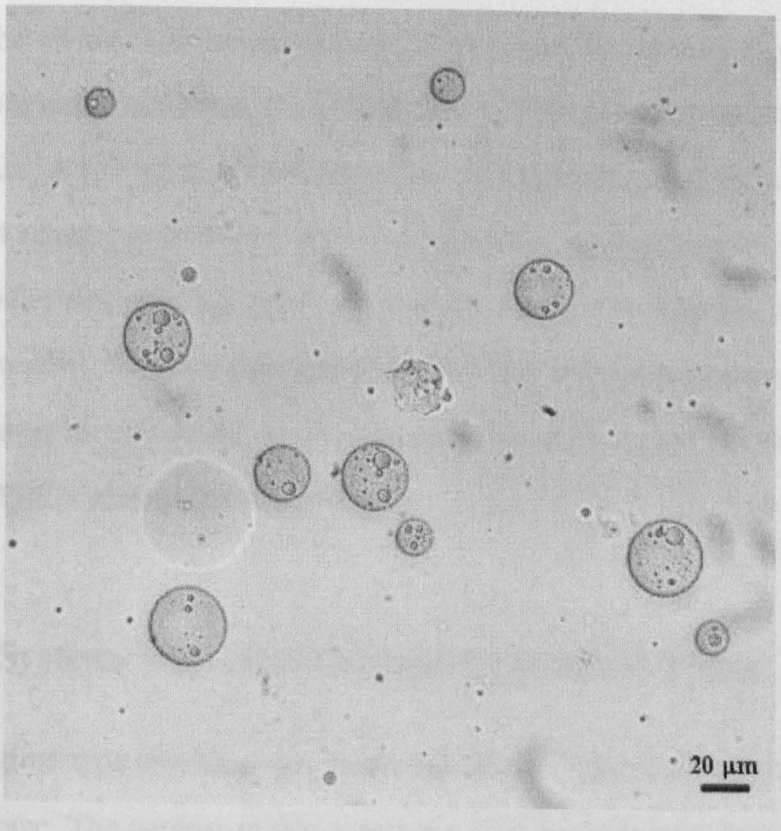

Figure 7.27: Skinned capsules dispersed into water. Smaller capsules are observed within.

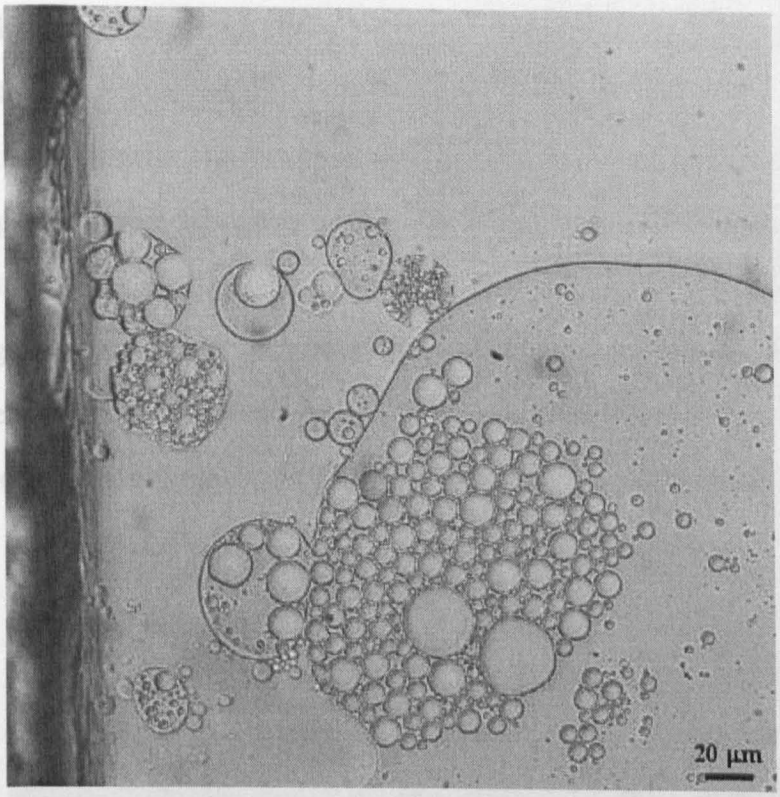

Figure 7.28: Skinned capsules crenellating within oil droplets that are dispersed in CTAB solution

could stabilize the capsules in water. The majority of the capsules were observed to have sedimented at the oil-water interface, without passing into the aqueous phase, but a small quantity was observed to have been forced along the centrifuge tubes' walls and had entered the aqueous phase. A few ml of the aqueous phase was pipetted off in each case. The white material that had adhered to the tubes' walls did not readily disperse in the water, but formed large white globules that creamed. Microscopically it is not clear whether the capsules had retained their integrity. Capsules were observed, but they contained droplets. Some broken shell structures were also observed. There seemed little difference in behaviour between the different TEGOPREN surfactant concentrations.

7.3.8 W/O Systems with an n-Heptane Continuous Phase

An ammonia regime-type emulsion was made, but with an n-heptane continuous phase instead of hexadecane. The purpose of this experiment was to determine if the skinned dispersions could be made in shorter chain alkanes, which may allow capsules to be transferred to

an aqueous medium through formation of a multiple emulsion with subsequent evaporation of the organic phase.

An emulsion was formed, but it did not exhibit the same behaviour as hexadecane analogues. The capsules seemed to behave more like a true emulsion, forming a honeycomb foam-like structure when concentrated at the evaporating n-heptane boundary on a microscope slide (Figure 7.29). There seemed to be no obviously stabilizing shell layer, as no crenellations were observed, but precipitated silica artifacts were observed upon drying (Figure 7.30). It is possible that the higher solubility of heptane in water disrupted skin formation.

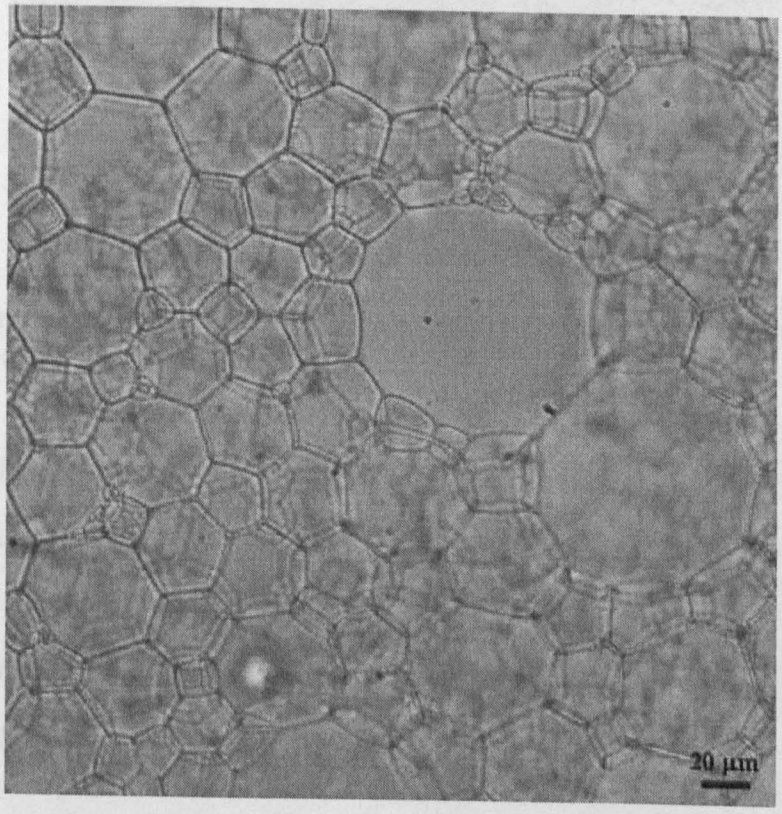

Figure 7.29: n-Heptane system. The formed capsules behave more like an emulsion, forming a honeycomb morphology upon compression

7.3.9 The Effect Catalyst Concentration

The Effect of Decreasing Catalyst Concentration

Capsules formed with with lower (0.1 %) NH_3 concentrations were examined. In addition, the use of 0.1 % HCl as an alternative catalyst was also explored. In both cases the skins persisted longer than the higher NH_3 systems. In the case of the NH_3 system, particle shrinkage

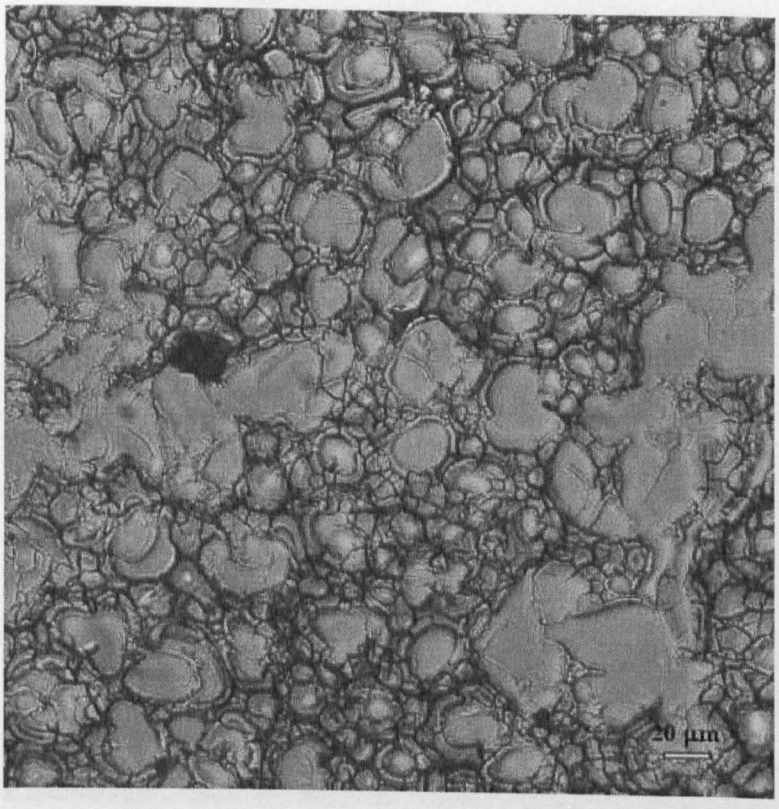

Figure 7.30: Dried n-heptane system. Drying of the n-heptane leaves silica artifacts, suggesting the silica did reside at the interface, but it was thin and soft.

followed by collapse occurred. The discarded skin became invisable thereafter (Figure 7.31). In the case of the HCl system, the skins persisted far longer after the initial collapse (Figure 7.32). The nature of silica produced under acidic or basic conditions differs. Silica formed in conditions of low pH is linear or randomly branched, whereas at high pH silica is denser, which may account for the difference in skin behaviour.

7.3.10 Inverse TEGOPREN emulsions

An aqueous TEGOPREN solution (1 wt %) was prepared. A silica-skinned W/O system was then added with shearing, which yielded an apparent W/O/W system (Figure 7.33). Such systems were observed to cream and coalesce; skinned capsules were observed to persist in the creamed phase. If the W/O/W systems were tumbled, a thick curd-like material was observed to form within 30 minutes (Figure 7.34); this was probably a consequence of particle collision and rupture.

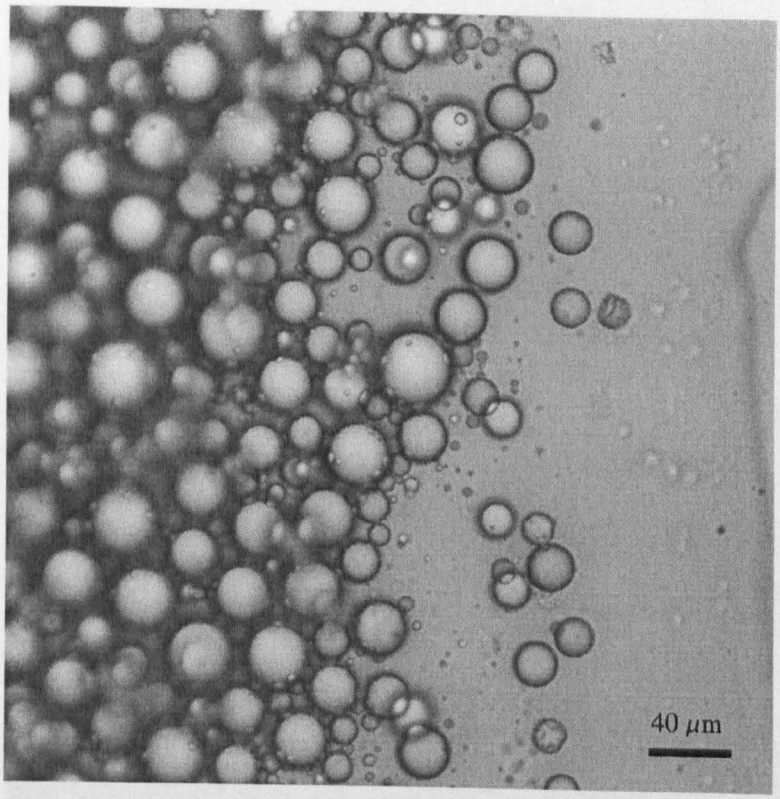

Figure 7.31: Optical micrograph of skinned 0.1 % NH_3 capsule collapse near the oil-air interface, the skins remain visible only momentarily following this process

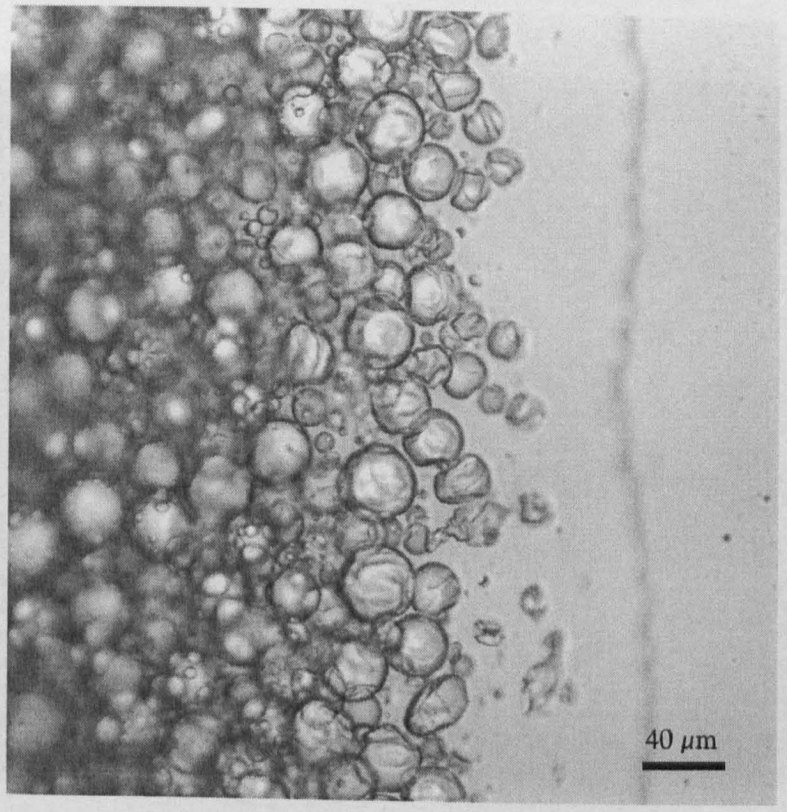

Figure 7.32: Optical micrograph of 0.1 % HCl particle collapse near the oil-air interface, the skins persist thereafter

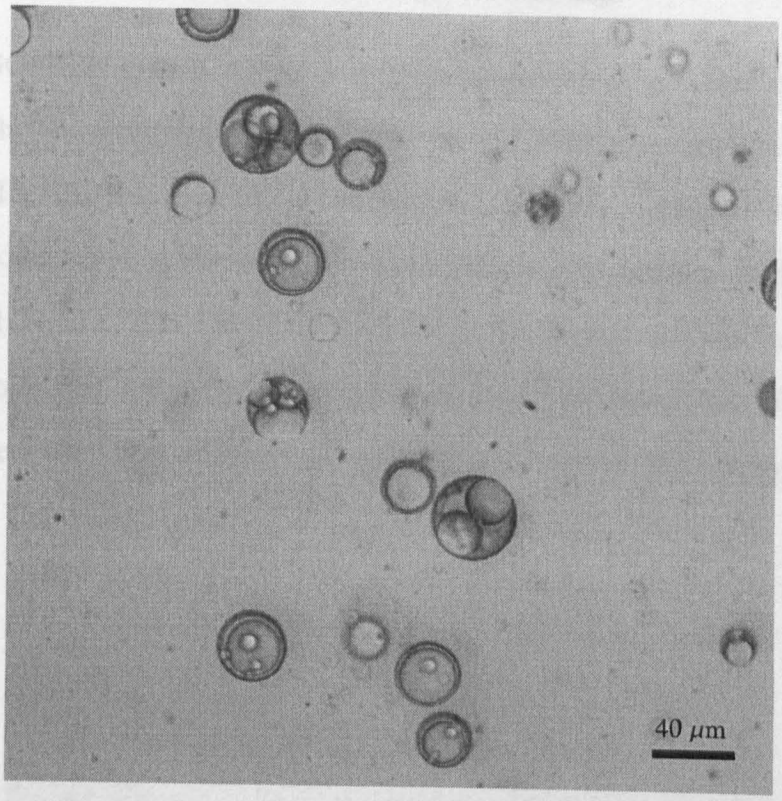

Figure 7.33: W/O/W system stabilized by TEGOPREN 7008; the internal water phase is silica-skinned

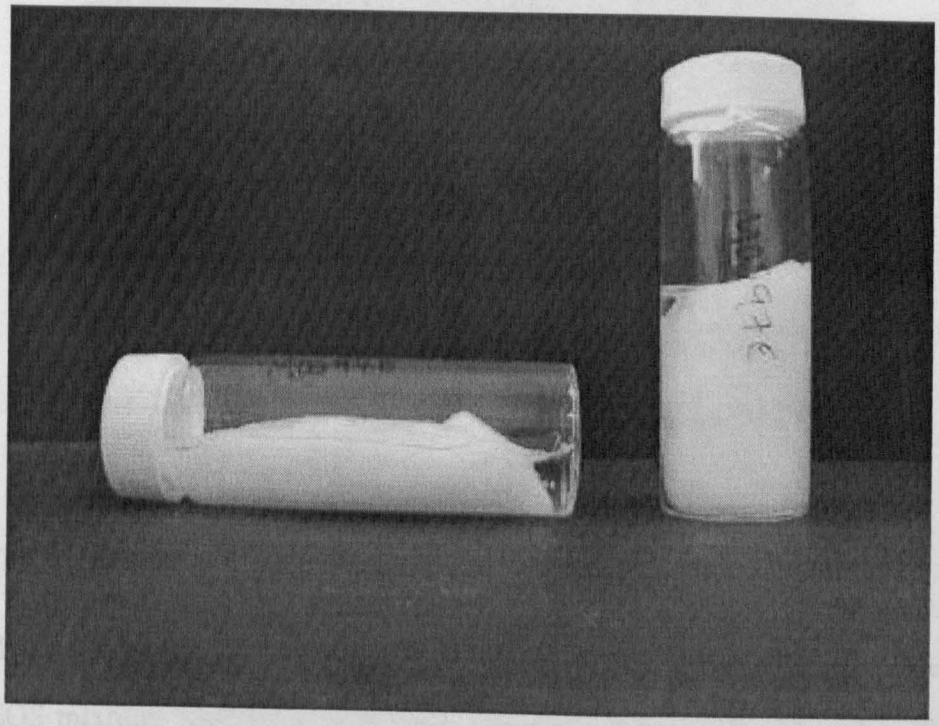

Figure 7.34: Tumbling the W/O/W system pictured in Figure 7.33 leads to formation of a curd-like material

Attempted shell growth on TEGOPREN W/O/W emulsions

A W/O/W TEGOPREN system, whose internal water phase had been skinned was subjected to Stöber growth: The multiple emulsion (125.5 ml) was added to a stirred mixture of ethanol (150 ml) and NH_3 (210 ml), then TEOS (14.5 ml, 1.2 ml $hr^{-}1$) was added. Two types of dispersion were produced: an apparent W/O/W emulsion that creamed; and aggregated capsules that sedimented (Figure 7.35). Under the microscope the aggregated capsules were observed to be crushed following applied gentle pressure on the cover-slip surface (Figure 7.36), the shards of apparent shell that remained seem to indicate that shell thickening may have been achieved.

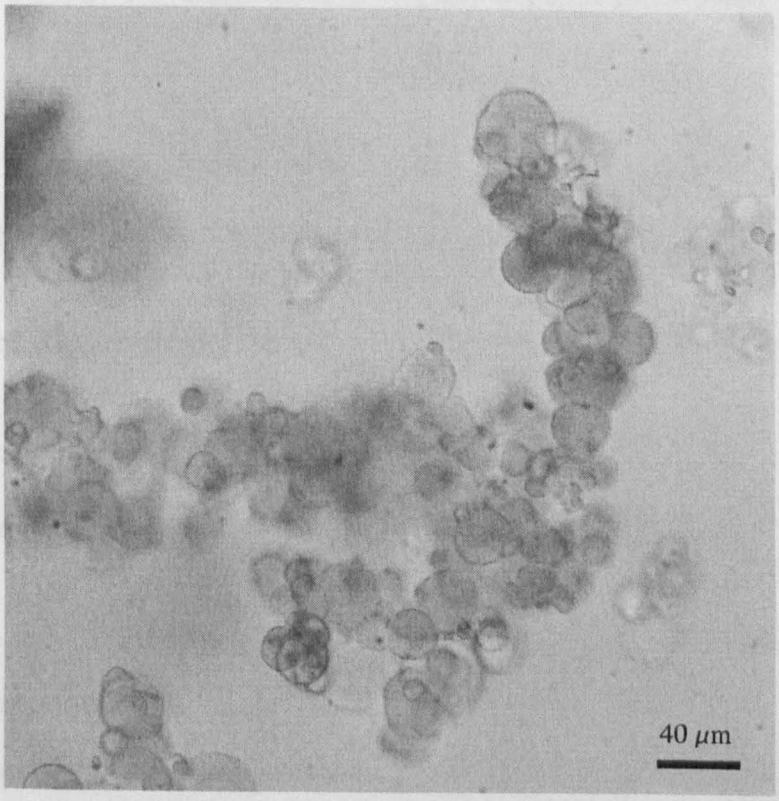

Figure 7.35: Capsules from the sediment following shell growth

TEOS/MTES addition to TEGOPREN W/O/W

Multiple TEGOPREN emulsions were also subjected to Stöber growth with addition of an MTES/TEOS mixture. Multinuclear W/O/W systems were observed (Figure 7.37), with an apparent flexible silica skin on the oil droplet surface that could be ruptured upon application of gentle pressure (Figure 7.38). The small droplets observed in the oil phase may have been

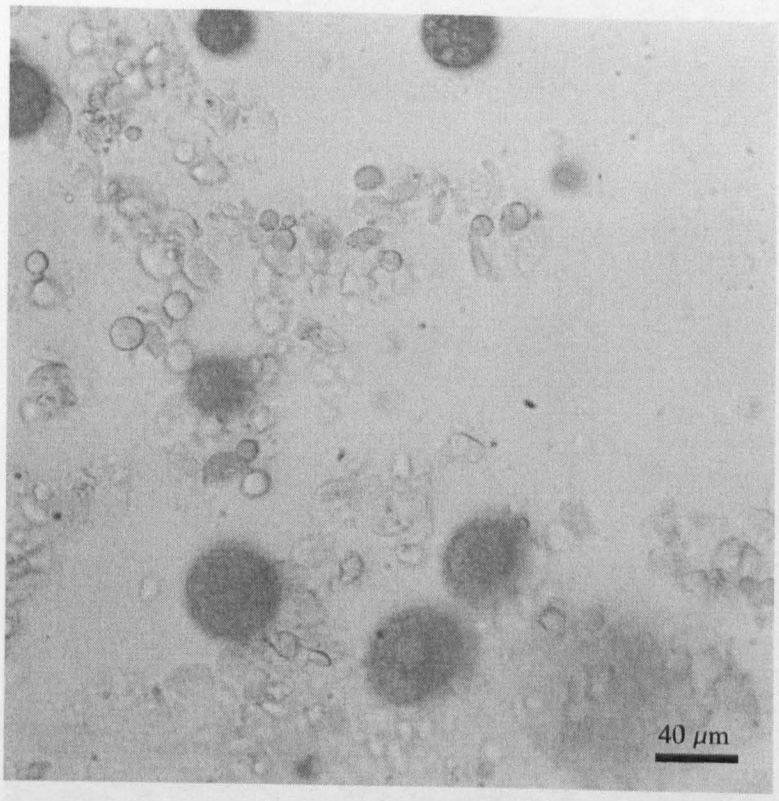

Figure 7.36: Squashed sediment revealing broken shells; darker oil droplets are also visible

a consequence of skinned emulsion break-up during the W/O/W preparation.

7.3.11 Solvent exchange in W/O emulsion

To assist in the transfer of the skinned W/O system from hexadecane into water a series of solvent exchanges were attempted. 5 ml of dispersion was added to 20 ml of n-heptane and shaken. The capsules were left to sediment, then the oil was decanted off and replaced with further heptane. Care was taken not to expose the sediment to air to prevent drying. The same procedure was used to transfer the capsules to ethanol. No capsules could be viewed under the microscope on a conventional slide as the continuous phase in both cases evaporated causing particle collapse. To view the capsules in these solvents it was first necessary to put drops of the dispersions into probe-clip press-seal incubation chambers (Sigma) to prevent solvent evaporation (Figure 7.39). Creaming was observed in the ethanol dispersion, indicating that the hexadecane may not have been effectively removed from the particle surfaces.

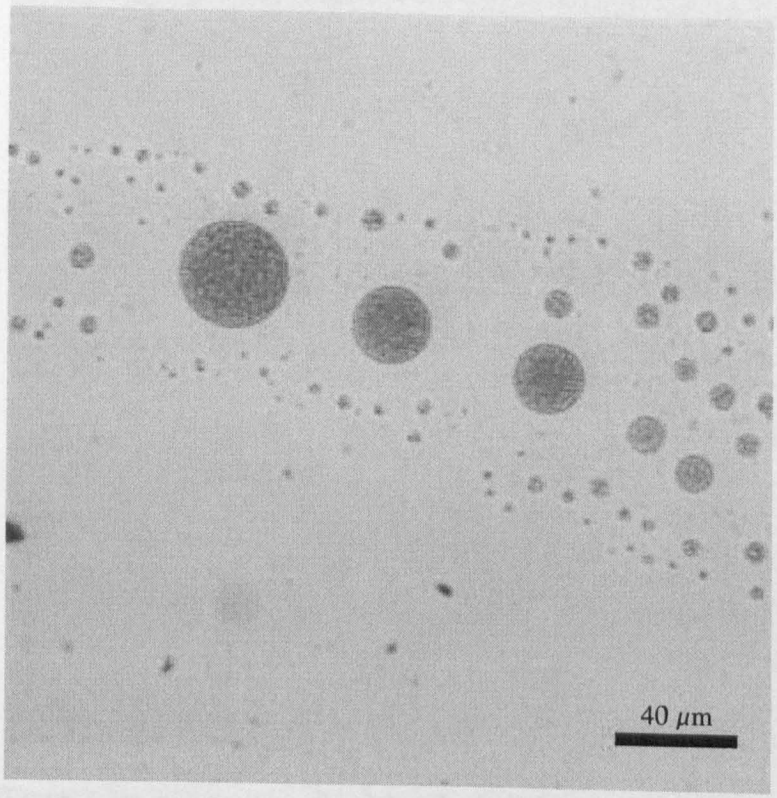

Figure 7.37: Skinned oil droplets, inside of which are smaller water droplets

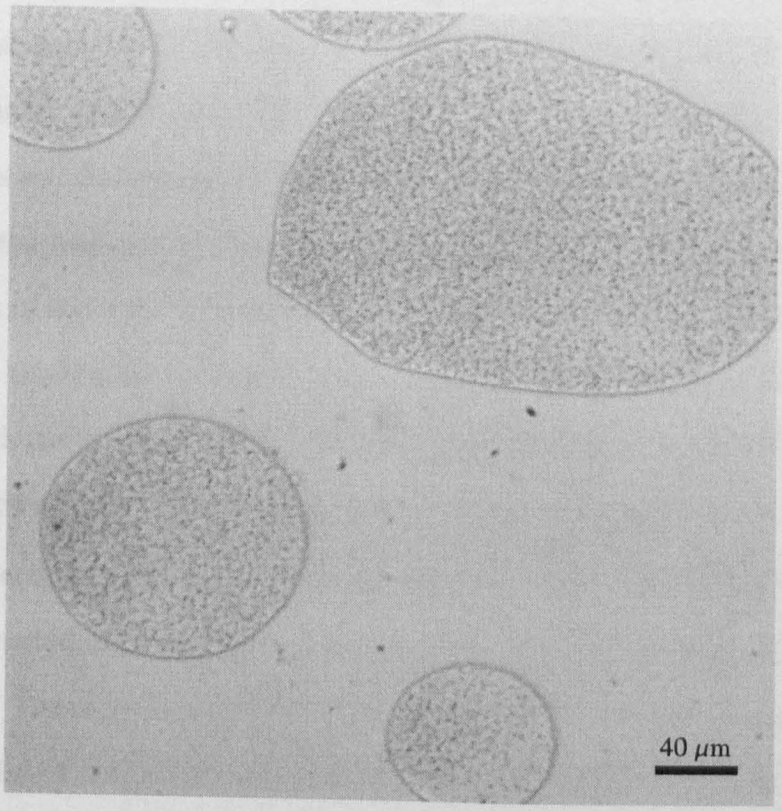

Figure 7.38: Skinned oil droplets that have been ruptured under pressure

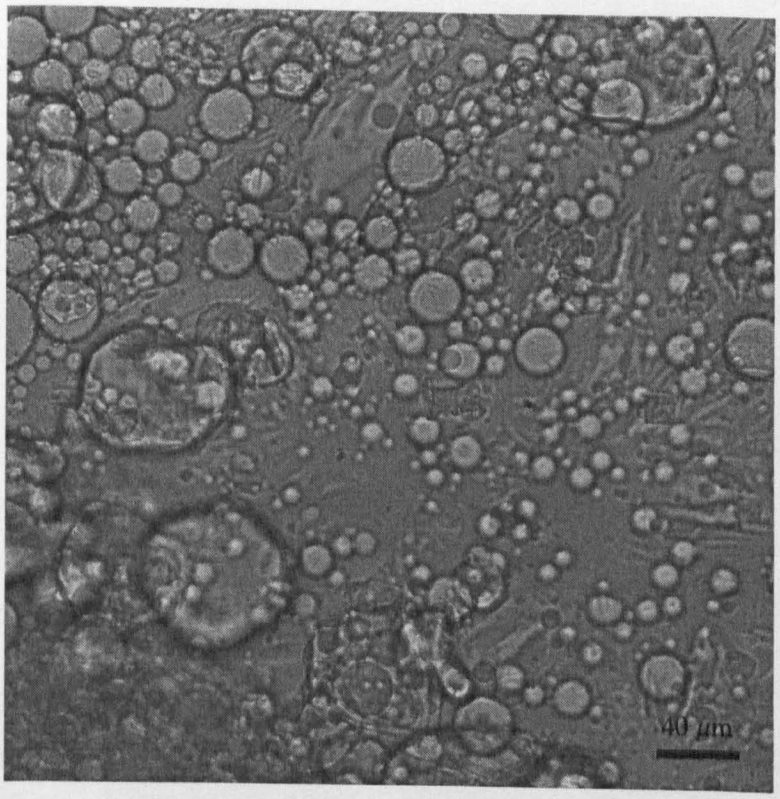

Figure 7.39: Silica-skinned water droplets dispersed in ethanol

7.3.12 PDMS in the Internal Aqueous Phase

Interfacial polymerization of TEOS had only yielded thinly skinned W/O droplets. A new approach was attempted (Figure 7.40). A low MW PDMS aqueous dispersion was prepared, left for 18 hours and then homogenized into hexadecane with 1 wt. % TEGOPREN. This process was repeated with post addition of TEOS and again with TEOS present in the mixture uppon addition of the aqueous dispersion. The aim was to make an initial O/W/O system, with PDMS as the internal oil phase, while residual DMDES could contribute to skin formation: an anologue of the Secondary DMDES approach to form solid shells around PDMS droplets (Section 4.2.3).

All three versions yielded successful dispersions. Sediment formed on standing, but could be redispersed with shaking. Under the microscope, no internal PDMS oil droplets were observed. The capsules collapsed at the oil-air interface, though subjectively the skins seemed to persist for longer and were smoother. It is likely that some of the PDMS adsorbed at the water/hexadecane interface and may have had a surfactant effect, but it seems likely that there was some contribution to the skin too. Compressed capsules left wall artifacts

(Figure 7.43).

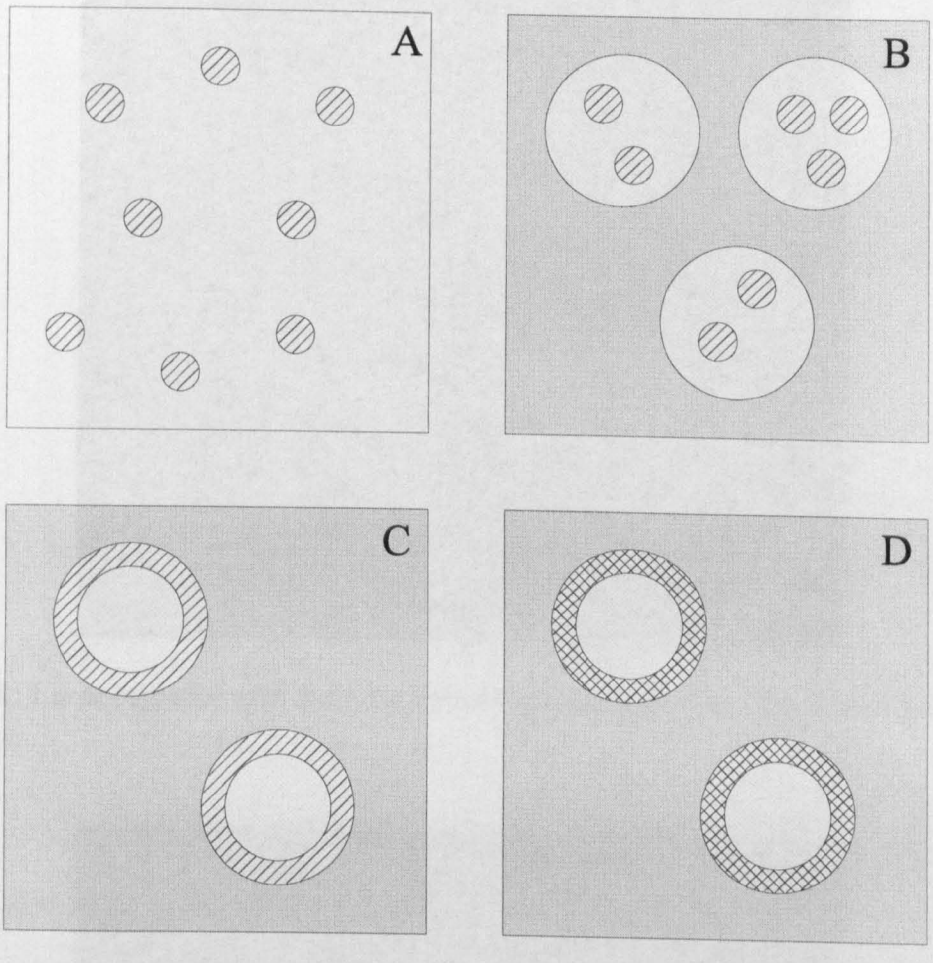

Figure 7.40: Internal PDMS scheme and possible capsule formation mechanism. A. PDMS emulsion in water. B. PDMS emulsion dispersed into oil to form an O/W/O emulsion. C. Surface-active PDMS adsorbs at the interface. D. TEOS diffused from the continuous phase and condenses with aqueous DMDES residues to form a wall.

Drying of Internal PDMS Systems

W/O capsules that had been shelled by the internal PDMS method were washed into n-heptane and allowed to dry. Unlike previous TEGOPREN systems, the shell structure persisted following drying and survived splutter coating to be viewed under the SEM (Figure 7.44).

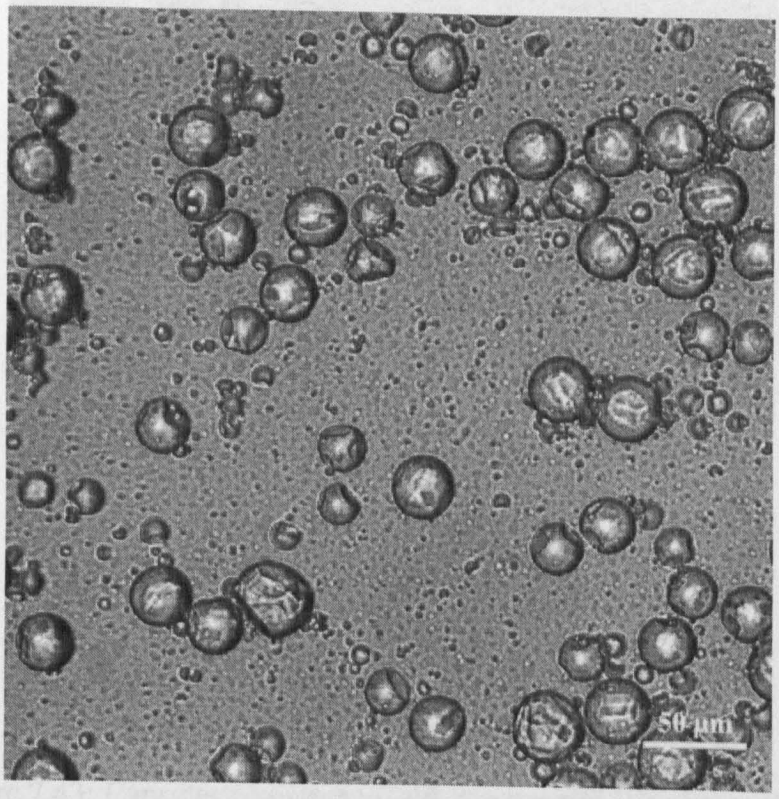

Figure 7.41: Large capsules with skins formed in the presence of an internal PDMS emulsion

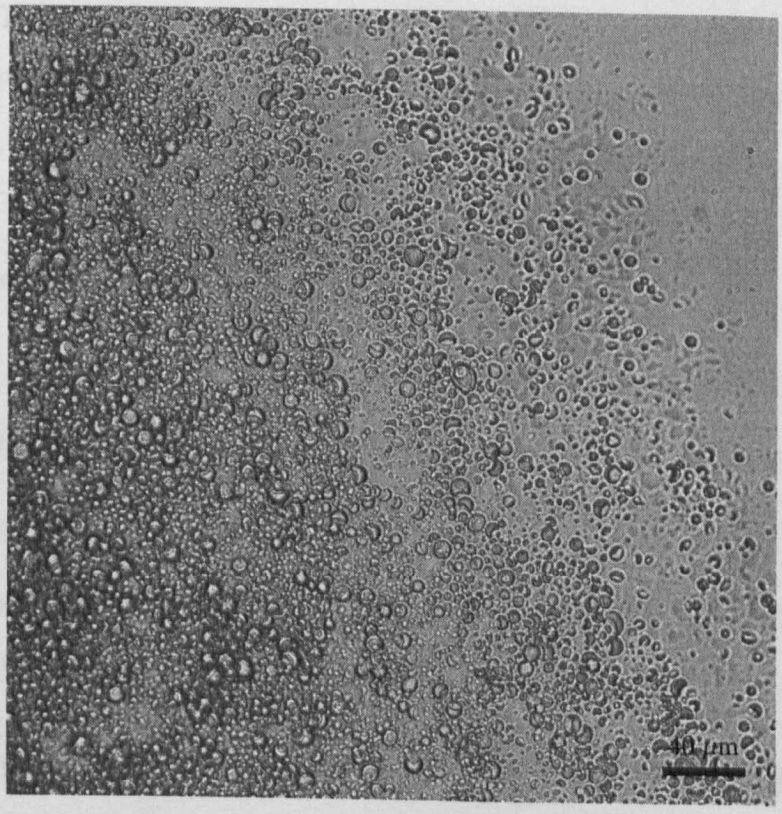

Figure 7.42: Small collapsed capsules formed in the presence of a PDMS emulsion.

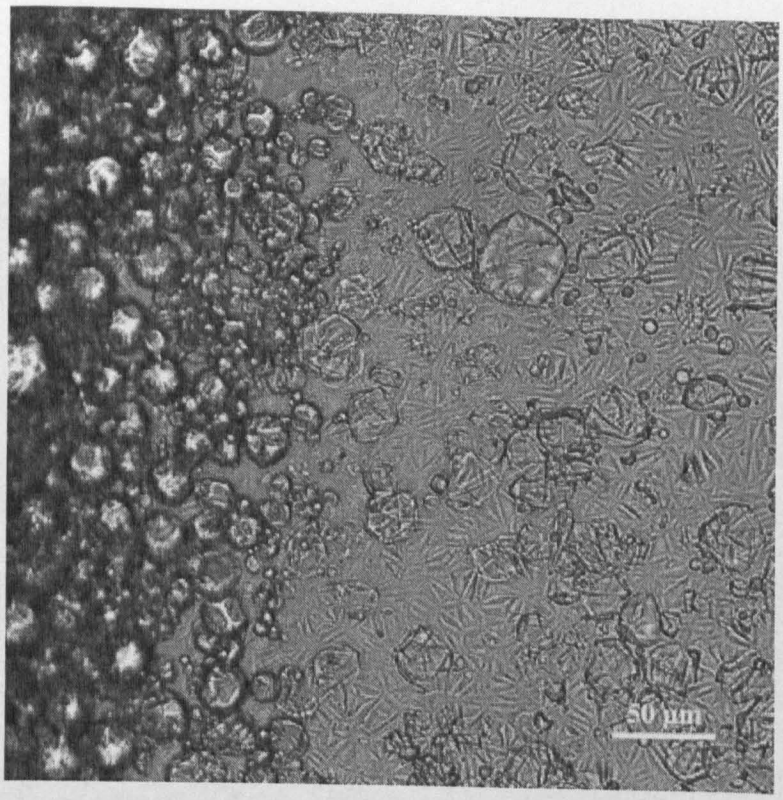

Figure 7.43: Capsules compressed with a cover slip left wall artifacts.

TEOS/DMDES Capsule formation

Three different TEGOPREN W/O systems were made. The aqueous phase was homogenized into the TEGOPREN/hexadecane mixture at 3000 rpm for 30 minutes. The shell monomer was then added to the formed emulsion and homogenization continued for a further 5 minutes.

Several regimes were investigated:

- A control experiment. The external hexadecane phase contained TEOS (30 g dm^{-3}) and DMDES (27 g dm^{-3}), but no monomer was included in the aqueous phase (Figure 7.45).

- An internal aqueous phase that contained 2 vol. % DMDES. TEOS (58 g dm^{-3}) was added to the external hexadecane phase (Figure 7.46).

- The internal aqueous phase contained 2 % DMDES, while TEOS (30 g dm^{-3}) and DMDES (27 g dm^{-3}) were added as shell monomer to the hexadecane phase (Figure 7.47).

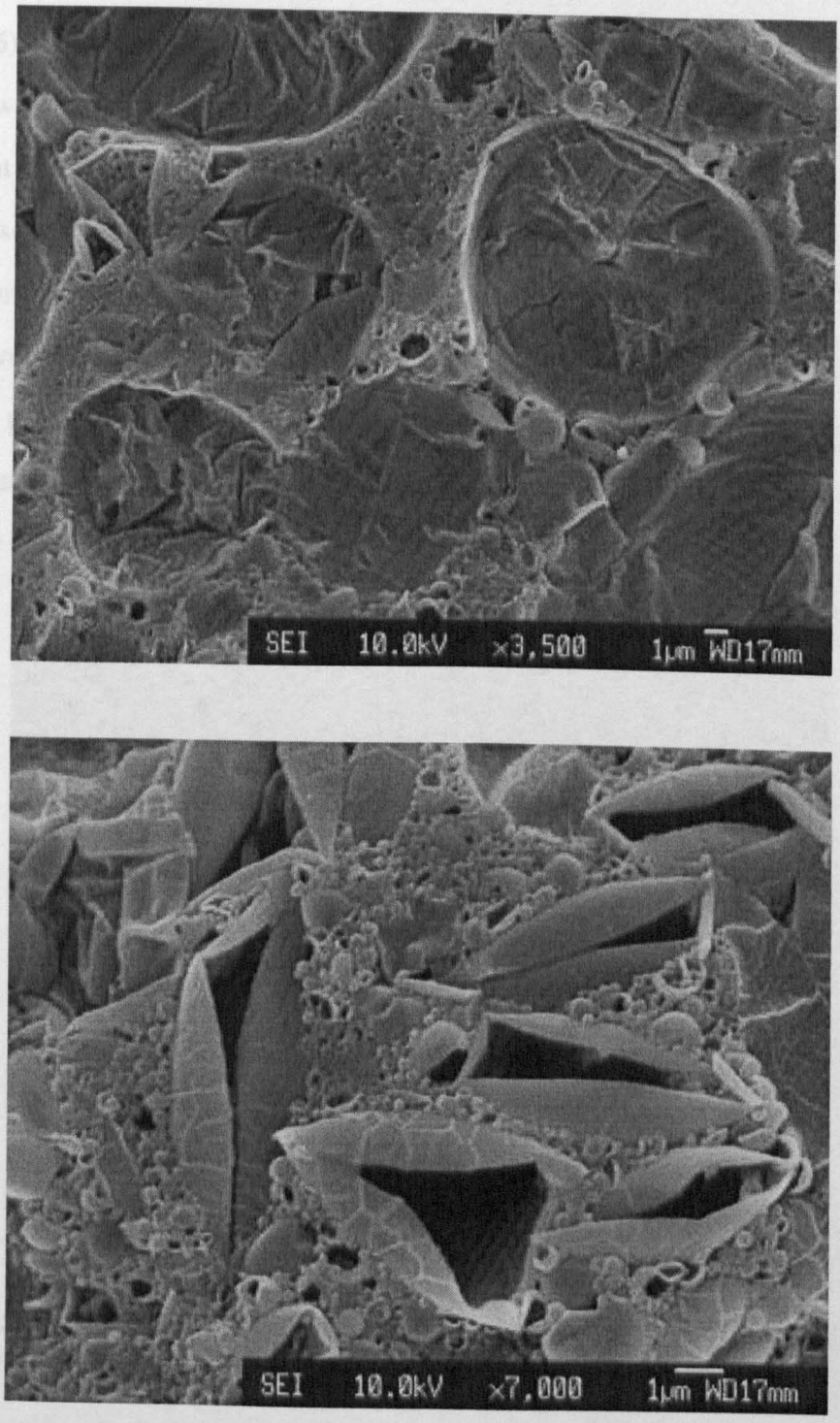

Figure 7.44: Capsules formed in the presence of an internal PDMS emulsion. Washed with heptane and dried

The control experiment, in contrast to TEOS-only systems, produced shells that survived washing in n-heptane and subsequent drying to be viewed with SEM (Figure 7.45). The dispersion that contained DMDES in the aqueous phase did not produce such structures (Figure 7.46). This suggests that for successful shells in such systems, DMDES must either be allowed sufficient time to form PDMS oligomers prior to the shelling step to have a co-surfactant effect, or be available in sufficient quantity to form a silica-silicone composite membrane (see Section 7.3.12); the DMDES concentration relative to the total alkoxysilane concentration was small in this case and the final structures resembled those produced by TEOS-only regimes. The dispersion that contained DMDES in both the aqueous and hexadecane phases produced the thickest shells, probably because that system enhanced DMDES enrichment at the interface (Figure 7.47) allowing formation of the Zoldesi shell material (see Chapter 4, Figure 4.1).

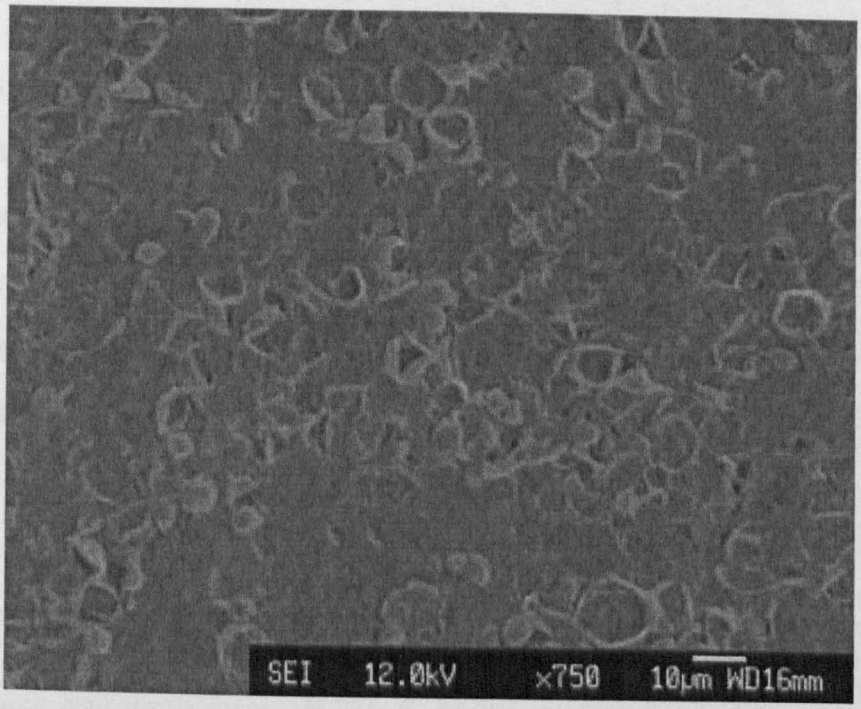

Figure 7.45: Shells formed from equal volumes of TEOS and DMDES upon a TEGOPREN-stabilized W/O emulsion

PDMS stabilized W/O emulsions

It is possible that the PDMS had acted as a co-surfactant. To determine if the PDMS could stabilize such emulsions in the absence of TEGOPREN, 1, 5 and 7 % aqueous PDMS emul-

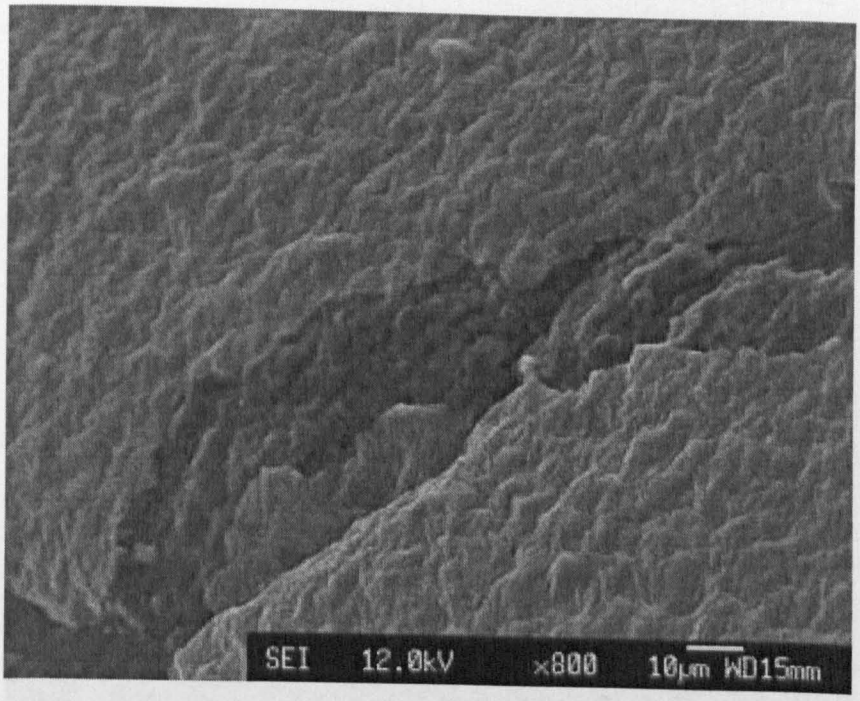

Figure 7.46: When DMDES (0.117 mol dm^{-3}) was present in the aqueous phase, but not in the organic phase, no capsule artifacts were observed with SEM.

sion systems were respectively homogenized into hexadecane. Upon ceasation of homogenization, phase separation was observed, though turbidity persisted in both the top hexadecane phase and the lower aqueous phase. The process was repeated, but with the addition of TEOS in the final 5 minutes of homogenization in an attempt to capture any emulsion in a shelled system. Again, pronounced phase separation was observed with turbidity observed in both phases. Although PDMS probably acts to reduce interfacial tension, the oligomers are too small to provide any steric stabilization in the oil phase.

Skins derived from DMDES-TEOS Mixtures

A series of skinned W/O dispersions was made in conditions of fixed TEOS volume fraction (5 %) with varying DMDES volume fractions, ranging from 1–7.5 % v/v. Following overnight sedimentation the dispersions could be redispersed with gentle shaking. Dispersions formed with DMDES volume fractions $\geq$ 5 % v/v became increasingly difficult to redisperse however, and, in time, formed solid plugs. It is probable, at higher alkoxysilane concentrations, in the sedimented state that the aqueous phase exuded into inter-particle space and reacted with monomer there to bind the capsules togethter.

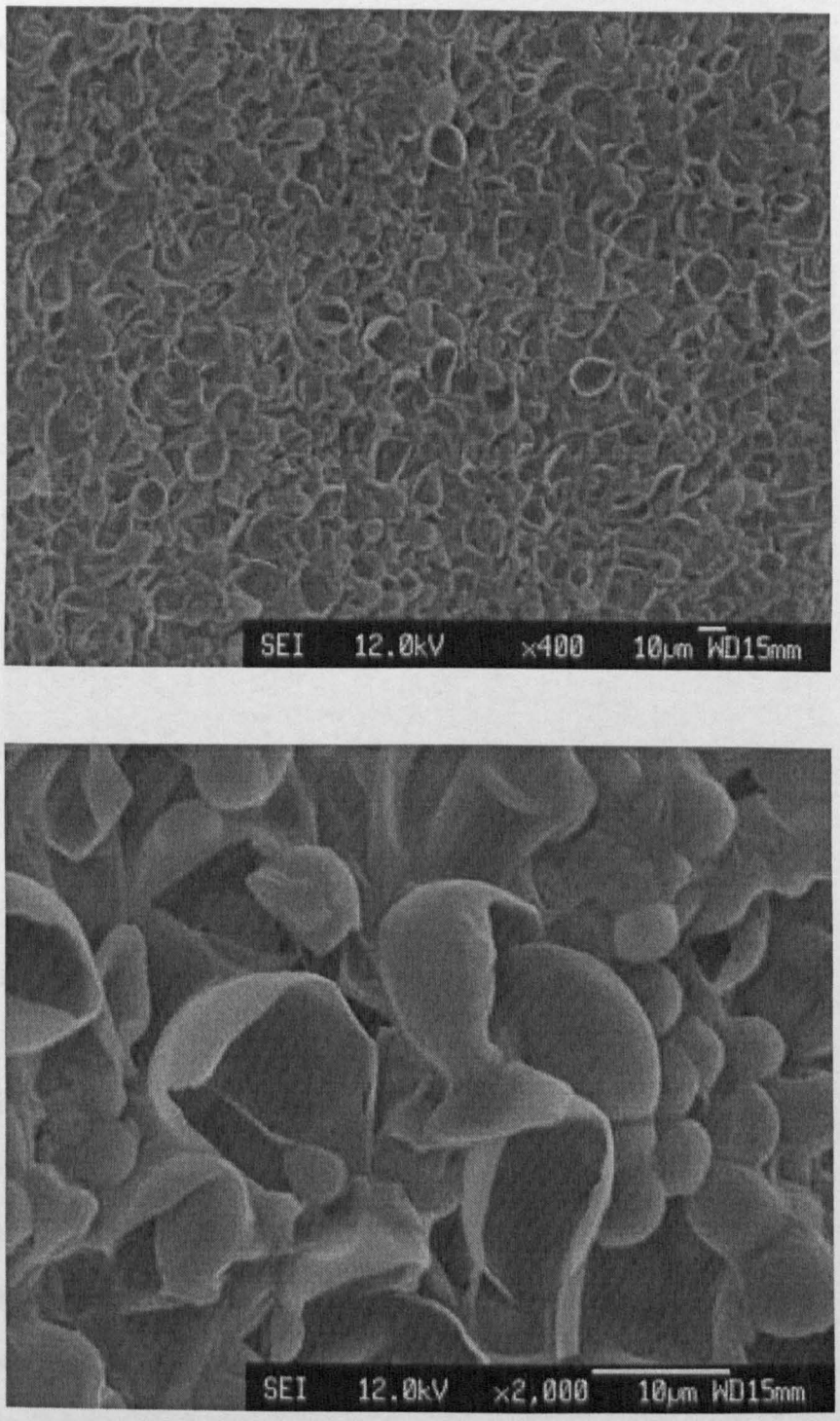

Figure 7.47: The presence of DMDES in both the aqueous and organic phases lead to formation of thicker shells.

The dispersable regimes were successfully subjected to centrifugation with sequential washing from hexadecane (Figure 7.48) to n-heptane to ethanol, whereupon aggregates were observed (Figure 7.49). Centrifugation and washing from ethanol to 1 wt. % aqueous INUTEC SP1 solution lead to formation of denser aggregates that could not be dispersed, even with sonication (Figure 7.50).

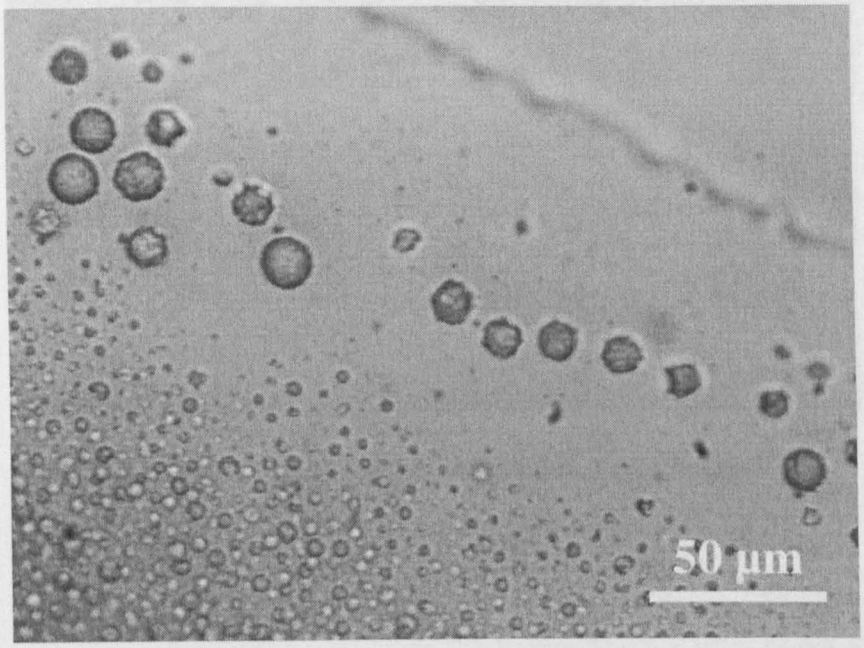

Figure 7.48: DMDES-TEOS Skinned droplets in hexadecane

A further series of skinned dispersions were made, whose aqueous phase (20 % v/v) contained $CaCl_2$ (2.5 mol dm^{-3}) and DMDES (58–292 mmol dm^{-3}), while the hexadecane phase consisted of 1 wt. % TEGOPREN 7008, 5 % v/v TEOS, and sufficient DMDES to bring the total DMDES volume fraction to 3.75 % v/v. These dispersions were directly centrifuged from hexadecane (Figure 7.51) to 1 wt. % INUTEC SP1 solution, without intermediate washing steps into other solvents. Although capsules persisted in the organic phase, sediment was present in the lower aqueous phase. Following removal of the hexadecane phase, the sediment could be dispersed with shaking, although some aggregates persisted (Figure 7.52). The presence of $CaCl_2$ in the aqueous cores did not trigger any obvious osmotic pressure effects, such as exploding capsules, which means that either the skins were sufficiently strong to withstand such pressures or, more plausably, the salt had diffused into the continuous phase.

Drying of the aqueous phase on a microscope slide, for 6 hours, revealed apparent uncol-

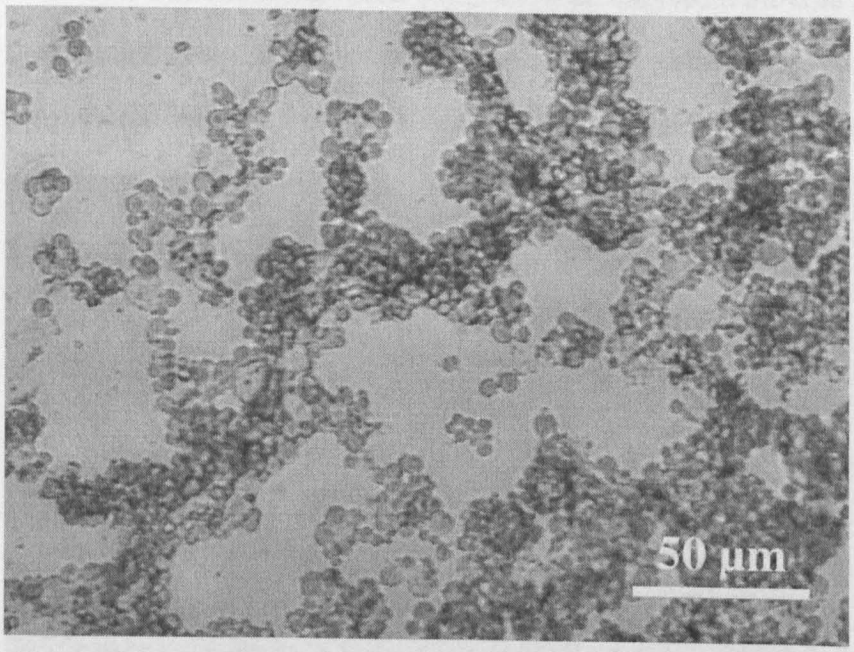

Figure 7.49: Skinned droplets washed into ethanol

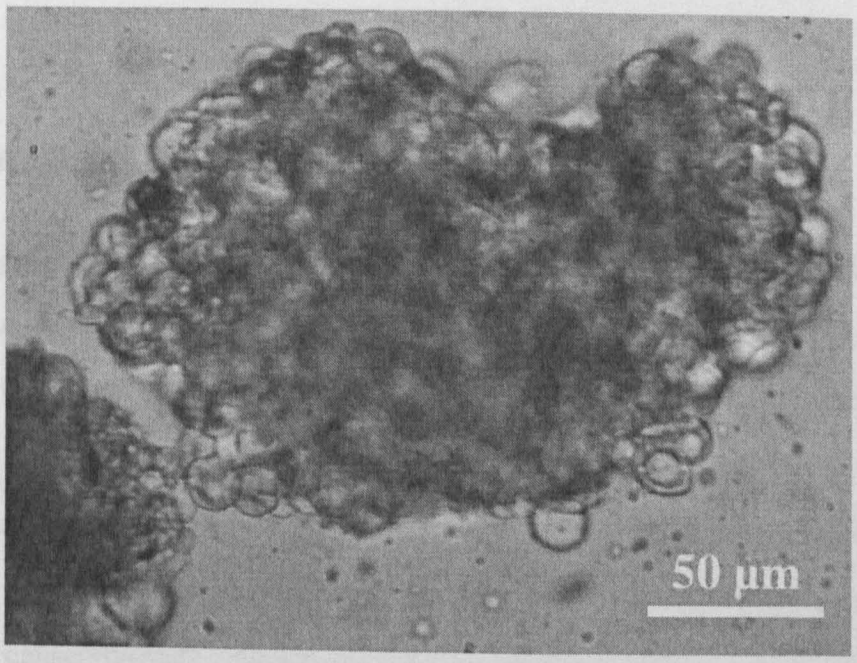

Figure 7.50: Following washing of the ethanol phase with 1 wt. % INUTEC SP1, no obviously discrete capsules were observed.

lapsed capsules, but no capsules of diameter larger than 20 μm were evident (Figure 7.53). Some mild crenellation was observed, which suggests water loss from the core was ongoing. It is possible that precipitating $CaCl_2$ was acting to support the skins; spherical structures of this size had not previously been observed in dried systems (Figure 7.44, Section 7.3.12).

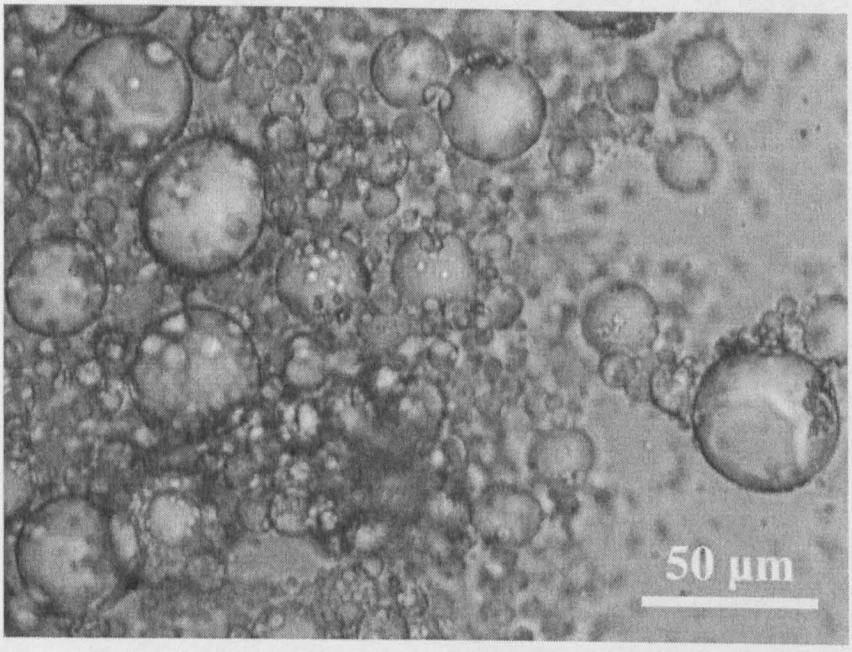

Figure 7.51: Skinned droplets, whose aqueous phase contained both DMDES, NH_3 and $CaCl_2$, in hexadecane.

7.4 Summary

Silica or cross-linked silicone membranes were formed around ammoniacal W/O emulsion droplets through condensation of alkoxysilanes at the oil-water interface. The principal surfactant used was TEGOPREN 7008, although membranes were also formed in the presence of SPAN 80 or, possibly, hydrophobic fumed silica. Membranes could be visualized with a microscope when the capsules were in a crenellated state of collapse, attributed to core evaporation. The presence of high TEOS volume fractions in the organic phase, in excess of 50 % v/v, caused particle collapse, possibly as an osmotic effect. Use of low TEOS concentrations, $\leq$ 5 % v/v, formed membrane-bound droplets that appeared to be stable for over two years.

Monomer condensation was base catalysed if ammonia was present in the aqueous phase.

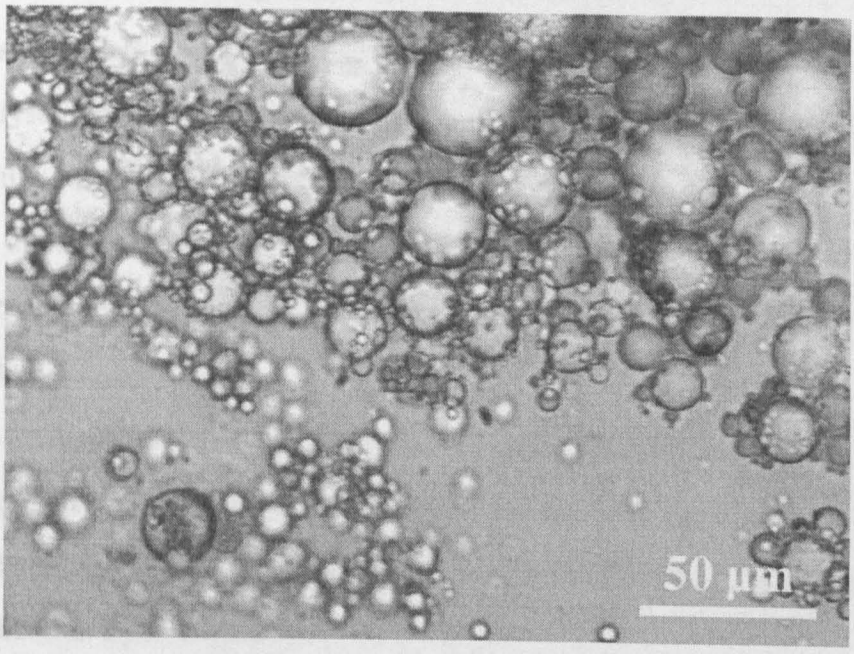

Figure 7.52: The $CaCl_2$ regime dispersed into water

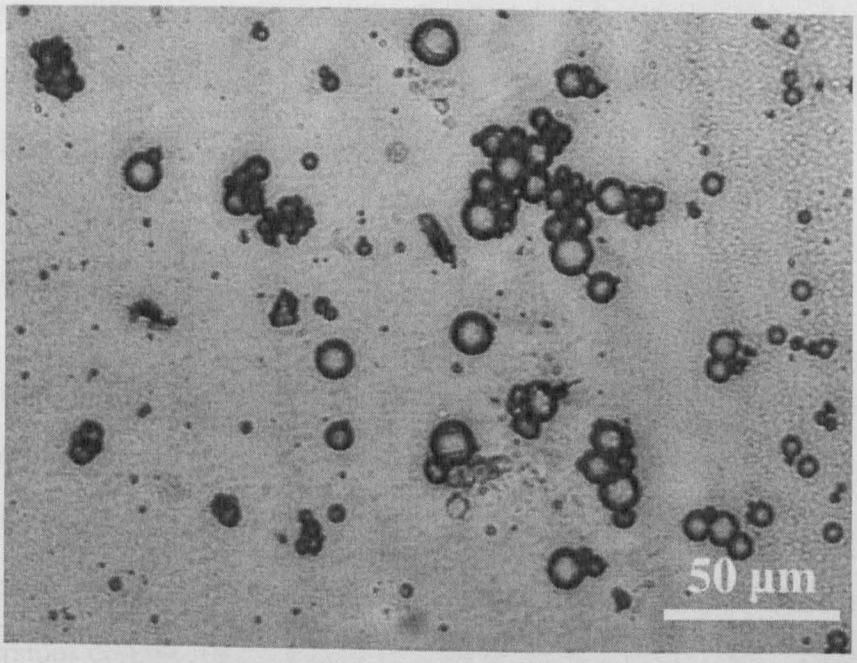

Figure 7.53: Skinned droplets air dried for 6 hours. Surprisingly the capsules remained spherical, possibly due to the precipitation of $CaCl_2$

Use of octanoic acid as an alternative catalyst in the organic phase was examined: membranes formed, but non-spherical morphologies were adopted with ageing, also, in contrast to similar basic regimes, collapsed capsules were observed in the bulk phase. Use of acetic acid as a catalyst in the aqueous phase also lead to the formation of non-spherical dispersions. This behaviour could be attributed to a gel-like membrane nature, but membranes formed in the presence of HCl were similar to the ammonia-catalysed analogues. The organic acids may have been absorbed into the growing membrane to cause the gel-behaviour, but this was not investigated.

Attempts to transfer skinned dispersions into an aqueous continuous phase included solvent exchange and centrifugation. Direct centrifugation from hexadecane into a 1 wt. % INUTEC SP1 solution was the most successful method, as a skinned discrete dispersion was observed in the final aqueous phase.

Formation of a W/O/W dispersion, in which the internal aqueous phase was skinned was succeeded by an attempted Stöber growth, but this generally lead to formation of gross precipitate. Use of DMDES as a co-monomer, including enrichment of the aqueous phase with this monomer, lead to formation of apparently thicker membranes that could be dried and observed with SEM. When $CaCl_2$ was present in the aqueous phase of the latter regime, droplets with spherical morphology were observed with an optical microscope, following air drying. It is possible that precipitating salt acted to support the structures.

7.5 Future Work

No study of shell thickness was undertaken for the W/O systems. Use of freeze fracture SEM could be considered for this. Capsules have been formed with $CaCl_2$ in the internal aqueous phase and, following their transition to an aqueous continuous phase, conductivity experiments could be used to investigate their release and permeability behaviour.

The dispersions collapse upon drying, so further work to form tougher shells that would more effectively contain the aqueous phase is necessary. Use of a multiple shell using both the silica membrane and a precipitated polymer could be explored. Such shells could engender several benefits such as improved retention of core active, or resistance to pressure or

temperature. A multiple W/O/W emulsion approach could be of interest if the oil phase could be solidified; use of polymerizable organic phases could be explored. Further use of particle stabilizers, both in simple and multiple emulsion approaches could also be considered.

Advances in microfluidic technology have allowed formation of monodisperse emulsions [43]. This technology could be employed to form aqueous skinned dispersions; a systematic study of the influence of TEOS and DMDES concentrations in the internal aqueous phase, analogous to that carried out in Chapter 4, could then be made.

Spherical capsules were observed upon drying if $CaCl_2$ was present in the internal aqueous phase. Investigation into the stabilizing influence of the salt, if any, is necessary. Furthermore any diffusion of $CaCl_2$ across the silica membrane could be exploited if the capsules are centrifuged into an aqueous carbonate solution; insoluble calcium carbonate may form at the interface and act to further seal the capsule.

Chapter 8

Thesis Summary

PDMS emulsions, formed from surfactant-free emulsion polymerization, were used as templates to form core shell particles. These dispersions have narrow size distributions and are simple to make.

Bogush silica growth upon silica-skinned PDMS templates was investigated following Goller's method [34]. It had previously been observed that it was necessary to form cross-linked PDMS cores to prevent disrupting swelling by ethanol during shell growth. PDMS swelling as a function of MTES cross-linker and external ethanol concentrations was measured, and solid-type PDMS regimes were found to be the most suitable for shelling.

Microcapsules with tunable shell thicknesses have been developed by modifying previous work in which TEOS was added to growing PDMS droplets and acted to cross-link newly formed PDMS to create a discrete solid layer, without recourse to Stöber silica growth conditions [35]. The thickness of the solid layer was dependant upon the time of TEOS addition relative to the initiation of DMDES polymerization: in effect the residual DMDES concentration controls shell thickness.

The modified method involved addition of DMDES and TEOS to a matured PDMS system so that shell formation was independent of the initial core synthesis and the thickness was found to be proportional to the secondary DMDES concentration up to a threshold concentration, beyond which secondary nucleation reduced the shelling efficiency. Shell thickness could also be controlled, in both methods, by quenching the shell maturation step.

The Secondary DMDES method also allowed study of the effects of using MTES in the

place of TEOS and DMDES, and various combinations thereof. Substitution of TEOS by MTES lead to formation of nodular shell growth at low MTES concentrations with respect to TEOS, while thin soft shells were observed at higher MTES concentrations. Substituting secondary DMDES by MTES, at high DMDES/MTES ratios, lead to formation of softer shells, but improved shell hardness was observed at lower DMDES/MTES ratios, together with pronounced secondary material production.

Micromanipulation studies found an apparent linear proportionality between breaking force and shell thickness, although such a trend was less defined between the shell thickness/total radius ratio and the breaking force. Low DMDES/TEOS monomer ratios formed shells with Young's moduli in the region of 10 GPa, higher DMDES concentrations formed shells with Young's moduli of 1-3 GPa, which is similar to those observed for polymers.

Dyes may be incorporated into the PDMS using vector solvents, such as chloroform, and subsequently shelled. These solvents have implications for droplet density and enhance creaming or sedimentation, which leads to a broadening template size distribution. Attempts to incorporate a 4-nitroanisol dye into PDMS by polymerizing dye-loaded DMDES were unsuccessful because the basic aqueous conditions rendered the dye water-soluble, which limits the usefulness of the technique for pH sensitive material encapsulation.

Silica, or cross-linked silicone, membranes were formed around W/O emulsions to form capsules with aqueous cores. The membranes were formed via an interfacial sol-gel reaction, whereby the alkoxysilane monomers were present in the oil phase, while water and catalyst were available in the aqueous phase. Thicker shells were formed if the aqueous phase was also enriched with monomer: a process analogous to the shell formation upon PDMS. The capsules were successfully transferred from oil to water by centrifugation if a stabilizer were present in the external aqueous phase. The presence of salt in the internal aqueous phase seemed to stabilize drying capsules, possibly due to precipitation at the shell-air interface.

Colophon

This thesis was written using Free and Open Source Software. Text was written and edited using Bram Moolenaar's Vim, and typeset with LaTeX running on Slackware Linux and Ubuntu. Graphs were plotted with Gnuplot, illustrations drawn with Inkscape, and image manipulation was carried out with the GNU Image Manipulation Program (GIMP) or scripted with ImageMagick. Custom Python scripts were written to automate document markup and process data files.

Bibliography

[1] C. Thies. A survey of microencapsulation processes. In S. Benita, editor, *Microencapsulation: Methods and Industrial Applications*, pages 1–19. Marcel Dekker, New York, 1996.

[2] C. Graf and A. van Blaaderan. Metallodielectric colloidal core-shell particles for photonic applications. *Langmuir*, 18(2):524–534, 2002.

[3] W. Sliwka. Microencapsulation. *Angewandte Chemie International Edition*, 14(8):539–550, 1975.

[4] R. Georgieva, S. Moya, M. Hin, R. Mitlohner, E. Donath, H. Kiesewetter, H. Möhwald, and H. Baumler. Permeation of macromolecules into polyelectrolyte microcapsules. *Biomacromolecules*, 3:517–524, 2002.

[5] G.B. Sukhorukov, A.A. Antipov, A. Voigt, E. Donath, and H. Möhwald. ph-controlled macromolecule encapsulation in and release from polyelectrolyte multilayer nanocapsules. *Macormolecular Rapid Communications*, 22(1):44–46, 2001.

[6] L.Y. Chu, S.H. Park, T. Yamaguchi, and Nakao S. Preparation of micron-sized monodispersed thermoresponsive core-shell microcapsules. *Langmuir*, 18(5):1856–1864, 2002.

[7] W.B. Stockton and M.F. Rubner. Molecular-level processing of conjugated polymers. 4. layer-by-layer manipulation of polyaniline via hydrogen-bonding interactions. *Macromolecules*, 30(9):2717–2725, 1997.

[8] K. Little and J. Parkhouse. Tissue reactions to polymers. *Lancet*, 2(7261):857–861, 1962.

[9] K. Shiga, N. Muramatsu, and T. Kondo. Preparation of poly(d,l-lactide) and copoly(lactide-glycolide) microspheres of uniform size. *Journal of Pharmacy and Pharmacology*, 48(9):891–895, 1996.

[10] I.G. Loscertales, A. Barrero, I. Guerrero, M. Cortijo, R.and Marquez, and Ga nán Calvo. Micro/nano encapsulation via electrified coaxial liquid jets. *Science*, 295:1695–1698, 2002.

[11] A. Loxley and B. Vincent. Preparation of poly(methylmethacrylate) microcapsules with liquid cores. *Journal of Colloid and Interface Science*, 208(1):49–62, 1998.

[12] R. Atkin, P. Davies, J. Hardy, and B. Vincent. Preparation of aqueous core/polymer shell microcapsules by internal phase separation. *Macromolecules*, 37(21):7979–7985, 2004.

[13] H.K. Mahabadi, T.H. Ng, and H.S. Tan. Interfacial/free radical polymerization microencapsulation: Kinetics of particle formation. *Journal of Microencapsulation*, 13(5):559–573, 1996.

[14] C.S. Peyratout and L. Dähne. Tailor-made polyelectrolyte microcapsules from multilayers to smart containers. *Angewandte Chemie International Edition*, 43(29):3762–3783, 2004.

[15] A.P.R. Johnston, C. Cortez, A.S. Angelatos, and F. Caruso. Layer-by-layer engineered capsules and their applications. *Current Opinion in Colloid and Interface Science*, 11:203–209, 2006.

[16] E. Donath, G.B. Sukhorukov, Caruso F., S.A. Davis, and H. Möwald. Novel hollow polymer shells by colloid-templated assembly of polyelectrolytes. *Angewandte Chemie International Edition*, 37(16):2202–2205, 1998.

[17] T. Serizawa, S. Kamimura, N. Kawanishi, and M. Akashi. Layer-by-layer assembly of poly(vinyl alcohol) and hydrophobic polymers based on their physical adsorption on surfaces. *Langmuir*, 18(22):8381–8385, 2002.

[18] X. Yang, T. Dai, M. Wei, and Y. Lu. Polymerization of pyrrole on a polyelectrolyte hollow capsule microreactor. *Polymer*, 47:4596–4602, 2006.

[19] Z.F. Dai, L. Dähne, H. Möwald, and B. Tiersch. Novel capsules with high stability and controlled permeability by hierarchic templating. *Angewandte Chemie International Edition*, 41(21):4019–4022, 2002.

[20] R.H. Ottewill, A.B. Schofield, J.A. Waters, and N.S.J. Williams. Preparation of core-shell polymer colloid particles by encapsulation. *Colloid and Polymer Science*, 275(3):274–283, 1997.

[21] H. Li, J. Han, A. Panioukhine, and E. Kumacheva. From heterocoagulated colloids to core-shell particles. *Journal of Colloid and Interface Science*, 255(1):119–128, 2002.

[22] A. D. Dinsmore, M. F. Hsu, M. G. Nikolaides, M. Marquez, A. R. Bausch, and D. A. Weitz. Colloidosomes: Selectively permeable capsules composed of colloidal particles. *Science*, 298(5595):1006–1009, 2002.

[23] O. D. Velev and K. Nagayama. Assembly of latex particles by using emulsion droplets .3. reverse (water in oil) system. *Langmuir*, 13(6):1856–1859, 1997.

[24] L. M. Croll and H. D. H. Stöver. Mechanism of self-assembly and rupture of cross-linked microspheres and microgels at the oil-water interface. *Langmuir*, 19(24):10077–10080, 2003.

[25] A.K. van Helden, J.W. Jansen, and A. Vrij. Preparation and characterization of spherical monodisperse silica dispersions in non-aqueous solvents. *Journal of Colloid and Interface Science*, 81(2):354–386, 1981.

[26] A. van Blaaderen, J. van Geest, and A. Vrij. Monodisperse colloidal silica spheres from tetraalkoxysilanes: Particle formation and growth mechanism. *Journal of Colloid and Interface Science*, 154(2):481–501, 1992.

[27] H. Ono and K. Takahashi. Preparation of silica microcapsules by sol-gel method in w/o emulsion. *Journal of Chemical Engineering of Japan*, 31(5):808–812, 1998.

[28] P.S. Smith and J.A. Hibbert. Stabilizing emulsions, 2000. United States Patent no. 6,156,805.

[29] E.G. Kaneva. Silicone oil emulsions and microgel particles with application to the oil recovery industry. Msc, University of Bristol, 2002.

[30] K.P. Velikov and A. van Blaaderan. Synthesis and characterization of monodisperse core-shell colloidal spheres of zinc sulphide and silica. *Langmuir*, 17:4779–4786, 2001.

[31] Wilhelmy D.M. and E. Matijević. Preparation and properties of monodispersed spherical colloidal particles of zinc sulphide. *Journal of the Chemistry Society Faraday Trans. 1*, 80:563–570, 1984.

[32] R. Vacassy, S.M. Scholz, J. Dutta, C.J.G. Plummer, R. Houriet, and H. Hofmann. Synthesis of controlled spherical zinc sulphide particles by precipitation from homogeneous solutions. *Journal of the American Ceramic Society,*, 81:2699–2705, 1998.

[33] T.M. Obey and B. Vincent. Novel monodisperse silicone oil/water emulsions. *Journal of Colloid and Interface Science*, 163:454–463, 1994.

[34] M. I. Goller and B. Vincent. Silica encapsulation of liquid PDMS droplets. *Colloids and Surfaces A-Physicochemical and Engineering Aspects*, 142(2-3):281–285, 1998.

[35] C.I. Zoldesi and A. Imhof. Synthesis of monodisperse colloidal spheres, capsules, and microballoons by emulsion templating. *Advanced Materials*, 17:924–928, 2005.

[36] C.I. Zoldesi, C.A. van Walree, and A Imhof. Deformable hollow hybrid silica/siloxane colloids by emulsion templating. *Langmuir*, 22:4343–4352, 2006.

[37] K. Glinel, G.B. Sukhorukov, H. Möhwald, V. Khrenov, and K. Tauer. Thermosensitive hollow capsules based on thermoresponsive polyelectrolytes. *Macromolecular Chemistry and Physics*, 204(14):1784–1790, 2003.

[38] A.J. Khopade and F. Caruso. Stepwise self-assembled poly(amidoamine) dendrimer and poly(styrenesulfonate) microcapsules as sustained delivery vehicles. *Biomacromolecules*, 3(6):1154–1162, 2002.

[39] F. Caruso, W.J. Yang, D. Trau, and R. Renneberg. Microencapsulation of uncharged low molecular weight organic materials by polyelectrolyte multilayer self-assembly. *Langmuir*, 16(23):8932–8936, 2000.

[40] Y.J Wang, A.M. Yu, and F. Caruso. Nanoporous polyelectrolyte spheres prepared by sequentially coating sacrificial mesoporous silica spheres. *Angewandte Chemie International Edition*, 44(19):2888–2892, 2005.

[41] D. V. Volodkin, A. I. Petrov, M. Prevot, and G. B. Sukhorukov. Matrix polyelectrolyte microcapsules: New system for macromolecule encapsulation. *Langmuir*, 20(8):3398–3406, 2004.

[42] P.J. Dowding, J.W. Goodwin, and B. Vincent. Production of porous suspension polymer beads with a narrow size distribution using a cross-flow membrane and a continuous tubular reactor. *Colloids and Surfaces A: Physical and Engineering Aspects*, 180(3):301–309, 2001.

[43] D.R. Link, E. Grasland-Mongrain, A. Duri, F. Sarrazin, Z. Cheng, G. Cristobal, M. Marquez, and D.A. Weitz. Electric control of droplets in microfluidic devices. *Angewandte Chemie-International Edition*, 45(16):2556–2560, 2006.

[44] D.H. Everett. *Basic Principles of Colloid Science*. Royal Society of Chemistry, London, 1988.

[45] D.J. Shaw. *Colloid and Surface Chemistry*. Butterworth-Heinmann, Oxford, 4 edition, 1992.

[46] S.A. Davis. Electron microscopy. In T. Cosgrove, editor, *Colloid Science*, pages 266–282. Blackwell, Oxford, 2005.

[47] W. Stöber, A. Fink, and E. Bohn. Controlled growth of monodisperse silica spheres in the micron size range,. *Journal of Colloid and Interface Science*, 26(1):62–69, 1968.

[48] B. Neumann and B. Vincent. Stability of various silicone oil/water emulsion films as a function of surfactant and salt concentration. *Langmuir*, 20:4336–4344, 2004.

[49] K.T. Rees. *Behavioural Study of the Deposition and Removal of Cross-Linked PDMS Droplets on Macroscopic Surfaces*. PhD thesis, University of Bristol, 2005.

[50] S.A. Nespolo, M.A. Bevan, D.Y.C. Chan, F. Grieser, and G.W. Stevens. Hydrodynamic and electrokinetic properties of decane droplets in aqueous sodium dodecy sulfate solutions. *Langmuir*, 17:7210–7218, 2001.

[51] M. Goller, T.M. Obey, D.O.H. Teare, and B. Vincent. Inorganic "silicone oil" microgels. *Colloids and Surfaces A: Physiochemical and Engineering Aspects*, 123–124:183–193, 1997.

[52] R.G. Dunleavey. *Colloidal Supports for Catalysts*. PhD thesis, University of Bristol, 2005.

[53] M.J. Murray and M.J. Snowden. The preparation, characterisation and applications of colloidal microgels. *Advances in Colloid and Interface Science*, 54:73–91, 1995.

[54] D.O.H. Teare. *Cross-linked Silicone Oil/Water Emulsions*. PhD thesis, University of Bristol, 1997.

[55] J. Stachurski and M. Michałek. The effect of the zeta potential on the stability of a non-polar oil-in-water emulsion. *Journal of Colloid and Interface Science*, 184:433–436, 1996.

[56] A. Goebel and K. Lunkenheimer. Interfacial tension of the water/n-alkane interface. *Langmuir*, 13(2):369–372, 1997.

[57] G.H. Bogush, M.A. Tracy, and C.F. Zukoski. Preparation of monodisperse silica particles—control of size and mass. *Journal of Non-Crystalline Solids*, 104(1):95–106, 1988.

[58] S. Simovic and C.A Prestidge. Hydrophilic silica nanoparticles at the PDMS droplet-water interface. *Langmuir*, 19:3785–3792, 2003.

[59] S Simovic and C.A. Prestidge. Adsorption of hydrophilic silica nanoparticles at the pdms droplet-water interface. *Langmuir*, 19:8364–8370, 2003.

[60] C.A. Prestidge, T. Barnes, and S. Simovic. Polymer and particle adsorption at the pdms droplet-water interface. *Advances in Colloid and Interface Science*, 108–109:105–118, 2004.

[61] S. Simovic and C.A. Prestidge. Nanoparticles at the polydimethylsiloxane droplet/water interface. *Australian Journal of Chemistry*, 58:664–666, 2005.

[62] C. Graf, D.L.J. Vossen, A. Imhof, and A. van Blaaderan. A general method to coat colloidal particles with silica. *Langmuir*, 19:6693–6700, 2003.

[63] C.I. Zoldesi. *Hollow Colloidal Particles by Emulsion Templating: from synthesis to self-assembly*. PhD thesis, Universiteit Utrecht, September 2006.

[64] A. van Blaaderen and A. Vrij. Synthesis and characterization of monodisperse colloidal organo-silica spheres. *Journal of Colloid and Interface Science*, 156:1–18, 1993.

[65] K. Anderson, T.M. Obey, and B. Vincent. Surfactant stabilized silicone oil in water emulsions. *Langmuir*, 10:2493–2494, 1994.

[66] A.R. Spurr. A low-viscosity epoxy resin embedding medium for electron microscopy. *Journal of Ultrastructure Research*, 26(1–2):31–43, 1969.

[67] C.V. Stevens, A. Meriggi, Peristeropoulou M., P.P. Christov, K. Booten, B. Levecke, A. Vandamme, N. Pittevils, and T.F. Tadros. Polymeric surfactants based on in-

ulin, a polysaccharide extracted from chicory. 1. synthesis and interfacial properties. *Biomacromolecules*, 2:1256–1259, 2001.

[68] Th.F. Tadros, A. Vandamme, K. Booten, B. Levecke, and C.V. Stevens. Stabilisation of emulsions using hydrophobically modified inulin (polyfructose). *Colloids and Surfaces A: Physicochem. Eng. Aspects*, 250:133–140, 2004.

[69] J. Nestor, J. Esquena, C. Solans, B. Levecke, K. Booten, and T.F. Tadros. Emulsion polymerization of styrene and methyl methacrylate using hydrophobically modified inulin and comparison with other surfactants. *Langmuir*, 11:4837–4841, 2005.

[70] J. Esquena, F.J. Domínguez, C. Solans, B. Levecke, K. Booten, and T.F. Tadros. Stabilization of latex dispersions using a graft copolymer of inulin based surfactants. *Langmuir*, 19:10463–10467, 2003.

[71] M.D. Abramoff, P.J. Magelhaes, and S.J. Ram. Image processing with ImageJ. *Biophotonics International*, 11(7):36–42, 2004.

[72] R Development Core Team. *R: A Language and Environment for Statistical Computing*. R Foundation for Statistical Computing, Vienna, Austria, 2006. ISBN 3-900051-07-0.

[73] G.Z. Lu, F.G. Thompson, and M.R. Gray. Physical modelling of animal cell damage by hydrodynamic forces in suspension cultures. *Biotechnology and Bioengineering*, 40:1277–1281, 1992.

[74] T. Ohtsubo, H. Takeda, S. Tsuda, M. Kagoshima, and K. Tsuji. A study of the physical strength of fenitrothion microcapsules. *Polymer*, 32(13):2395–2399, 1991.

[75] D. Poncelet and R.J. Neufeld. Shear breakage of nylon membrane microcapsules in a turbine reactor. *Biotechnology and Bioengineering*, 33:95–103, 1989.

[76] J. Su, Li. Ren, and L. Wang. Preparation and mechanical properties of thermal energy storage microcapsules. *Colloid and Polymer Science*, 284:224–228, 2005.

[77] A.W.L. Jay and M.A. Edwards. Mechanical properties of semipermeable microcapsules. *Canadian Journal of Physiology and Pharmacology*, 46:731–737, 1968.

[78] W.R. Jones, H.P. Ting-Beall, G.M. Lee, S.S. Kelley, R.M. Hochmuth, and F Guilak. Alterations in the young's modulus and volumetric properties of chondrocytes isolated from normal and osteoarthritic human cartilage. *Journal of Biomechanics*, 32(2):119–127, 1999.

[79] B. Schoeler, N. Delorme, I. Doench, G.B. Sukhorukov, A. Fery, and K. Glinel. Polyelectrolyte films based on polysaccharides of different conformations: Effects of multilayer structure and mechanical properties. *Biomacromolecules*, 7:2065–2071, 2006.

[80] A. Rehor, L. Canaple, Z. Zhang, and D. Hunkeler. The compressive deformation of multicomponent microcapsules: Influence of size, membrane thickness and compression speed. *Journal of Biomaterials Science Polymer Edition*, 12(2):157–170, 2001.

[81] Z. Zhang, R. Saunders, and C.R. Thomas. Micromanipulation measurements of the bursting strength of single microcapsules. *The 1994 IChemE Research Event*, 2:722–724, 1994.

[82] Z. Zhang, R. Saunders, and C.R. Thomas. Mechanical strength of single microcapsules determined by a novel micromanipulation technique. *Journal of Microencapsulation*, 16(1):117–124, 1999.

[83] G. Sun and Z. Zhang. Mechanical strength of microcapsules made from different wall materials. *International Journal of Pharmaceutics*, 242:307–311, 2002.

[84] V. Chan, K.K. Lui, C. Le Visage, B-.F. Ju, and K.W. Leong. Bioadhesive characterization of poly(methylidene malonate 2.12) microparticles on a model extracellular matrix. *Biomaterials*, 25:4327–4332, 2004.

[85] T. Liu, A.M. Donald, and Z. Zhang. Novel manipulation in an environmental scanning electron microscope for measuring mechanical properties of single particles. *Materials Science and Technology*, 21(3):289–294, 2005.

[86] V.V. Lulevich, I.L. Radtchenko, G.B. Sukhorukov, and O.I. Vinogradova. Deformation properties of nonadhesive polyelectrolyte microcapsules studied with the atomic force microscope. *Journal of Physical Chemistry B*, 107:2735–2740, 2003.

[87] V.V. Lulevich, D. Andrienko, and O.I. Vinogradova. Elasticity of polyelectrolyte multilayer microcapsules. *Journal of Chemical Physics*, 120(8):3822–3826, 2004.

[88] V.V. Lulevich, T. Zink, H-.Y. Chen, F-.T. Liu, and G. Liu. Cell mechanics using atomic force microscopy-based single-cell compression. *Langmuir*, 22:8151–8155, 2006.

[89] F. Dubreuil, N. Elsner, and A. Fery. Elastic properties of polyelectrolyte capsules studied by atomic-force microscopy and ricm. *European Physical Journal E*, 12:215–221, 2003.

[90] A. Ashkin. Optical trapping and manipulation of neutral particles using lasers. *Proceedings of the National Academy of Sciences of the United States of America*, 94(10):4853–4860, 1997.

[91] E. Helfer, S. Harlepp, L. Bourdieu, J. Robert, F.C. MacKintosh, and D. Chatenay. Buckling of actin-coated membranes under application of a local force. *Physical Review Letters*, 87(8):088103(1–4), 2001.

[92] A.R. Bausch, W. Möller, and E. Sackmann. Measurement of local viscoelasticity and forces in living cells by magnetic tweezers. *Biophysical Journal*, 76:573–579, 1999.

[93] S.C. Kuo. Using optics to measure biological forces and mechanics. *Traffic*, 2:757–763, 2001.

[94] T. Liu and Z. Zhang. Mechanical properties of desiccated ragweed pollen grains determined by micromanipulation and theoretical modelling. *Biotechnology and Bioengineering*, 85(7):770–775, 2004.

[95] M. Rachik, D. Barthès-Biesel, M. Carin, and F. Edwards-Lévy. Identification of the elastic properties of an artificial capsule membrane with the compression test: Effect of thickness. *Journal of Colloid and Interface Science*, 301:217–226, 2006.

[96] K.K. Liu, D.R. Williams, and B.J. Briscoe. Compressive deformation of a single microcapsule. *Physical Review E*, 54(6):6673–6680, 1996.

[97] A. Fery, F. Dubreuil, and H. Möhwald. Mechanics of artificial microcapsules. *New Journal of Physics*, 6(18):1–13, 2004.

[98] M. Ashby, editor. *Materials Selection in Mechanical Design*. Elsevier, Cambridge, 2 edition, 1999.

[99] M.J. Crawley. *Statistics: An Introduction using R*. John Wiley & Sons Ltd, Chichester, UK, 2005.

[100] R. Richardson. Scattering and reflection techniques. In T. Cosgrove, editor, *Colloid Science*, pages 228–254. Blackwell, Oxford, 2005.

[101] P. Klán, R. Růžička, D. Hegar, J. Literák, P. Kulhánek, and A. Loupy. Temperature-sensitive photochemical aromatic substitution on 4-nitroanisole. *Photochemical and Photobiological Science*, 1:1012–1016, 2002.

[102] P. J. Dowding, R. Atkin, B. Vincent, and P. Bouillot. Oil core/polymer shell microcapsules by internal phase separation from emulsion droplets. ii: Controlling the release profile of active molecules. *Langmuir*, 21(12):5278–5284, 2005.

[103] David R Lide, editor. *CRC Handbook of Chemistry and Physics*. CRC Press, Cleveland, Ohio, 83 edition, 2003.

[104] B. P. Binks and C. P. Whitby. Temperature-dependent stability of water-in-undecanol emulsions. *Colloids and Surfaces A-Physicochemical and Engineering Aspects*, 224(1–3):241–249, 2003.

[105] B. P. Binks and S. O. Lumsdon. Catastrophic phase inversion of water-in-oil emulsions stabilized by hydrophobic silica. *Langmuir*, 16(6):2539–2547, 2000.